# CHARGE-COUPLED DEVICES IN TRANSMISSION ELECTRON MICROSCOPY

PATRICIA T E ROBERTS

Submitted for the degree of Doctor of Philosophy in the University of Glasgow.

November 1980



ProQuest LLC.
789 East Eisenhower Parkway
P.O. Box 1346
Ann Arbor, MI 48106 – 1346

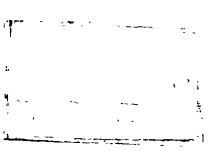

## DECLARATION

This thesis is a report of work which I have undertaken in the Department of Natural Philosophy, University of Glasgow. The work described is my own apart from the design and construction of the Data Accumulation and Control Unit, the Driver Circuit Modifications, and the holders for the CCD in the electron microscope. The first two were designed by Dr A M MacLeod, and several members of the Solid State Physics Group collaborated on the design of the latter.

The following papers have been published, containing details of some of the work reported in Chapters 3, 4 and 5.

1. Chapman J N, Roberts P T E, MacLeod A M, Ferrier R P "Image Recording in the CTEM using Charge-Coupled Devices", in Developments in Electron Microscopy and Analysis 1979, ed T Mulvey, publ Institute of Physics.

2. Roberts P T E, MacLeod A M, Chapman J N, "Application of CCDs as Electron Detectors in Electron Microscopy", in Proceedings of 5th International Conference on Charge-Coupled Devices, Edinburgh 1979, ed J Mavor, publ University of Edinburgh, Centre for Industrial Consultancy and Liaison.

3. Chapman J N, Roberts P T E, MacLeod A M, Ferrier R P, "The Performance of an Imaging System for CTEM based on a Charge-Coupled Device", in Electron Microscopy 1980, Vol 1, ed P Brederoo & G Boom, publ 7th European Congress on Electron Microscopy Foundation (Leiden 1980)

4. Chapman J N, Ferrier R P, MacLeod A M, Roberts P T E, "The use of Charge-Coupled Devices for Direct Electron Recording", in Microbeam Analysis 1980, Proceedings 15th Annual Conference of Microbeam Analysis Society, ed D B Wittry, publ San Francisco Press Inc.

ACKNOWLEDGMENTS

I am grateful to everyone who helped with the work described in this thesis. In particular, I thank my supervisors, Dr J N Chapman and Dr A M MacLeod for their invaluable advice and encouragement, and for many useful and enlightening discussions on experimental results. I am grateful to Professor R P Ferrier for his interest, and for the provision of facilities within the Solid State Group of the Natural Philosophy Department in the University of Glasgow.

With regard to the instrumental aspects of the work, I thank Dr A M MacLeod for the design of the electronics for the Data Accumulation and Control Unit. I would also like to thank Mr D Dickson of the Natural Philosophy Electronics Laboratory for building the Unit, and for his frequent help with maintenance and modifications. The electron microscope is maintained by Mr J Simms and Miss M Low, to whom I am most grateful for their help,

I would also like to thank the members of the Solid State Workshop for the construction of various pieces of apparatus. I am grateful to Dr E H Darlington for the design of equipment for testing the display oscilloscope and for his help and interest in various aspects of the work. I thank Dr W R K Clark for specimens of chlorinated copper phthalocyanine, and Fairchild Semiconductor for the provision of four CCD 202s.

In the preparation of this thesis I am most grateful to Miss S M Sinclair for her skilful typing and willing help. I thank Mrs M Waterson for preparation of the diagrams and Mr I MacVicar for photographic work.

Finally, I thank the Science Research Council and Kratos Ltd for the provision of a CASE award.

SUMMARY

This thesis describes the results of experiments to test the suitability of charge-coupled devices (CCDs) for electron imaging. An electronic imaging system based on a CCD has several advantages over conventional imaging methods, particularly for image processing applications where quantitative data is required. The Introduction outlines the advantages of an electronic imaging system, and discusses available systems, and the possible merits of solid state devices, in particular CCDs. The operation of CCDs is described in Chapter 1, with particular reference to the Fairchild CCD 202, the device used in these experiments.

The desirable properties for an imager with a quantitative output for computer processing are described in Chapter 3. In this chapter are reported the results of experiments to test the properties of the CCD 202 and these results show it to be suitable as a recording device for producing a quantitative output for image processing. It has a DQE in the range of 0.46 - 0.6, has an output which is linearly related to the incident electron intensity, and has an electron gain of $\sim 10^3$ for 20 keV and $\sim 10^4$ for 60 and 100 keV electrons.

An undesirable property of MOS devices such as CCDs is their limited lifetime under exposure to ionizing radiation. Chapter 4 reviews radiation effects in MOS devices, presents results on experiments to test the CCD lifetime under irradiation, and discusses ways in which the useful life of the device can be extended.

The output of the CCD is an analogue video signal. A Data Accumulation Unit was built to digitise and store the output signal and to transfer it to a computer or to magnetic tape for storage. In addition the image can be displayed on a CRT screen, and photographed to produce a permanent record. Chapter 5 describes the use of the CCD 202 to record electron images of various specimens and shows the images which were obtained.

Chapter 6 summarises the findings on the suitability of CCDs for electron microscopy, and suggests modifications to the devices and to the imaging system which would extend the range of applications of CCDs.

C O N T E N T S

# INTRODUCTION

The electron microscope was first developed in 1931 by Ernst Ruska in an attempt to overcome the resolution limit of the optical microscope, set at ≈ 0.2 μm by the diffraction limit for visible light. The advantage of using electrons as illumination results from their very short wavelength ( ≈ 0.05Å for 60 keV electrons) which allows imaging of detail at considerably smaller spacing than the light microscope. However, for the electron microscope the resolution is determined not only by the electron wavelength but also by lens aberrations, resulting in a minimum lattice resolution ≈ 1Å, and a point-to-point resolution ≈ 3Å.

In Conventional Transmission Electron Microscopy (CTEM) a thin specimen ( ≈ 100Å thick) is illuminated with a uniform beam of electrons, and the electrons transmitted by the specimen are used to form an image. The optical system in CTEM is analogous to that of a light microscope, with magnetic lenses being used to focus the electron beam onto the specimen and to form and magnify the image. Contrast in the electron microscope is obtained by 1) amplitude contrast, in which electrons scattered through large angles by thick areas of specimen are stopped by an aperture placed below the specimen, or 2) phase contrast resulting from interference effects between the unscattered electron beam and the elastically scattered electrons.

The resulting image in the electron microscope is normally recorded on photographic emulsion which is subsequently developed to produce a permanent record. Photographic emulsion consists of a suspension of silver halide crystals in gelatine, of thickness typically 12 μm, supported on a plastic backing film. An electron incident on the emulsion loses little energy in the gelatine, but does interact with the silver halide crystals (grains) producing local aggregates of silver atoms so that the grain readily reduces to silver in the development procedure[1]. Thus any grain which has been hit by an incident electron appears dark on development. The number of grains developed by an electron depends on the electron energy and on the grain size, but is typically 3 - 4 for conventional emulsions for energies of 30 - 60keV.[2] Thus every electron incident on the photographic film may be recorded. The detective quantum efficiency (DQE) of photographic film or any other recording medium is defined as $(S/N)^2_{Out}/(S/N)^2_{In}$ where S = signal amplitude and N = noise amplitude. This is a measure of the additional noise introduced into the recorded data by the photographic plate, and

for an ideal recorder the DQE is 1. The DQE of photographic film has been measured by Valentine for a variety of emulsions, and values in the range 0.4 - 1 were obtained for the emulsions tested[3]. These values indicate that photographic film can be an excellent recorder of electrons, with the noise in the recorded data being approximately equal to the shot noise in the electron beam.

The number of incident electrons determines the number of grains exposed in the emulsion and thus the optical density of the micrograph. The relationship between optical density and electron dose has been experimentally determined and has been shown to have the form $D = K(1 - e^{-Ek})$ where D = optical density, E = exposure, and K and k are constants.[3] However the relationship can be approximated as linear up to optical densities of $\approx$ 1 and thus electron micrographs are normally recorded with an optical density of $\lesssim$ 1. The number of electrons required to reach this density is a measure of the speed of the emulsion, and has a typical value of 1 - 3 electrons/$\mu m^2$ for standard electron microscope emulsions.[4]

Thus, photographic emulsion is a good electron recorder, with a high DQE and a linear response over part of its range. In addition, photographic film stores a large amount of information and in many cases image processing can be used to extract information from the recorded image which is not accessible by visual inspection. The types of image processing normally performed fall into 4 main categories[5]. These are 1) Image enhancement procedures such as contrast improvement and enhancement of high spatial frequencies, 2) Image averaging of radiation sensitive specimens to improve the signal to noise ratio, 3) The formation of composite images from several micrographs of the same specimen recorded under different conditions to obtain, for example, information about the 3-dimensional structure of a specimen, and finally 4) Determination of the focus conditions of the microscope by examination of the Fourier transform of an amorphous specimen such as a carbon film.

Before image processing can take place, the intensity distribution in the image must be measured and converted to a digital form. This is normally done using a densitometer, which measures the optical density in the micrograph by scanning a small spot of light in a raster of points across it and measuring the transmitted intensity at each point. The transmitted intensity is exponentially related to the optical density, and so requires some method of conversion to produce an output

signal proportional to the optical density, that is, to the number of electrons incident on the film (assuming an optical density $\leq 1$). The output of the microdensitometer is in graphical or digital form, with the latter recorded on magnetic tape or paper tape, or transferred directly to a computer. The number of picture points normally used in image processing at present is 256 x 256, although the trend is towards using larger 512 x 512 arrays as cheaper computer memory becomes available.

Densitometry of photographic film, while it is the most common method of obtaining quantitative intensity information, is unsatisfactory in several respects. Firstly, the process involves several stages before the digital information is obtained, that is recording, development and densitometry, and is thus time-consuming. In particular, the necessary development stage means that several hours may elapse between recording the image and obtaining the quantised data. No selection of data for processing can be done before the development stage is complete. In addition, both development and densitometry normally take place remotely from the microscope. Thus the above procedure is wasteful in terms of operator time and certainly rules out the use of image processing for instrumental adjustment.

A method of obtaining quantitative information immediately from the microscope is to replace the photographic plate with a television-type imaging system based either on a camera tube or a solid state imaging array. The output of such a system is a series of voltage pulses corresponding to a raster of picture points in the image, ideally with the amplitude of a voltage pulse being linearly related to electron intensity on the corresponding picture point. Such a signal is simply converted by an analogue to digital converter (ADC) into the digital form required for computer processing. Thus the output of a television-type image sensor can be transferred via an ADC immediately to a computer, thus avoiding the multistage and time consuming process necessary with photographic film. In addition, the form of the video output signal is such that the recorded image can be displayed on an oscilloscope screen allowing the prior selection of suitable data for processing.

A further advantage of such a system is its superiority over the phosphor screen for work with radiation sensitive specimens. Such specimens damage under the electron beam, so that after a certain critical electron dose the specimen is no longer representative of the original structure. Thus for these specimens it is important to

minimise the electron dose on the specimen during the area selection and focusing stage, so that the maximum number of electrons can be used in recording the image[6]. This is normally achieved by focusing on one area of specimen while viewing the image on a phosphor screen, and then recording a new and unseen area of the specimen. Clearly, this is unacceptable, since images are recorded without prior selection of the area, resulting in a high percentage of wasted films. In addition, focus conditions may vary from one specimen area to the next due to, for example, specimen buckling.

The advantages of electronic imaging systems for radiation sensitive materials are two-fold. Firstly, by suitable amplification of the output signal, images can be seen on a display oscilloscope at beam currents too low to be seen with the naked eye on the phosphor screen. Secondly, once recorded in digital form the output signal can be stored and cycled, so that the image can be continuously displayed on an oscilloscope screen without further irradiation of the specimen. Using this method area selection and focusing can be done at considerably lower electron doses than with the phosphor screen, and the area for recording can be selected at a low electron dose.

As mentioned earlier, the choice of a TV type image sensor lies between television camera tubes and the more recent solid state image sensors. All of these devices are designed for photon imaging, although the latter may be suitable for direct electron imaging. Camera tubes have been investigated for electron microscopy over a number of years, and in many cases have been used simply to amplify the electron image and allow the specimen to be viewed at low intensities. Their quantitative performance and suitability for image processing has been investigated in particular by Herrmann, Krahl & Rust et al[7,8,9,10,11] and by other workers[12,13,14].

The system of Herrmann et al is based on an Electron Bombarded Silicon (EBS) camera tube. Since this is designed for light imaging, the electron signal is converted to a photon signal by a transmission fluorescent screen made of ZnS, so that a photon image is incident on the camera tube. The EBS camera tube operates in the following way. The photons are incident on a photocathode, from which they liberate photo-electrons. These are accelerated to a silicon target maintained at a positive potential of typically 5 - 10 keV with respect to the photocathode. The target consists of an array of reverse biased photodiodes which are discharged by the photo-electrons, so producing

a charge pattern on the target corresponding to the optical image. An electron beam accelerated to a potential of < 1kV scans the target on the other side from the photocathode. The current in the reading beam depends on the potential (and thus the stored charge) of the point being scanned, and is therefore related to the image intensity. Thus, measurement of the current pulse produces the video signal. The camera is enclosed within an evacuated glass tube.

This system has been shown by Herrmann et al to have excellent response in pulse counting mode, in which the number of electrons incident on each picture point is either 0 or 1. The system has an efficiency of 65% for the detection of single electrons, equivalent to a DQE of 0.6, which is in the range available with photographic plate. Signal processing of the video output is necessary in this mode to avoid multiple counts due to signal spread to adjacent picture elements and image lag between successive frames. In pulse counting mode an image intensifier before the camera tube is used to increase the photon signal. The stage which is least efficient in this system and leads to the loss of DQE is the fluorescent screen in which the electron-photon conversion takes place. This point has also been made by Kuo & Glaeser[12], who obtained ≈ 10% efficiency in single electron detection with a Secondary Electron Conduction (SEC) camera tube. Kerzendorf & Hoppe[13] have suggested that the DQE of the system could be improved to ≈ 0.95 by the replacement of ZnS by $CaF_2$ as the screen material. However, this method has not been tested experimentally.

Although television camera tubes provide the necessary quantitative output for image processing and can have a high DQE in electron counting mode there are several areas in which they could be improved. Firstly, the noise introduced into the output signal in the electron-photon-electron conversion degrades the performance of the camera in analogue mode and limits the maximum number of electrons which can be discriminated. Secondly, a non-uniformity of response of image elements is introduced by non-normal scanning by the electron beam of elements at the edge of the array[15]. Finally, from the practical point of view, they are expensive, have a high power consumption, are of fragile construction and are relatively large compared with the space available in an electron microscope. Thus there is an incentive to test solid state arrays as alternative to camera tubes for electron imaging.

The two main types of solid-state detector array now available are

charge-coupled devices[16] and photodiode arrays[17]. Both devices are based on silicon substrates, the first consisting of an array of metal-oxide-semiconductor (MOS) capacitors, and the second of an array of p-n diodes. In both devices incident radiation creates electron-hole pairs in the silicon substrate which are collected in the MOS capacitors in the CCD and in the reverse-biased diodes in the photodiode array. The amount of charge collected is directly proportional to the intensity of the incident radiation. The main difference in the two devices is in the readout method employed. In the photodiode array, a depletion region is formed at the p-n junction of the diodes by connecting each diode in turn momentarily to a reverse bias voltage. The charge stored on the depletion layer capacitance is discharged by the electron-hole pairs created by the incident radiation. An output signal is obtained when the diode is once more connected to the reverse bias voltage, with the signal being the quantity of charge required to restore the diode to its previous level.

In CCDs, the signal charge is stored in the depletion region formed in the silicon substrate by the application of a suitable potential to the metal electrode. The charge is read out by removing the potential from the storage electrode and placing it on an adjacent electrode, so moving the depletion region and therefore the stored charge. This process continues, moving the charge one electrode at a time until it is read out of the device through an output amplifier.

Although designed for photon imaging, both of these devices can be used as electron detectors, since incident electrons can create electron-hole pairs in the silicon substrate. Of the two devices the CCD area imaging array seemed the more suitable, for the following reasons[18]:

1. The output noise in the photodiode array is greater than that of the CCD array due to the large capacitance of the output video bus, which is connected to all of the elements in the array. As a result, in the photodiode array the output noise increases with $\sqrt{n}$ where n is the number of image elements. In the CCD the output noise is due to the capacitance of the single output element and to the noise which is introduced in charge transfer.

2. Photodiode arrays suffer from non-uniformity in the response of the image elements. This is caused by spatial variations in the switches which connect the diodes to the reverse bias voltage, and in the scan pulses which control them.

3. For the reason given in 1 above commercial development of solid state arrays for cameras for video recorders is tending to concentrate on CCDs rather than photodiode arrays. Therefore CCDs are available commercially in larger arrays sizes than are photodiode arrays, and the price of CCDs is less for equal numbers of elements. For computer processing an array size of at least 256 x 256 elements is desirable, and while this is available in CCDs, the largest photodiode array commercially available has 100 x 100 image elements.

However, there are aspects of CCD structure which are less suitable for electron imaging than photodiode arrays. Foremost among these is the degradation in the MOS structure of the device caused by ionising radiation[19,20,21]. The oxide layer in the MOS structure gains fixed positive charge under ionising radiation, and this affects the threshold voltage levels and the shape of the potential wells of the device. This problem does not affect the p-n structure of the photodiode array.

On balance, it was decided that CCDs held greater promise for electron imaging because of their lower noise and more advanced commercial development.

This thesis is concerned with an investigation of the performance of a particular CCD as an electron imager, with a view to using it to obtain quantitative information for image processing. The CCD chosen for these experiments is the Fairchild CCD 202, which is a 100 x 100 element array. Although this is smaller than the number of elements which is desirable for image processing, it allows assessment of the performance of CCDs as electron detectors, since the results obtained with this device should be applicable to larger arrays. The cost of the device is $\approx$ £200, with a further £200 required for driver circuitry. Although the CCD 202 is designed for photon imaging, it was decided to use it in direct electron imaging mode, to avoid the degradation in the image associated with electron-photon conversion.

Chapter 1 of this thesis describes the operation of CCDs and of the Fairchild CCD 202 in particular, and outlines the differences between using the CCD for electron and photon imaging. Chapter 2 describes the apparatus used in the experiment, including the modifications to the CCD drive circuitry required for electron imaging and the Data Accumulation and Control Unit which was designed to drive the CCD in the microscope, to collect data, and to output it for storage and processing.

Since the CCD is intended for photon imaging, little was known about its performance as an electron imager. As a result a series of experiments was done to investigate its performance in this mode, that is, to measure the gain, resolution, uniformity of response, single electron detectability and cell capacity. The results of these experiments, their implications for the suitability of CCDs for electron microscopy, and a comparison of the CCD performance with that of other imagers is reported in Chapter 3. Chapter 4 deals with the damage caused to the device by electron irradiation, and the measures which can be taken to extend the device lifetime after damage has occurred. In Chapter 5 results on using the CCD for recording electron images, including images of radiation sensitive materials, are presented.

Although this thesis is concerned with the role of CCDs in CTEM, there are several other branches of electron microscopy in which they may prove useful. Thus the results of the performance tests in CTEM are a guide to the potential usefulness of CCDs in other fields, and will be discussed in this light where appropriate.

In Electron Energy Loss Spectroscopy (EELS), the energy lost by the electron beam in passing through the specimen is analysed to determine the chemical structure of the specimen material[22]. An electron spectrometer after the specimen converts the energy distribution into a spatial distribution. The resulting spectrum is normally recorded either by scanning it across a slit in front of a scintillator-photomultiplier, or by recording it directly on photographic plate. The second method involves all the problems of densitometry of photographic plate described earlier. The first method provides a quantitative output immediately, but has the serious drawback that all the channels of data are recorded serially, resulting in a long recording time and inefficiency in the collection of the transmitted electrons. Typically 512 or 1024 channels of data are recorded for good energy resolution, thus the recording time and the electron dose on the specimen are both increased by a factor of $\sim 10^3$ over the necessary values. This may well result in problems with radiation sensitivity and specimen drift. As a result, a parallel recording system which could record all channels simultaneously would be of considerable advantage[23]. A linear CCD imaging array is potentially suitable for this application.

Another field in which a position sensitive recorder such as a CCD would be advantageous is in Scanning Transmission Electron Microscopy

(STEM). In this mode a fine electron probe is scanned in a raster across the specimen and information about the specimen is contained in the angular intensity distribution in the transmitted beam. Thus detectors with different geometrical configurations can extract different information about the specimen. The detector configurations which can yield useful information are the common circular bright and annular dark field detectors, the split detector[24], the quadrant detector[25] and the Rose multiannular detector[26]. All of these modes require detectors with a specific geometry, and some of them require multiple detectors with matched gains. An area imaging array with a large number of individual imaging elements such as a CCD would produce an output which, when suitably processed, would be capable of representing any of the above geometries[23]. This would remove the need for more than one type of detector in a STEM instrument, and would avoid the undesirable changing of detectors in high vacuum instruments.

While the CCD 202 is not used in any mode other than CTEM imaging, its performance in that mode gives a guide to its suitability as a detector in these other applications. This is discussed in Chapter 3.

# CHAPTER 1

# CHARGE COUPLED DEVICES

## SECTION 1.1 INTRODUCTION

Imaging charge coupled devices (CCDs) are produced commercially as solid state television cameras. They were first proposed in 1969 by Boyle & Smith[1] and the first device was manufactured in 1973 by Fairchild Camera and Instrument Corporation. Their design is based on a metal - oxide - semiconductor (MOS) structure and as a result has the advantage of being compatible with standard semiconductor manufacturing technology. This, in addition to their small size (typically 5mm x 5 mm for the image sensing area) and their robustness when compared with traditional television cameras, means that they are very suitable for the home video market, and has resulted in extensive commercial interest and development.

Although CCDs are intended for photon imaging they are also sensitive to other forms of radiation, and, in particular, can detect electrons. In this chapter their basic operation is described in Section 1.2. Section 1.3 deals with the particular structure of the CCD used in our experiments, the Fairchild CCD202, and Section 1.4 discusses the differences encountered in using the devices for electron, rather than photon, imaging.

## SECTION 1.2 OPERATION OF CHARGE COUPLED DEVICES

### 1.2.1 Introduction

An imaging CCD consists of a large array (typically 100 x 100 or more) of MOS capacitors (known as photocells) each of which can store an amount of charge proportional to the intensity of the radiation incident on it. The charge packets from the photocells are read out of the CCD serially to form a video signal which represents the image on the front face of the device. This section describes firstly the method by which charge is collected and stored in the photocells, secondly the way in which the signal charge is read out of the device, and finally the various available readout organisations of CCDs. The information in this Section is taken largely from Hobson's book "Charge Transfer Devices"[2].

### 1.2.2 Storage of Charge

The simplest form of CCD, known as a surface channel device, consists of a doped silicon substrate of thickness $\approx 250\ \mu m$, covered with

an insulating layer of $SiO_2$ of thickness $\approx 0.1 - 1\mu m$ overlaid with an array of conducting electrodes made, for example, of aluminium. Figure 1.1 shows a cross-section of a CCD cell. The application of a suitable potential to the electrode drives away the majority carriers in the silicon, producing a depletion region under the electrode and creating a potential minimum for minority carriers at the interface. The electron-hole pairs produced in the substrate by incident radiation are separated by the applied field, with the minority carriers being attracted to and stored at the interface, and the majority carriers being swept into the silicon bulk. Figure 1.2a shows the electric field and potential profiles in a single cell in the absence of stored charge, and Figure 1.2b shows the profiles when charge is present.

In Appendix 1 the relationship of the surface potential Vs to the stored charge $\rho$ is calculated for a surface channel CCD. It is shown that for this case Vs is approximately linearly related to $\rho$ with the MOS structure behaving as a capacitor having the capacitance of the oxide layer $\varepsilon_r\varepsilon_0/d$ . As a result, as charge collects at the interface, the depth of the potential minimum decreases until it becomes the same as that in neighbouring cells which do not have an applied electrode voltage. At this point, which is defined as saturation, spillage of charge from the collecting cell to adjacent cells occurs. The stored charge at saturation is the saturation charge, and the corresponding output voltage is the saturation voltage.

The storage of charge at the interface has the disadvantage of allowing it to interact with interface states, energy levels within the silicon band gap which can trap charge making it unavailable for readout. These interface states result from the mismatch between the Si and $SiO_2$ lattices, and from impurities trapped at the interface which distort the periodic potential. They are discussed in greater detail in Sections 4.2.2 and 4.2.5. To avoid the interaction of signal charge with interface states, buried-channel CCDs are used in which charge is stored and transported, not at the interface but in the silicon bulk $\approx 0.5\mu m$ away from the interface. This is accomplished by the insertion at the interface of a thin channel of doped silicon typically $\approx 1\mu m$ thick of opposite polarity to the substrate material. The channel-substrate junction is reverse biased by applying a suitable potential to the channel, so depleting the buried channel.

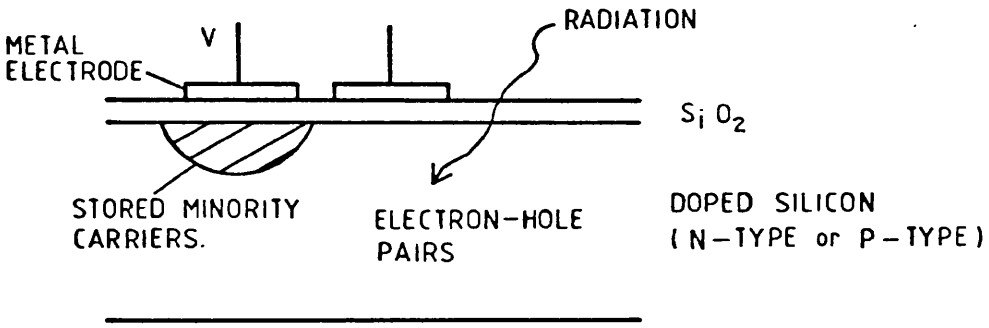


Figure 1.1: Cross-Section of CCD cell

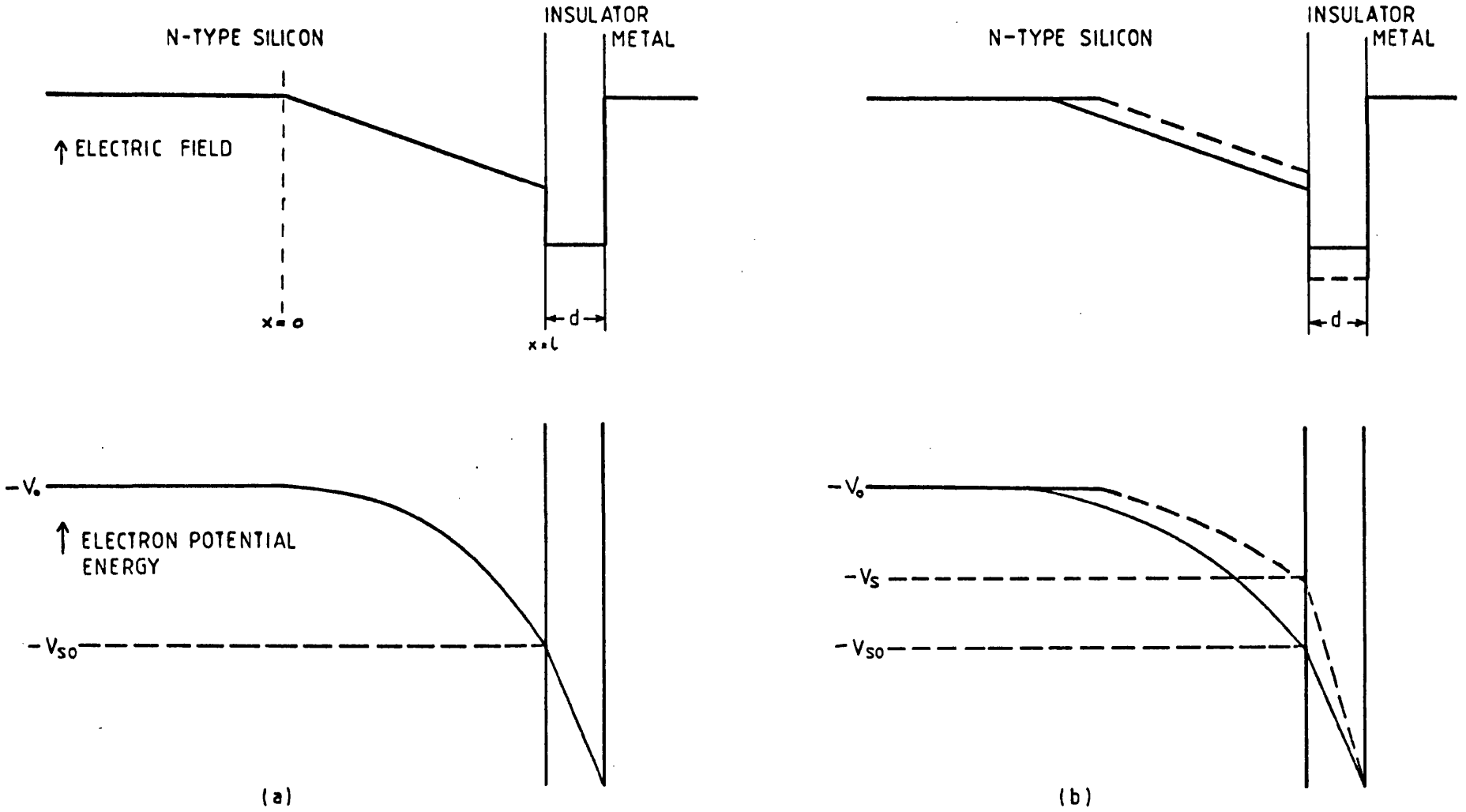


Figure 1.2: Electric field and potential profiles in surface channel CCD
a) in absence of stored charge
b) with charge present

Figure 1.3 shows the electric field and potential diagrams for a buried-channel device with and without stored charge. It can be seen that the potential minimum, and therefore the position at which charge is stored, is displaced from the interface, and that its position depends on the value of the applied voltage. As signal charge is created by incident irradiation it is attracted to and stored at the potential minimum. The density of the stored charge is such as to maintain a zero electric field and therefore a potential minimum in the storage region. Since the electric field is constant there can be no net charge in this region, implying that the density of stored charge is equal to the doping density of the n-channel. The charge in a buried channel device is therefore stored in a finite volume of the buried channel layer. Saturation charge for a buried channel device can be defined as the stored charge which causes the volume of the storage region to increase so that some charge is stored at the interface. At this point the CCD is working in surface channel mode since the charge at the interface can interact with interface states and may be trapped by them. In practice, the electrode voltages are arranged so that saturation by spillage to an adjacent cell occurs before this point is reached. In addition, it can be seen that if the edge of the storage region reaches the n-type - p-type junction the electric field becomes zero in the former depletion region so that the potential minimum exists throughout the silicon bulk and the storage well is no longer defined. The distance $l_{b0}$ shown in figure 1.3, the distance of the potential minimum with no charge stored from the n-type - p-type junction, is the quantity which sets the absolute maximum limit on stored charge for a given electrode voltage. The maximum charge which can be stored in a well is therefore $eN_D Al_{b0}$ where $N_D$ is the doping density of the n-layer and A is the area of the electrode.

### 1.2.3 Readout of Charge

The stored charge in a CCD cell is read out to an output sensing amplifier using the charge transfer method first suggested by Boyle & Smith. The charge is transferred out of the CCD by removing the electrode voltage on the storage cell and applying it to an adjacent cell, so translating the potential minimum and therefore moving the charge. This process can be continued, moving the charge packet one electrode at a time until it is transferred to an output gate which senses the charge and produces a voltage pulse of size proportional to the charge packet.

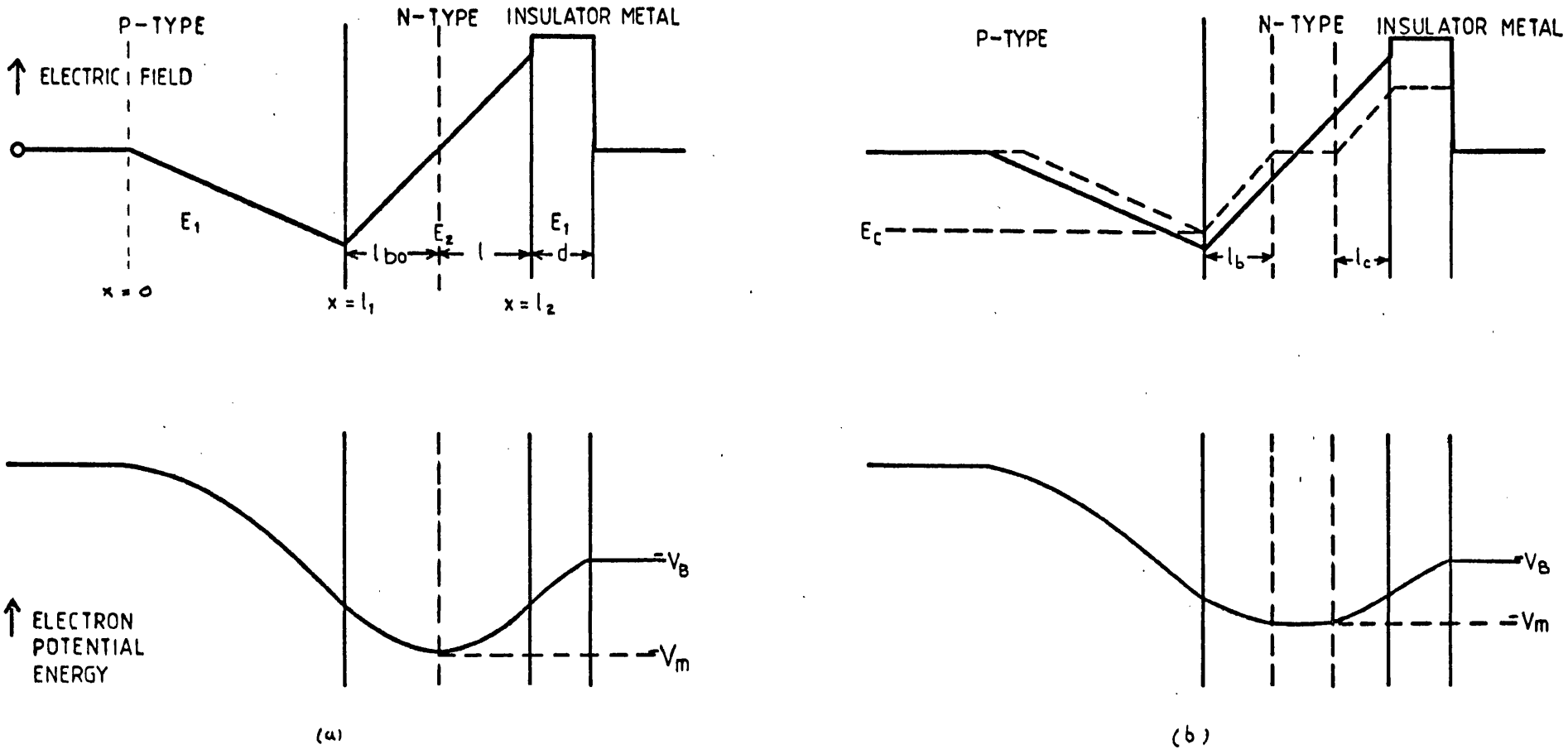


Figure 1.3: Electric field and potential profiles in buried channel CCD
a) in absence of stored charge
b) with charge present

When the electrode voltage is applied to the adjacent cell, there are 3 mechanisms by which the charge transfer takes place:

1. Mutual Repulsion. Application of the electrode voltage to the adjacent cell removes the potential barrier which previously existed round the storage cell. Charge at the edge of the storage electrode which experiences a repulsive force due to the rest of the charge packet is then free to move until it comes within the electric field of the receiving well, at which point it can be stored there.

2. Self-Induced Drift. The non-uniform charge density in the well caused by the transfer of charge in (1) above produces a non-uniform surface potential in the emptying cell. The surface potential energy is lowest at the edge of the cell (where the charge density is least) and so there is a movement of charge towards the receiving cell.

3. Diffusion. The non-uniformity of charge also causes diffusion of charge towards the receiving cell, aiding the charge transfer process.

Clearly it is necessary to have at least two electrodes per cell so that there is one empty well available to collect charge transferred from the adjacent cell. In the most simple transfer structure each cell has three identical electrodes, only one of which is used during the storage phase to store charge. Figure 1.4 shows how transfer occurs. The purpose of the third electrode is to provide a potential barrier during transfer to define the direction in which transfer takes place. Charge is initially stored under electrode 1 , which has a potential of typically 10V on the electrode. The application of a positive potential to electrode 2 removes the potential barrier between electrodes 1 and 2 allowing charge transfer to take place. Finally, removal of the positive potential from electrode 1 creates a potential barrier confining the charge to the region under electrode 2. This process is repeated to transfer the charge to electrode 3. A third transfer would result in the charge being stored under electrode 1 of the adjacent cell.

This transfer mode in which there are 3 electrodes per cell is known as 3-phase clocking. While allowing a simple CCD structure, it has the disadvantages of requiring a driver circuit with 3 different clocking phases and of being inefficient both in terms of storage space and transfer time. A more efficient organisation is 2-phase clocking

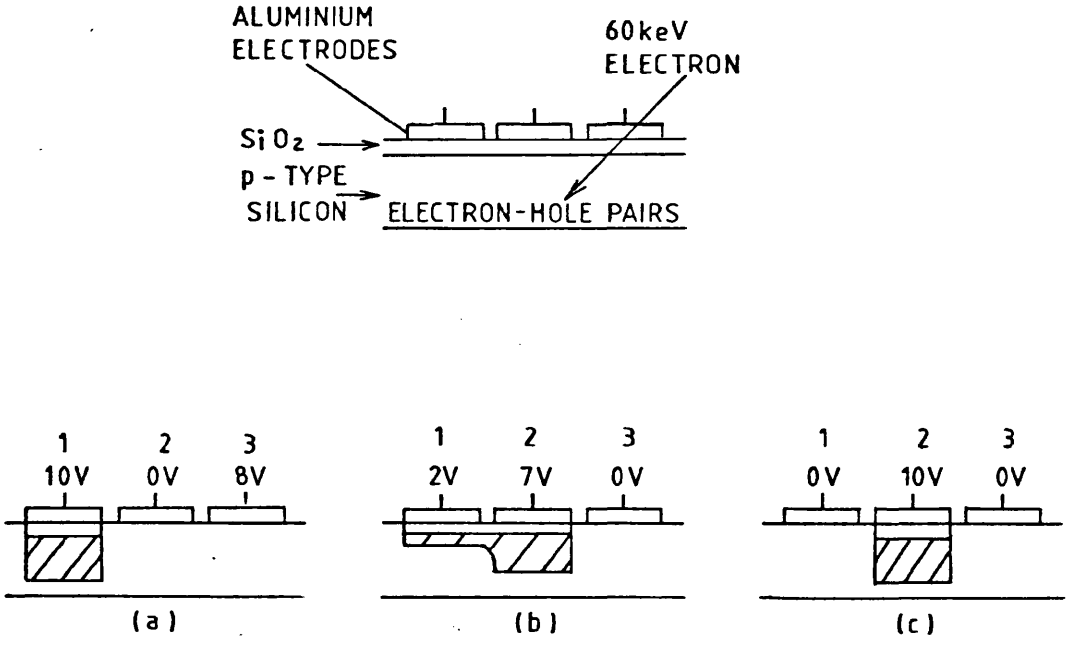


Figure 1.4: Charge transfer in a 3-phase CCD

in which there are 2 electrodes per cell and in which the surface potential under each electrode is profiled to provide a potential barrier and ensure unidirectional charge transfer. Figure 1.5 shows a 2-phase CCD with profiled wells. There are several ways in which the surface potential can be increased to provide the potential barrier. The most common methods are 1) to increase the oxide thickness at one side of the well, so increasing the potential drop across the oxide under it, or 2) to insert a more highly doped region of material of the same polarity as the substrate immediately under the electrode. The 2-phase clocking method is used in the Fairchild CCD202, the device used in these experiments.

### 1.2.4 Organisation of CCDs

The above subsections have discussed the storage of charge in the CCD cells and the transfer of charge from one cell to the next. In imaging CCDs the readout of signal has to be organised in such a way that the resulting video signal can be used to reconstruct the image incident on the device. There are 3 main readout organisations by which this can be done, and these will be described separately:

1. Interline Transfer Method. This is the readout organisation employed in the Fairchild CCD202, the device used in these experiments. Figure 1.6a shows schematically the organisation of the device. There are N columns of light sensitive cells (called photocells) in which charge is collected, interlaced with N columns of transport cells through which the signal charge is transferred. (N is typically $\sim$ 100 - 500). The transport cells are shielded from the incident light by a thin layer ( $\approx$ 1 $\mu$m thick) of aluminium so that there is no signal charge produced in these cells. When an electrode voltage is applied to the photocells signal charge collects in them. To read out the charge the electrode voltage is removed so that charge transfers into the adjacent transport cell which has an applied electrode voltage. The electrode voltage is immediately restored to the photocell so that signal collection can recommence. The potential wells are profiled, as described in the previous subsection, to create a potential barrier between photocell and transport cell, allowing both to have an applied electrode voltage and to store charge simultaneously. Once in the transport cells a 2-phase clocking mode transfers the charge along the vertical transport register towards the horizontal transport register. As each row of charge packets reaches the horizontal

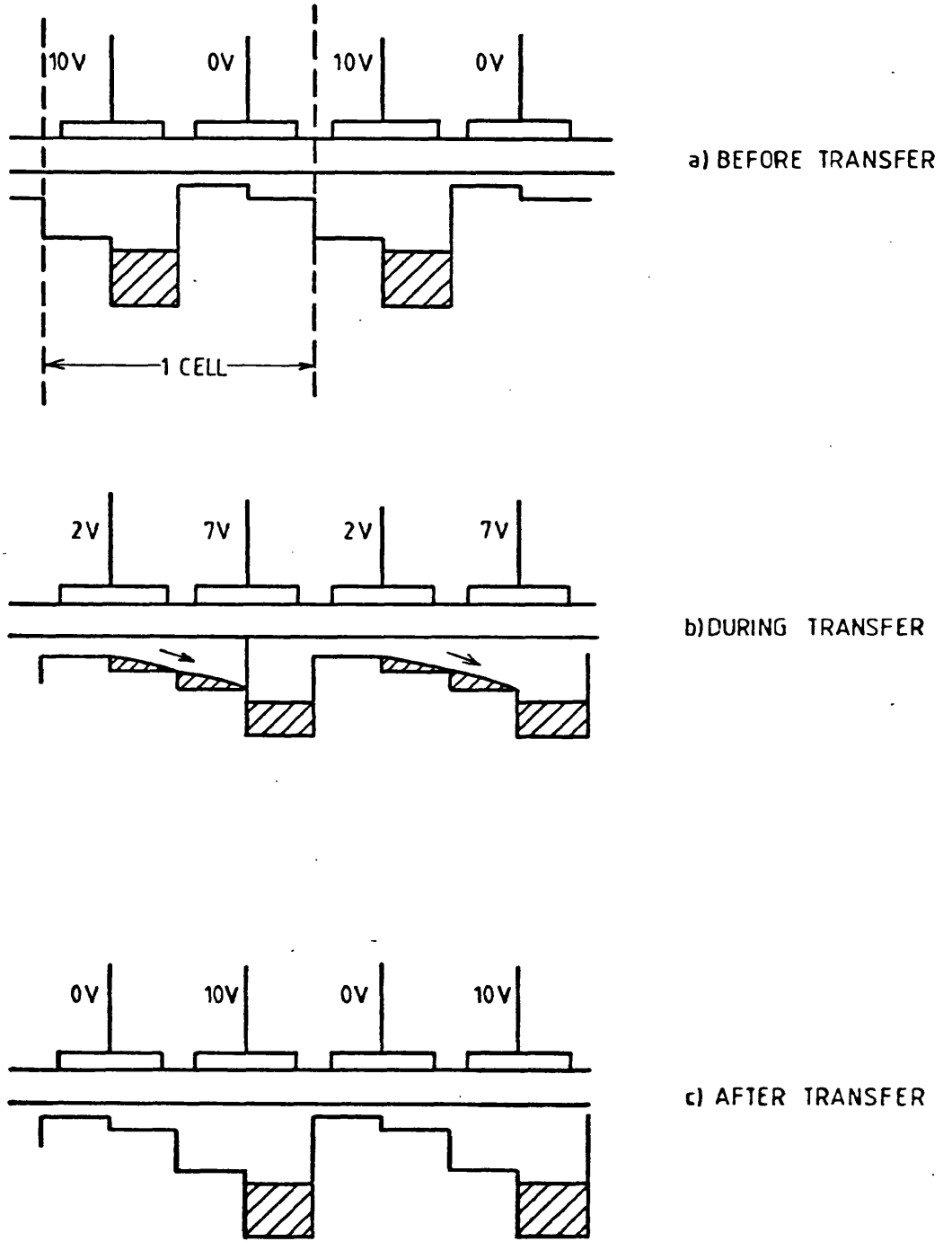


Figure 1.5: Charge transfer in a 2-phase CCD

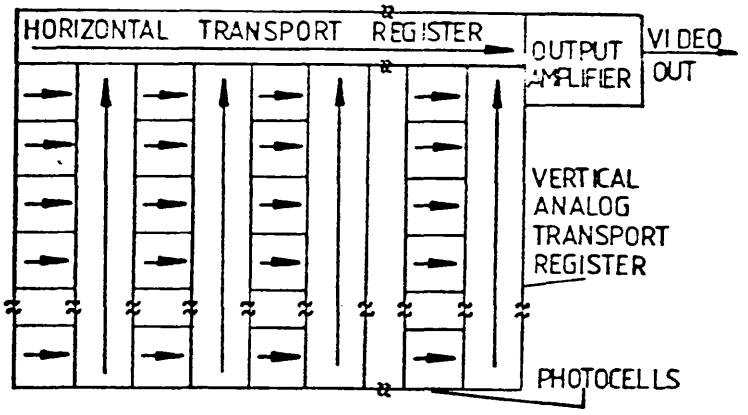


a) INTERLINE TRANSFER

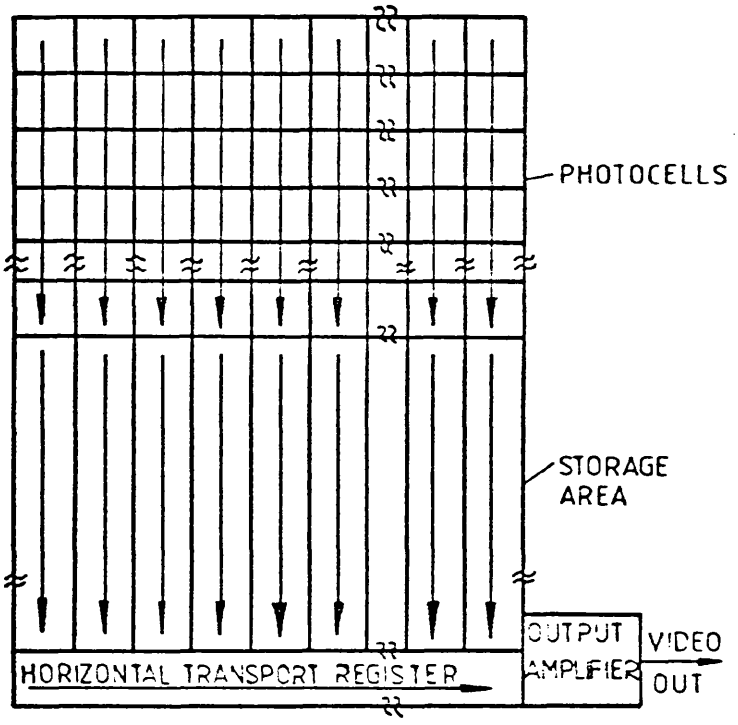


b) FRAME TRANSFER

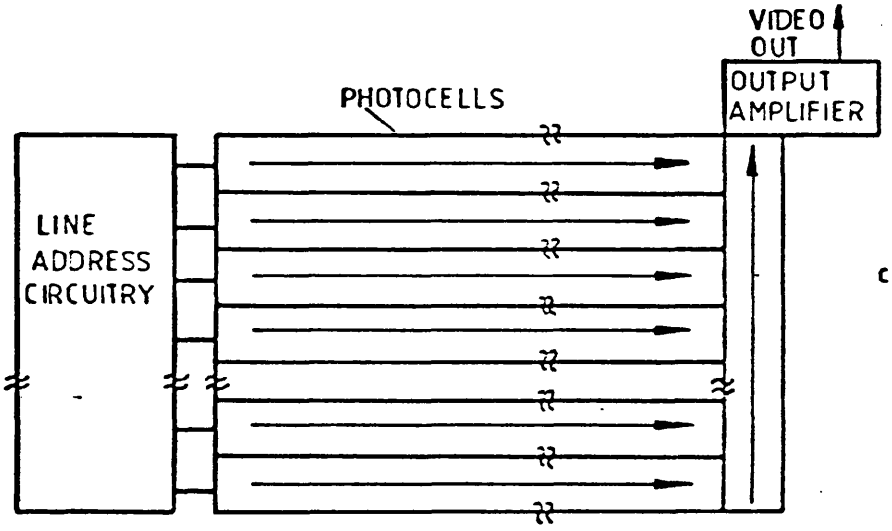


c) LINE TRANSFER

Figure 1.6: Readout organisations of CCDs

register it is read out horizontally by 2-phase clocks to the video output amplifier which senses each charge packet and produces a voltage pulse at the device output of size proportional to the magnitude of the signal charge. After each horizontal row has been read out a vertical transfer puts the next horizontal row into the output register. This process continues until all charge packets have been transferred out of the transport cells.

Interline transfer devices employ a television type readout in which alternate fields of odd and even-numbered rows of photocells are read out separately. This method has the advantage of producing a flicker-free display at a lower clocking frequency than would be possible if both odd and even rows were read out simultaneously. In addition, since only N/2 charge packets are transferred into each column of transport cells at any one time only N/2 transport cells each with 2 electrodes are required.

2. Frame Transfer Method. The second readout method commonly employed in imaging CCDs is the Frame Transfer structure. A schematic diagram is shown (Figure 1.6b). The device consists of an N x 2N array of cells of which half (N x N) are photocells, and half (N x N) are shielded from light to form a storage area from which the charge is output via an amplifier. Incident light creates charge in the photocells in the upper half of the device (Figure 1.6b). To read out the signal, the charge is transferred vertically out of the photocells to the shielded storage cells in the lower half of the device. From there the signal is read out in the same way as in the Interline Transfer organisation described above by clocking the charge vertically into a horizontal output register and reading it out row by row.

Separating the photocells and transport cells in this way has the advantage that none of the information in the image is lost by being incident on shielded transport cells, resulting in a twofold increase in efficiency over the interline transfer method. However, it has the drawback that charge transfer takes place through an irradiated region, so that charge is added to the cells during transfer through the photocells to the storage region, resulting in charge smearing. This is minimised by clocking the charge at a high rate (typically 10 MHz) in to the storage cells, and ensuring that the transfer time is short compared with the charge integration time. A typical transfer time of 50μs and integration time

of 25 ms reduces the smeared charge to $\approx$ 0.2% of the output signal.

With this structure an interlaced output where alternate fields of odd and even-numbered rows of photocells are read out separately can be obtained by suitable application of electrode voltages to alternate rows of photocells during the integration time.

3. Line Transfer Method. The final readout method, and one which is not in common use, is the line transfer method. A schematic diagram is shown in Figure 1.6c. The signal is read out of the device one horizontal row at a time, with charge transfer taking place through the photocells. Although the absence of storage cells constitutes a X2 saving in device area, the complicated drive circuitry required to clock the charge through the device has made manufacture of this device difficult.

Of the 2 readout organisations available, the second, the Frame Transfer Method, would seem to be the most suitable for electron imaging, because it avoids the problem of electron penetration to the transfer and storage cells. This will be discussed in more detail in Section 1.4.3. However, there was difficulty in obtaining information and devices from manufacturers using the Frame Transfer structure, and as a result the Fairchild CCD202, which is an Interline transfer device, was used throughout this project.

## SECTION 1.3 FAIRCHILD CCD 202

### 1.3.1 Introduction

This section describes the Fairchild CCD202, the imaging device used in these experiments. The CCD202 is commercially produced for photon imaging, and no attempt has been made by the manufacturers to harden the device to ionizing radiation. (The effect of radiation damage on the CCD performance and the desirable features for a radiation hard CCD are described in Chapter 4). The only modification to the standard commercial devices adopted in these experiments was to have the glass window over the device removed by the manufacturers to avoid absorption of the incident electrons when the CCD was used in electron imaging mode. Figure 1.7 shows the Fairchild CCD202 with the glass window removed. The CCD is mounted on a ceramic base in a 24-pin dual in-line format. The dimensions of the base are 3cm x 1.5cm and the active area of the device measures 4 mm x 3 mm.

### 1.3.2 Device Organisation and Drive Signals

The Fairchild Design Development Board Brochure[3] describes the

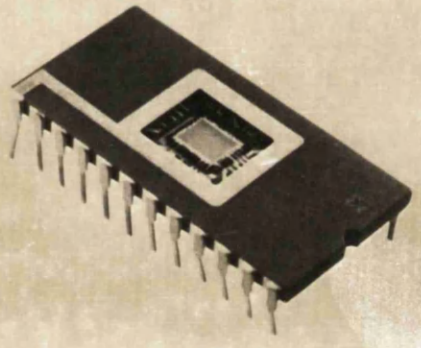

Figure 1.7: Fairchild CCD 202

electrical properties of the CCD202 and the clocking voltages which drive it. The CCD202 has the interline transfer organisation described in the previous subsection, and consists of a 100 x 100 array of photocells interlaced with a 50 x 100 array of shielded transport cells. The structure is buried channel, with a p-type silicon substrate and an n-type silicon buried channel, with minority electrons from the substrate constituting the signal charge.

The driver voltages are provided by the Fairchild Driver Board SL61268 and consist of 6 clock pulses for charge readout together with several dc voltage levels which are required for the charge sensing circuitry and output amplifiers. In particular, the buried channel is depleted by the application of a +16V level to the drain of the output diode and the substrate is grounded at several points.

Figure 1.8 shows the clocking signals required to read out the CCD202, and their timing with respect to each other. One photogate pulse, $\phi_p$, controls the transfer of charge from photocells to transport cells, two complementary vertical clocking pulses $\phi_{v1}$ and $\phi_{v2}$ transfer the charge along the transport cells and two complementary horizontal clocking pulses $\phi_{H1}$ and $\phi_{H2}$ transfer the charge along the output register to the output amplifier. A sixth clocking pulse, $\phi_R$, is used in the CCD202 to reset the output diode after each charge packet has been sensed. With respect to the video output, $\phi_D$ occurs at the start of each frame, $\phi_V$ at the start of each horizontal row, and $\phi_H$ and $\phi_R$ have the same clock frequency as the video signal. The amplitude of the clocking pulses can be varied, with the upper and lower rail voltages being continuously variable by means of potentiometers from -10V to +10V. Both $\phi_{v1}$ and $\phi_{v2}$ and $\phi_{H1}$ and $\phi_{H2}$ remain complementary when the clocking voltage is varied and diode protection ensures that the polarity of the clocking voltages cannot be reversed.

The charge sensing circuitry consists of an output diode whose voltage changes linearly with the applied charge. The output of the diode is connected to the gate of a MOS transistor, the first stage of a two-stage amplifier. The output video signal from the amplifier is in the range 0 - 1V, with the saturation charge corresponding to an output of 1V, and the output voltage proportional to the number of minority carriers in the photocells.

### 1.3.3 Cell Structure of CCD202

The details of the cell structure are important in the understanding of the response of the CCD202 to electrons reported in Chapter 3

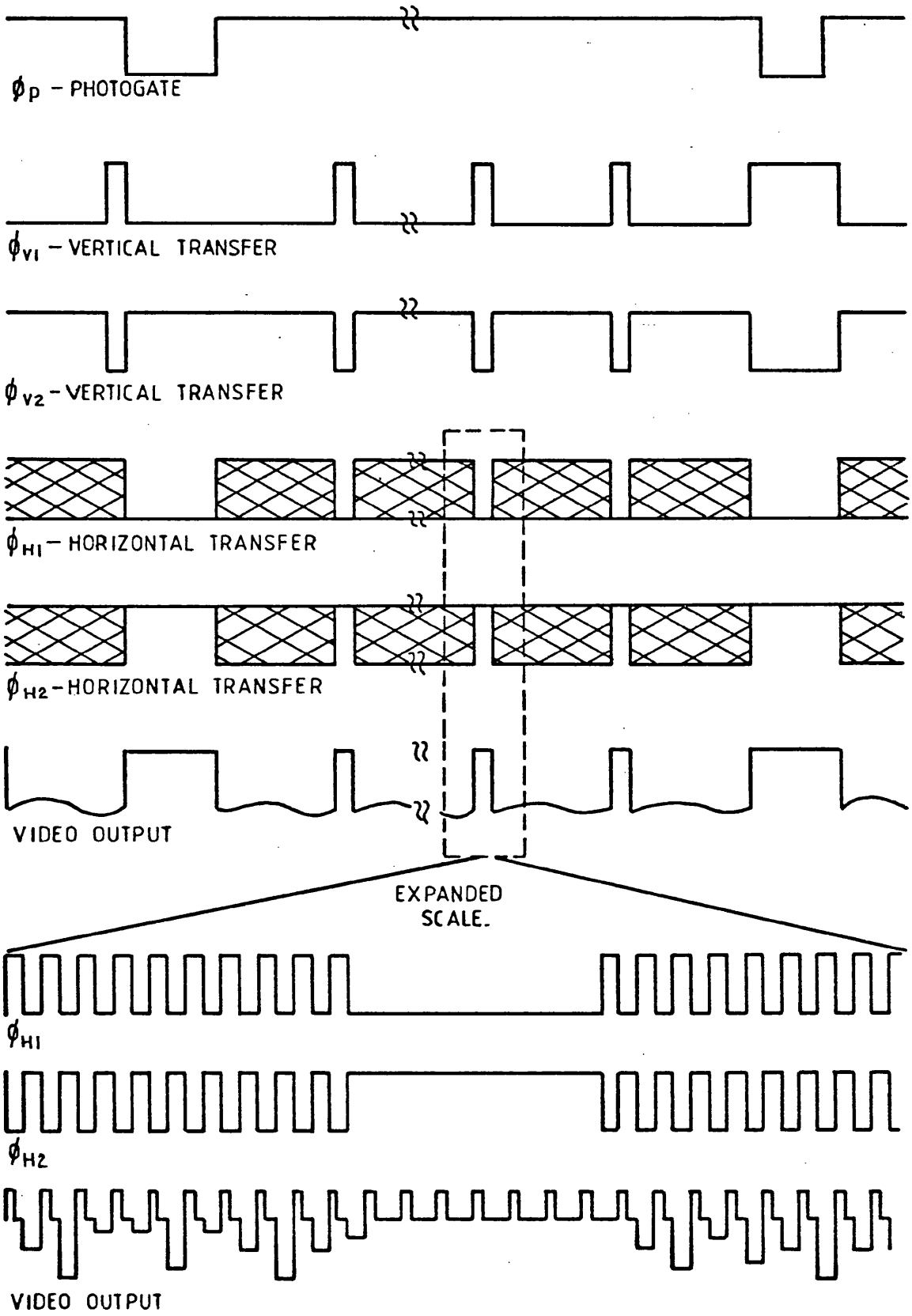


Figure 1.8: Clocking signals for Fairchild CCD 202

and the results on radiation damage in Chapter 4. The structure described here is given by Killiany et al[4].

The CCD202 is a buried channel device with an arsenic implanted n-type buried channel. Since a 2-phase clocking method is used, the potential wells are profiled by the implantation of boron in selected regions of the n-channel. Figure 1.9a shows a cross-section through a column of transport cells, while Figure 1.9b is a cross section through a row showing a photocell and transport cell. The n-channel is covered by a thin layer (0.12μm) of $SiO_2$. In this device the electrode structure is formed by depositing a layer of high resistivity polycrystalline silicon over the $SiO_2$ insulator, and selectively doping it to form conducting regions which are used as electrodes. The remaining regions of undoped polycrystalline silicon provide insulation between adjacent electrodes. Polycrystalline silicon is used as the electrode material because, unlike aluminium, it is transparent to light. A thick layer of vapour deposited $SiO_2$ covers the device above the polycrystalline silicon layer and a layer of aluminium above the transport cells shields them from light.

The boron implanted barrier between the photocell and transport cell ensures that no charge spills between them, even when the potential on both electrodes is held high. The p+ silicon implants at the edges of the photocells and transport cells provide potential barriers to define the potential wells. Figure 1.10 shows the potential profile under the photocells and transport cells during a) integration of charge and b) transfer of charge from the photocells to transport cells.

Values for the thicknesses of the various layers overlying the silicon substrate are necessary to allow calculation of the energy lost by an incident electron before it reaches the silicon substrate, and thus of the electron gain of the CCD. Unfortunately this information is not available from the manufacturers. However some figures are given by Killiany et al[4], and further data was calculated from the work of Currie[5]. Currie's data applies to the Fairchild CCD201, of which the CCD202 is an improved version. It is not known if the improvements in the device affect the thicknesses of the various layers, but throughout this description it is assumed that the two structures are identical. The known thicknesses are given in Figure 1.9.

The $SiO_2$ channel layer thickness of 0.12μm and the n-channel thickness of 0.3 μm are given in the paper by Killiany et al[2]. The figure for the thickness of the aluminium layer of 0.8μm, for the combined

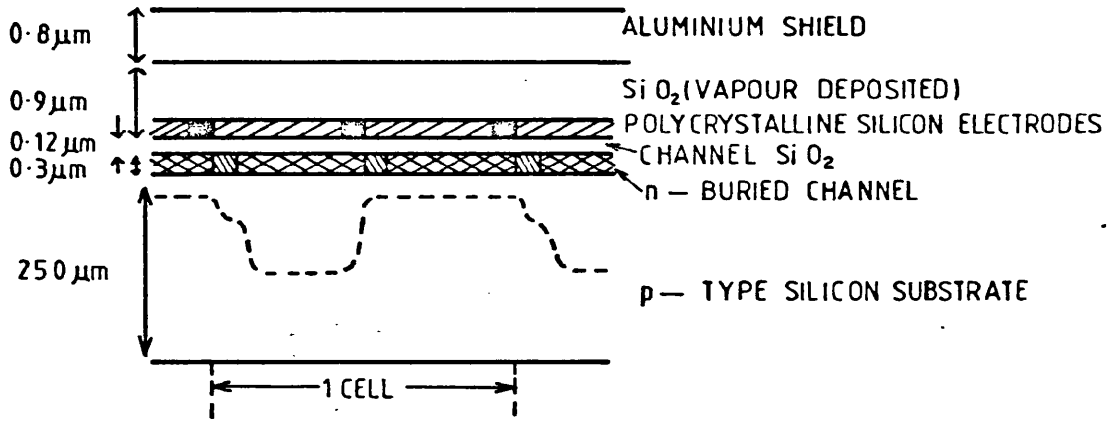


a) SECTION THROUGH COLUMN OF TRANSPORT CELL

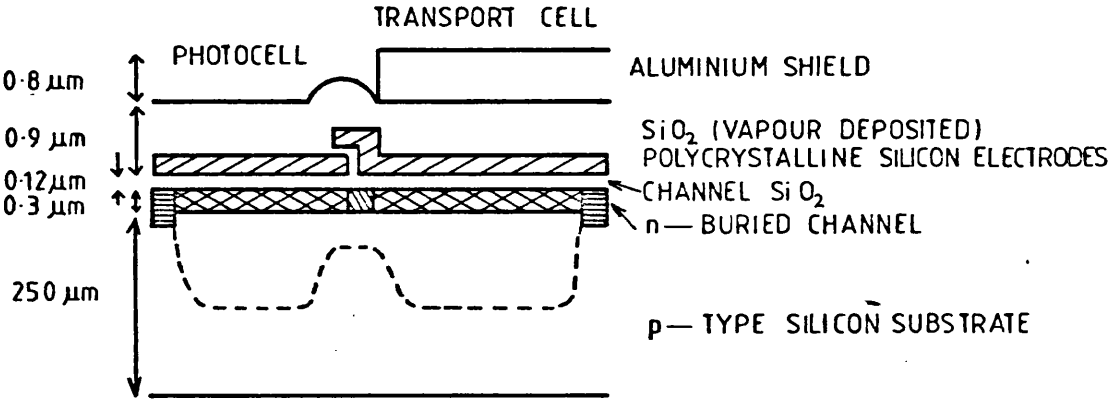


b) HORIZONTAL SECTION THROUGH PHOTOCELL AND TRANSPORT CELL

ARSENIC IMPLANTED n—LAYER
DOPED POLYCRYSTALLINE SILICON
UNDOPED POLYCRYSTALLINE SILICON
BORON IMPLANTED BARRIER
p+ SILICON

Figure 1.9: Cross-section of Fairchild 100 x 100 imaging array (similar to CCD 202)

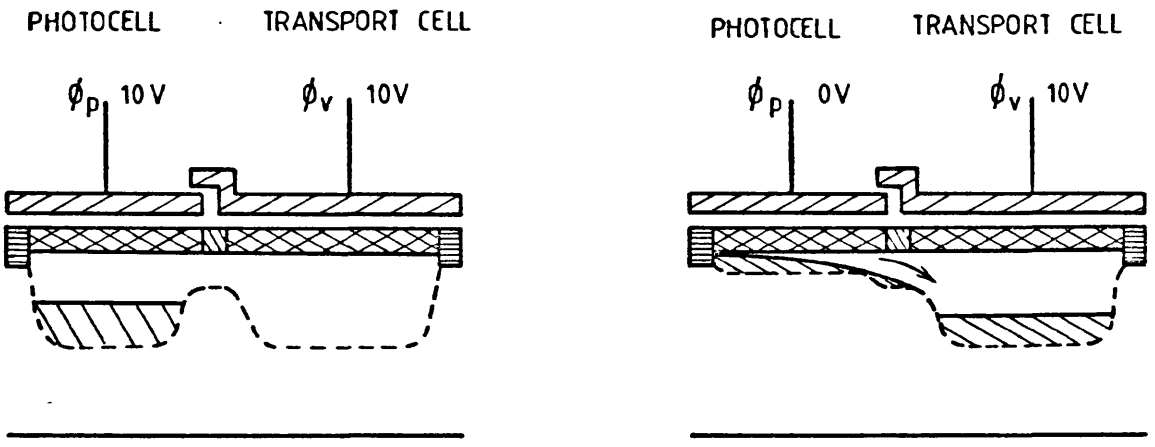


Figure 1.10: Charge transfer in CCD 202

thickness of the polycrystalline silicon and the upper $SiO_2$ layer of 0.9 μm and for the thickness of the insulator step between the photocells and transport cells of 0.2μmare approximate values which were calculated from data given by Currie[5]. Currie gives a figure of 14.6 keV for the maximum electron energy which can be absorbed by the overlying layers of the transport cells, that is the aluminium, vapour-deposited $SiO_2$, polycrystalline silicon and channel $SiO_2$, and gives 8.5 keV and 9.6 keV as the energy remaining after a 14.6 keV electron has penetrated the thick and thin regions of the photocells respectively. Application of the Thomson-Whiddington law for energy loss[6] and knowledge of the range of electrons in the various materials[7] gives the approximate thickness figures quoted above.

The areas of the photocells and transport cells are given in the Fairchild Design Development Board brochure and are respectively 18 μm x 30 μm for photocells and 22 μm x 60 μm for transport cells. The total area of the device is therefore 4 mm x 3 mm with slightly more than half of the area being transport cells.

### 1.3.4 Full Well Capacity of CCD202

In investigating the response of the CCD to high energy electrons it is important to know the relationship of the CCD output voltage to the number of minority electrons present in the potential well. Knowledge of this relationship allows calculation of the number of electron-hole pairs produced by each incident electron which are collected in the potential well and therefore of the electron gain and efficiency of the device. Once again this information is unavailable from the manufacturers. However Currie[5] quotes a figure of $4 \times 10^5$ as the number of minority electrons required to saturate a photocell of the CCD201. Although this figure may not apply to the CCD202 it gives an order of magnitude value for cell capacity.

## SECTION 1.4 DIFFERENCES BETWEEN ELECTRON AND PHOTON IMAGING WITH CCD 202

### 1.4.1 Introduction

While the Fairchild CCD202 is designed for photon imaging an electron image incident on the front face of the device will also be detected as signal charge in the CCD wells. An incident electron creates many electron-hole pairs in the silicon substrate, and the resulting charge packet is collected by the photocells in the same way as the charge produced by an incident photon. However the very

different energies of visible photons and of electrons used in electron microscopy ($\approx$ 2eV and $\approx$ 60keV respectively) and the different interactions which they can have means that there are several differences between the CCD operation in the two modes. The main differences and their consequences are listed below.

### 1.4.2 Energy Deposited in Silicon Substrate

A visible photon incident on the silicon substrate creates one electron-hole pair. In contrast, when an electron enters the silicon one electron-hole pair is created on average for every 3.66eV of energy deposited in the substrate. For a 60keV electron this is equivalent to a charge packet of $\approx 1.6 \times 10^4$ minority electrons created by each incident electron. Clearly the number of incident electrons required to cause saturation will be very much less than the number of incident photons.

### 1.4.3 Interaction with Overlying Layers

The polycrystalline silicon electrodes and the $SiO_2$ layers do not absorb visible photons of wavelength greater than $\approx$ 450nm, although reflection at the interfaces between materials causes some loss of intensity. As a result there is no photon energy deposited in the electrode layers. However electrons of energies in the range used in these experiments (20 - 100keV) interact with the overlying layers, causing ionization and a resultant loss of electron energy. There are two consequences of this interaction. Firstly, the energy deposited in the electrode structure causes damage in the $SiO_2$ layer resulting in a deterioration in the CCD performance. This is discussed in detail in Chapter 4 which also presents experimental results on the lifetime of the device under electron bombardment. Secondly, the loss of energy in the overlying layers of the device means that less than the full incident electron energy is deposited in the silicon substrate, and the output signal from the CCD is correspondingly smaller. In addition, the amount of energy lost is a function of the incident electron energy, with electrons with energy less than $\approx$ 15keV being completely absorbed, and, above 15keV, the deposited energy decreasing as electron energy increases. As a result the electron gain of the device (the number of minority carriers collected/incident electron) is not simply related to the electron energy. This is discussed in Chapter 3, Section 3.2.4

In the transport cells the electron interaction with the overlying layers is again different from that of photons. The aluminium layer

over the transport cells (≈ 1μm thick) is sufficient to shield the transport cells from visible photons, thus ensuring that no signal charge is introduced into the transport cells during charge transfer. However, in the case of electrons of the energies used in these experiments, the incident electrons can penetrate the aluminium shield and can create electron-hole pairs in the silicon substrate under the transport cells. Currie[5] reports a threshold electron energy of 14.6 keV below which electrons are stopped by the aluminium shield, and above which the incident electron is sufficiently energetic to create electron-hole pairs in the silicon. Consequently continuous irradiation and readout of the CCD202 results in image smearing with incident electrons creating signal which adds to the charge packets being transferred through the transport cells. It becomes desirable to remove the electron beam from the CCD during readout, and to interrupt clocking of the transport cells during electron irradiation. This problem, and the modifications to the drive circuitry required to implement the new readout cycle, are described in Chapter 2, Section 2.5.2.

This problem of electrons penetrating the transport cells is peculiar to the interline transfer readout organisation. In the frame transfer organisation described in Section 1.3.2 the separate storage cell area can be shielded from the electron beam, so that electron imaging can take place in the same way as photon imaging. For this reason the frame transfer structure is more desirable for electron imaging, but, as explained before, these devices were difficult to obtain.

### 1.4.4 Volume of Electron-hole Pair Production

A visible photon entering the silicon substrate interacts with an atom and produces an electron-hole pair within a distance of typically ≈ 4μm from the point at which it entered the silicon[8]. As a result, practically all minority carriers are produced well within the depletion region under the electrode on which the photon was incident, giving very little spread of signal to adjacent cells, and ensuring that little signal charge is lost due to recombination.

An electron incident on the silicon substrate, however, produces a roughly pear-shaped cloud of electron-hole pairs over a volume which is determined by the electron energy. For a 20keV electron the depth of penetration of the electron-hole pair cloud into the material is ≈ 2μm, whereas for 100keV electrons the corresponding distance is

$\approx 60\mu m$[7]. The diameter of the cloud is approximately equal to its depth with the shape becoming less spherical and more elongated for higher energy electrons. The implication of this large volume of electron-hole pair production for, eg,100keV electrons is twofold. Firstly, the width of the distribution ( $\sim$ 60$\mu$m) compared with the dimensions of the CCD photocells (18$\mu$m x 30$\mu$m) means that an incident electron will produce signal charge in several cells other than the one on which it was incident, resulting in a reduction of the effective number of picture elements in the device and a loss of resolution. This effect is less severe for lower energy electrons, eg 20keV, where the 2$\mu$m width of the electron-hole pair cloud ensures that most of the minority carriers are collected in the appropriate cell. Secondly, for high energy electrons a significant fraction of the electron-hole pairs produced in the substrate will be created outside the depletion region which typically extends to a depth of 10$\mu$m from the Si - $SiO_2$ interface. The minority carriers produced outside the depletion region do not experience a force towards the potential minimum and so will only be collected if they enter the depletion region by diffusion. Lateral diffusion is responsible for further smearing of signal charge to surrounding cells and, in addition, since the diffusion length of electrons in silicon is $\sim$ 50$\mu$m, significant recombination of minority electrons will occur. The electron gain of the CCD will thus be reduced by inefficiency in the collection of minority carriers created far from the potential minimum.

These effects are discussed in Chapter 3 where experimental results on CCD gain and electron spread are presented.

# CHAPTER 2

## INSTRUMENTATION

### SECTION 2.1 INTRODUCTION

This chapter deals with the apparatus used in the experiments reported in this thesis. Figure 2.1 shows the main features of the experimental system, which is attached to the JEOL JEM100C electron microscope. The CCD is housed under vacuum in the camera chamber of the microscope, and is driven by a Fairchild driver board, supplied by the manufacturers, which provides the necessary clock signals. This driver board also amplifies the output signal from the CCD and provides X and Y scan pulses to drive a display oscilloscope. Since the CCD is designed for photon, rather than electron, imaging, modifications to the driver board were necessary to produce a clocking cycle suitable for CCD operation in the electron microscope. The driver circuit and the modifications for electron imaging will be described in Section 2.5.

The simple driver board shown in Figure 2.1 was later incorporated in the Data Accumulation and Control Unit, designed by Dr A M MacLeod specifically for this work. It performs two main functions. Firstly, since the cell capacity of the CCD 202 is small (Section 3.2.3) it is necessary to superimpose the data from several frames of CCD output to obtain an image in which the electron shot noise is satisfactorily low. The unit does this by digitising the video signal, adding the data from successive frames, and storing the result in a solid state memory. Its second function is to provide flexible facilities for data transfer so that the accumulated image can be displayed on an oscilloscope screen, can be transferred to the departmental computer for permanent storage or can be stored in digital form on magnetic tape. This Unit will be described in Section 2.6.

The interline transfer readout mode employed in the Fairchild CCD 202, the device used in these experiments, would result in image smearing if the CCD was irradiated by the electron beam during the readout time. It is therefore desirable to remove the electron beam from the CCD during readout. This was achieved in the JEOL JEM100C by the application of a deflecting pulse, synchronised with the CCD readout cycle, to the alignment coils. The deflection system and its performance is described in Section 2.3. An electron counting system adjacent to the CCD was used throughout these experiments to monitor the electron dose on the device and will be dealt with in Section 2.4.

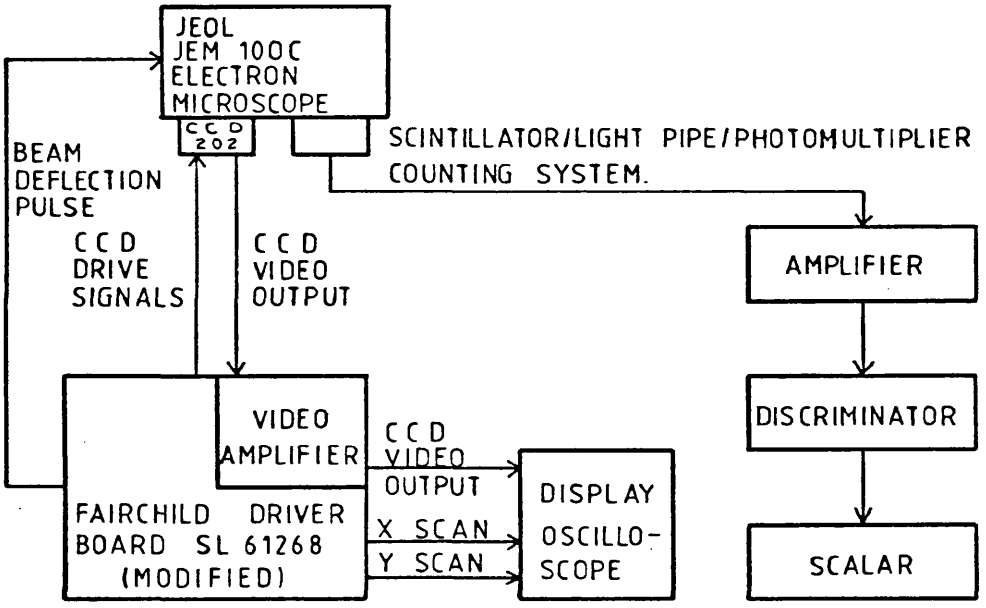


Figure 2.1: Block diagram showing main features of CCD-based imaging system

## SECTION 2.2 HOLDERS FOR THE CCD IN THE ELECTRON MICROSCOPE

### Section 2.2.1 Basic Holder

The holder for the CCD and electron counting equipment is shown in Figure 2.2. It is attached to the JEOL JEM100C electron microscope below the camera chamber in the position normally occupied by the single STEM detector. O-ring seals on all joints allow the system to be held under vacuum. The holder is made of brass, with walls of thickness ≈ 1.5 cm to absorb X-rays generated by high energy electrons hitting the walls. The CCD is mounted on a 24 pin dual in-line holder, which is sealed with Araldite into a Dural plate, which in turn is attached by three screws and an O-ring seal to the bottom of the brass holder. Electrical signals are transferred to and from the CCD via the pins of the dual in-line holder, and the terminating resistors for the CCD drive pulses are on the outside of the Dural plate as is the transistor circuit to drive the video signal down the line to the video amplifier.

So that the CCD can be illuminated with light in the electron microscope, two LEDs are mounted on the top surface of the Dural plate ≈ $2\frac{1}{2}$ cm above the device. The LED brightness is varied by an external control, which adjusts the diode current. This arrangement was used routinely to check the CCD performance without the necessity for electron irradiation. In particular it was used in the radiation damage experiments described in Chapter 4 to monitor the deterioration in CCD performance with electron dose.

In the radiation damage experiments (Chapter 4) small areas of the CCD ( ≈ 150 photocells) were irradiated with electrons and their subsequent performance compared with that of unirradiated areas. For these experiments the whole area of the CCD was shielded by a brass plate ( ≈ 1.5 mm thick) with an aperture of ≈ 0.5 mm diameter to allow irradiation of the chosen area. The plate was mounted on brass studding approximately 1 cm above the CCD. Several plates were made, with apertures in different positions, to allow different areas of the CCD to be irradiated.

The scintillator and light-pipe assembly occupying the other half of the holder forms part of the electron counting system whose operation is described in detail in Section 2.4. The scintillator is NE 102A plastic scintillator and is ≈ 3 mm thick. The top surface of the scintillator is silvered to reflect back-scattered light into the light-pipe, thus increasing collection efficiency. The light-pipe is made

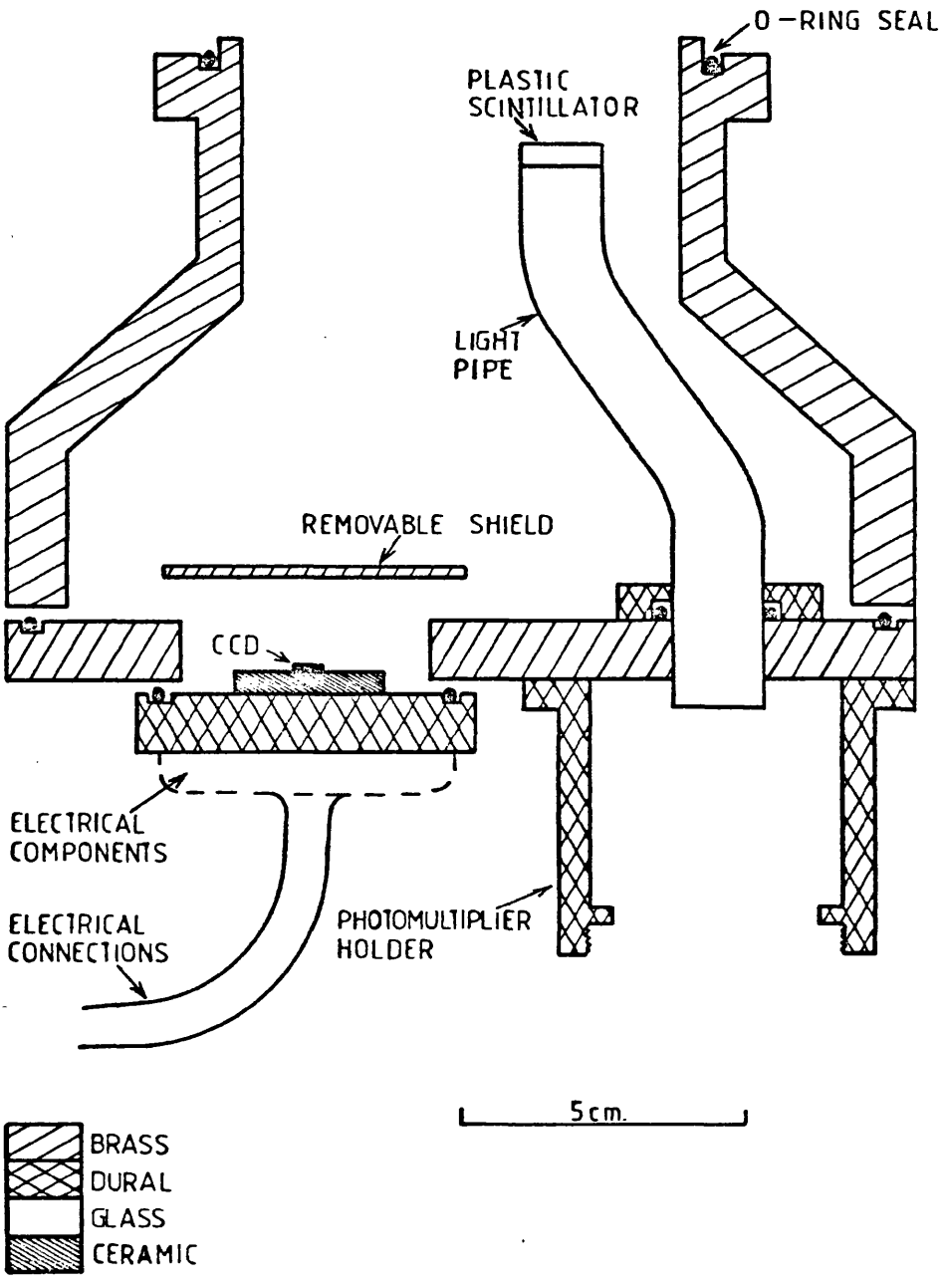


Figure 2.2: Holder for CCD in electron microscope

of glass which is covered with 250 μm thick aluminium foil to reduce signal loss due to transmitted light and partially reduce unwanted signals from stray X-rays generated by the electron beam striking the brass holder. The light-pipe passes through the base-plate of the brass holder, to which it is sealed by an O-ring. A screw fitting below the light-pipe holds the photomultiplier which is held in contact with the light-pipe by a spring and coupled to it by optical grease. To ensure that no stray electrons penetrate the aluminium foil and enter the light-pipe this half of the holder is shielded from the incident beam by a 1.5 mm thick semicircular aluminium plate on the top of the holder and ≈ 0.3 mm thick aluminium foil dividing the centre of the holder. A small hole in the aluminium plate (2 mm diameter) above the scintillator supports an AEI electron microscope aperture with, typically, a 500 μm diameter hole in the centre. This aperture is removable to allow the size to be varied to match the electron beam intensity, so that the maxiumum rate of the counting system is not exceeded (see Section 2.4).

Section 2.2.2. Cooling Holder

As will be described in Section 4.3.4, the increased dark current resulting from damage to the CCD necessitates cooling the device to temperatures below 0°C. The cooling system built to accomplish this is attached below the brass holder in the position occupied by the Dural plate in Figure 2.2. A cross-section of the cooling holder is shown in Figure 2.3. Heat is conducted from the CCD by a copper braid via an aluminium cylinder and a copper rod to copper braid which is cooled at one end by liquid nitrogen. The dimensions of these components are given in the table on Figure 2.3. They are encased by a 1 cm thick brass canister which is at room temperature and which prevents condensation on the cooled areas. The cooled sections are attached to the brass shield by a hard-solder joint between the copper rod and the stainless steel rod, with the temperature differential being maintained by the high thermal resistance of the thin-walled (0.25 mm) stainless steel tube. The CCD is held in a zero-force holder which is supported by 2 lengths of plastic studding. Electrical connections are made by means of thin insulated copper wires which pass through PTFE-lined copper-nickel tubes through the bottom brass plate and have a high thermal resistance. Since the inside of the CCD holder is under vacuum the electrical feed-throughs are sealed to the copper-nickel tubes with stiecast adhesive and the copper-nickel tubes are hard-soldered to the brass plate so forming a vacuum seal.

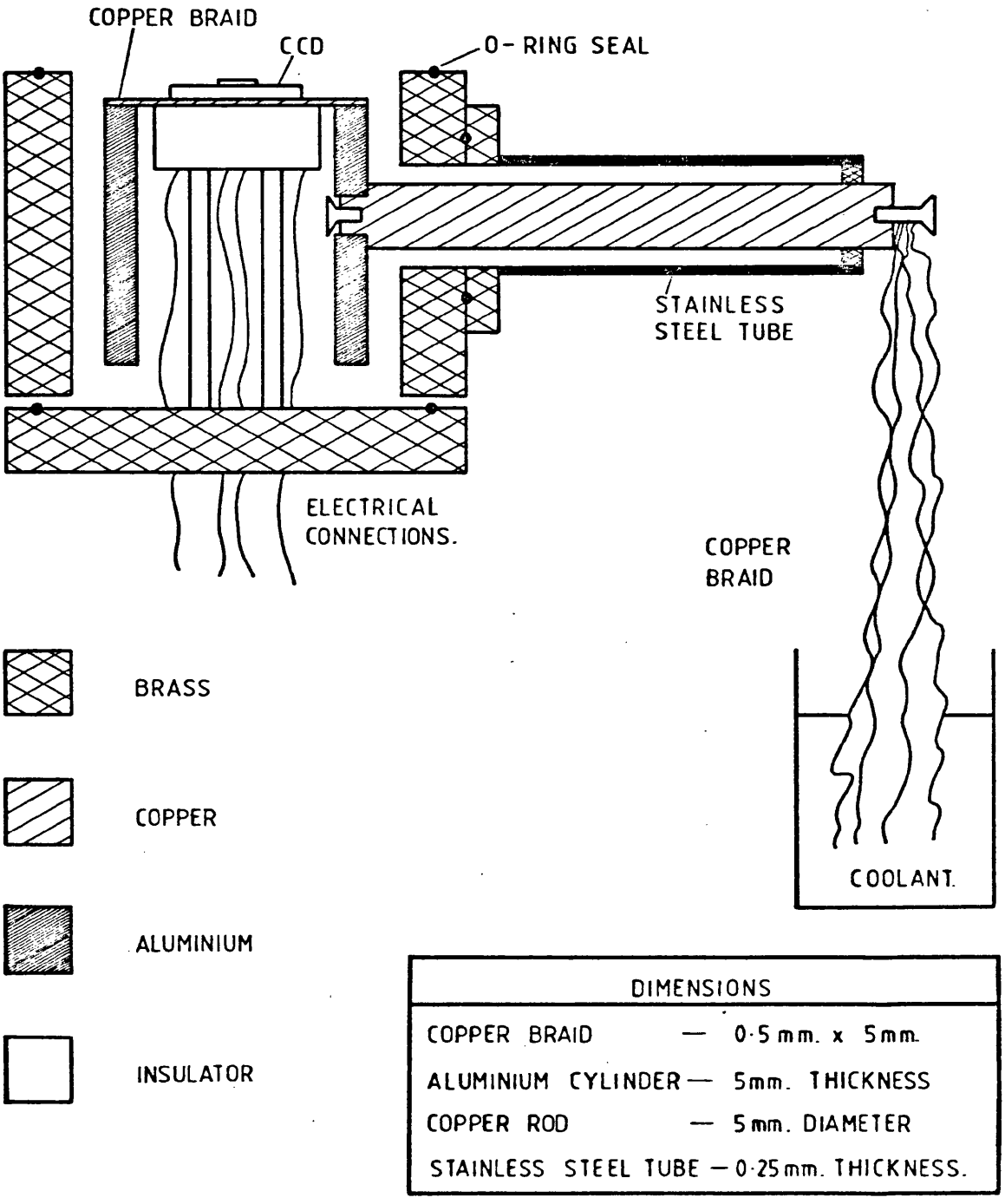


Figure 2.3: Cooling holder for CCD 202

An aluminium can below the brass holder contains the terminating resistors for the drive pulses and supports the 12-way plug by which connection is made to the driver circuit. There are 47 Ω terminations between all driver signals and ground. The circuit to drive the video signal down the coaxial cable to the amplifier is contained in this holder. Two LEDs mounted inside the vacuum system and above the CCD provide a light source for the CCD in the electron microscope. These were used for the same purpose and are controlled in the same way as the LEDs described in the previous section. A brass plate mounted on top of the aluminium cylinder inside the brass holder supports apertures to define the irradiated area of the CCD. These are used in performance tests to select a small area ( ≈ 150 photocells) for irradiation, and in imaging experiments to mask off the surrounding circuitry from the electron beam.

The CCD temperature is measured by means of a Cu/Cu-Ni thermocouple attached to a Comark electronic thermometer Type 1625. One junction of the thermocouple is taped to the top surface of the ceramic base of the brass holder which is assumed to be at room temperature. Copper feedthroughs in the brass plate connect the thermocouple to the thermometer via sockets in the base of the aluminium can. If the temperatures of the brass plate on the CCD holder and the socket in the thermometer which receives the thermocouple connections are the same, this arrangement is equivalent to a simple Cu/Cu-Ni thermocouple with leads connected directly to the thermometer, in which case the CCD temperature is given directly by the thermometer reading. Throughout these experiments it was assumed that this condition held.

Using this system the lowest CCD temperature achieved is -66°C. The temperature was varied by adjusting the length of the copper braid between the liquid nitrogen and the copper rod by raising or lowering the liquid nitrogen flask using a platform jack. Typically -20°C was chosen as the working temperature of the device and the CCD could be stabilised at this temperature in ≈ 20 minutes by cooling as rapidly as possible for 15 minutes and then lowering the liquid nitrogen flask to leave a 6 inch length of copper braid outside the vessel. This level of cooling, ie to ≈ -20°C, can conveniently be achieved using a Peltier element in contact with the back of the ceramic base of the CCD[1], and this method has been used in X-ray imaging work[2] and latterly in electron microscopy[3]. In addition, in the experiments on radiation damage to the CCD and its removal by annealing described in Chapter 4, it was found that the properties of annealed devices are very sensitive

to the CCD temperature, requiring the temperature to be controllable to within a few degrees. As a result, a Peltier element, in which the temperature is controlled by the current through the device, would be extremely useful for setting device temperature. However, when the cooling system was designed we had expected to require cooling to considerably lower temperatures, and had not foreseen the necessity for fine temperature control. In future work a Peltier element cooling system would be advisable.

## SECTION 2.3 BEAM DEFLECTION SYSTEM

### Section 2.3.1 Description of System

As explained in Section 1.3.3, it is desirable to remove the electron beam from the CCD while charge packets are transferred through the transport cells to avoid image smearing due to penetration of the transport cells by incident electrons. In the JEM100C this has been accomplished by the application of a deflection pulse either to the beam alignment coils or the gun alignment coils. These coils usually provide small corrections to the direction of the electron beam to ensure that it passes centrally through the microscope column. Figure 2.4 shows the position of the coils in the microscope column and the three modes in which the alignment coils can be used to deflect the electron beam from the CCD. These are described below:

1) Gun translate mode: The electron beam is moved approximately laterally across the electron microscope column with negligible tilt of the beam by applying a current to gun alignment coils 1. The beam is deflected through an angle $\theta$ by coils 1, and is bent by the field of the first condenser lens so that it is approximately parallel to the column axis. Therefore, at the first condenser lens the beam has been approximately laterally translated through a distance $\theta D$, where D is the distance from coils 1 to the first condenser lens. If the beam is translated through a large distance ($\simeq$ 100 um) in this mode it is cut off by the condenser aperture, so stopping irradiation of the specimen and CCD.

2) Gun tilt mode. This mode compensates for any beam tilt which is present when the beam leaves the electron gun. It tilts the beam about a point on the electron gun without causing any translation in this plane. In this mode the beam is again cut off by the condenser aperture, stopping irradiation of the specimen and CCD.

3) Objective alignment mode : The electron beam is moved approximately

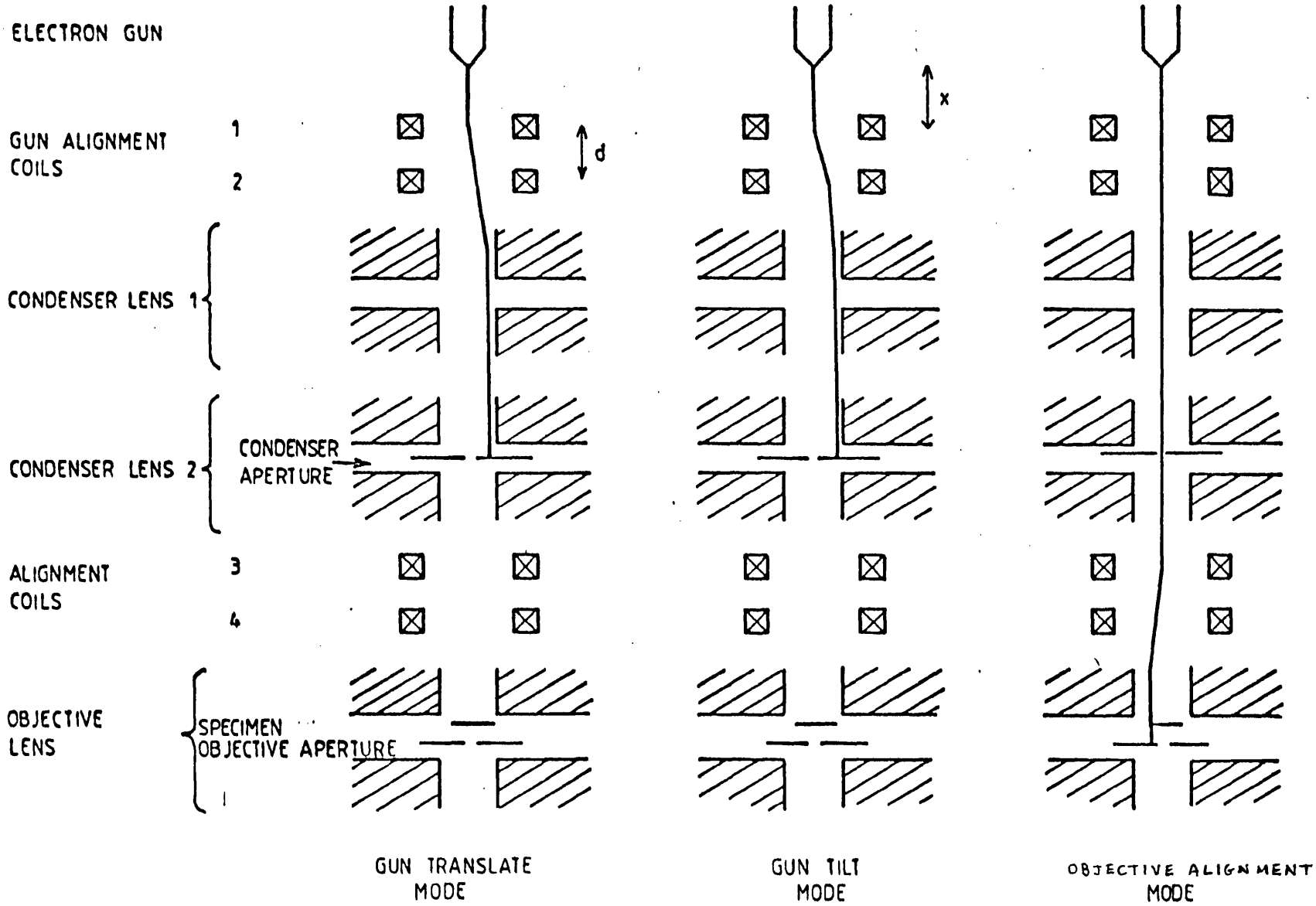


Figure 2.4: Beam deflection modes in JEOL JEM 100C electron microscope

laterally across the specimen by the application of a current to the alignment coils 3. After deflection by coils 3 the field of the objective lens bends the deflected beam so that it is approximately parallel to the column axis. In this mode translation through a large distance results in the electron beam being cut off by the objective lens aperture and so removed from the CCD although it may still be present on the specimen.

In normal use of the microscope the three modes are operated by separate manual controls which move the centre slider on a potentiometer control. This varies the voltage applied to the appropriate operational amplifier circuit feeding the beam alignment or gun alignment coils. In order to deflect the electron beam from the CCD during readout a deflection pulse is supplied by the modified driver circuit (Section 2.5 and 2.6) and added to the voltage from the manual potentiometer control by an operational amplifier circuit.

The adder circuit used is shown in Figure 2.5. The magnitude of the deflection signal is 0V during the time for which the CCD is irradiated and transfer is stopped (the irradiation time) and is 3V at all other times. As a result the electron beam is deflected from the CCD at all times other than the irradiation time. To allow the microscope to be aligned before the CCD is used a d.c. level is provided which cancels the 3V signal from the Data Accumulation and Control Unit during alignment, and can be switched off to remove the beam from the specimen. The magnitudes of both the deflection pulse and the d.c level can be varied by potentiometers to allow the amount of beam deflection to be controlled. Since the deflection pulse height is within the voltage range provided by the manual deflection control (-5 - +5V) no unusual deflection conditions occur.

Section 2.3.2 Performance of the Deflection System

For the deflection system to be useful the time for which the electron beam moves across the specimen must be small compared with the irradiation time. This condition is necessary to avoid variation of the electron dose across the specimen and to avoid loss of contrast in phase contrast microscopy due to a change in the angle of incidence of the electron beam. This was checked for the 3 deflection modes described above by exposing the scintillator - photomultiplier arrangement in the camera chamber to the electron beam during deflection and measuring the time for which the signal on the photomultiplier varied. Figure 2.6 shows a typical output from the photomultiplier displayed on an

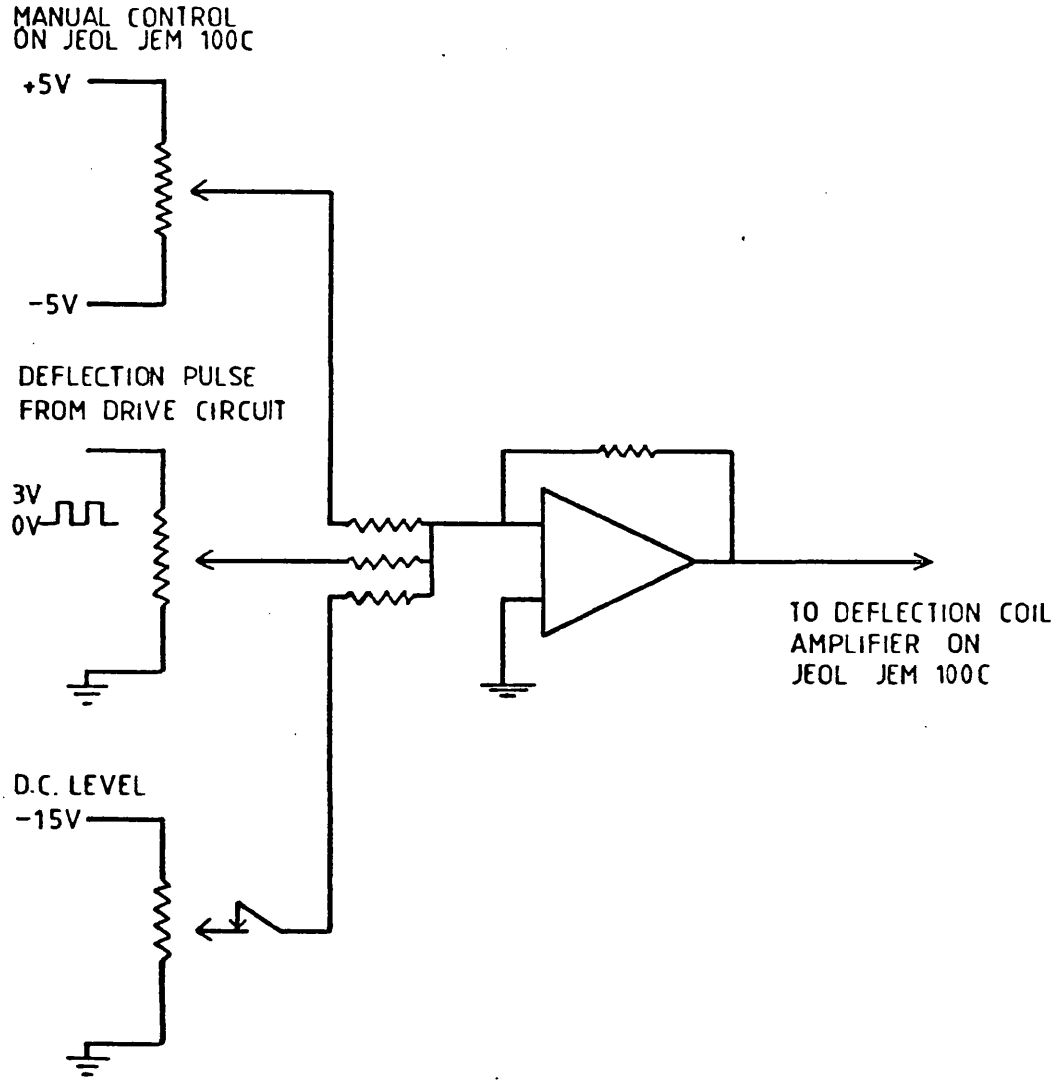


Figure 2.5: Adder circuit for beam deflection system

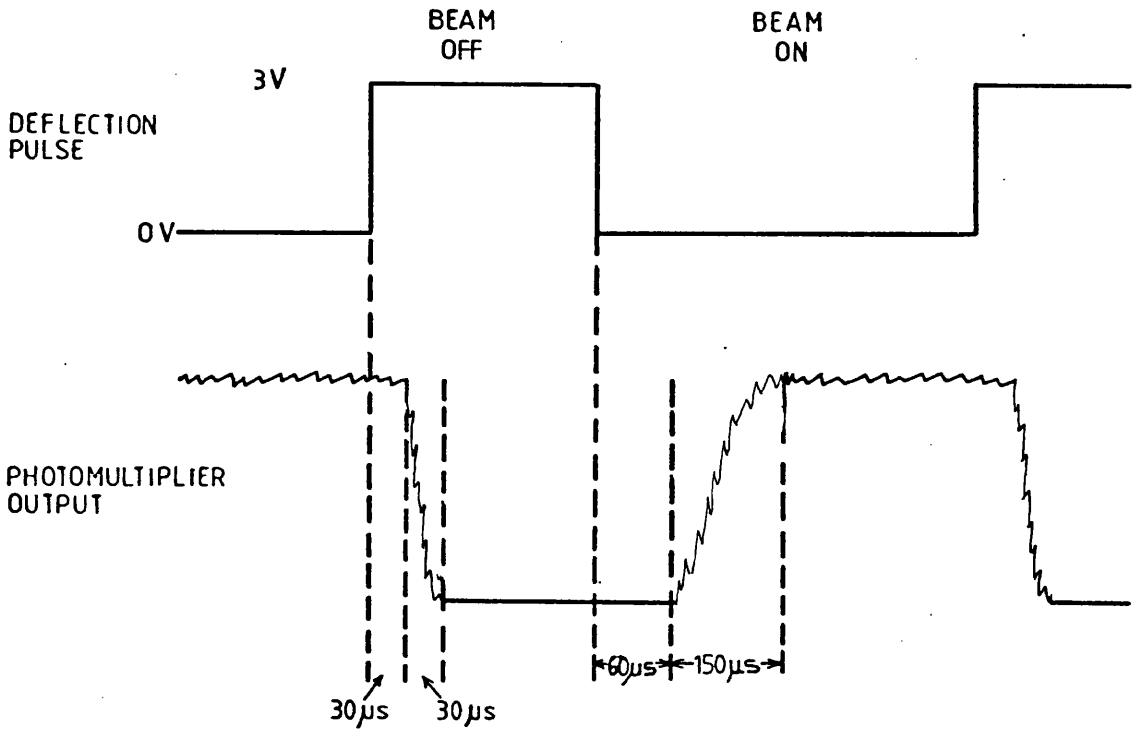


Figure 2.6: Output of photomultiplier for beam deflection in gun translate mode showing effect of exponential variation of current in alignment coils

oscilloscope (in this case for deflection by the gun translate mode).

For deflection by the gun translate coils there is a delay of ≈ 60 μs after the deflection pulse switches to 0V before any signal is seen on the photomultiplier. This is followed by a period of ≈ 150 μs during which the intensity of the signal from the photomultiplier changes before a steady output is reached. When the deflection pulse switches to 3V, there is a delay of ≈30 μs before any change in signal is seen and a further period of ≈30 μs during which the intensity of the signal varies. These delay times and variation times result from the exponential variation of the current in the alignment coils as the applied voltage is changed, and the corresponding variation in the magnetic field and beam position. The beam position at time t can therefore be given by an expression of the form $X = X_0 e^{-t/\tau}$ , where X is the distance of the centre of the beam from the centre of the viewing screen $X_0$ is the corresponding position at t = 0, and $\tau$ is the time constant of the alignment coils. From the figures above $\tau$ was calculated to be 84 μs.

The deflection times were also measured for deflecting in gun tilt mode and alignment translate mode, and the times for gun tilt mode were comparable with the above results. However, in alignment translate mode an extremely long delay of 2 ms for switch-on was encountered, and variation times were approximately twice as long as in the other two modes. The time constant $\tau$ in this case was ≈ 1.25 ms. Of the three deflection modes, alignment translate is least satisfactory due to long variation and delay times. There is little difference between the other two modes, gun translate and gun tilt, but gun tilt mode was most commonly used for deflection in these experiments. These experiments measure only the time for which the beam intensity varies, and a constant photomultiplier output can be obtained even if the angle of incidence of the beam varies. This is of interest in phase contrast microscopy where variation in the angle of incidence of the electron beam on the specimen causes a loss of contrast. However, from the time constant for deflection for gun translate mode, the residual movement in the beam after the intensity becomes constant is calculated to be ≈ 15% of the half-angle of the electron beam. Therefore the image blurring in phase contrast microscopy caused by beam movement after the beam intensity has become constant causes little degradation beyond that already present as a result of non-axial illumination. Intensity variation time is thus sufficient to determine the required irradiation time.

The time for which the electron beam intensity on the CCD varies

imposes a limit on the minimum usable irradiation time. With the variation encountered here of approximately 250 μs an irradiation time of not less than 2.5 ms is necessary so that the intensity variation is small compared with the total signal on the CCD. The irradiation time was 11.4 ms in the preliminary driver circuit and was in the range 4.8 ms to 158 ms for the Data Accumulation and Control Unit.

## SECTION 2.4 COUNTING SYSTEM

During electron irradiation the number of electrons incident on the CCD was monitored by an electron counting system. This information was necessary for the experiments on CCD performance and on device lifetime under electron bombardment described in Chapters 3 and 4 respectively. The counting system consists of 1) the scintillator and light-pipe assembly described in Section 2.1.2 which converts each electron to a pulse of photons; 2) a photomultiplier which detects the photon pulse from the scintillator and produces a voltage pulse of amplitude proportional to the incident electron energy; 3) an amplifier; and 4) a discriminator which detects voltage pulses greater than a chosen threshold value and produces a square wave at the output for each suitable input pulse; and 5) a fast scalar which counts the pulses from the discriminator.

The scintillator used in the experiments was Nuclear Enterprises NE102A with an absolute scintillation efficiency of 2.6% and a maximum emission wave length of 423 nm[4,5]. As described earlier, the top surface of the scintillator is coated with aluminium to increase the collection efficiency, and the light-pipe, which is made of optical glass, is surrounded with aluminium foil for the same reason.

The photomultiplier is an EMI model 9824B, which has a photocathode with quantum efficiency $\approx$ 18% for photons of wave length 423 nm and a typical electron gain in the dynode chain of $\approx 4 \times 10^6$ electrons/photoelectron (for an applied voltage of 1000V)[6]. Assuming a typical value of 10% for the efficiency with which the scintillator-light-pipe assembly transfers created light to the photomultiplier, gives a typical figure of $\sim 10^7$ electrons for the charge packet created at the photomultiplier output by an incident 60keV electron. The last electrode is connected to earth via a 100kΩ resistor across which a voltage pulse is produced. The voltage output from the photomultiplier depends on the pulse length and on the resistance of the load it drives but for a 50Ω cable the output signal is typically 25 mV. Figure 2.7 shows the pulse height distribution from the photomultiplier, recorded using a multi-

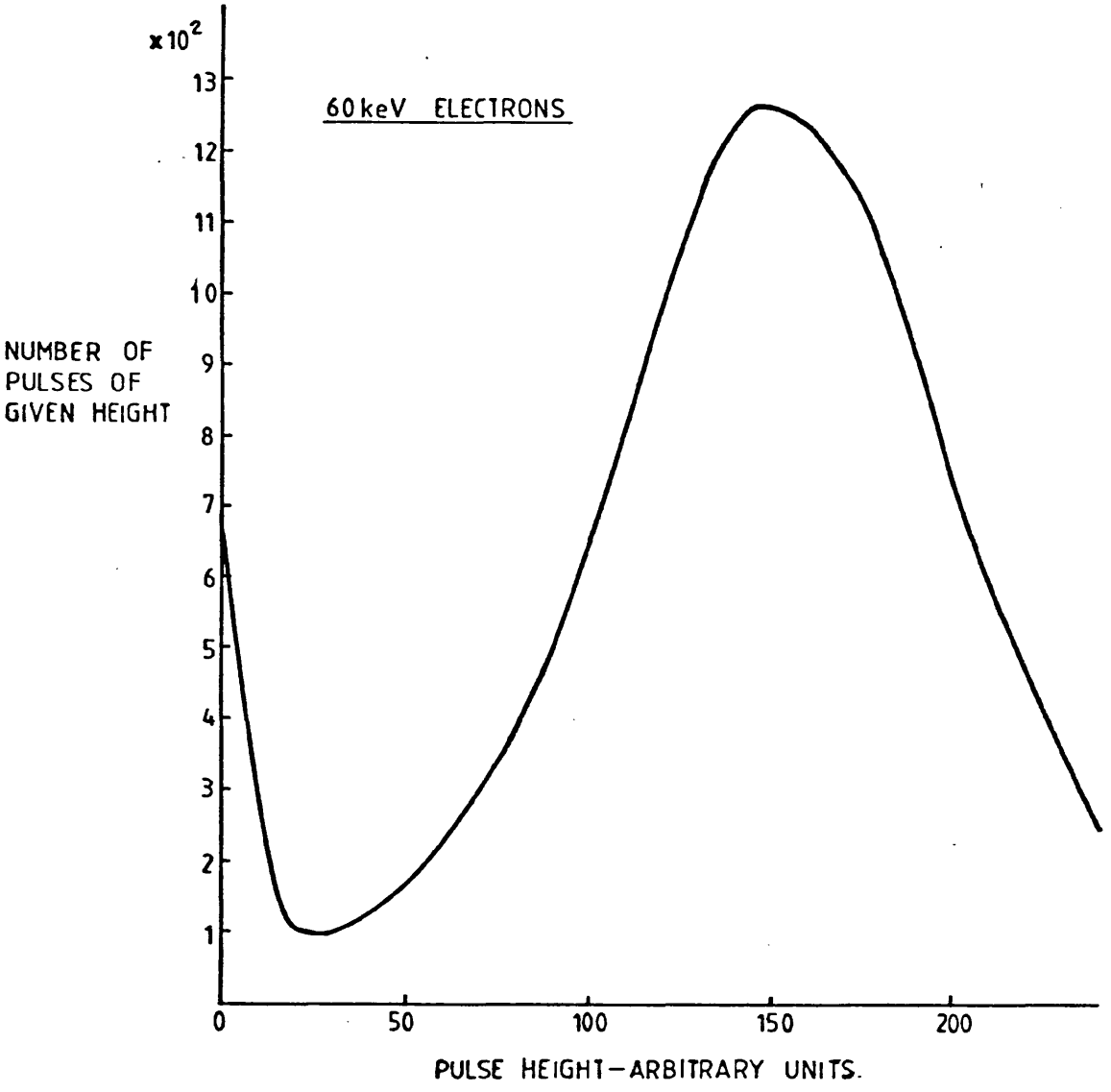


Figure 2.7: Electron pulse height distribution from photomultiplier for 60 keV electrons

channel analyser. Clearly, from this graph it can be seen that the pulses due to single electrons are well separated from those due to noise, allowing a discriminator threshold level to be set to ignore noise pulses.

The voltage pulses from the photomultiplier are transferred via an amplifier (EG & G Type AN101) to a discriminator unit (EG & G Type T100A). The discriminator unit produces a 1V square pulse for each input pulse greater than a chosen threshold voltage. This allows the spurious pulses due to dark signal in the photomultiplier to be ignored by the subsequent counting system. The amplifier has a gain of X16, and both the discriminator threshold voltage and the length of the output pulse can be varied. The discriminator output pulses are counted by a fast scalar (Borer & Co Fast Scalar Type 613) capable of a count rate of 100 MHz with a digital display to $10^{15}$ counts.

The maximum count rate of the whole system is determined by the length of the output pulse from the photomultiplier, which was $\approx 0.3$ μs at half height when driving the 50 Ω input impedance of the amplifier. An output pulse length of 0.16 μs was chosen for the discriminator and the threshold voltage suitably chosen to ensure that each photomultiplier output pulse was sampled once only. This gives a maximum count rate of 6 MHz for regular pulses, but since the arrival times of the incident electrons are random a maximum average count rate of 0.6 MHz was chosen to ensure that 99.5% of pulses would be counted. To maintain the electron count rate below 0.6 MHz, an aperture was placed above the scintillator (as described in Section 2.2.7) and the aperture size chosen to match the electron beam intensity. Since the efficiency of the system allows the detection of single incident electrons, the error in a measurement of number of counts is due mainly to the random nature of the electron arrival at the scintillator. Assuming a Poisson distribution, this is $\sqrt{N}$ where N is the number of electrons counted. There is a small background count due to dark current signals which are greater than the discriminator threshold but this signal is only 0.001% of the typical count rate, and so is insignificant compared with the statistical error. In addition, with an electron beam in the column but deflected off the CCD and photomultiplier there is a spurious count due to stray electrons of 0.05% of the typical count rate, again insignificant compared with the statistical error.

## SECTION 2.5 PRELIMINARY DRIVER CIRCUIT FOR CCD

### Section 2.5.1 Fairchild Driver Board

The Fairchild Driver Board SL 61268 provides the clock signals and d.c. bias voltages for the CCD 2027. It also amplifies the video signal from the CCD and provides X and Y scan signals to enable the image to be displayed on an oscilloscope. A schematic diagram of the Driver Circuit together with modifications to allow electron imaging is shown in Figure 2.8. A basic clock pulse is converted to the required CCD driver pulses by a clock generator consisting of a TTL logic circuit. The clock pulses required to drive the CCD are described in Section 1.1.4 and are shown in Figure 1.6. These square waves are amplified by discrete transistor circuits whose upper and lower rail voltages are set by variable resistors. The circuit allows the heights of $\phi_H$, $\phi_V$, $\phi_D$ and $\phi_R$ to be set independently to the required level, and the value of pulse height typically used in these experiments was 0-6V.

For operation in the electron microscope the CCD is mounted in one of the holders described in Section 2.2. The clock pulses and d.c. levels to the CCD are transferred from the Driver Board via 50Ω cable terminated with 47Ω resistors which are located outside the Dural base in the basic holder, and within the aluminium can in the cooling holder. An emitter follower circuit is used to drive the video signal from the CCD to the amplifier, and is held in the same place as the terminating resistors. This puts a d.c. level of 8V on the CCD signal, which is removed by the a.c. coupled amplifier on the Fairchild Driver Board.

### Section 2.5.2 Modifications to Driver Circuit for Electron Microscope Operation

Several modifications to the Fairchild Driver Board were necessary to allow the CCD to be used for electron imaging. The design of these modifications was done by Dr A M MacLeod, and the circuitry was built by the Electronics Laboratory in this Department.

As described in Section 1.3.3, the aluminium layer over the transport cells in the CCD 202, which shields them from incident photons, is not thick enough to stop electrons, and so it is desirable to deflect the electron beam from the CCD during readout and to stop all clocking signals during irradiation. The resulting irradiation and

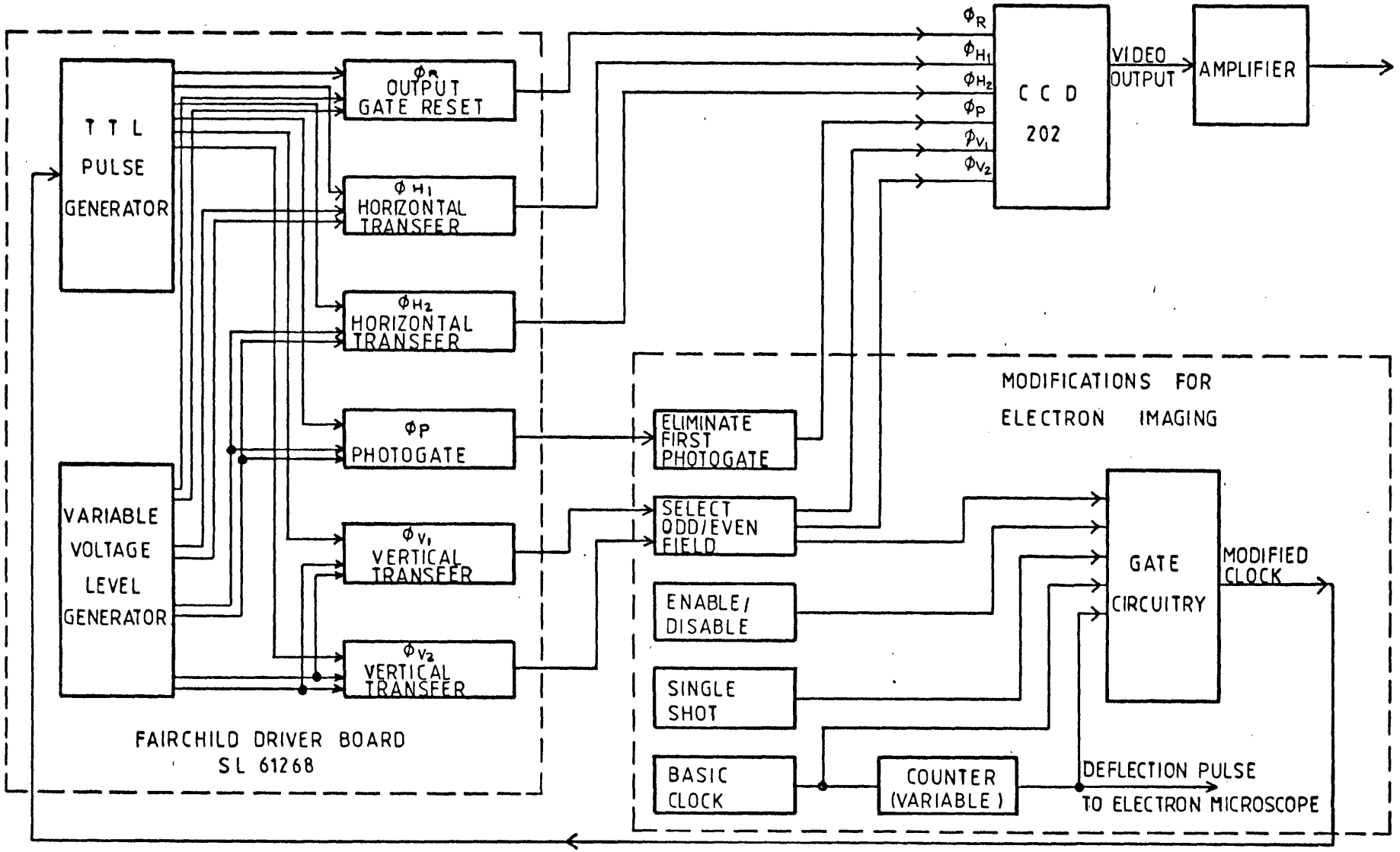


Figure 2.8: Schematic diagram of Driver Circuit for CCD 202 including modifications for electron imaging

readout cycle is shown in Figure 2.9 and is as follows:

1) The CCD is illuminated by the electron beam, and all clocking signals are stopped.

2) The electron beam is removed from the CCD, clocking restarted and the signals in the transport cells are read out. Since no photogate pulse occurs to transfer charge from photocells to transport cells only signal from electrons incident on the transport cells is contained in this field.

3) A photogate pulse transfers charge from the even numbered rows of photocells into the transport cells and this is read out in the second data field.

4) Charge from odd numbered rows of photocells is read out in the third data field.

5) A final readout cycle occurs, clocking out the even numbered rows of photocells again. This field should be empty, and the presence of electron signals in it indicates charge transfer inefficiency.

This ends the irradiation/readout cycle which is repeated for a preset number of times. The irradiation time can be varied in steps of 2.25 ms from 2.25 ms to 36 ms, the readout time being fixed at 25 ms. This 4-field readout cycle was adopted at the time for simplicity in the design of the electronic circuitry. With hindsight, since the information in the fourth frame is seldom used, a 3-field cycle with the corresponding saving in readout time would be preferable.

## SECTION 2.6 DATA ACCUMULATION AND CONTROL UNIT

### Section 2.6.1 Introduction

The driver circuit described in the previous section was used in some of the experiments to test the CCD performance as an electron imager (Chapter 3). However, this simple system was inadequate for later work for 2 main reasons. Firstly, the full-well capacity of the CCD, that is the number of incident electrons which saturate a photocell of the CCD, is $\approx$ 50 electrons/photocell, for electrons of energies in the range 60 - 100 keV (Section 3.2.3). As a result, to obtain a statistically significant image, the data from many cycles of irradiation and readout must be superimposed. Secondly, computer processing of data and images requires conversion of the CCD video

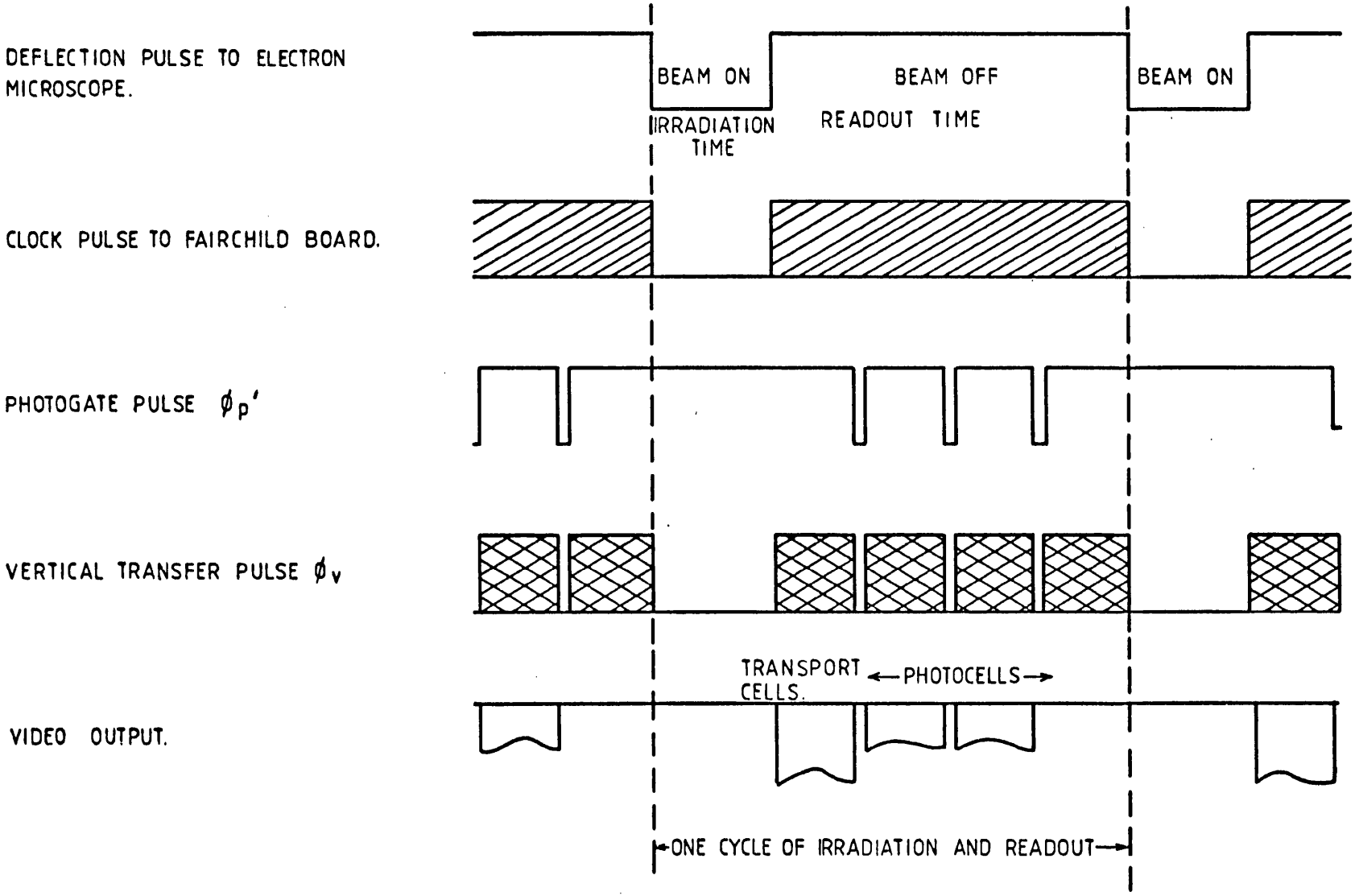


Figure 2.9: Irradiation and readout cycle for CCD 202 for imaging in the electron microscope

output into a form suitable for transfer to a computer, and makes it desirable that the output can be stored in a readily accessible form. Therefore, to provide these functions a unit was designed to drive the CCD 202 in the electron microscope, with flexible facilities for data storage and transfer.

This Data Accumulation and Control Unit was designed by Dr A M MacLeod and was built in the departmental Electronics Laboratory. It digitises the analogue video signal from the CCD, and stores the result in solid state memory, so allowing the use of logic circuitry to modify, organise and output the video data. A block diagram of the unit is shown in Figure 2.10, and its main functions are outlined below.

Firstly, to circumvent the problem of the small well capacity described above, the data from many cycles of irradiation and readout can be summed cell-by-cell, stored in the memory, and output as a single array to produce an accumulated image. In a similar manner, a subtraction can be performed on the data in the memory allowing, for example, dark current to be subtracted from an image. Secondly, the data stored in the memory can be output in several ways. To display an accumulated image the data is transferred via a digital to analogue converter (DAC) to a display monitor for viewing or photography. For processing and storage the data is transferred on-line to an IBM 370/145 computer. Finally, the data can be output via an interface to magnetic tape for permanent storage.

The transfer of data through the system to the outputs is controlled by the driver circuit, which provides the timing pulses to the various components. Its operation is described briefly in the following sub-section, and in the remainder of this section the transfer of data through the individual components and their interaction with the driver circuitry will be described.

Section 2.6.2 Driver Circuit

The driver circuit incorporates the Fairchild Driver Board SL61268 and from the CCD clocking signals derives the timing pulses for the other components of the system. The elements of the driver circuit are: 1. the basic clock; 2. the Fairchild driver board; 3. the mode select controls; 4. the logic circuitry to provide the irradiation and readout cycle described in Section 2.5.2; 5. the logic circuitry to control components; 6. the microprocessor section for controlling the

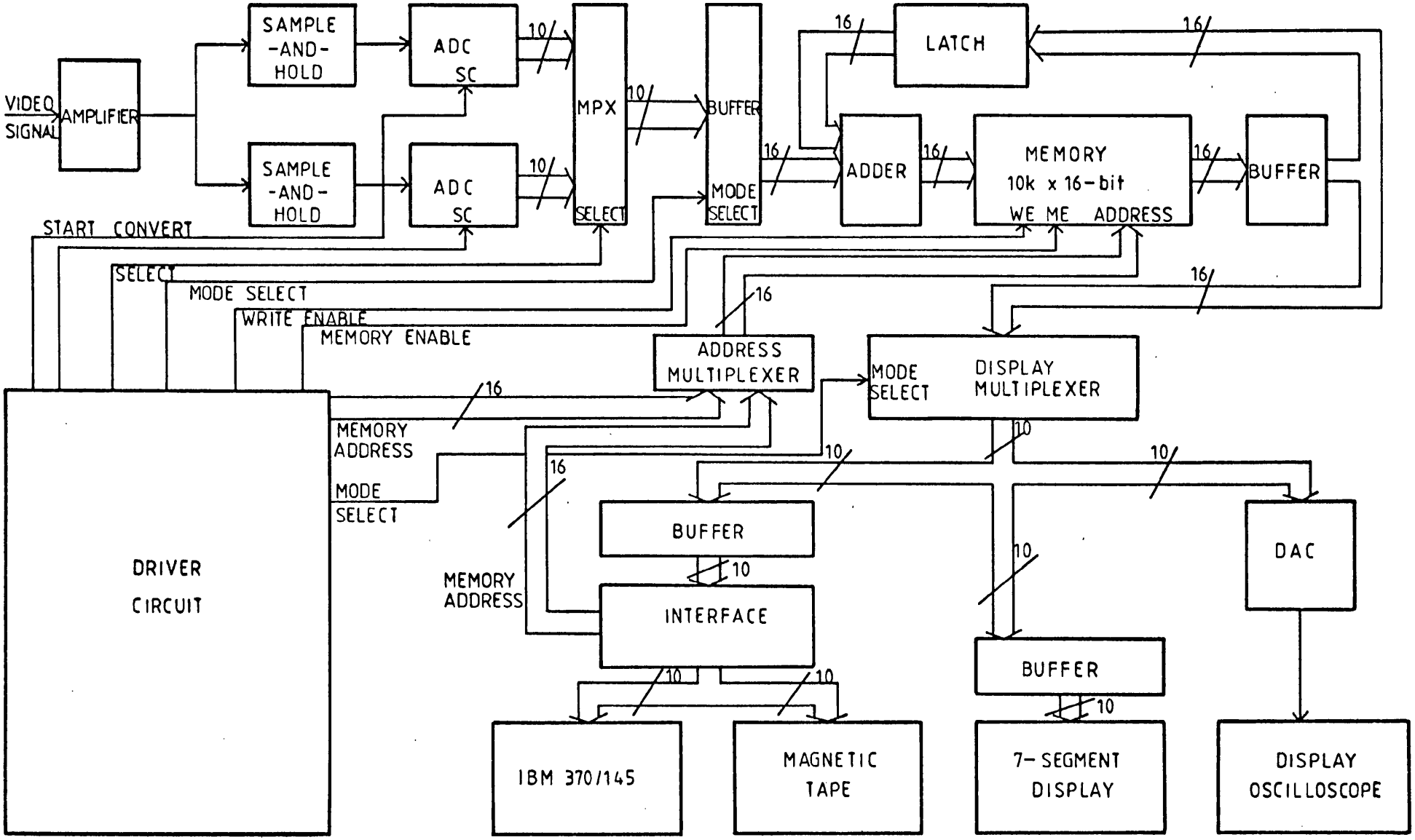


Figure 2.10: Block diagram of Data Accumulation and Control Unit

seven-segment displays and addressing the memory.

1. The basic clock is produced by a Schmidt trigger oscillator with a period of ≈ 2 μs. This pulse provides the basic clock for the Fairchild board and the logic circuitry.

2. The Fairchild driver board has been described in Section 2.5.1. One change has been made in this system and that is to remove the amplifier from the Fairchild board and to use instead a video amplifier with a higher and variable gain to amplify the video signal. This is described in Section 2.6.3. The clock pulses $\phi_H$, $\phi_V$, $\phi_P$ and $\phi_R$, are derived from the basic clock and are used to drive the CCD, in the logic circuitry to produce the irradiation and readout cycle, and in the logic circuitry to produce the component timing pulses.

3. The mode select controls produce voltage levels which are used in the logic circuitry to enable and disable components and select data, thereby controlling the path of the data through the system and the operations which are performed on it.

4. The logic circuitry to produce the irradiation and readout cycle uses the basic clock fed to a counter to produce the 'beam deflect' pulse to deflect the microscope beam (see Section 2.3 ). This pulse is gated with the basic clock to provide the clock for the Fairchild board which is stopped during the irradiation time. In addition this section contains controls and circuitry for selecting either a 2-frame mode of operation, where the data from a 100 x 100 array of photocells is transferred to the memory, or a 3-frame mode where an 82 x 82 array of photocells together with the corresponding 41 x 82 array of transport cells is transferred. The curtailed image which is transferred in 3-frame mode is a result of the memory capacity, which is limited to 10k words. This will be discussed in Section 2.6.5.

5. The logic pulses to control the component timing and thus the flow of data through the system are derived from the basic clock pulse, the clock pulses from the Fairchild board, and the mode select levels.

6. The microprocessor section converts the XY position of a given cell into a memory address and controls a seven-segment LED display which displays both the cell location and content. The location of the cell to be examined is selected by two variable resistors

connected to ADCs.

Section 2.6.3 Amplifier

The video data from the CCD is transferred during the readout cycle to a video amplifier with a variable gain. The amplifier consists of two stages, the first with a fixed and the second a variable gain. The amplifier gain can be varied from X1.35 to X23.5 with a maximum output signal of 12V. A d.c. level can be added to the video input from the CCD at the first amplifier stage to remove the 8V d.c. level added by the emitter-follower drive circuit. The d.c. level is variable to compensate for shifts in the video d.c. level due to temperature changes, and to match the input d.c. level to the amplifier gain so that the output level remains constant. The amplifier response was checked, and it was found to be linear for output voltages in the range 0 - 11 V.

Section 2.6.4 Sample-and-Hold and ADC

The video output from the amplifier is transferred to the input of the sample-and-hold. The sample-and-hold circuit samples the video signal and on a command pulse from the ADC holds its output at the instantaneous value of input voltage. The output of the sample-and-hold is connected to the input of the ADC which is commanded by a 'start convert' pulse to convert it to a 10-bit digital signal. At the end of the conversion time the ADC produces an 'end-of-conversion' pulse which commands the sample-and-hold circuit to hold the next video pulse.

To increase the rate at which video data is converted to digital form two ADCs were used to convert alternate pulses. The video data is presented to the inputs of two sample-and-holds and the start convert pulses to the ADCs determine the timing. The data rate of the entire system is determined by the maximum speed of the ADCs.

The ADC accepts input signals in the range 0v to 10v and converts to a 10-bit number in 4 μs. The system data rate was therefore chosen to be ≃ 0.5 MHz and the basic clock set to give this figure. This conversion time is by no means the shortest available in commercial ADCs, and the data rate could be increased by the use of a more expensive device. However, the cost of ADCs increases greatly with speed because of the more complex design of the faster devices, and the data rate is thus a compromise between system speed and cost.

An ADC with 10-bit accuracy was chosen to match the dynamic range

of the CCD which is given as 300:1 in the manufacturer's Data Sheet. This dynamic range is not used in electron bombardment mode due to the large signal produced by each incident electron, but will be of use in the future if an electron-photon conversion mode is used. Therefore, for the direct electron bombardment mode, a gain in system speed could be achieved by using a less accurate (eg 8-bit) but faster ADC.

Section 2.6.5 Memory and Adder

There are 5 modes in which data can be transferred into the memory. These are selected by switches on the front panel of the Data Accumulation and Control Unit, and control the 'mode select' levels mentioned previously. The input modes operate as follows:

1) Accumulate Mode: This is the mode which is used to record the images from the CCD. In this mode the data from the ADCs is added cell by cell to the data already stored in the memory. Thus the memory content is a digitised image accumulated from many cycles of CCD irradiation and readout. Referring to Figure 2.10, the data is transferred from the ADCs through a multiplexed latch which converts the 2 parallel data streams into 1. It then passes unchanged through a buffer circuit and multiplexer to a two-input adder, where it is added to the memory contents. The result is then stored in the appropriate location in the memory. The number of cycles of accumulation is selected by a control on the Data Accumulation and Control Unit, and can be varied from 1 to 128 in factors of 2.

2) Subtract Mode: In this mode the data from the ADCs is subtracted from the data in the memory. Its operation is identical to that of Accumulate Mode with the exception that the data is inverted by the exclusive or buffer, which is gated with a mode select pulse. The complement of the ADC output is thus added to the memory content. This mode is normally used, after data has been accumulated, to subtract the signal due to the d.c. level on the amplifier output.

3)Run Mode: This is similar to accumulate mode, but has no provision for selecting the number of cycles of data for accumulation. Cycling continues until stopped manually.

4) Test I Mode: This mode transfers a content of $(10^{16} - 1)$ to all memory locations, and is used in testing the output facilities of the unit. The multiplexer before the two input adder is gated with

a mode select level to present all 1's at its output in this mode.

5) Test 0 Mode: This is similar to Test I Mode, but is used normally to zero the memory content before data is accumulated. In this case the multiplexer is gated with a mode select level to present all 0's to its output.

In all of the input modes the driver board provides write enable, memory enable and address signals to the memory section. The address signals are derived from a counter which is operated by the basic clock and determines the memory location which can be accessed. The memory enable signal determines whether an operation can be carried out on the memory, and the write enable pulse determines whether the operation is data input to the location or data output.

The type of memory used in this system is static RAM capable of storing 20k 8-bit words, which is used in parallel to give a capacity of 10k 16-bit words. This word length was chosen to match the 10-bit output of the ADC, and allow a large number of accumulations at signals near ADC saturation. The 10k word capacity is sufficient for storing an image produced by the photocell contents, but is inadequate when transport cell contents are also stored. This results in the curtailed 82 x 82 array described earlier. It would be desirable at a later date to increase the memory capacity to eg 16k, so that the full array can be stored, and to modify the output to combine the data from photocells and transport cells to produce a single image.

Once stored in the memory, the data can be output in several ways. In all output modes, the memory data is transferred to a display multiplexer, which selects which 10-bits of the 16-bit number are to be output. For example, if the content of the memory locations is high, the 10 most significant bits will be selected for output. Conversely, if the memory content is low, and the most significant bits are zero, then the 10 least significant bits will be transferred. The bits to be selected are set by a control on the unit. There are three ways in which data can be output from the memory. Firstly, in all modes the data is transferred to the DAC where it is converted to analogue form to reproduce the video signal. Secondly, the data can be output via a tristate buffer output interface for transfer to storage systems. Finally, in several modes the data from a selected location is transferred to a seven segment display.

The 10-bit accuracy of the output signal was chosen as being

suitable for image processing work. Although the frame stores now used in image processing use 8-bit words, this accuracy is inadequate for processing requiring, for example, Fourier transformation[8] and for operations where the result is the difference of two similar quantities as in, for example, difference images. However 10-bit accuracy is sufficient for these applications.

Section 2.6.6 Digital to Analogue Converter.

The data from the display multiplexer is transferred to the DAC for conversion to a video signal. The 10-bit binary number at the DAC input is converted to a positive going sampled-and-held pulse with a maximum voltage of 10v. This pulse is used to modulate the brightness of a Tektronix 608 display monitor which has X and Y scan pulses provided by the Fairchild board. In 3-frame mode, in which data from both the photocells and transport cells are stored in the memory, the output from the DAC can be chosen to be either the transport cell or photocell contents. Thus the data from the photocells and transport cells are used to produce separate images on the oscilloscope. To display the image the memory is addressed by the memory counter, which is cycled continuously so that the video signal to the display oscilloscope is also continuously cycled. Thus, once an image is stored in the memory it can be displayed for viewing or photography without further irradiation of the specimen.

Section 2.6.7 Numerical Display

The microprocessor unit allows the data from a selected location in the CCD to be displayed continuously on a seven-segment display in accumulate subtract, run and display modes. The slider of a variable resistor is connected to the input of an ADC which produces a digital output of value determined by the position of the slider. The ADC output is transferred via a tristate buffer to a set of seven-segment displays where it is displayed as the coordinates of a row and column of the CCD. The output of the ADC is also transferred as data to a microprocessor which calculates and outputs the corresponding memory address. This address becomes the input of a comparator circuit whose other input is the output of the counter which provides the memory address and which is constantly cycled. When the two memory addresses become equal the memory content is transferred to the seven-segment display and remains there until the next cycle is completed.

Section 2.6.8 Output Interface and Storage Systems

The output interface transfers the data to the IBM 370/145 computer

or to magnetic tape for storage. The data is transferred as 10-bit numbers and stored temporarily in the interface memory before permanent storage. The interface directly addresses the memory of the data accumulation and control unit, and the rate at which it addresses can be varied.

A Conversational Remote Job Entry (CRJE) system on the IBM 370/145 allows data and programmes to be submitted to the computer using a VDU. By linking the interface with the VDU, the data from the CCD can be transferred to the IBM 370/145 as if it was typed in at the VDU. The creation of a file in the IBM 370/145 and the saving of data is done from the VDU but data transfer takes place automatically from the interface. Once in the computer the data from the CCD can be treated as any other dataset. The rate of data transfer is determined by the CRJE rate of $\simeq$ 10 words/sec, giving a transfer time of $\approx$ 15 minutes for a 4k dataset. This transfer time is undesirably long and is determined solely by the CRJE system, which is a multi-user system linked to the departmental computer. However, CRJE is subsidiary to the computer's main function and accepts data from many users at the same time, so that the data transfer rate is reduced accordingly. The transfer time could therefore be considerably reduced by using a separate computer.

The maximum memory capacity of the interface is 4k, so at present it is not possible to transfer complete images to the IBM 370/145. In 2-frame mode the first 80 rows of one frame of photocells can be transferred, as can the transport cells and a small area of photocells in 3-frame mode. As a result, the system is not yet suitable for image processing although the addition of memory cards to the output interface will remedy this. However, it was used to transfer video data to the IBM 370/145 in the tests on CCD performance described in Sections 3.3 - 3.5.

The system for storing data on magnetic tape uses the frequency shift keying method in which the data is stored on tape in digital form, with a binary 1 being represented by a high frequency signal and a zero by one of low frequency. These signals are produced by the interface and transferred to a cassette tape recorder at a rate of $\approx$ 10 words/sec where they are stored on audio cassettes. One C60 cassette is capable of storing 120k 10-bit words, the equivalent of 12 stored images. Data can be transferred from the cassette to the IBM computer via the same interface.

Section 2.6.9 Summary of System Parameters

The data accumulation unit accepts analogue video signals from the CCD at a rate of ≈ 0.5 MHz, digitises them to 10-bit numbers and stores them in random access memory with a capacity of 10k 16-bit words. The data from many cycles (1 to 128 in factors of 2) of irradiation and readout can be accumulated in the memory and output as a single image. The system stores either a complete 100 x 100 array of photocells, or a smaller 82 x 82 array of photocells and transport cells.

In addition to storing the CCD data the Data Accumulation and Storage system provides the clocking signals to drive the CCD 202 and the deflection pulse to deflect the electron beam off the CCD during readout.

The data in the memory can be output in several ways. In all cases the data is output as 10-bit numbers, with a display multiplexer selecting 10 of the 16-bits. The content of a chosen location of the CCD can be shown on a numerical display. In display, accumulation and subtract modes the accumulated data is converted to analogue form and displayed on a monitor oscilloscope. Finally, the data can be output for permanent storage via an interface to the IBM 370/145 computer or to magnetic tape at a rate of ≈ 10 words/sec.

Section 2.6.10 Tests performed on System

The Data Accumulation and Control Unit was tested to investigate the system performance and to eliminate any faults in the system. As an overall test which checked most functions of the system the CCD was illuminated with electrons and the digital output on the numerical display vs. the number of electrons incident on the CCD was measured. When this test was done the output of the CCD had already been shown to be linear with electron dose, up to the saturation voltage of the device (Section 3.2.2). As a result this tests the amplifier, sample and hold, ADC, memory adder, and the logic circuitry driving them since a fault in this section will be evident in a non-linearity of the output signal with respect to the input signal. Displaying an image incident on the CCD checked the memory address system, since a fault in this area would be seen as a fault in the organisation of the image. The address in external mode was similarly tested by transferring an image of an aperture edge to the IBM 370/145 and printing the stored data in digital form.

No problems were found with the logic circuitry but several were

identified at the input stage with the amplifier and sample-and-hold. Firstly, the preliminary test showed that it was necessary to bypass the amplifier on the Fairchild board, because this was a.c. coupled and resulted in a varying base line, giving a change in the digital output of a cell if the signal in adjacent cells was changed. This amplifier had previously been responsible for removing the 8v d.c. level of the CCD output and so a negative voltage was provided at the input of the amplifier which was added to the video signal to give a base line of 0V. This voltage was made variable to enable its height to be adjusted to suit the amplifier gain.

A problem arose in operating the amplifier at high gain. The frequency of the video signal is 0.5 MHz, requiring an amplifier bandwidth of 10 MHz to maintain the square wave shape of the pulse at the amplifier output. At low amplifier gain this condition holds. However the gain bandwidth product of the amplifier is such that at high gain the bandwidth is reduced to a level where the pulse edges are distorted. This means that the point at which the video signal is held by the sample-and-hold has to be chosen to be on the flat top of the pulse where it is least affected by the distortion at high gain. This was set accordingly.

A non-linearity in the output signal on the numerical display against the CCD output was seen for low values of CCD output. This was identified as a problem arising from the non-linearity of the amplifier for low signals and was solved by setting the bias voltage on the amplifier input to give a larger input signal which was in the range with constant gain.

A problem arose in the linearity tests when it was noted that the digital output for a given signal was a function of temperature of the CCD. This was investigated by measuring the digital output as a function of CCD output for various temperatures. The result is shown in Figure 2.11. It appears from this result that the 8V d.c. bias voltage on the CCD drifts with temperature by $\approx$ 1mV/$^{o}$C. This result means that it will be necessary to stabilise the CCD temperature to avoid drifts in the digital output.

With the temperature stabilised and the above adjustments made, the system was linear throughout the range of CCD signals.

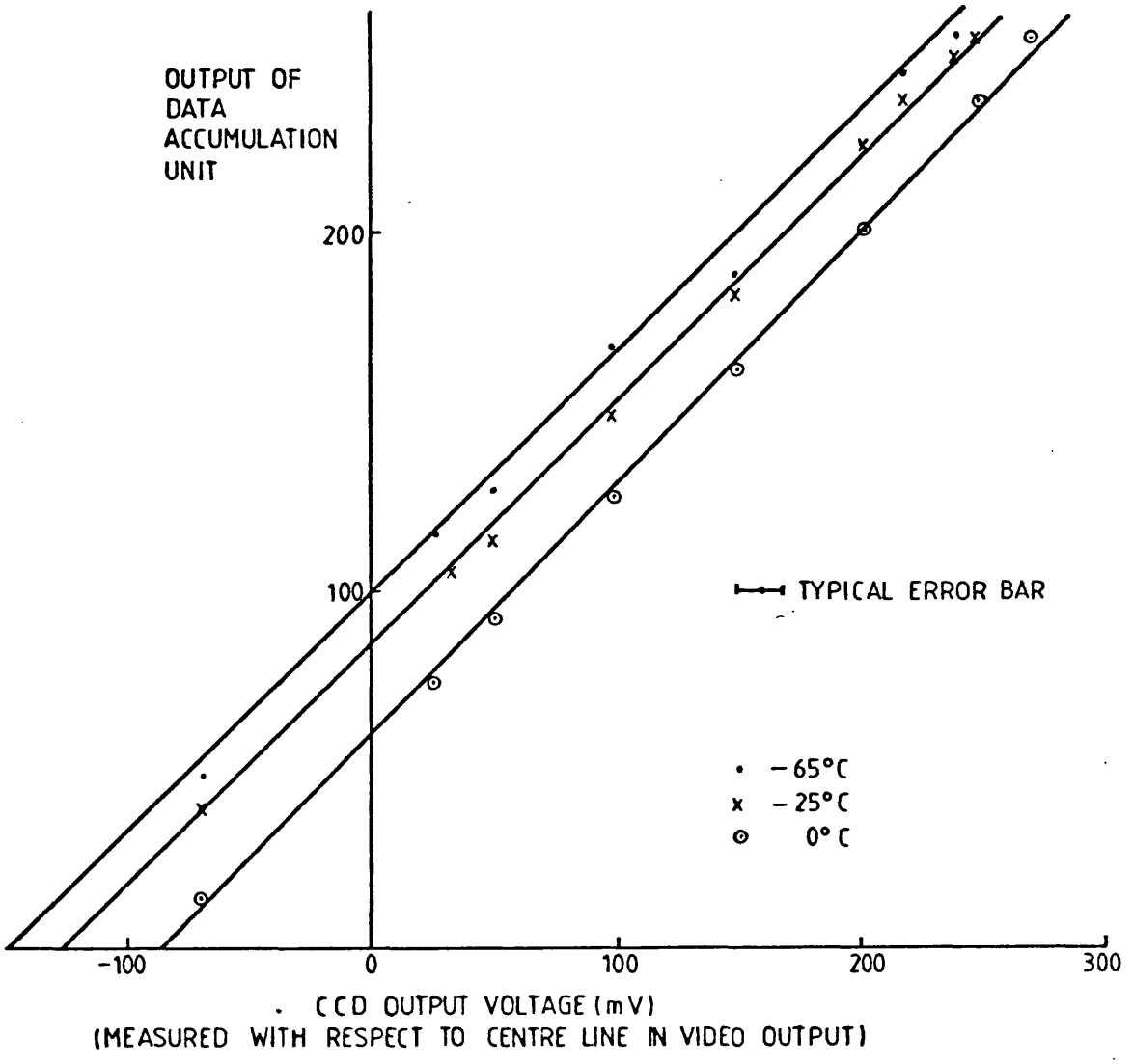


Figure 2.11 Variation in DC Voltage level of CCD 202 with CCD temperature

## SECTION 2.7 DISPLAY OSCILLOSCOPE

The output signal from the DAC is displayed on a Tektronix 608 monitor to allow the accumulated image to be viewed and photographed. The monitor consists of a cathode ray tube with a high brightness phosphor screen, with the electron beam intensity and thus the screen brightness modulated by the voltage output from the DAC. The Fairchild Driver Board SL 61268 provides the X and Y scan signals to produce the image raster. The images on the phosphor screen are recorded on photographic plate; either on Polaroid 107C film for immediate prints or on Ilford HP5 220 roll film. The high brightness phosphor allows the image to be seen when the room is moderately well lit.

The display monitor has a gain control and a variable d.c. level to match the input signal level to the usable voltage range of the Cathode ray tube and thereby to use the full brightness range of the monitor. The voltage range on the CRT input required to give the maximum number of grey levels distinguishable to the eye was measured using a step function generator designed by Dr E H Darlington and built in the departmental Electronics Laboratory. This unit generates a step function consisting of $2^n$ voltage steps of equal magnitude which is used to modulate the monitor brightness. The start of the pulse can be triggered by the horizontal scan pulse, giving a series of vertical stripes of increasing brightness. By suitably adjusting the gain and d.c. level controls and the number of voltage steps, the usable voltage range was determined and the maximum number of grey levels which could be seen on the monitor was found to be 14, with a voltage on the CRT input of 0 - 70v. A series of calibration photographs of the step function displayed on the screen allowed the optimum exposure time and aperture setting to be estimated.

# CHAPTER 3

## EXPERIMENTS ON CCD PERFORMANCE AS AN ELECTRON IMAGER

## SECTION 3.1 INTRODUCTION

### Section 3.1.1 Desirable Properties of CCDs for Electron Imaging

The Fairchild CCD 202 is designed for photon imaging and since differences exist between the interactions of electrons and photons with the MOS structure of the device, it is not clear, a priori, whether the CCD 202 will be equally suitable for electron imaging. These differences are outlined in Section 1.3. As a result, a series of experiments were performed to test the suitability of the CCD 202 for imaging in the electron microscope. There are several criteria which the CCD must fulfil if it is to compete with established imaging methods such as photographic film and more sophisticated equipment such as television-type image intensifiers.

1. Detective Quantum Efficiency (DQE). In an ideal recording system no noise is introduced into the output signal by the detector. This is not achieved in practice and the DQE of the system, defined as $(S/N)^2_{output}/(S/N)^2_{input}$ is used as a measure of noise increase. (S = signal amplitude; N = noise amplitude). A DQE of 1 corresponds to an ideal recording system with no additional noise. This condition holds in an electron imaging system if all electrons in the image are detected, so that the noise in the detected image is equal to the original shot noise in the electron beam. This requires firstly that the imaging device is sensitive enough to detect single electrons, that is, the gain of the device should be high enough that the output signal from 1 electron is greater than the output noise. If this condition holds, the imaging system can be used in electron counting mode, as in the system of Herrmann et al.[1,2,3,4,5] In this mode, the electron dose on the detector is low enough that the number of electrons incident on each cell is either 1 or 0, and a discrimator set on the output signal produces a 1 or 0 signal accordingly. This method yields a high DQE (0.6 in that of Herrmann et al) but has the disadvantage that a large number of cycles of readout and data accumulation must be performed to produce a statistically significant image.

In an ideal detection system, the detector would be able to discriminate between the signals due to n - 1 and n electrons, where n is the number of electrons which saturates the device. For this to be the case requires that $\sqrt{n}\Delta S < S$ where S is the signal produced by one

electron and $\Delta S$ is the noise in that signal. Therefore for discrimination of high numbers of electrons the width of the probability distribution for signals due to one electron must be small. Finally, so that no additional shot noise is introduced into the output, the CCD must make use of every incident electron, that is there must be no inactive areas on the device. This will be the case for the CCD 202 for electron bombardment, since both the photocells and the transport cells are sensitive to electrons.

Two experiments were performed to see whether these conditions held.

Firstly, the gain of the CCD in terms of output voltage/incident electron was measured and this is described in Section 3.2. In addition, experiments were done specifically to test single electron detection ability and to determine the single electron distribution and these are reported in Section 3.5.

2. Linear Response. An important and desirable feature of a detector for image processing is an output which is simply related to the number of electrons incident on each picture element. A linear relationship clearly fulfils this requirement, and Section 3.2.2 describes experiments to check that this holds for the CCD 202

3. Spatial Resolution. It is important that the spatial resolution in the image is degraded as little as possible by the resolution of the detector system. This can normally be achieved by magnifying the image to match the required resolution to the minimum resolvable distance in the recorder. For example, in the JEOLJEM 100C, a lattice resolution of 1.4 Å is possible in the image. For this to be resolved on a typical photographic emulsion (with a resolution of $\simeq$ 30 $\mu m$[6]) requires a minimum electron microscope magnification of $\approx$ 200,000. In this case considerable enlargement of the image on the photographic plate would be required to make the detail at 1.4 Å spacing visible to the naked eye.

The best resolution possible with the CCD 202 is determined by the cell size of 18 $\mu m$ x 30 $\mu m$ for photocells and 20 $\mu m$ x 60 $\mu m$ for transport cells. If this was the only limitation on CCD resolution the CCD could in theory detect image detail as small as 2 x 30 $\mu m/250 \times 10^3$ (where the latter figure is the maximum magnification of the JEM100C). This gives a figure of 2.4 Å for the smallest resolvable lattice repeat distance, suggesting that it should always be possible, with this microscope and CCD to come close to the resolution limit of the microscope by suitable adjustment of the magnification.

However, the CCD resolution may be degraded beyond the limit imposed by the cell size. As described in Section 1.3.4 an incident electron creates a cloud of electron-hole pairs in the silicon substrate, with the diameter of the cloud increasing with the incident electron energy[7].

Experiments were performed to measure the spread of an electron signal to adjacent cells and these are described in Section 3.4.

4. Uniformity of Response. Since the CCD consists of an array of detectors it is important that there is good cell-to-cell uniformity of response. If this condition is not met separate calibration of the response of each cell and manipulation of the video output would be required before the output data could be used to reconstruct the image. Since the CCD is a monolithic device, it is expected that variations in cell size and in depletion layer depth, both of which can affect electron gain, will be minimal. In addition, the readout method employed in CCDs has the advantage of sensing all charge with the same output amplifier, so avoiding the problems of matching the gain of individual amplifiers encountered in some types of photodiode arrays and other solid state imaging devices[8]. An experiment to study the uniformity of response of the CCD 202 for electrons is described in Section 3.3.

5. Speed of Data Collection. This is an important factor in determining the applications in electron microscopy for which CCDs are best suited. Ideally, the collection system should impose no limitations on the beam current density, so that collection time is minimised, and instabilities in the specimen and in the microscope are unimportant. However, the maximum readout rate of the CCD 202 is limited by the device structure to 2 MHz, and the Data Accumulation and Control Unit further reduces this figure to $\approx$ 0.5 MHz.

The time $\tau$ required to accumulate an image with an average of N electrons/photocell is:

$$\tau = nT_I + nT_R$$

n is the number of cycles of irradiation and readout required and is = 2N/Nf.w where Nf.w is the full well capacity of the CCD, that is, the number of incident electrons which fill a cell of the device. (It is assumed that the cells are half-filled at each accumulation)

$T_I$ is the time for one irradiation and has the minimum value $T_I = \frac{1}{R_{BEAM}}$ where $R_{BEAM}$ is the electron beam intensity measured in electrons/photocell/second.

$T_R$ is the time for 1 readout cycle.

Therefore $\tau = \frac{2N}{N_{f.w}} \frac{N_{f.w}}{R_{BEAM}} + \frac{2N}{N_{f.w}} T_R$

$= 2N \left(\frac{1}{R_{BEAM}} + \frac{T_R}{N_{f.w}}\right)$

With $T_R$ fixed, and N chosen, $\tau$ is determined by the electron beam intensity and the full well capacity of the CCD. Experiments to measure the full well capacity together with the implications of the data collection rate on possible uses of CCDs in microscopy are described in Section 3.2.3.

6. Radiation Damage to CCD. An ideal detector would suffer no degradation in performance due to the incidence of ionizing radiation but the CCD, being an MOS device, does undergo such a deterioration. Since this aspect of CCD performance is crucial to its use as an electron imager a large amount of time was spent in investigating the effects of radiation damage and in combating these effects. The results of this work merit a separate chapter and so are described in detail in Chapter 4.

## SECTION 3.2 MEASUREMENT OF GAIN AND CELL CAPACITY

### Section 3.2.1 Experimental Method

In these experiments the relationship of output voltage to the number of electrons incident on the device was studied and from the results the number of incident electrons required to fill a cell was found. This was done for electrons of energy 20, 60 and 100 keV, these being representative of energies of interest in electron microscopy. The experiments were performed on the Fairchild CCD 202 described in Chapter 1 using the apparatus described in Chapter 2. The CCD was mounted in the cooling holder in the camera chamber of the JEOL JEM 100C electron microscope and was typically cooled to -20°C. The number of electrons incident on the device was measured using the scintillator-photomultiplier counting system and the output voltage was measured by displaying the video output on an oscilloscope. The number of incident electrons was varied by adjusting the electron gun bias voltage to vary the beam intensity. A small aperture ( $\approx$ 500 μm diameter) above the CCD allowed an area of $\approx$ 150 photocells and $\approx$ 75 transport cells to be irradiated for each energy, while shielding all other areas from the incident radiation. Since the radiation damage described in Chapter 4 affects the gain of the device, all measurements were made on areas

which had not previously been irradiated.

In the experiments described in this Section the preliminary driver board with modifications was used to drive the CCD. The saturation output voltage of the CCD was therefore 2.5V.

Section 3.2.2 Results for Output Voltage versus Number of Incident Electrons

Figure 3.1 shows the results of the experiments to determine the variation in output voltage with the number of incident electrons. The number of incident electrons/cell/irradiation was limited to $\approx$ 60 in these experiments by the speed of the counting system and the maximum irradiation time available in the system (35 ms). With hindsight, the size of the aperture over the scintillator should have been reduced to allow the beam intensity to be increased to cover the full range of output voltage of the CCD. However, this was not done at the time, and only the data for 100 keV electrons is complete. The experimental errors arose from the scale reading error on the oscilloscope together with the shot noise in the electron beam encountered with the low electron doses measured here.

Clearly, within experimental error the output voltage of the CCD increases linearly with the number of incident electrons over the voltage range studied. There is, as expected, an increase in the output voltage/incident electron with the electron energy and this quantity is shown in Table 3.1 for the 3 electron energies used in the experiment. The table also shows the output voltage per unit of energy for the 3 electron energies (in mV/keV). This is a measure of the efficiency with which the CCD collects the energy from the incident electrons, and it can be seen that the value for 20 keV electrons is considerably lower than for 60 and 100 keV. This is consistent with the large fraction of the energy of 20 keV electrons which is deposited in the overlying layers of the CCD and which therefore does not create electron-hole pairs in the silicon.

The linearity of the CCD output voltage with the number of incident electrons augers well for its use in image processing. Digitising the CCD output thus gives a figure which is directly proportional to the number of electrons incident on the corresponding photocell, which is not true (except in a limited range) of the output of the photographic plate-densitometer system[9].

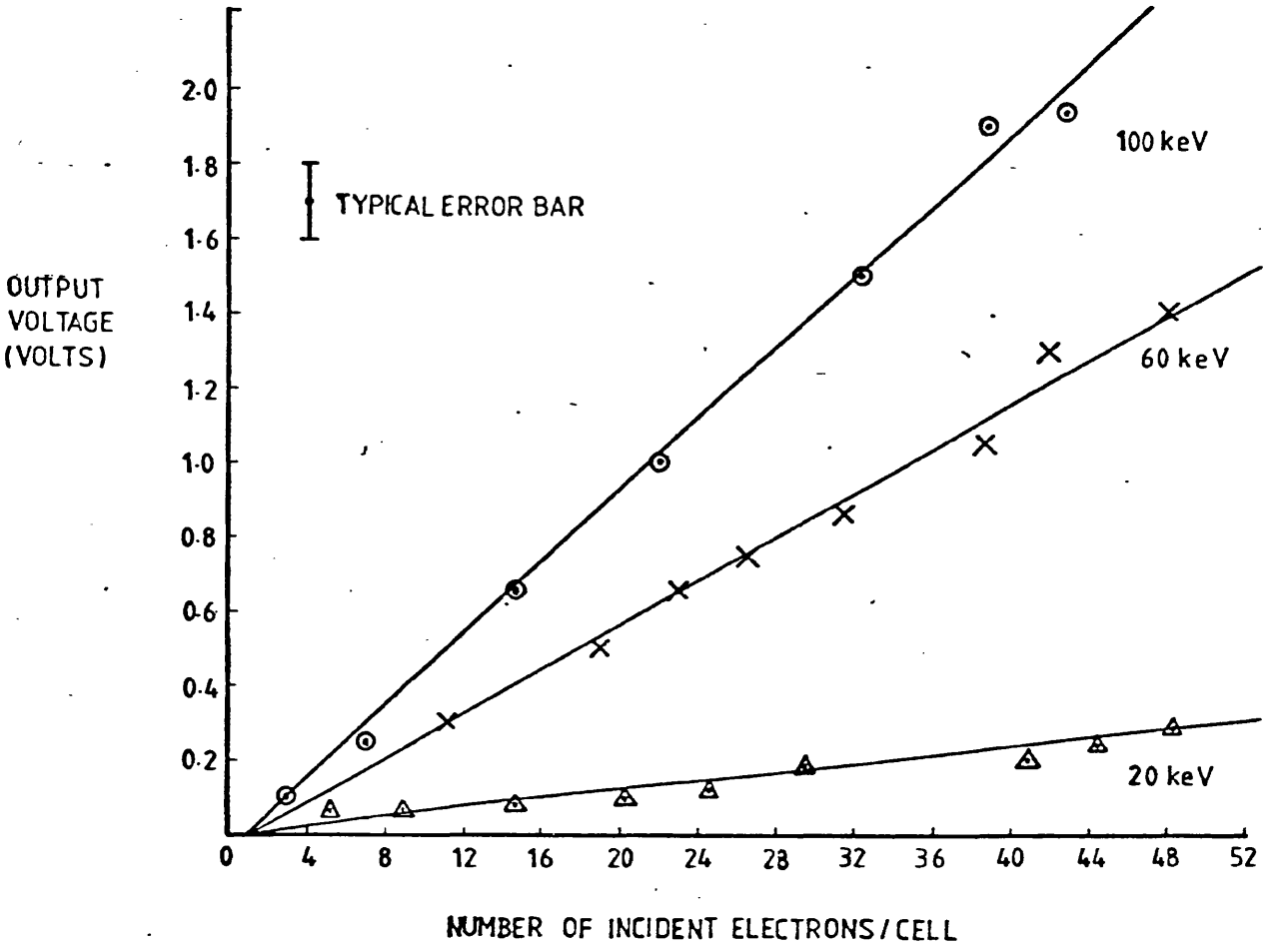


Figure 3.1: Output voltage against incident electron intensity for electrons of energy 20, 60 and 100 keV

| Electron Energy (keV) | 20 | 60 | 100 |
|---|---|---|---|
| Output voltage/incident electron (mV) | 5.6 | 38.4 | 55.5 |
| mV/keV | 0.28 | 0.64 | 0.55 |
| Cell capacity (electrons/photocell) | 440 | 65 | 45 |

Table 3.1: Response of CCD 202 for various electron energies

Section 3.2.3 Cell Capacity

The number of incident electrons required to fill a cell of the CCD can be calculated from Figure 3.1. The results are given in Table 3.1 for reference and are respectively 45, 65 and 440 electrons/cell for 100, 60 and 20 keV electrons. This low cell capacity implies that many cycles of irradiation, readout and accumulation will be required before the number of incident electrons/cell of the CCD is statistically significant. This was the motivation for designing the Data Accumulation and Control Unit described in Section 2.6 to allow the data from many cycles to be digitised, added and stored. Table 3.2 shows the number of accumulations required at each electron energy to collect an acceptable image with an average of $10^3$ electrons/photocell and the time taken to do this using the Data Accumulation and Control Unit (assuming that the shortest possible accumulation time of 5 ms is used). It is assumed in this calculation that $10^3$ electrons/photocell are sufficient to produce an image suitable for image processing and in which statistical variations are not visible to the human eye.

While these cell capacities and accumulation times are acceptable for producing images in CTEM, the limited cell capacity rules out the use of CCDs in direct bombardment mode as detectors in EELS. The height of the zero-loss peak in the EELS spectrum compared with the heights of the energy loss peaks requires a detector with a large dynamic range ( $\geq 10^4$) if the full spectrum is to be recorded in parallel[10]. Clearly, the limited full well capacity of the CCD for electrons means that the direct electron bombardment mode cannot be used in EELS. However, an optical coupling system which converts the electron signal into a photon signal, which is then detected by the CCD, would effectively reduce the CCD gain, and increase the cell capacity of the device. Such a system, incorporating a microchannel plate image intensifier, has been reported by Hicks et al[11].

As described in the introduction, CCDs could be used in place of the single detector normally used in STEM, and the output signal processed to simulate different detector geometries. It is unlikely in this case that more than one accumulation will be required, since the signal processing involves the addition of signals from areas containing a large number of cells. For electrons of energy in the range 60 - 100 keV, a signal which half fills the photocells is equivalent to a total signal of $\approx 5 \times 10^5$ electrons on the CCD. However, even if the signal from 1 accumulation provides sufficient data for each

| Electron Energy (keV) | 20 | 60 | 100 |
|---|---|---|---|
| Cell Capacity (electrons/photocell) | 440 | 65 | 45 |
| Number of accumulations for 3% shot noise | 4 | 30 | 45 |
| Time to accumulate image with 3% shot noise (seconds) | 0.24 | 1.8 | 2.7 |

Table 3.2: Cell capacity and accumulation time

picture point in the image, the CCD must be read out for each picture element, resulting in an accumulation time of $\approx$ 1 hour for an image of 256 x 256 picture elements at the present data rate.

Neither the data rate nor the cell capacity are fundamental limitations on the performance of CCDs as electron imagers. CCDs have been manufactured which operate at $\gtrsim$ 100 MHz[12], and the CCD cell capacity can be increased by increasing the cell area. The latter is particularly simply done in the case of linear arrays.

Section 3.2.4 Electron Gain of CCD 202

Exact values for the electron gain of the CCD 202 cannot be calculated from the measured results because of lack of information on the full well capacity of the device. In addition, values for the thicknesses of the overlying layers of the device and for the depth of the depletion region are necessary for a theoretical calculation of electron gain. As discussed in Chapter 1, these figures are available for the CCD 201, the forerunner of the CCD 202, but not for our device.

However, it can be assumed that the full well capacity of the CCD 202 is of the same order as that of the CCD 201 which is $4 \times 10^5$[13]. This gives figures of $\approx 0.9 \times 10^3$, $6.0 \times 10^3$ and $9 \times 10^3$ for the electron gains of 20, 60 and 100 keV electrons respectively. These figures are considerably less than the theoretical maximum number of electron-hole pairs created if it is assumed that 3.66 eV is required for the production of each electron-hole pair ( $\approx 5 \times 10^3$, $16 \times 10^3$, $27 \times 10^3$ for 20, 60 and 100 keV respectively). There are 2 factors which act to reduce this figure below the theoretical value.

Firstly, energy is deposited in the overlying layers of the CCD, and is therefore not available for the creation of electron-hole pairs in the silicon substrate. This mechanism is most important in the case of 20 keV electrons, where the range of the electrons in silicon is comparable with the thickness of the electrode layers. Therefore, the gain for 20 keV electrons is relatively smaller compared with that of 60 and 100 keV than would be at first expected.

Secondly, only electron-hole pairs created in the depletion region of the cell experience the force due to the electric field which collects them in the potential minimum. Electron-hole pairs created outside the depletion region may diffuse into it and so be collected in the signal charge packet. However, since diffusion occurs in all

directions, a large fraction of the charge created outside the depletion region is not collected, and the number is further reduced by the recombination of electron-hole pairs. A typical value for the thickness of the depletion region is 5 μm[14], and with ranges in silicon of 20 and 60 μm respectively for 60 and 100 keV electrons[15], it is clear that most of the electron energy is deposited outside the depletion region. A very rough calculation, which assumes $dE/dx$ is constant throughout the range of the electron in the silicon and is zero thereafter, that half of the created electrons diffuse towards the interface, and that the diffusion length of electons in silicon is 50 μm, was done to determine the fraction of the electron energy collected in the potential minimum. This suggests that $\approx$ 30% of the energy of 100 keV electrons is collected as signal, and that the equivalent figure for 60 keV electrons is 40%. The figures are reasonable in the light of the experimental results. The calculation for 20 keV electrons is highly dependent on the thickness of the overlying layers of the CCD, and the data for the CCD 201 does not give a figure compatible with the experimental results.

Despite the uncertainty in the figures for electron gain, it is clear that the value for gain for 20 keV electrons is $\sim 10^3$, while for 60 and 100 keV this figure is $\sim 10^4$. These large gains suggest that single electron detection by the CCD should be possible at all 3 energies given the approximate random noise figure of $\approx$ 0.1% of full well signal for a cooled CCD (equivalent to $\approx$ 300 minority electrons) given by Currie[13], and the statistical variation in the number of electron-hole pairs created in the silicon ( $\approx$ 1% for 100 keV).

## SECTION 3.3 UNIFORMITY OF RESPONSE OF CCD 202 TO ELECTRONS

### Section 3.3.1 Experimental Method

As described in the introduction to this Chapter, it is important that the response of the individual cells of the CCD is uniform over the device to avoid the necessity of scaling the cell outputs. The uniformity of response was checked by illuminating the CCD with a uniform electron beam, ie one in which variations in the number of electrons incident on each cell are due only to the shot noise in the electron beam, and producing a histogram of output cell contents.

In this experiment the CCD was housed in the cooling holder in the electron microscope and was typically cooled to 10- -20°C. An area of 82 x 82 photocells and the associated transport cells in the centre of

the device was exposed to the electron beam with the rest of the device being shielded from electrons by a copper aperture of thickness 75 μm to avoid irradiation of the output amplifiers. The counting system described previously monitored the number of electrons incident on the CCD, so that the variation in output signal from the CCD cells could be compared with the shot noise in the electron beam.

In the experiments described in this Section the CCD was driven by the Data Accumulation and Control Unit, and the video output was digitised and stored by the Unit. Either 31 or 63 accumulations were performed to collect each data-set. Once accumulated, the data was transferred to the IBM 370/145 computer using the output interface described in Section 2.6.9. The data stored in the computer was analysed to produce a histogram of cell contents. From the width of this distribution, knowing the contributions from shot noise, non-uniform illumination, and random noise the uniformity of response of the CCD photocells can be calculated.

It is important to ensure that the illumination on the CCD is uniform for these experiments, since otherwise variations in CCD output may occur which cannot be attributed to the device itself. In these experiments an irradiation time of 47 ms and a readout time of 56 ms were used with the beam deflected by the translate coils. Variation in intensity across the device should therefore be $\approx$ 1% (see Section 2.3). Before the data was accumulated the photomultiplier output was checked on the oscilloscope to see if this condition held. The intensity variation could have been further reduced to $\approx$ 0.5% by deflecting via either the gun tilt or gun translate coils but this was not realised at the time.

After each set of accumulations the background signal due to the d.c. level on the CCD was subtracted to ensure that the signal stored in the memory was due only to electron signals.

Results were obtained at 2 electron energies, 40 and 100 keV. 20 keV was not used in these experiments due to the rate at which electrons of this energy cause damage in the CCD (see Section 4.3). The data from photocells was transferred by operating the Data Accumulation and Control Unit in 2-frame mode, and transport cell data was transferred by operating in 3-frame mode. Normally the data from 4096 cells (the maximum memory capacity of the interface) was transferred to the computer for analysis. The computer program calculates the mean and standard deviation of the content of irradiated cells and produces a printed histogram of cell contents.

Section 3.3.2 Experimental Results

The experimentally measured standard deviation in the output signal from the photocells is in the range 3-5% for the 2 energies studied. Figure 3.2 shows the histogram of cell contents for 40 and 100 keV outputs. Taking the contribution to this figure from the shot noise in the electron beam and the 1% variation due to beam deflection into account gives a non-uniformity of response in the CCD in the range 2-4% of the output signal. This variation is of the same size as that quoted by the CCD manufacturers for irradiation with light which is 2% typical and 10% maximum 'shading'. 'Shading' is described as the variation in output signal across a row of photocells when the CCD is uniformly illuminated with light. It is not certain how this relates to the standard deviation in output signals but is probably of the same order of magnitude.

This uniform response of the CCD photocells suggests that the noise introduced into the video output by the CCD does not seriously degrade the video data. It is assumed that the variation in output signal is due to fixed pattern noise since the random noise in the output signal should be low. From Currie's data, the random noise due to the output amplifier is calculated at $\approx$ 1% of the total signal, and at the temperature used in these experiments the random noise due to dark current is negligible. That the variation is due to fixed pattern noise could have been verified by comparing two sets of video data collected from the CCD at different times, since the same pattern of signal should be observed for both datasets. However, this was not done due to lack of time.

It is probable that the fixed pattern noise is due to variations in the efficiency of collection of the created electron-hole pairs from cell to cell. This results from variations in lifetime of the electrons in the silicon due to non-uniformities in the composition of the substrate[16].

Thus it is to be expected that the noise introduced into the signal for 100 keV electrons should be greater than that for 40 keV electrons, since 100 keV electrons have a range of $\approx$ 60 $\mu$m in silicon, and 40 keV electrons have a range of $\approx$ 8 $\mu$m. As a result, the electron-hole pairs created by 100 keV electrons have to diffuse a greater distance to the potential minimum and so are more affected by variations in diffusion length. This is consistent with the experimental results, which give a noise introduced into the output signal of 2% and 3.5% for 40 and 100

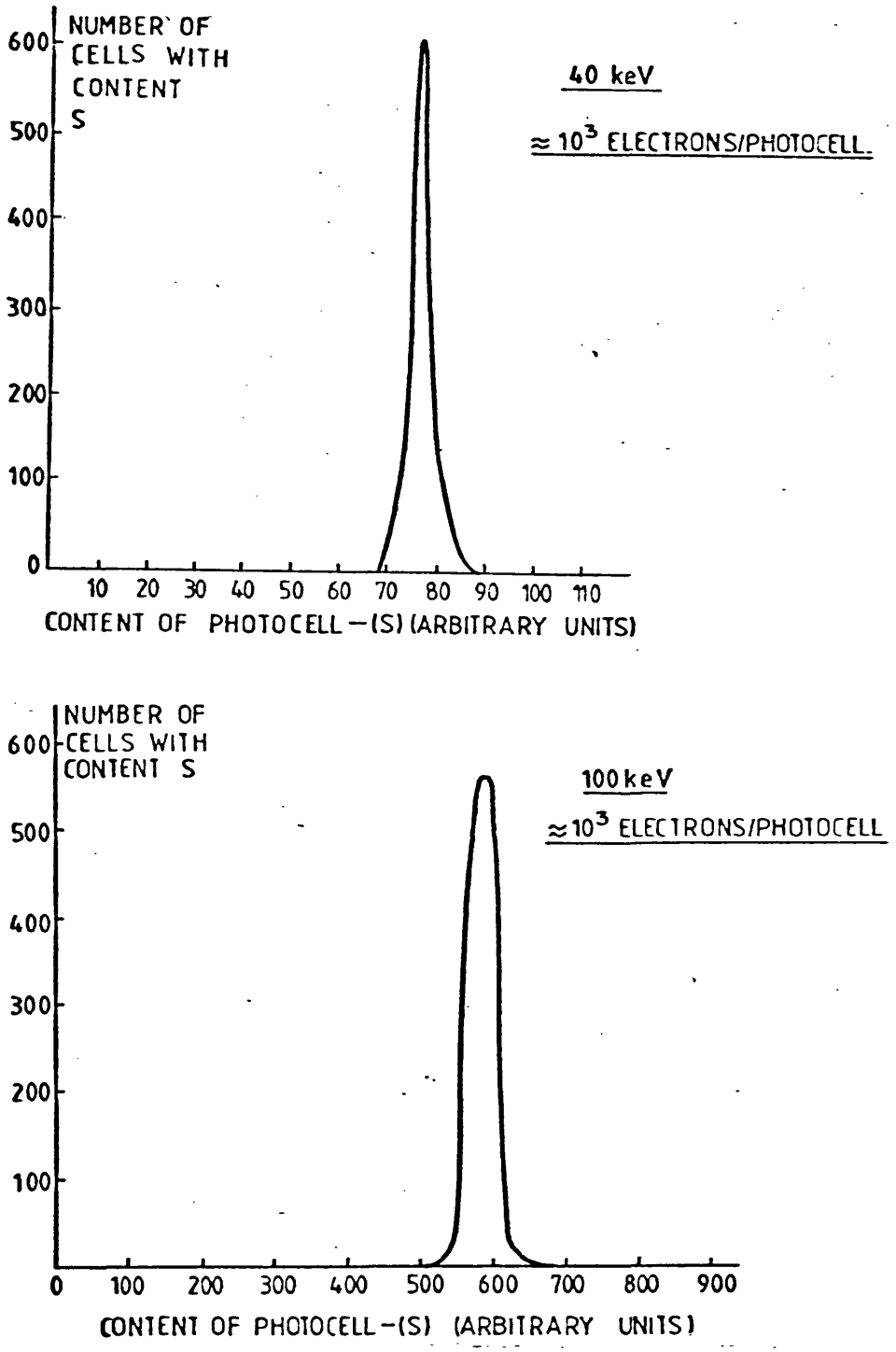


Figure 3.2: Uniformity of response of CCD 202 for 40 and 100 keV electrons. Noise introduced into output signal by imaging system for 40 keV electrons ≈ 2% (DQE = 0.6) Noise introduced into output signal by imaging system for 100 keV electrons ≈ 3.5% (DQE = 0.46)

keV electrons respectively.

The DQE of the CCD for electrons can be calculated from the figures for output noise in the signal. For 40 keV electrons a DQE of $\approx 0.6$ is obtained which is satisfactorily high. For 100 keV electrons the DQE is lower, due to the greater dependence of charge collection on diffusion, and is 0.46. Since DQE may be a function of the number of incident electrons, these figures apply only to a dose of $\approx 10^3$ electrons/photocell.

During the course of these experiments it was observed that the noise introduced into the video signal by the CCD increased dramatically (to $\approx 12\%$) if the CCD temperature fell below $\approx -20^{o}C$. It was postulated that this may be due to ice forming on the surface of the CCD but it is not clear whether this is the case.

## SECTION 3.4 SPATIAL RESOLUTION OF CCD 202

### Section 3.4.1 Experimental Method

This Section describes the measurement of the spread of the signal from an incident electron from the cell on which it was incident to other cells. This proves to be more important than the cell size in determining the resolution of the CCD for 100 keV electrons. The experiment was performed for 40 and 100 keV electrons. A copper aperture, of thickness 75 $\mu$m, was placed above the CCD, and the device was illuminated with a uniform electron beam. As a result there is a transition at the aperture edge from an area which has been illuminated with electrons to one which has received no illumination. If there is no scattering at the edge of the aperture the variation in output signal at the aperture edge reflects only the spread of charge from the irradiated to the unirradiated cells. It is assumed that this condition held for these experiments. However, under an optical microscope the edge of the aperture is uneven on the scale of $\approx$ 6$\mu$m so that there should be an intensity variation over this distance at the aperture edge. However, since this is $\approx \frac{1}{5}$ of the width of a photocell the effects of edge non-uniformity should

normally be limited to 1, and at worst to 2, cells.

The CCD output was collected and transferred to the IBM 370/145 using the Data Accumulation and Control Unit. The digitised values for cell content were plotted at the aperture edge to show the intensity variation.

Section 3.4.2 Experimental Results

Figure 3.3 shows the variation in photocell content along a horizontal row at the aperture edge for 100 keV electrons. A significant variation in cell content can be seen over 4 photocells. The total digital output from these 4 cells is equivalent to the content of one full photocell and one which is 75% full. We can therefore assume that cell 1 has received its full quota of incident electrons, that cell 2 is partly irradiated, and that cells 3 and 4 have not been irradiated. This suggests that the aperture edge is positioned in cell 2 so that a distance of 15 μm on the left-hand side is irradiated and the remainder of the device (5 μm) is shielded by the aperture.

In electron microscopy, the diffusion width at an aperture edge for photographic film is defined as the point at which the density of the emulsion falls to 1/10th of its maximum value[17]. This criterion gives a figure of 50 μm for the diffusion width for 100 keV electrons in the CCD. Thus a significant signal is created in an area of diameter 100 μm.

Figure 3.4 shows schematically a horizontal section through this row of the CCD showing how the spread of charge to nearby cells occurs. The finite width of the electron-hole pair clouds created by the incident electrons, results in the creation of electon-hole pairs under electrodes which have not been irradiated (as in the case of the transport cell between photocells 2 and 3). In addition, the lateral diffusion of the minority electrons results in charge diffusing to and being collected over a still larger area. In this case the charge collected in photocells 3 and 4 is due to minority carrier diffusion. Returning to figure 3.3, the loss of charge in cell 1 is due to the smaller amount of charge which spills over to it from cell 2 than to the other cells from their fully irradiated neighbours.

Figure 3.5 shows the same effect for 40 keV electrons. In this case the signals from both photocells and transport cells were collected and suitably scaled to show the variation in output across the edge. As can be seen from looking at the outputs of the photocells alone,

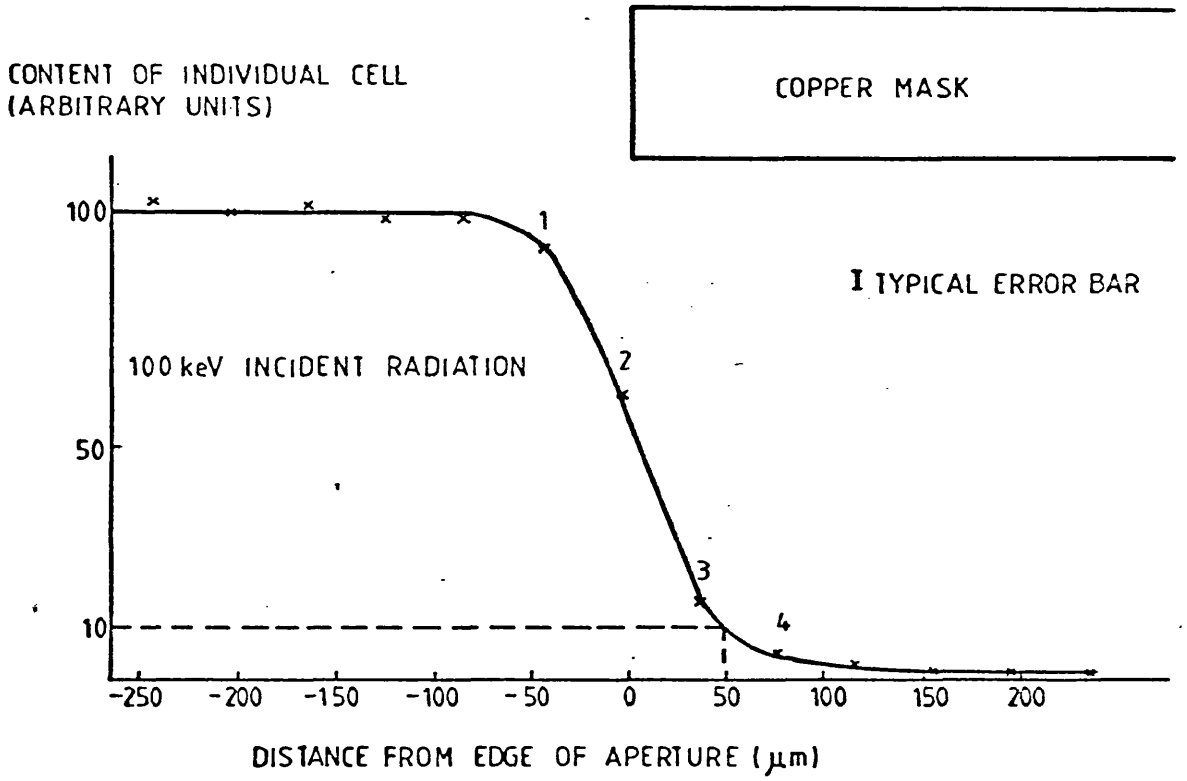


Figure 3.3: Charge spreading at aperture edge for 100 keV incident electrons, showing significant charge spread to a distance of ≈ 50 μm

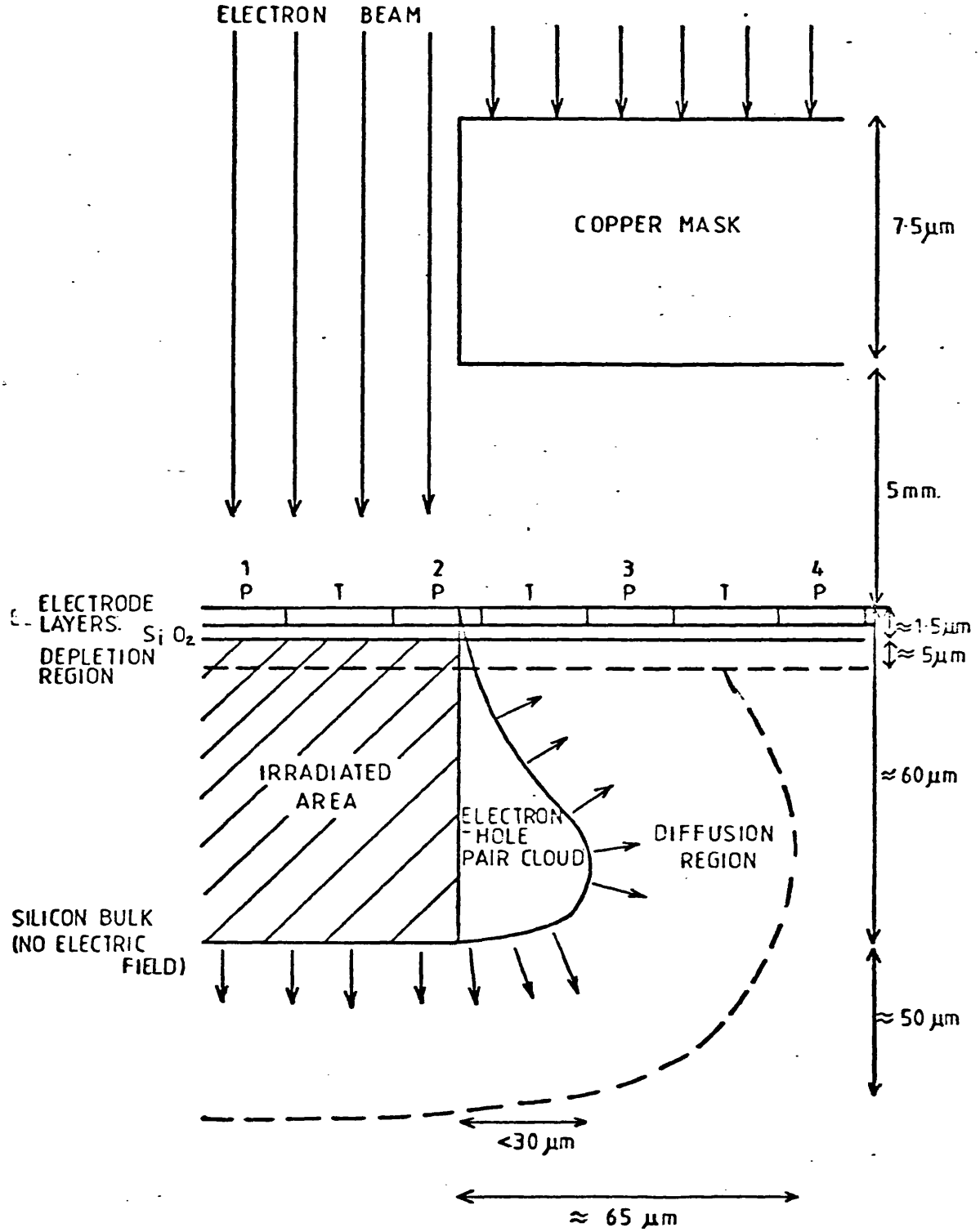


Figure 3.4: Schematic diagram showing charge spreading in CCD for 100 keV electrons

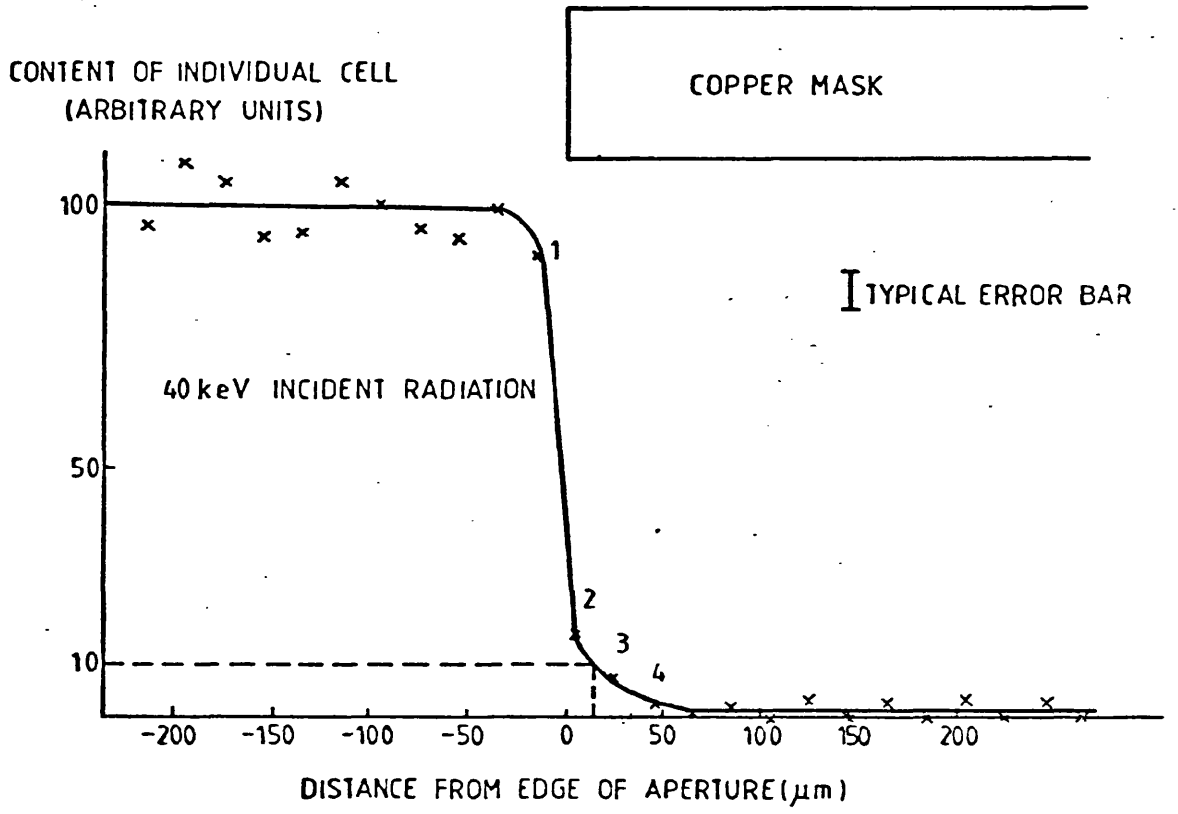


Figure 3.5: Charge spreading at aperture edge for 40 keV incident electrons, showing significant charge spread to a distance of ≈ 14 μm

there is no smearing of signal to nearest neighbour photocells for 40 keV electrons. There is some charge spillage from a photocell to the adjacent transport cell, and vice versa. From the contents of the cells at the edge of the aperture it appears that cell 1 (a transport cell) was completely irradiated, cell 2 (a photocell) was irradiated over $\approx$ 25% of its area and cell 3 (a transport cell) was unirradiated. The output signal falls to 1/10th of its maximum value in $\approx$ 14 μm in this case, giving a diameter of $\approx$ 28 μm for the area over which 40 keV electrons create a significant signal. The effect of diffusion on the spread of charge is less significant in the case of 40 keV electrons than 100 keV electrons, since a large fraction ( $\approx$ 40%) of the electron energy is deposited within the depletion region as compared with 4% for 100 keV electrons.

These calculations of signal spread assume that there is negligible charge smearing as a result of charge transfer inefficiency in the horizontal output register. Since the CCD clocking voltages were adjusted according to the manufacturer's instructions to ensure that this was the case, it is assumed that the charge transfer inefficiency was negligible. However, since this was not measured directly, these experiments can only set an upper limit on the area over which charge is created.

Section 3.4.3 Comparison of Results with Expected Values

Experimental results on the shapes of the electron-hole pair cloud volumes in bulk material are not available in the literature for 40 and 100 keV electrons, and there is unfortunately a wide variation in the electron-hole pair cloud diameters predicted by various theories[7] (eg ranging for 100 keV electrons from 19 μm (Reed) to 100 μm (Duncumb)). However, a rule-of-thumb guide generally used by electron microscopists is that the diameter of the volume of X-ray production ( $\approx$ the volume of electron-hole pair production) is approximately equal to the electron range in the material and that the shape of the distribution is roughly spherical. This assumption becomes less true with increasing electron energy and with decreasing atomic number, resulting in a more elongated distribution with diameter less than the electron range. This is the case for 40 and 100 keV electrons in silicon. The range of the electrons 8.5 μm for 40 keV and 60 μm for 100 keV thus puts an upper limit on the expected diameter of the electron-hole pair cloud. This is approximately a factor of 2X smaller than the spread of charge observed in the CCD, where the variations in signal at the aperture

edge suggest that an incident electron creates a significant signal over an area of diameter 28 μm and 100 μm respectively for 40 and 100 keV electrons. The probable explanation for this greater spread is the diffusion of electrons created outside the depletion region into the potential wells of distant cells. This effect is most important in the case of 100 keV electrons where a large fraction ($\approx$ 96%) of the electron-hole pairs are collected by diffusion. In the case of 40 keV electrons $\approx$ 60% of the electron-hole pairs are created outside the depletion region.

Section 3.4.4 Implications of Charge Spreading

Charge spreading has the effect of degrading the resolution of the CCD by decreasing the effective number of picture elements in the device. In the mode in which we intend using the CCD there is no advantage in having CCD cells which are smaller than the charge spread distribution and the number of effective picture elements is the active area divided by the area over which charge is created. The CCD 202 with photocells of size 18 μm by 30 μm is therefore well suited for imaging with 40 keV electrons, but its resolution is reduced by a factor of $\approx$ 4 when imaging with 100 keV electrons.

Thus for future use, it would be desirable to have a CCD with a larger cell size, which matches the diameter of charge spreading for 100 keV electrons. A cell size of 100 x 100 μm would be suitable. However no such devices are currently available and it may be necessary to have a device specially made for electron imaging.

SECTION 3.5 SINGLE ELECTRON DISTRIBUTION

Section 3.5.1 Introduction

A series of experiments was performed at various electron energies to investigate the ability of the CCD to detect single electrons, and to determine the spread of output signals produced by a single electron incident on a cell. As discussed in the introduction to this Chapter, this will determine whether the CCD can discriminate between output pulses due to large numbers of electrons.

The initial plan in these experiments was to perform only one cycle of accumulation and readout and transfer the output of the CCD to the IBM 370/145 for analysis. However, in the course of the experiments a problem arose in the CCD performance which made this method unworkable. Since this problem necessitated some modification of the apparatus and

alteration of the experimental plan it will be discussed first.

Section 3.5.2 Charge Barrier Problem

A 100 keV electron incident on a CCD cell should create a signal of $\approx$ 22 mV at the CCD output. At maximum amplifier gain this should give a signal of $\approx$ 53 units in the Data Accumulation Unit. However, in the experiments to detect single electrons, the CCD was irradiated with a signal of 1 electron/5 photocells, and the content of the cells in the Data Accumulation Unit was zero, instead of the expected average of $\approx$ 11 units. Further experiments were performed to investigate this phenomenon and as a result the following observations were made:

At low signal levels, the output signal/incident electron depends on the number of accumulations performed, being approximately zero for 1 - 3 accumulations and increasing thereafter. The number of accumulations required before a charge output is seen depends on the number of electrons incident per accumulation. Figure 3.6 shows the output of the ADC versus the number of accumulations for a low and a high intensity electron beam. From these and other measurements it appears that an electron dose of 4 - 7 electrons/cell must be collected before any output is produced.

This effect may be due to charge trapping in states in the CCD bulk, suggesting that there are $\approx$ 3 -6 x $10^4$ such states per photocell. This figure is of the order of the number of bulk states present in a photocell[18,19] ($\sim 10^{17} - 10^{19}/m^3$). These states are approximately in the middle of the band gap and are due mainly to metallic impurities in the silicon, such as gold[20]. Since the CCD is cooled, and is cycled continuously while not being irradiated, the bulk states which normally retain charge can be emptied, and become ready to trap any minority carriers present. The absence of dark current in the cooled CCD means that the signal charge due to incident electrons provides the only available minority carriers and so is trapped. Cooling the CCD to -20°C reduces the dark current from its room temperature figure of $\approx 10^5$ minority electrons/photocell/accumulation to $\approx 10^2$ minority electrons/photocell/accumulation.

Section 3.5.3 Modification to Data Accumulation and Control Unit

This charge trapping effect means that it is not possible to carry out the experiment to detect single electrons according to the original plan of irradiating the CCD with a very low dose of electrons for one accumulation and examining the output. Clearly, it will be necessary

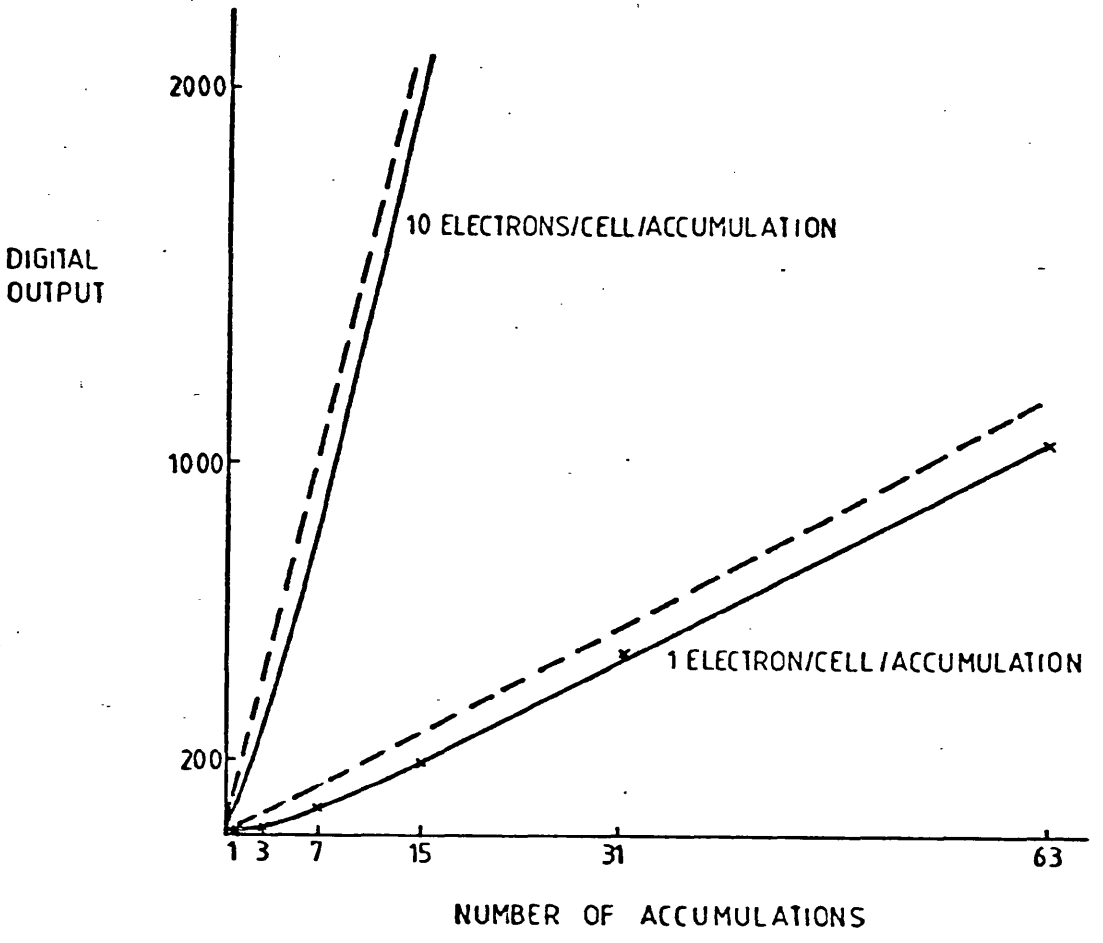


Figure 3.6: Non-linearity in CCD output for low numbers of accumulations, probably due to bulk trapping in the silicon substrate. The solid line shows the experiment results, the broken line is the expected output signal

to provide some signal charge for the trapping states, so that the CCD is reading out normally, before collecting the output. A modification to the driver circuitry was built to accomplish this. It allows the CCD to be irradiated and read out for a chosen number of times without data being transferred to the memory or adder circuitry, then allows the data from a chosen number of cycles to be stored in the memory, and finally allows cycling to continue with no storage of data. In this way the contents of the CCD can be examined midway through the accumulation of data rather than at the beginning of the accumulation when the CCD has not come to equilibrium. This modification was used in the following experiment to measure the single electron distribution.

Section 3.5.4 Experiment to Measure Single Electron Distribution

The experiment was performed with electrons of energy 40, 60 and 100 keV. The CCD was cycled for 63 periods of irradiation and read out without storing data, and then the data from the 64th cycle was stored in the memory and output to the IBM 370/145 computer for analysis.

Since the electron dose used in these experiments was $\approx 1/5$ electron /photocell, from the previous results 15 - 35 accumulations would have been sufficient to ensure that the empty states in the silicon bulk had been filled and that the CCD was working normally. Therefore, 63 accumulations was chosen so that the output was examined in the region where the CCD has come to equilibrium. The CCD was cooled to $\approx -10^{o}C$ during the experiments to reduce the signal due to dark current noise, and 1 subtraction was performed after the data had accumulated to remove the signal due to the d.c. offset on the CCD output. The electron dose on the CCD was monitored by the counting system, and an aperture of diameter 2 mm (equivalent to 3272 photocells) was placed above the scintillator to match the number of electrons incident on the scintillator to the maximum count rate of the system. The count rate was measured for the 127 accumulations and was suitably scaled to obtain the number of electrons incident/cell for 1 accumulation. An amplifier gain of 23.5x was used to give the maximum signal amplitude into the ADC.

Section 3.5.5 Experimental Results

The histograms of cell contents obtained for 40, 60 and 100 keV electrons are shown in Figure 3.7. The electron dose on the CCD was 0.19, 0.13 and 0.33 electrons/photocell respectively for the 3 energies. From the results no obvious difference in cell content can be seen between irradiated and unirradiated cells. This suggests that the

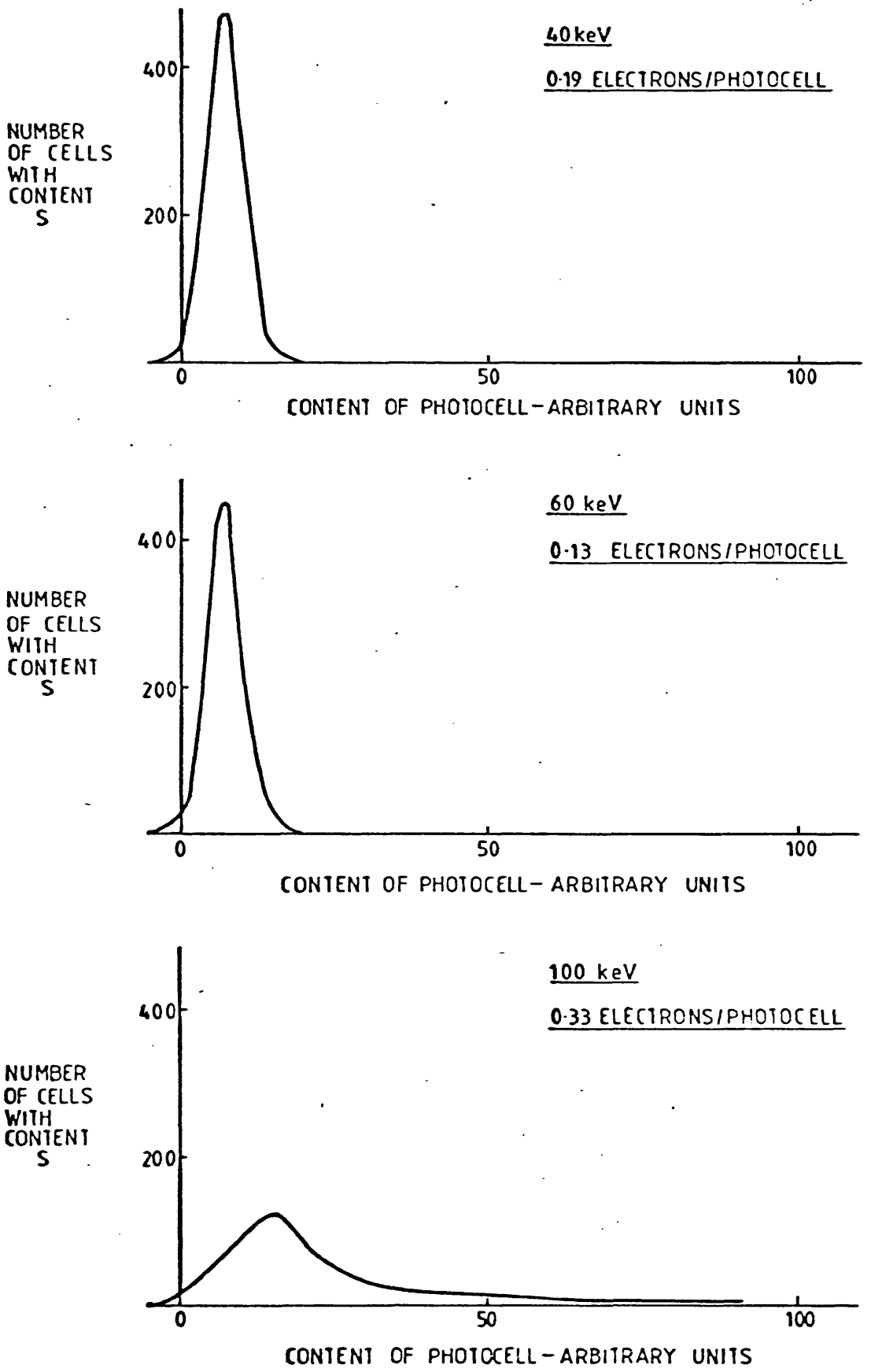


Figure 3.7: Histogram of CCD photocell contents for very low electron doses. Note absence of expected zero peak

effect of charge smearing from an irradiated to an unirradiated cell is to produce at least a small signal in all cells in the device. This should have been anticipated in the case of 100 keV electrons, where an incident electron creates a signal in ≈ 9 photocells. However, the result is surprising for 40 keV electrons, where the created charge could be expected to be limited to ≈ 4 cells. With a dose of ≈ 1 electron/5 photocells, by Poisson statistics ≈ 45% of the photocells should receive no signal at all, neither by direct bombardment nor by spread of charge. Therefore there should be a large zero peak in the distribution for 40 keV electrons.

The probable reason for the disappearance of the zero peak is the emptying of the bulk traps discussed in Section 3.5.2 during the time in which there are no electrons incident on the cells. This effect is well documented for buried channel CCDs for the case in which a series of high pulses (ones) followed by a series of low pulses (zeros) is transferred through the device. Signal trapped from the series of ones is re-emitted into the first zero, whereas the first one of a series loses charge to the bulk states[18,19]. The equivalent mechanism for the case of electron bombardment could be as follows. When an electron is incident on the cell, the traps fill since the trapping time is very much shorter than the emission time. The photocell is then read out leaving no signal in the cell. In the period until the next readout time ( ≈ 28 ms) the bulk traps empty, and some of their electrons are swept by the field gradient to the potential minimum and are stored there. Others are re-trapped by bulk states. Thus when the photocell is next read out signal has collected in it from the bulk states and is read out in the usual way as signal charge. Only bulk states within the depletion region will contribute to the signal charge so that the maximum possible signal packet due to bulk states is ≈ $0.25 - 1 \times 10^4$ minority carriers, ie is ≈ 15 - 60 on the ADC output. This will be reduced by trapping, but the magnitude of this effect is not known. The length of time between readouts ( ≈ 28 ms) compared with a typical emission time of ≈ 250 μs[18] means that practically all traps will have emptied during the cycle. This explanation seems possible in the light of the average signal height of ≈ 8 units obtained for both 40 and 60 keV electrons.

It may be possible to reduce this effect to some extent by using a small background charge, such as is normally supplied by dark current, to provide a source of charge which maintains equilibrium between

trapping and emission by the bulk states[18]. This could be achieved either by increasing the device temperature to increase the dark current or by continually illuminating the device with a low level of photon illumination. The first method has the disadvantage of increasing dark current noise, while the second has no effect on the bulk states in the transport cells. However, since the transport cells are clocked at a considerably higher frequency than the photocells, they are less affected by emission of charge from bulk traps.

Assuming the above explanation to be correct, these results suggest that the detection of single electrons by the CCD may be hampered by the effects of bulk traps, but that this effect can perhaps be avoided by the use of a background charge $\approx$ 10% of the output signal. If this can be done, the noise level of the CCD is low enough for the detection of single electrons.

The effect of trapping and emission by bulk states is less important for the case of 100 keV electrons, since at the electron dose used here (0.33 electrons/photocell) the probability of a cell receiving a zero signal is $\approx$ 0.05. However the zero peak is smaller than would be expected for this probability. Since 100 keV electrons create signal in a region of diameter $\approx$ 100 $\mu$m around the point of impact, charge is produced in $\approx$ 9 photocells and 4 transport cells (equivalent to an area of $\approx$ 17 photocells). Very roughly, the distribution of charge can be approximated as uniform over this area and zero elsewhere. Thus the distribution of cell contents may be expected to be a Poisson distribution of mean 17n, where n is the number of incident electrons/photocell. However, the distribution of cell contents for 100 keV is well fitted by a Poisson distribution of mean 5n, suggesting that the major part of the signal is created within a distance of 1 cell from the point of impact, giving a diameter of $\approx$ 60 $\mu$m for the area over which a significant signal is collected.

Section 3.5.6 Implications of Single Electron Distribution

Clearly, at present the distortion in the output signal, due possibly to bulk trapping, is too large to allow single electron discrimination. However if this problem can be removed by the use of a background signal, it should be possible to detect single electrons and identify the irradiated cell, if the CCD is used in an electron counting mode. This requires that the electron dose on the device is extremely low, so that there is little overlap of the distribution from incident electrons. It also requires processing of the output signal from the CCD to

identify the centre of the charge distribution and so the irradiated cell. This technique has been used by Herrmann, Krahl and Rust[1,2,3,4,5] using a TV camera tube with an electron-photon conversion.

Figure 3.8 is a contour plot of the distribution of energy in the region over which charge is collected (assuming a spherical distribution), and shows the size of the photocells relative to the width of the collection area for 40 and 100 keV electrons. For 40 keV electrons, an electron hitting a cell creates a significant charge in it and in at most 3 adjacent cells. Since the size of the charge distribution is approximately equal to the cell size, the signal in the cell will be highly sensitive to the point of impact of the incident electron. In addition, by determining which adjacent cells contain charge it should be possible to assign the point of impact of the electron to one of the 4 quadrants of the cell. Finer determination of the position of impact may be possible by examination of the relative magnitudes of the signals in the cells. For the case of 100 keV electrons, where the size of the electron-hole pair cloud is very much greater than the photocell size, a large number of photocells receive approximately equal signals when a nearby cell is hit by an electron. As a result it is not possible to relate the output of a cell to the number of electrons directly incident on it, and identification of an irradiated cell will require processing of a large area of cells.

This problem in determining the irradiated cell for 100 keV electrons results from the electron spread to adjacent cells and reinforces the need for a CCD with a larger cell size outlined in Section 3.4.4. In addition, the time required to accumulate an image in electron counting mode would be prohibitive at present readout speeds, being $\simeq$ 15 mins for 40 keV electrons and considerably longer for 100 keV.

## SECTION 3.6 COMPARISON OF CCD WITH OTHER ELECTRON IMAGERS

This section compares the performance of the CCD as measured in the previous sections with that of other electron detectors. The detectors discussed will be photographic film, TV cameras, and photodiode arrays.

### Section 3.6.1 Photographic Film

Photographic film is the recording medium which is most commonly used in electron microscopy. Its main drawback, as discussed in the Introduction, is the difficulty in extracting quantitative information from the recorded intensities. Photographic emulsion consists of a layer, $\simeq$ 12 $\mu$m thick, of a suspension of silver halide crystals in

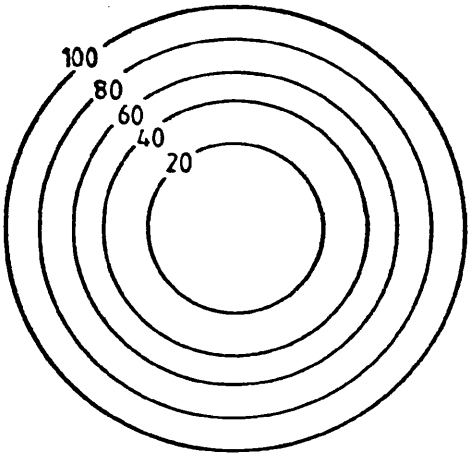


CONTOUR PLOT OF ELECTRON-HOLE PAIR DISTRIBUTION

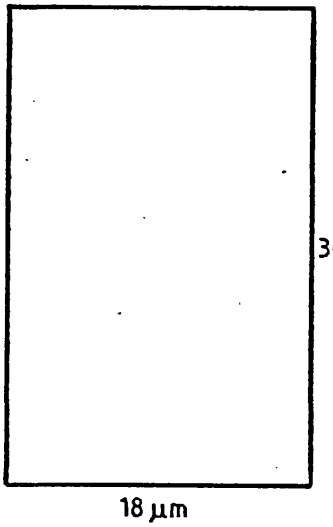


SIZE OF PHOTOCELL RELATIVE TO WIDTH OF ELECTRON-HOLE PAIR DISTRIBUTION FOR 40 keV ELECTRONS

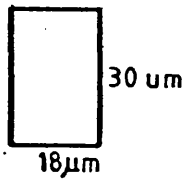


SIZE OF PHOTOCELL RELATIVE TO WIDTH OF ELECTRON-HOLE PAIR DISTRIBUTION FOR 100 keV ELECTRONS

Figure 3.8: Contour plot of electron-hole pair distribution in CCD, assuming a spherical distribution of electron energy. The sizes of the CCD photocells relative to the charge distribution predict charge will be collected in 3 and 13 surrounding cells for 40 and 100 keV electrons respectively

gelatine, covered with a protective layer, ≈ 1 μm thick, of clear gelatine. This is supported on a plastic base. The size of the silver halide crystals, ie the grain size, is typically ≈ 0.5 μm in emulsions used in electron microscopy[9].

An electron incident on the photographic film deposits energy in any silver halide grains with which it interacts, making them susceptible to reduction to silver in the development process. The number of grains developed by an electron depends on the range of the electron in the emulsion and thus on its energy, with lower energy electrons developing fewer grains. Thus the ultimate resolution limit of photographic plate is set by the range of the electrons in the emulsion and by the emulsion thickness(although in practice statistical considerations are more important). This is a function not only of electron energy, but also of the emulsion structure. The width of the profile of an aperture edge has been measured by several workers[6,9,21] and gives results which can be compared with those of the CCD. All of the figures give the distance from the aperture edge at which the signal falls to 1/10th of its maximum value (the diffusion width). The results are given in Table 3.3. It can be seen that for a standard emulsion thickness of ≈ 12 μm, at low energies the diffusion width is approximately the same as for the CCD (14 μm for 40 keV electrons - see Figure 3.7). At higher energies, the diffusion width is highly dependent on emulsion thickness, but for all emulsions is lower than the value of ≈ 60 μm measured for 100 keV electrons in the CCD. At low emulsion thicknesses, the diffusion width is reduced.

The DQE of photographic plates is degraded by non-uniformities in the number and areas of grains exposed by an incident electron[17,22]. Valentine has measured the increase in noise in the recorded image caused by the photographic emulsion for a range of developers and emulsions. Taking the figures for each emulsion with the most suitable developer gives a range of DQE of 0.4 to 1 for 60 keV electrons. These figures are clearly better than the results for the CCD, which had a DQE of 0.6 for 40 keV electrons, and of approximately 0.46 for 100 keV electrons. However, the DQE of photographic plate is also a function of energy, being a maximum for the range 60 - 100 keV and decreasing considerably below 60 keV[20].

For low electron doses the number of grains developed and thus the optical density of the micrograph is linearly related to electron dose. However as electron dose increases a significant fraction of the grains

| Author | Electron Energy (keV) | Emulsion Thickness (μm) | Diffusion Width (μm) |
|---|---|---|---|
| Farnell & Flint[9] | 75 | - | 7.5 |
| Zeitler & Hayes[6] | 52 | 13.4 | 14 |
| | " | 22.4 | 14 |
| | 68 | 13.4 | 13.5 |
| | " | 31.4 | 17.5 |
| | 82 | 13.4 | 13 |
| | " | 53.9 | 30 |
| Burge & Garrard[21] | 60 | 13 | 13.8 |
| | 60 | 10.5 | 8 |
| | 60 | 2 | 5.52 |
| | 40 | 13 | 6.44 |
| | 7.3 | 13,10.5,2 | 1.15 |

Table 3.3: Diffusion widths in photographic emulsions measured by various workers.

is already developed and so is unaffected by the electron beam, resulting in a departure from linearity. The linear region corresponds to a density range of 0 - 1.4. The electron dose required to achieve density ≈ 1.4 varies with emulsion type, but a typical value is 3 electrons/$\mu m^2$ at 100 keV[17], compared with 0.08 electrons/$\mu m^2$ for the CCD at the same energy. Thus the range of intensities for which the photographic plate is linear is considerably greater than that of the CCD.

The information capacity of photographic plate is considerable, with a typical film of dimensions 8 x 5 cm containing $\sim 10^6 - 10^7$ picture elements (assuming a cell size of 30 x 30 μm to match the resolution of the film).

Clearly, from the above discussion, photographic plate is an excellent electron recorder, with its only disadvantage compared with the CCD 202 being the inaccessibility of quantitative information.

Section 3.6.2 TV Camera

Several groups of workers have used commercial television tubes for electron recording, either for image intensification or for quantitative work. All of these systems use a fluorescent screen to convert the electron image into a photon image, and in most cases use an image intensifier before the camera to intensify the photon signal. Electron counting mode is normally used in the systems which are reported in the literature, so that the DQE of the system can be maximised. In these systems the DQE is determined mainly by the response of the fluorescent screen. Kuo and Glaeser[23] using a Secondary Electron Conduction (SEC) camera tube, preceded by an image intensifier and a Zn S screen, obtained an electron counting efficiency of only 10 - 20%. They suggest that this is due mainly to the effect of scattering and diffusion of the light in the Zn S screen. Herrmann et al[1,2,3,7,23] obtained a counting efficiency of 65% (equivalent to a DQE of 0.6) using a similar system with an Electron Bombarded Silicon (EBS) camera tube, an image intensifier and Zn S scintillator. However, due to image lag and signal spread to adjacent picture elements, it is necessary to process the camera output to achieve this low noise figure. This figure is not attainable in analogue mode, but no figures are given for DQE in that mode. Once again the DQE degradation is due mainly to the performance of the scintillator, which in this case has an efficiency of ≈ 70%[11]. Kerzendorf & Hoppe[25] suggest that the DQE of the scintillator and thus

of the system could be improved to 0.95 if a $CaF_2$ screen was used in place of the Zn S screen. In addition, they suggest cooling the TV camera to $\approx -40^{\circ}C$ to reduce image lag and eliminate fixed pattern noise, so reducing the processing requirements. Thus the DQE of present imaging systems based on TV cameras is comparable with or worse than that of the CCD 202, when the TV camera is used in pulse counting mode and the CCD is used in analogue mode although there is a possibility that the performance of TV cameras will be improved by using a more efficient fluorescent screen.

From the data of Herrmann et al the resolutions of TV cameras and CCDs are comparable. The target of the EBS camera is a 256 x 256 array of silicon diodes each of size 35 x 46 μm[5]. The thickness of each diode is ≈ 12 μm[25]. In processing the output the data from a 3 x 3 array of cells is processed to find the point of impact of the electron on the array. This corresponds to a radius of signal spread at the array in the range 23 - 69 μm.

Section 3.6.3 Photodiode Arrays

The use of photodiode arrays in electron microscopy has been investigated by Jones, Jenkins et al [26,27,28]. Results have been published on the performance of linear photodiode arrays as detectors in EELS. The arrays used consisted of either 64[26,27] or 96[28] diodes with centre-to-centre spacing 100 μm. In the latter array the active area of each diode had dimensions 80 μm x 800 μm, and the maximum charge on each diode was $2 \times 10^8$ electrons. The efficiency of this array has been measured for incident electrons in the range 10 - 100 keV by measuring the time taken to saturate the device at a specific beam current, and is > 0.5, in the above energy range, being ≈ 1.0 at 40 keV[27]. This high gain figure requires a very thin oxide layer above the silicon substrate and a depletion region which extends to a depth of ≈ 8 μm from the surface, so that practically all of the signal from 40 keV electrons is created within the depletion region.

In the 64 diode array the depth of the p-type diffusion is 1.0 μm below the silicon surface[26], and in measurements up to 30 keV a charge collection efficiency of ≈ 1 is obtained for every keV above a threshold energy. The threshold energy depends on the thickness of the overlying oxide layer. In this case no signal is created in the silicon bulk below the depletion region.

The spatial resolution of photodiode arrays should be similar to

that of CCDs, since in both cases it is determined by the width of the electron-hole pair cloud in the silicon substrate, and by the diffusion of electrons in silicon. There is no information available on the DQE of photodiode arrays as electron detectors, but the cell-to-cell non-uniformity in response is typically ± 10%[29,30]. This is due mainly to non-homogeneity in the silicon and thus to variations in carrier life time[16].

Despite the encouraging performance of photodiode array imagers, the number of elements in an array is restricted by the necessity of maintaining a low capacitance in the output bus line. The noise in the output signal is proportional to $C^{\frac{1}{2}}$ where C is the output capacitance. With an XY addressed imager, the output capacitance is proportional to the number of picture elements, so that the output noise also increases with the number of picture elements[8]. Thus it is unlikely that area photodiode arrays will match the noise performance of equivalent sizes of CCDs.

# CHAPTER 4

## EXPERIMENTS ON RADIATION EFFECTS ON CHARGE COUPLED DEVICES

### SECTION 4.1 INTRODUCTION

As commercially available CCDs are designed for photon rather than electron imaging it was important to investigate the performance of the Fairchild CCD202 under electron irradiation before using it in earnest for imaging in the electron microscope. It is known that a deterioration in performance occurs in single MOS capacitors, the structure on which CCDs are based, after exposure to ionizing radiation doses as low as $10^3$ rads (Si). Extensive investigation of these effects has been undertaken[1-7], and positive charge build-up in the oxide layer and an increase in the number of interface states have been identified as the main causes of device degradation. Although the effects of these are well known and empirical methods of producing radiation hard devices are reported[7], there is little agreement among workers about the mechanisms for damage production.

Killiany and co-workers[8-10] and Chang[11] have studied the effect of ionizing radiation on CCD performance and have suggested CCD structures which are radiation hard to $10^6$ rads (Si). Despite this, radiation hard CCDs are not yet in production. There are reports in the literature on MOS radiation effects of the removal of radiation damage by annealing devices to temperatures between 150 and 400°C. However there are no reports of similar annealing of CCDs to remove radiation damage.

The three areas to be investigated to determine the suitability of CCDs for imaging in the electron microscope are:

1. Whether changes in device performance eventually render the device unusable as an electron detector, and if so what the device lifetime is.

2. Whether the radiation effects can be minimised by suitable operating conditions.

3. Whether radiation effects can be reversed by annealing and if so whether a cycle of irradiation and annealing can extend the device lifetime indefinitely.

The results of these tests are reported in this chapter.

## SECTION 4.2 REVIEW OF RADIATION EFFECTS IN MOS DEVICES

### 4.2.1 Positive Charge Build-up in the Oxide Layer

Positive charge build-up in the oxide layer in MOS devices has the effect of changing the operating voltage of the device by causing a negative shift in the flat band voltage. The flat band voltage is defined as the bias voltage which must be applied to the electrode to make the energy bands flat throughout the semiconductor. Since this voltage shift can be large ( $\approx$ 30V) the change in its characteristics can render a device inoperable.

Early reviews (Snow et al[2] (1967), Zaininger & Holmes Siedle[1] (1967), Lamb[5] (1970)) and experimental work (Zaininger[4] (1966)) suggest that the oxide charge build up is caused by the production of electron-hole pairs in the oxide by the incident radiation and the subsequent trapping of holes within the oxide near the Si-$SiO_2$ interface. Zaininger's model states that if no field is present in the oxide the electron-hole pairs will recombine, but that under the influence of an electric field electrons are free to drift to the more positive electrode, the less mobile holes being trapped. Electron-hole recombination can still occur in regions of the oxide through which the electrons drift, but no electrons are available to recombine with the trapped holes which are at the interface furthest from the positive electrode. Thus if the metal electrode is positive with respect to the substrate there is a build-up of positive charge in the oxide at the Si-$SiO_2$ interface, whereas if the metal electrode is negative with respect to the substrate charge build-up occurs near the Metal - $SiO_2$ interface. This agrees with the observation that the flat band voltage shift is greatest for irradiation under positive bias and Zaininger and Holmes-Siedle (1967) suggest that the hole traps are non-bridging oxygen atoms (that is oxygen atoms in which only one electron forms a bond with an adjacent silicon, and in which the other valence electron is not bonded). These sites can trap a hole to become $SiO^{\cdot}$. The increase in radiation damage in oxides containing metallic impurities such as sodium may be a result of the greater number of non-bridging oxygen atoms caused by the impurities.

The work of Powell & Derbenwick[12] (1971) substantiates the electron-hole pair creation model. By irradiating MOS structures with ultra-violet photons they estimated the threshold photon energy required to cause positive charge build-up to be 8.8eV, consistent with the energy for electron-hole pair formation. However their results support a

'mobile hole' model in which holes are transported to the $Si-SiO_2$ interface and subsequently trapped. Their evidence for this model is that all of the positive charge is located within 30 nm of this interface even in the case in which all the photon energy is deposited in the upper layers of the oxide.

Rewesz[13] (1971) suggests several possible hole traps present in the oxide. Firstly, hole trapping is an intrinsic property of the Si-O bond due to the discontinuity of the $\pi$ energy band within the oxide. Therefore if a hole appears in a lower continuous energy level, an electron from the $\pi$ -band can recombine with it, leaving a trapped hole in the $\pi$ -band. Secondly, defects can be generated by irradiation, in particular, breaking of Si-O-Si bonds produces non-bridging oxygen and trivalent silicon (ie silicon in which only 3 of the 4 valence electrons are bonded to oxygen atoms) both of which are traps. Thirdly, impurities at the interface form bonds with the silicon, in particular producing Si-H and Si-OH which can dissociate under ionizing radiation to produce trivalent silicon and interstitial hydrogen which again behave as traps. Finally, Sah[6] (1976) suggests trivalent silicon and interstitial oxygen as the centres responsible for positive charge trapping in the oxide. Both centres can capture holes produced by ionizing radiation and both can be ionized by energetic electrons, with the free electrons in both cases drifting to the more positive electrode.

4.2.2 Interface State Production

Interface states are energy levels within the forbidden energy gap of silicon which can readily exchange charge with the silicon. They provide states for the thermal generation of electron-hole pairs and thus contribute to device dark current. They result from irregular potential distributions at the interface which perturb states in the conduction and valence bands of the silicon into the forbidden gap. Sah[6] identifies trivalent silicon resulting from the mismatch between the $SiO_2$ and Si lattices to be the centre responsible for interface states. This model assumes that the trivalent silicon bonds to $OH^-$ ions during oxide growth so that the number of pre-irradiation interface states is reduced considerably in a steam grown oxide. Under irradiation, however, the generated electrons and holes can interact with this bond to release the $OH^-$ ion and regenerate the trivalent silicon. The $OH^-$ ion is then free to drift to the more positive electrode. This model is consistent with the observation

(due to Aubuchon) that there is very little increase in interface state density with irradiation in oxides in which there are few Si-OH bonds, and with the greater increase in interface state density obtained when devices are irradiated under positive gate bias. In another model, due to Rewesz[13], the trivalent silicon and interstitial hydrogen described in Section 4.2.1 provide the perturbation responsible for interface states.

### 4.2.3 Effect of Electron Energy on Damage Mechanism

The type of radiation damage caused in MOS devices depends on the energy of the incident radiation. The above discussion is confined to energies which are sufficient to break electronic bonds and so cause changes in the energy band structure, but are too low to cause displacement of an atom from its lattice site. For electrons this assumes that their energy is less than 140keV[14]. This is the energy region in which the experiments described in this thesis were performed and so the damage effects described apply to the experimental results in Section 4.3.

A further damage effect can occur which, while not applicable to these results, is seen with electron energies greater than 140keV[14]. In that energy range an incident electron has sufficient energy to displace an atom in the silicon substrate, so disrupting the periodic potential of the lattice and perturbing energy states into the band gap. The effect of these states, which are in the silicon bulk, is to increase the component of dark current produced in the bulk in both surface and buried channel devices, and to decrease the transfer efficiency of buried channel devices by charge trapping[15].

### 4.2.4 Effect of Oxide Charge on CCD Performance

In CCDs the trapped oxide charge causes a negative shift in the flat band voltage of the device which is equivalent to a permanent positive gate bias. In p-buried or n-surface channel devices in which a negative gate bias is required the potential wells eventually collapse as the flat band voltage shift becomes greater. In the more common p-surface channel and n-buried channel devices the oxide charge has the effect of increasing the depth of the potential wells but can nevertheless degrade device performance in several ways.

The first effect (and the most important in devices with a polycrystalline silicon gate structure) is the increased conductivity

induced in the polycrystalline silicon interelectrode isolation by the field due to the trapped positive charge[8]. The field bends the energy bands in the insulator allowing channelling of charge from the electrodes through the polycrystalline silicon. As a result, the clock wave forms on adjacent electrodes are no longer isolated but can be mixed, so decreasing the potential barrier between cells and allowing charge collected in the photo cells to leak continually into the transport cells. This has the effect of decreasing the amount of charge which a cell can contain and so decreasing saturation output voltage of the device. This effect is described by Killiany[8], and has been noted by him after a dose of $3 \times 10^4$ rads (Si) in a Fairchild imaging CCD with a similar structure to the CCD202.

Secondly, in buried channel devices it is important that the n- buried channel is maintained in a depleted state to avoid flooding the potential wells with the majority electrons from the n-layer thus causing dark current (Section 1.2.2 ). A large positive charge trapped in the oxide increases the channel bias required to deplete the n-channel region. If the required bias becomes greater than that provided on-chip, the channel is driven out of depletion and the device flooded with electrons. The maximum voltage which can be applied to the channel is limited by the breakdown voltage of the channel output diode and so cannot be increased indefinitely. This effect has been described by Killiany[8], and was first apparent at a dose of $10^4$ rads (Si).

A third effect is possible, which is not of interest in the CCD202 but occurs in devices in which more than one type of gate material is used. The amount of flat band voltage shift for a given dose depends on the oxide thickness (proportional to $t_{ox}^{11}$ and on the gate material[8]. The voltage shift is approximately twice as great under polycrystalline silicon gates as under aluminium gates for a dose of $10^5$ rads. This results in distortion of the potential well profile and in a reduction in the full well capacity, and thus in the saturation output voltage, which becomes worse with increasing dose.

To summarise, there are two possible effects of radiation induced oxide charge on the performance of the CCD202. The first is a decrease in the saturation voltage of the device due to a breakdown in the polycrystalline silicon interelectrode isolation as a result of the field due to the positive charge. The second effect is an

increase in the dark current in irradiated areas arising from the inability of the positive bias on the n-channel to deplete that region in the presence of fixed positive charge in the insulator. Both effects appear at a dose of $\approx 10^4$ rads (Si).

### 4.2.5 Effect of Interface States on CCD Performance

As described in Section 4.2.2 interface states are states within the forbidden energy gap of silicon which can interact readily with carriers in the silicon substrate. The effect of this interaction is to provide generation-recombination centres for electron-hole pairs[10]. In an unirradiated CCD there is a small leakage current (dark current) due to thermal generation of electron-hole pairs in the depletion region. These do not recombine but are separated by the field in the depletion region, the minority carriers falling to the potential minimum while the majority carriers are swept into the substrate. The minority carriers generated in this way add to the signal charge contained in the potential wells, and, if allowed to collect for long enough, will eventually swamp the signal. This sets an upper limit on the time for which charge can be stored in a potential well and therefore sets a lower limit on clock frequency. This generation process occurs not by direct excitation of an electron across the band gap but by a two stage process in which an electron is excited to an intermediate energy level in the gap and another electron is excited from that level to the conduction band[16]. The number of such transitions occurring, and therefore the dark current, increases linearly with the number of available states in the band gap[17, 18]. Since radiation damage increases the number of interface states (eg from $10^{10}$ to $10^{11}$ $eV^{-1}\,cm^{-2}$ for a dose of $\approx 3 \times 10^4$ rads[8]), the dark current in the device also increases. This holds for both buried channel and surface channel devices, since in both cases minority carriers created at the interface can fall to the potential minimum.

The second effect seen is on the transfer efficiency of surface channel and some types of buried channel devices. In surface channel devices it can be shown that the transfer inefficiency $\varepsilon$ is proportional to $N_{ss}$, the fast state density[8]. $\varepsilon$ is defined as the fraction of the signal charge which is lost after one transfer, and fast states are those which interact with the charge in the silicon substrate. Killiany[8] has shown that an electron dose of $3 \times 10^4$ rads (Si) on a surface channel device can cause a 10-fold increase in the number of interface states, resulting in a loss of 30% of the signal

charge after ≈ 500 transfers. In buried channel devices the charge packets are transported in the potential minimum which is displaced by ≈ 1 μm from the Si-$SiO_2$ interface, and so should not interact with the interface states, and should not be affected by transfer inefficiency. However the volume of the depletion region occupied by the charge packet increases as more charge is added, and some mixed-mode buried channel devices operate in surface channel mode for signals greater than 50% of full well signal[9,19]. As a result, surface trapping at interface states will become important in these devices for large signals. This effect is seen at doses of ≈ $2x10^4$ rads (Si)[9].

In summary, interface states increase dark current in both surface and buried channel devices and decrease transfer efficiency for all signals in surface channel and for large signals in mixed-mode buried channel devices.

4.2.6 Requirements for Radiation Hard CCDs

Killiany[9] et al have suggested features which are desirable for a radiation hard CCD. These relate to the effects described above and are:

1. Buried channel structures to minimise the effect of interface state trapping on transfer efficiency.

2. N-channel structures to avoid the collapse of the potential wells with positive charge trapping in the oxide. This structure has the added advantage that with a large positive bias on the n-channel the holes in the $SiO_2$ will be repelled from the $SiO_2$ - Si interface, so reducing their effect on the silicon substrate.

3. An electrode structure that avoids differences in flat-band voltage shifts between electrodes. This requires that the oxide thickness should be uniform and that the same material should be used for all electrodes.

4. Avoidance of polycrystalline silicon insulators, since channelling is induced in this material by the field due to the trapped positive charge in the oxide.

5. A structure which allows a large reverse bias to be applied to the channel-substrate junction to counteract the effect of the positive oxide charge and so maintain the channel depletion.

6. Some method of controlling the surface potential between

electrodes.

An attempt has been made by several workers, in particular Chang[11], to produce a radiation hard device following these specifications. This has resulted in CCDs which are radiation hard to $10^6$ rads, an improvement of X100 on non-hardened devices. However these devices are not generally available, although it is possible that a radiation hard 100 x 100 array imaging CCD may be manufactured commercially by Hughes Aircraft Company.

### 4.2.7 Suitability of Fairchild CCD202 for Electron Irradiation

The device used in this project, the Fairchild CCD202, fulfils some of the above requirements. It has an n-buried channel structure and the interelectrode surface potential is controlled by an oxide layer (requirements 1, 2 and 6). However the interelectrode isolation in the transport register is polycrystalline silicon[9]. The reverse bias applied to the buried channel ( $\approx$ 16 V) does not appear to be large enough to deplete the channel in the presence of positive charge under certain experimental conditions (see Section 4.4.4). There may be some effect on the potential profile due to the variation in oxide thickness where the transport cell electrode overlaps with the photocell electrode, since the greater positive charge trapped in the thicker oxide in this region will tend to lower the potential barrier between photocell and transport cell. This will cause a decrease in the amount of charge which can be stored in the cell.

It is not clear from the manufacturers literature whether the CCD202 operates in buried channel mode for all signal heights or whether surface channel mode is employed for large signals. From the linear response of the device to an input signal it is assumed that the former is the case, and that therefore no transfer inefficiency is introduced by surface states.

### 4.2.8 Backface Imaging

The damage effects described in this section refer to the front face imaging mode in which the illumination incident on the CCD passes through the electrodes and the oxide layer before reaching the silicon substrate where it produces a signal. This is the more common imaging mode and is that employed in the Fairchild CCD202, the device used in these experiments. An alternative to this is the backface imaging method in which the CCD is illuminated from the substrate side so avoiding damage in the oxide layer and at the interface. In this mode

the substrate is thinned so that the incident radiation generates electron-hole pairs within a diffusion length of the potential minimum, thus avoiding signal loss through recombination of minority carriers.

The radiation hardness of thinned backface illuminated CCDs has been investigated by Borsuk et al[20]. They irradiated a buried channel CCD, in which the substrate had been thinned to 10 μm, with a dose of $\approx 10^8$ rads (Si) of 20keV electrons. A dose of 1600 rads (Si) was absorbed in the oxide during this irradiation due to X-rays produced in the silicon. This gave an increase of $\approx$ 2X in the dark current and no change in transfer efficiency, consistent with front face imaging results for a 1600 rads (Si) dose.

Although this is an attractive solution to the problem of radiation damage, at present there are no commercial backface devices available which are suitable for electron imaging. The range of electrons of the energies used in CTEM is such that a substrate thickness of 60 μm is required to maximise minority carrier collection efficiency while avoiding damage due to deposition of energy at the interface by the primary electron. However, since commercial devices are designed for photon imaging (in particular for the detection of photons of wavelength $\leq 6000\text{Å}$), the substrate is thinned to $\approx$ 10μm, which is incompatible with the requirements for electron imaging.

4.2.9 Removing Damage in MOS Devices by Annealing

It has been reported in the literature[1-4] that the effects of radiation damage can be completely removed in MOS devices by annealing to temperatures in the range 150 - 400°C

Mitchell & Wilson[3] quote results of damage produced by 10 - 20 keV electrons being removed by annealing for 15 minutes at 150 - 200°C, and of damage by 5keV electrons being removed at 200°C. Zaininger[4] reports that oxide charge can be removed by annealing, with most improvement occurring between 150 - 300°C and almost all charge being removed by 400°C. He suggests that the improvement is due to the recombination of trapped holes with electrons and shows that the same effect can be achieved by irradiating with UV photons of energy greater than 4eV. This suggests that the traps must be more than 4eV above the valence bond edge in $SiO_2$. Snow et al[2] attribute this energy threshold to the height of the Si-$SiO_2$ barrier (4.3eV)required for injection of electrons from the silicon into the conduction band of the oxide. The improvement in thermal annealing rate with positive electrode bias bears out this suggestion. Oxide charges are removed

eventually (after ≈ 1000 hrs) at 300°C but very quickly ( ≈ 15 mins) at 500°C. Interface states are completely removed at 300°C. Comparison of the isochronal anneal graphs of Zaininger for oxide charge and Snow et al for interface states suggests that there may be two different states contributing to the oxide charge, one of which has the same annealing behaviour as the interface states and is completely removed by 300°C, and the other which requires temperatures of 300-400°C to remove it. In addition Zaininger reports that damage can be removed completely by irradiating the damaged device under a slight negative bias.

A recently introduced technique for the removal of radiation damage in MOS devices is that of RF annealing[21], suggested by Ma & Ma. It is thought that the RF field interacts strongly with the centres at which the oxide charge is trapped and changes their state to give a more ordered $SiO_2$ structure. Electron-hole pairs are also generated and oscillate spatially in the $SiO_2$ under the action of the RF field, so that the probability of the free electrons recombining with trapped positive charge is high. An experiment has been done to compare the annealing of irradiated devices by the two methods, thermal and RF annealing. This shows that a 7.5 minute 500W RF anneal is equivalent to a 30 minute thermal anneal at 300-400°C, and that the temperature of the device during the RF anneal is less than 340°C.

### 4.2.10 Summary

To summarise, radiation damage is introduced into MOS devices at doses as low as $10^3$ rads (Si), and is evident in CCDs at doses greater than $10^4$ rads (Si). This damage is due to fixed positive charge in the oxide layer, and to interface states. Although investigations with MOS devices suggest that temperature annealing to 300-400°C restores device performance to its pre-irradiation level, there are no reports of similar annealing experiments on CCDs.

## SECTION 4.3 EXPERIMENTAL RESULTS ON RADIATION DAMAGE

### 4.3.1 Introduction

A series of experiments was performed to investigate the deterioration in performance of the CCD202 under bombardment with electrons of energies used in the electron microscope and hence to determine its useful lifetime as an electron imager. From the results of Killiany[8],

the performance should begin to worsen at $\approx 3 \times 10^4$ rads (Si), with increases in dark current and transfer inefficiency and a decrease in saturation voltage being the visible effects. Experiments were necessary to determine when these effects reduced image quality to an unacceptable level. In addition Killiany reports an improvement in device performance obtained by suitable adjustments of the clocking and bias voltages, and this effect was investigated.

In order to monitor damage effects a small area of the CCD was irradiated with electrons and the performance of the irradiated area was compared with that of the rest of the device after each irradiation. The CCD performance was studied under two sets of conditions. Firstly, the dark current in the irradiated area was measured at room temperature. Secondly, the transfer efficiency and saturation voltage were monitored by uniformly illuminating the whole device with light and comparing the output signal from electron irradiated cells with that of other areas. For this application a quantitative value of transfer inefficiency is not required and it is sufficient to determine the electron dose at which the characteristics of damaged cells become significantly different from those of other cells. Using light rather than electron irradiation to investigate the CCD performance has a two-fold advantage. Firstly, there is no further damaging exposure to the previously irradiated area, and, secondly, the unirradiated area which is used as control remains undamaged. As irradiation progressed the increased dark current masked the decrease in output signal due to transfer inefficiency, and so it became necessary to cool the CCD to $\approx -20^{\circ}C$ to allow independent measurement of the two effects.

### 4.3.2 Experimental Arrangement

The CCD was irradiated in the camera chamber of the JEM 100C. In the preliminary experiment the CCD was housed in the holder described in Section 2.2.1 and in all later experiments in that described in Section 2.2.2, which allows the device to be cooled. An AEI electron microscope objective aperture of 600 μm diameter was used to define the irradiated area. The aperture is made of molybdenum and the edge thickness varies linearly from 240 μm to 100 μm in the space of 200 μm.

The deflection system described in Section 2.3 was used to control the electron beam, with the beam being normally directed off the

CCD and being deflected onto the device during irradiation.

In these experiments the CCD was driven by the circuit described in Section 2.5 with a clocking rate of ≈ 1MHz, giving a readout time of 28 ms for 4 frames, and an irradiation time of 11.2 ms. The total cycle time was therefore approximately 40 ms. As described in Section 2.4 the electron dose on the CCD was monitored by the photomultiplier-based counting system with an aperture of the same type and size as that over the CCD being placed above the scintillator. The dose measured by the counting system is therefore equal to the dose collected on the irradiated area of the CCD. This figure allows calculation of the electron dose/photocell by noting the number of photocells and transport cells in which a signal could be seen during irradiation, and correcting for the different areas of the two cell types (18 x 30 μm for photocells, 22 x 60 μm for transport cells). This gives a figure of ≈ 350 photocell equivalents for the area of the apertures.

The number of electrons incident on the CCD is quoted in electrons/photocell in the remainder of this chapter. These units are convenient in practice in that they are simply calculated from the quantity measured by the counting system, and are more suitable than rads for describing imaging effects in electron microscopy.

To allow comparison of experimental results with those reviewed in Section 4.2 a comparison table from electrons/photocell to rads (Si) is given in Table 4.1 below:

| Electron Energy (keV) | Electrons/Photocell | Rads (Si) |
|---|---|---|
| 20 | 15.2 | 1 |
| 60 | 60 | 1 |
| 100 | 182 | 1 |
| 20 | $10^6$ | $6.6 \times 10^4$ |
| 60 | $10^6$ | $1.6 \times 10^4$ |
| 100 | $10^6$ | $0.5 \times 10^4$ |

TABLE 4.1

Conversion from electrons/photocell to rads (Si)

Throughout these experiments the output signal from the CCD was displayed on an oscilloscope to allow measurement of magnitude of the output signal and comparison of the signal from irradiated and unirradiated areas. Voltage measurements are average values across the

irradiated area resulting in errors of typically ± 0.1V (cf 2V saturation voltage).

Section 4.3.3 Preliminary Experiment on Dark Current Increase with Electron Dose

In a preliminary experiment to investigate damage effects the CCD was irradiated with 60 keV electrons. The electron dose on the device was increased gradually and no damage effect was seen up to a total dose of $\approx 10^5$ electrons/cell. After a further irradiation which increased the total dose to $2 \times 10^5$ electrons/cell a signal was seen in the irradiated area in all four frames in the absence of incident illumination being largest in frame 1, of equal size in frames 2 and 3 and smallest in frame 4. The signal was initially 14% of saturation in frame 2, but decreased to 10% when the CCD was returned to room temperature by allowing air into the camera chamber, and decreased further to 5% overnight with the device switched off and at room temperature. The temperature dependence of the signal suggests that it is dark current. That permanent damage has occurred is borne out by the fact that the dark current is still apparent after the device has returned to room temperature. Dark current caused by local heating alone would have disappeared in this time.

The CCD was next irradiated with seven doses of $\approx 10^5$ electrons/photocell and the dark current after each dose was monitored, both immediately after irradiation and at some time later when the dark current had come to a steady value (approximately 30 minutes). At the end of the experiment, after a total dose of $7.7 \times 10^5$ electrons/photocell (approximately $2 \times 10^4$ rads (Si)), the dark current at room temperature had increased to 17% of the saturation output voltage. Since in electron imaging mode the CCD will receive spatially non-uniform illumination and will therefore have a spatially non-uniform dark current a signal of this size makes the CCD unusable at room temperature. Experiments were therefore performed to investigate the effect of cooling on the CCD dark current.

4.3.4 Cooling CCD to reduce Dark Current

The CCD was placed in the ice box of a refrigerator (Tricity Polarfrost 5), inside a polythene bag to avoid icing on the device surface, and the temperature inside the bag was monitored using a Cu/Cu-Ni thermocouple with a Comark electronic thermometer type 1625. Cooling the CCD to $-11.5^{\circ}C$ considerably reduced the dark current in the irradiated area to 0.5% of the saturation voltage. The dark

current reappeared when the device returned to room temperature.

As a result of this experiment a cooling system was built to house the CCD in the electron microscope. This is described in Section 2.2.2 and was used in all the dark current experiments described hereafter.

A second area was irradiated with 60keV electrons to give a total dose of $2.1 \times 10^6$ electrons/photocell. The room temperature dark current at the end of this irradiation was 30% of the saturation output voltage. The effect of cooling on dark current was measured in this area with the CCD temperature monitored by a thermocouple in contact with the ceramic base of the device. The CCD was under vacuum in the JEM 100C camera chamber to avoid icing during the cooling process. The results of this experiment are shown in figure 4.1. The saturation output voltage is 2V in this case. The graph does not seem to be tending to 0V, but this is a result of the arbitrary choice of origin from which the voltage is measured. At $-2^{\circ}C$ there was no obvious difference in dark current between irradiated and unirradiated areas. A graph of log V vs 1/T gives a linear relationship with a characteristic energy of $1.4 \pm 0.1$ eV.

### 4.3.5 Experiments on CCD Dark Current

The increase in dark current with irradiation does not affect the CCD's potential as an electron imaging device because it can be made negligible by cooling the device to temperatures near $0^{\circ}C$. However the increase in dark current is a measure of the amount of damage which has occurred and so was included in a set of experiments to measure the effect of incident electron energy on degradation rate. These experiments were performed at 3 electron energies of 20, 60 and 100keV. As before, an aperture over the CCD defined a small irradiated area of $\approx$ 350 photocells, with the aperture being moved to a new area for each electron energy. The CCD was cooled to $\approx -20^{\circ}C$ during irradiation to avoid saturating the device with the combined dark current and electron signals. After each irradiation the CCD was heated to room temperature and the dark voltage measured.

The main points arising from the results of these experiments are:

1. Under bombardment with electrons in the energy range 20-100keV the dark current in the CCD increases with irradiation until the point is reached where the dark current saturates the device.

2. The rate at which the CCD dark current increases with dose is a function of incident electron energy, with damage occurring most

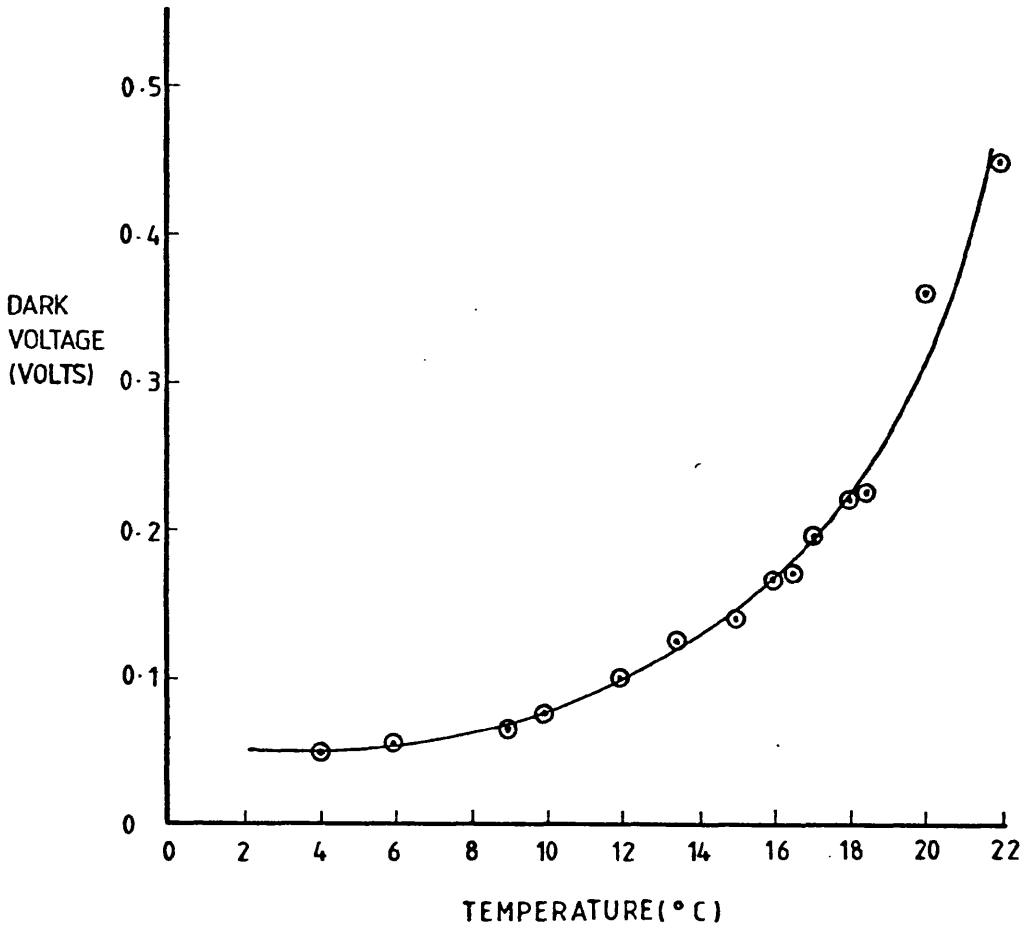


Figure 4.1 Effect of cooling on CCD dark voltage

quickly with lower energy electrons. Figure 4.2 shows the dark current increase with dose for the 3 electron energies. The electron dose required to half-fill the photocells is $1.4 \times 10^6$, $3.0 \times 10^6$ and $4.7 \times 10^6$ for 20, 60 and 100 keV electrons respectively under the conditions of Section 4.3.2.

The energy dependence is consistent with the damage models described in Section 4.2 in which dark current is attributed to an increase in the number of states at the Si-$SiO_2$ interface. The amount of energy deposited by an electron within a given distance is a function of its energy, and there are several empirical formulae by which this can be calculated. The Thomson-Whiddington law is one such formula which is commonly used in electron microscopy[22]. It states that for an electron with initial energy $E_o$, the energy $E_x$ remaining after traversing a distance X of material is $E_x = E_o \sqrt{1 - X/R_m}$ where $R_m$ is the range of the electron in the specific material.

Knowledge of the thicknesses of the electrode and oxide layers of the CCD202 would enable calculation of the energy deposited in the channel oxide layer between electrode and substrate. Although full information is not available from the manufacturer, a rough calculation can be made of the energy deposited in the channel oxide by taking its thickness as 0.1 μm[8], and ignoring electron energy loss in overlying layers (See Section 1.3.3 for device structure). The ranges of 20, 60 and 100keV electrons in $SiO_2$ are taken to be 2, 20 and 60 μm respectively[23]. This gives the energy deposited in the oxide as 0.5, 0.15 and 0.09keV for 20, 60 and 100keV electrons respectively, suggesting, for example, that a 20keV electron deposits six times more energy in this region than does a 100keV electron, and so should increase dark current six times faster.

As the damage to the CCD increases, a difficulty arises in separating the effect of dark current from that of transfer inefficiency. The dotted lines on the 20keV and 60keV curves of Figure 4.2 correspond to the doses at which the dark current signal becomes greater than the maximum usable output voltage (See Section 4.3.6 for explanation). Measured dark voltage for doses above the dotted line are lower than the true value since not all of the dark current produced by the device is transferred out as signal. For the 100keV curve this point occurs at $1.3 \times 10^7$ electrons/photocell and so is not shown.

Thus the results of these experiments show that dark current increases with electron dose and that damage occurs most rapidly for low energy electrons in a manner consistent with the proposed damage mechanisms.

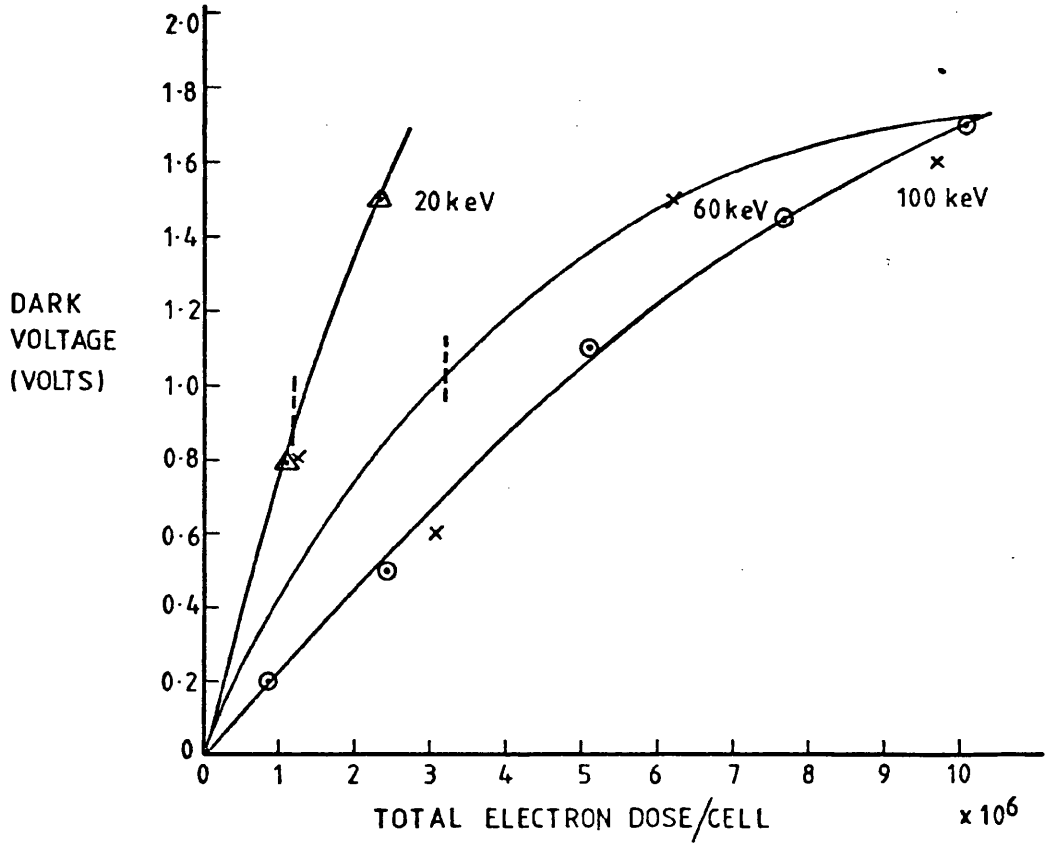


Figure 4.2 Radiation damage in CCD: increase in dark current with total electron dose (dotted line shows electron dose at which dark current becomes greater than maximum usable output voltage)

### 4.3.6 Preliminary Experiments on Decrease in Transfer Efficiency with Electron Dose

The object of this experiment was to detect any change in the response of irradiated cells to an electron or photon signal when compared with the response of previously unirradiated cells. The method by which this was done is described in Section 4.3.1.

Throughout these experiments the CCD was cooled (typically to -20°C) using the cooling system described in Section 2.?.2 to allow the output signal to be studied independently of the dark current. The electron energy used in this preliminary experiment was 60keV. The main points arising from these investigations were:

1. After a significant electron dose $\approx 1.5 \times 10^6$ electrons/photocell the output signal from electron irradiated cells is lower than that from other cells when the CCD is uniformly illuminated with light. The difference in output signal in the 2 areas under photon illumination becomes progressively larger as the total electron dose increases.

2. The efficiency with which the damaged area can transfer charge depends on the height of the output signal and therefore on the size of the charge packet which is being transferred. If the photon illumination on the CCD is low, producing a low output signal, the damaged cells appear to behave normally, producing the same magnitude of output signal as other cells. As the illumination is increased, the output signal in all cells increases until a point is reached where the output from damaged cells fails to increase at the same rate as that of other cells. A relatively lower output signal is then observed in the damaged cells and the discrepancy between damaged and undamaged cells increases as the illumination is increased. Figure 4.3 is an oscilloscope photograph of the output of a horizontal row of the CCD in a damaged area showing a normal output for a small signal, and a lower output in the damaged region for a large signal.

3. The performance of the damaged cells can be improved by increasing the voltages $\phi v$ and $\phi p$ which transfer the charge out of the CCD. For example, after a totaldectron dose of $2.2 \times 10^6$ electrons/cell, the damaged area behaved normally if the vertical clocking voltage $\phi_{V\ high}$ was greater than 2.8V, but became inefficient, exhibiting the effect described in (2) above, if $\phi_{V\ high}$ was smaller than 2.8V. A similar effect is seen with $\phi p$, the

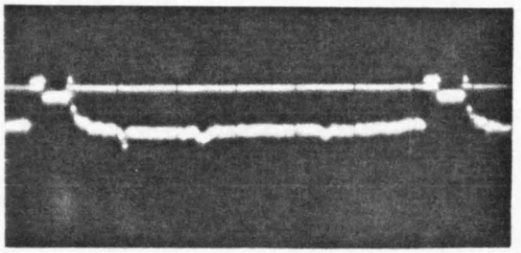

a) small signal

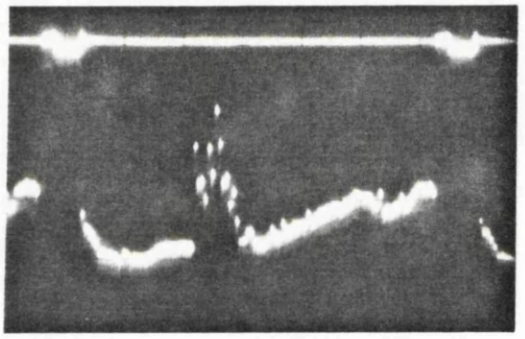

b) large signal

Figure 4.3: Output of horizontal row of CCD in damaged area.

a) small signal - output signal normal

b) large signal - note lower output signal in damaged region.

Photogate voltage. A 'threshold clocking voltage' can be defined for each of $\phi_V$ and $\phi_p$ which is the magnitude of the clocking signal required to achieve efficient transfer. As damage progresses the 'threshold clocking voltage' increases for both $\phi_V$ and $\phi_p$ until it becomes greater than the maximum clocking voltage provided by the Fairchild driver board. As a result of the effect described in (2) the magnitude of the threshold clocking voltage is a function of the height of the output signal.

### 4.3.7 Effect of Electron Irradiation on Threshold Clocking Voltage

An experiment was performed to obtain quantitative results on how the threshold clocking voltages of the CCD increase with electron dose. The experiment was done at three electron energies, 20, 60 and 100keV. After each irradiation the threshold clocking voltage for $\phi_V$ and $\phi_p$ was measured for three different output signal levels, namely 0.5V, 1.0V and 1.8V (Saturation Voltage = 2V). $\phi_V$ was held at 0-6V while the threshold value of $\phi_p$ was being measured and vice versa. Figures 4.4a and b show respectively the variation in the threshold value of $\phi_V$ and $\phi_p$ as electron dose increased for an output voltage of 40% of saturation. Clearly the threshold voltage increases with dose, until it eventually becomes greater than the maximum voltage of IOV supplied by the CCD driver board. The broken lines on figures 4.4a and b show the same effect for an output of 72% of saturation demonstrating that a larger threshold voltage is required to clock out higher signals. The energy dependence of the threshold voltage curve with dose shows again that the CCD damages most quickly under 20keV irradiation and most slowly under 100keV irradiation.

From these experiments the CCD behaves normally for the longest time if both $\phi_V$ and $\phi_p$ are set at their maximum levels. Both signals were therefore set at 0-10V. With the signals at this level, a maximum usable output voltage can be defined which is the voltage below which the output from irradiated and unirradiated cells is the same, and above which irradiated cells produce a lower signal than others.

### 4.3.8 Change in Maximum Usable Output Voltage with Electron Irradiation

The maximum usable output voltage was measured as the total electron dose increased, again for 20, 60 and 100keV electrons. $\phi_V$ and $\phi_p$ were set to 0-10V for this, and the measurements were made on frame 2. The CCD was uniformly illuminated with light and the output

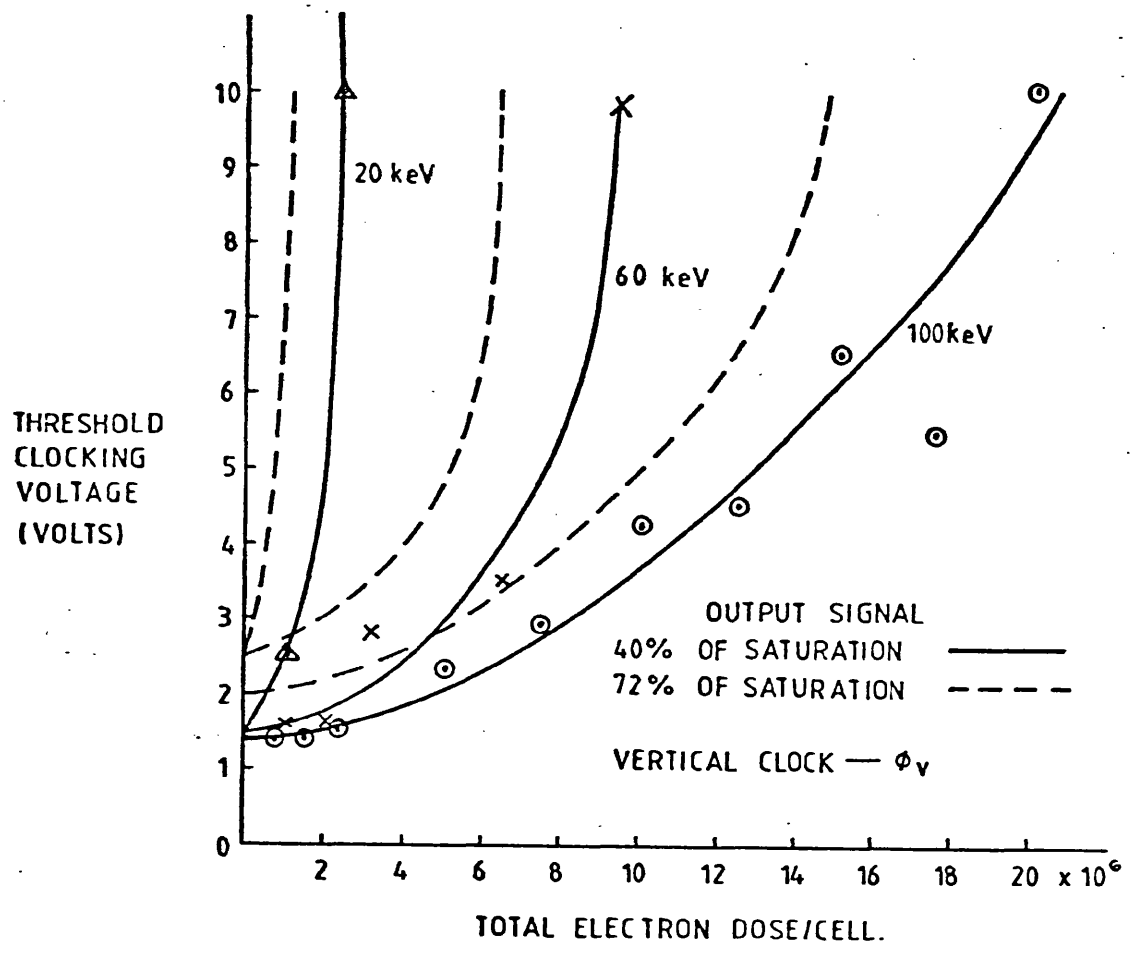


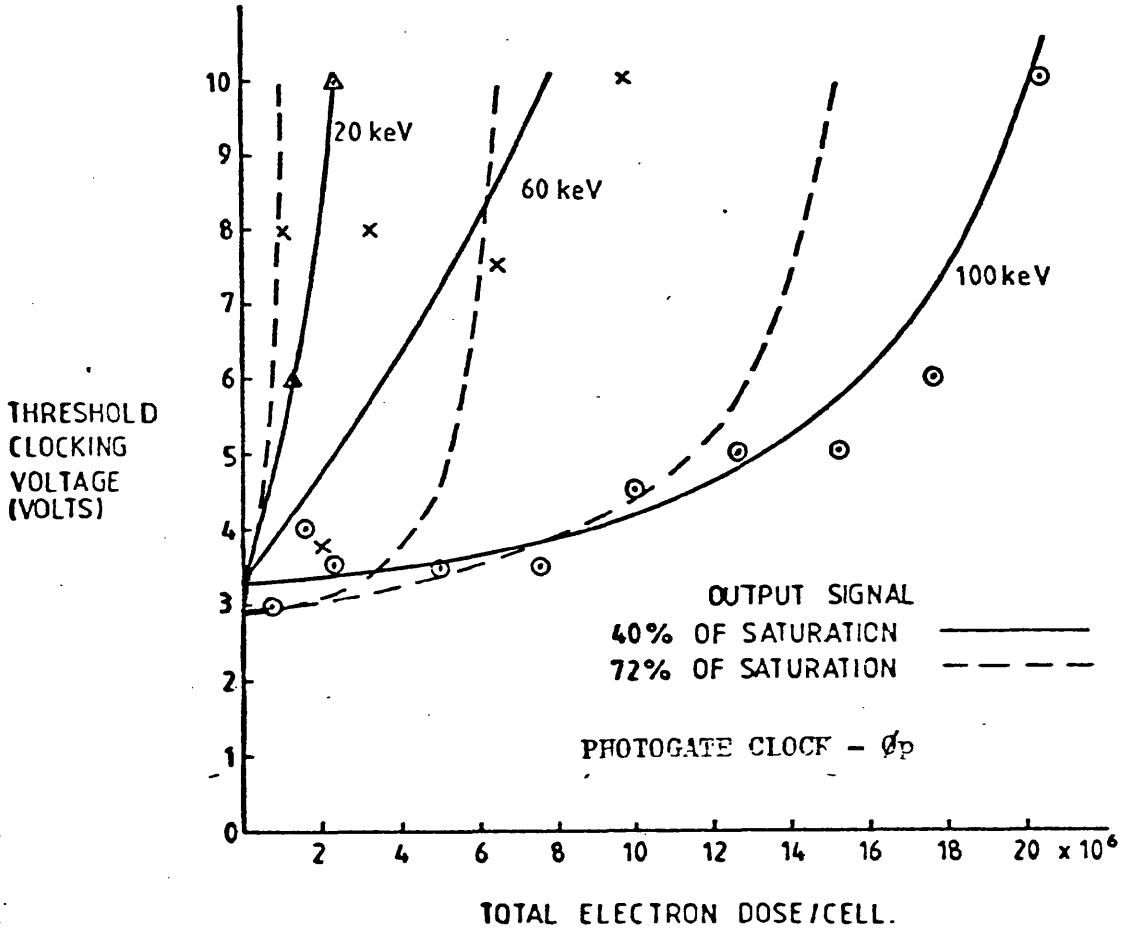


Figure 4.4: Radiation damage in CCD: Clocking voltage required to give normal output signal against total electron dose for various electron energies.

of a horizontal line was displayed on an oscilloscope. To determine the maximum usable output voltage the LED intensity was increased until the output voltage from the irradiated area first became lower than that of other areas. The experimental error in the maximum usable output voltage is $\pm$ 0.1V, arising from the difficulty in deciding when the output from damaged cells first becomes different from that of other cells. The results of this experiment are shown in figure 4.5.

The maximum usable output voltage falls with total electron dose as expected, and again falls more quickly as the incident electron energy decreases. The implication of this result is that as total electron dose increases, the size of signal that the CCD can collect and transfer normally decreases until a point is reached at which the device is no longer usable. Arbitrarily choosing this point to be when the maximum usable output voltage falls to half of its pre-irradiation value, this gives the CCD 202 the lifetimes shown in the table below for the three electron energies:

| Electron Energy (keV) | 20 | 60 | 100 |
|---|---|---|---|
| Lifetime (electrons/photocell) | $2 \times 10^6$ | $6 \times 10^6$ | $1.5 \times 10^7$ |
| Number of Images | $2 \times 10^3$ | $6 \times 10^3$ | $1.5 \times 10^4$ |

TABLE 4.2
Lifetime of CCD 202 for electrons of various energies

The second row in the table shows the number of images which can be produced within the lifetime of the device. This assumes that $10^3$ electrons/picture element is required to produce an acceptable image. This figure of $10^3$ arises because the shot noise in this number of electrons is 3%, the level below which contrast variations are not detectable by the human eye. This noise level is also a typical figure for satisfactory image processing.

These lifetimes, while showing that a CCD can produce a large number of images before the maximum usable output voltage is greatly reduced, restrict the range of possible applications of CCDs in electron microscopy. If the CCDs are to be used for locating the area of interest in the specimen and for viewing the image during focusing and adjustment, they will receive a considerably greater electron dose than if they are used solely for recording images. This continuous

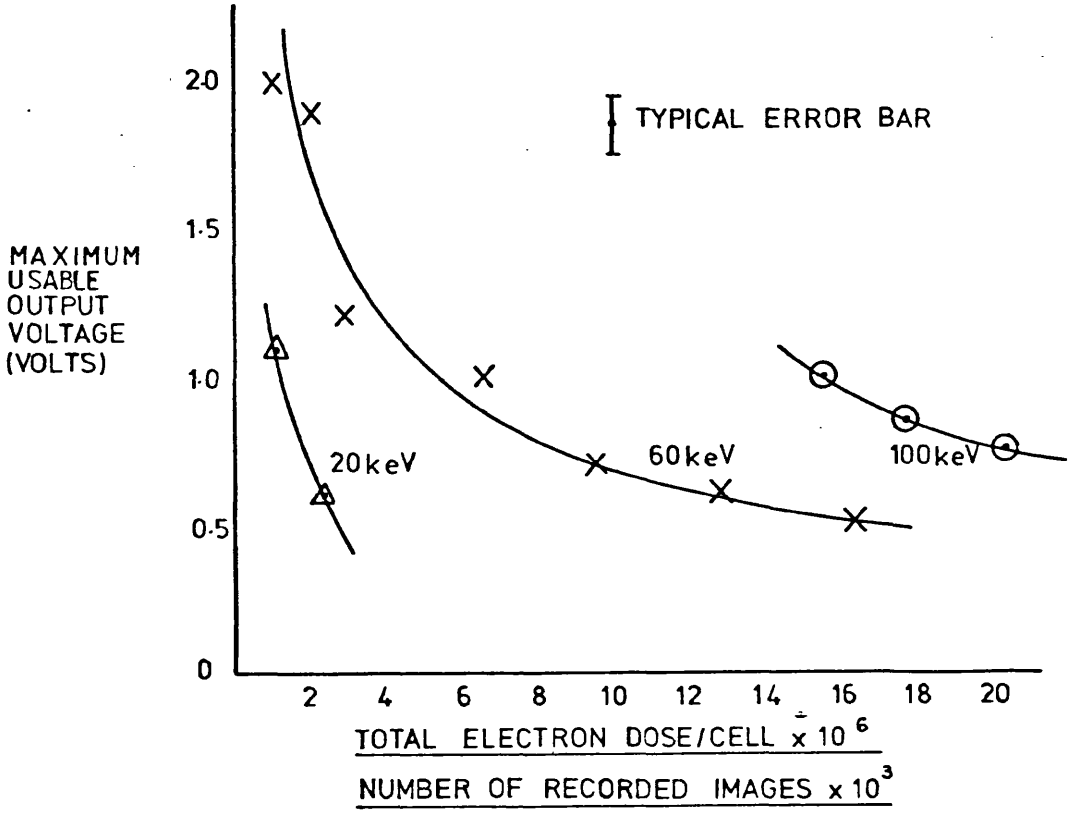


Figure 4.5 Radiation damage in CCD: Maximum usable output voltage against total electron dose for various electron energies. Figure for number of recorded images assumes $10^3$ electrons/photocell are required to produce a satisfactory image

mode of operation is particularly attractive in the field of radiation sensitive materials, for the reasons given in the Introduction and its routine use is at present precluded by the device lifetime. In summary, with these lifetimes CCDs are of use as recording devices giving a quantitative output, but a radiation hard device with a longer lifetime would widen their scope in electron microscopy.

### 4.3.9 Effect of Irradiation on CCD Gain

In earlier experiments (See Section 3.2.2 ) the output voltage of the CCD was shown to be linear with the number of incident electrons/cell. From the above results which show that after irradiation the CCD output is the same for damaged as for undamaged regions up to the maximum usable output voltage and is less thereafter, the gain is clearly reduced in the region beyond maximum usable output voltage. An experiment was done to investigate this in which the gain of the CCD for 60keV electrons was measured before it had received any significant irradiation and was remeasured after irradiation.

Figure 4.6 shows the change in CCD gain with irradiation for an area irradiated with $9.7 \times 10^6$ electrons/photocell. The post-irradiation curve follows the original until the output voltage increases to 0.7V, and thereafter has lower gain. The figure of 0.7V is equal to the maximum usable output voltage which was measured with the CCD illuminated by light, confirming that measurements of this quantity made with light are applicable to electron illumination.

This result is in agreement with the observed differences in output from irradiated and unirradiated cells described in Section 4.3.6 and shown in figure 4.3. Because of the scatter of experimental points it is not possible to say whether the curve is linear for output signals greater than the maximum usable output voltage.

### 4.3.10 Irradiating CCD under Negative Bias

The literature on radiation effects on MOS systems reports that the effects of positive charge build-up in the oxide can be minimised by negatively biasing the metal electrode during irradiation (See Section 4.2.1). This causes the positive charge to collect at the metal-insulator interface where it has a smaller effect on device performance than charge at the insulator-semiconductor interface. In an n-buried channel CCD the large positive potential applied to deplete the buried channel ensures that the electrode is negatively biased with respect to the semiconductor. However this negative bias

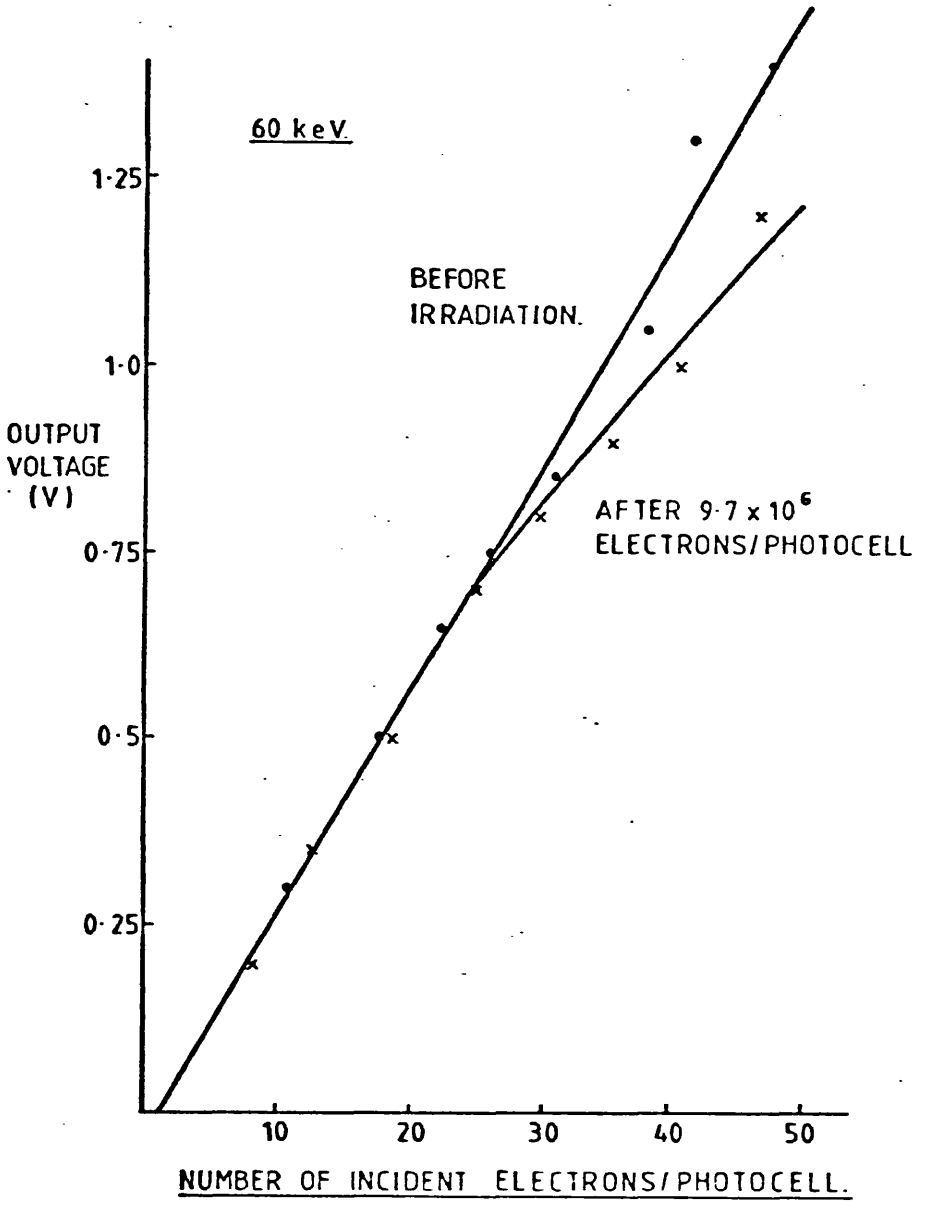


Figure 4.6: Non-linearity in CCD output caused by radiation damage. The point at which the 2 curves diverge is the maximum usable output voltage.

can be increased by applying negative clocking voltages to the electrodes, and this was done in the following experiment in an attempt to reduce the rate at which damage occurred in the CCD.

The experiment was performed in the same way as those described previously, but in this case the values of $\phi_v$ and $\phi_p$ were set at -6 to 0V during irradiation instead of 0 to +6V as before. The change in maximum usable output voltage with electron dose was used to monitor the radiation damage. No significant difference could be seen in the damage rates in positively and negatively biased areas, and it was concluded that negative bias on the electrodes does not reduce the rate at which the CCD damages.

4.3.11 Explanation of Results

The increase in dark current with total electron dose is simply explained by the increase in the number of interface states with irradiation as described in Section 4.2.5. However the decrease in transfer efficiency with dose requires further explanation. The transfer inefficiency is manifest as an inability of the CCD to transfer large charge packets efficiently, although transfer is normal for signals less than some maximum usable output voltage. There are several possible explanations for this:

1. Charge may be trapped in interface states, the number of which has certainly increased as shown by the large increase in dark current. This is the main cause of transfer inefficiency in surface channel devices, and since a buried channel CCD behaves as surface channel for large signals, with some charge being transported at the interface, interaction with interface states may occur. Small charge packets would not be affected since they are transported in the bulk of the channel and are not in contact with the interface states. However it is known (Section 4.3.7) that increasing the electrode bias voltages so that they have a more positive voltage during the charge collection phase improves performance by increasing the maximum usable output voltage. It is shown in Appendix 2 that increasing bias voltage moves the potential minimum closer to the interface, which should cause more interaction of minority carriers with interface states and should increase the charge loss. This explanation therefore seems unlikely.

2. When charge is added to a potential well in a buried channel device, the volume of the region of the n-channel used for charge storage increases, and saturation is reached when the edge of the

storage region reaches the interface[16]. In Appendix 5 it is shown that the amount of charge which can be stored before this occurs decreases as $V_B$, the electrode bias voltage, increases. The positive charge created in the $SiO_2$ insulator by electron bombardment behaves as a positive bias increase and may have the effect of causing the CCD to saturate at lower signal charges. However, once again the improvement in performance achieved by increasing the bias voltages disproves this theory, since a bias voltage increase should also reduce the saturation charge.

3. The positive charge induced in the $SiO_2$ layer by electron bombardment causes an increase in the effective bias voltage applied to the cell electrodes. If the increase in positive bias causes an unequal increase in $V_m$, the minimum potential, under wells with different initial bias voltages this will result in distortion of the potential wells which may cause a decrease in saturation charge. However, in Appendix 4 it is shown that for 2 wells with different initial bias voltages an equal increase in the bias voltage in both wells will result in an unequal increase in $V_m$, with the increase being greater for the cell with the higher initial value. Thus the voltage difference between the potential minima in 2 cells increases if a positive bias offset is added. This mechanism therefore predicts that trapping of positive charge in the oxide layer will cause an increase in the amount of charge which can be stored in the CCD. Thus this explanation is not consistent with the observed facts.

4. The final possibility is that suggested by Killiary et al[8] (Section 4.2.4). The positive charge trapped in the oxide layer causes field induced channelling in the undoped polycrystalline silicon interelectrode isolation. This reduces the resistance between adjacent electrodes at different potentials and allows the clocking waveforms to become mixed. Figure 4.7 shows the capacitance model for two adjacent CCD cells. $V_0$ and $V_1$ are the voltages produced by the power supplies to the two electrodes and r is the internal impedance of the supplies. $\mathcal{Z}$ is the impedance of the polysilicon isolation and $V_0'$ and $V_1'$ are the bias voltages on the insulator surface. The voltage drop across $\mathcal{Z}$ is:

$$V_1' - V_0' = \frac{\mathcal{Z}}{\mathcal{Z} + 2r} \quad (V_1 - V_0)$$

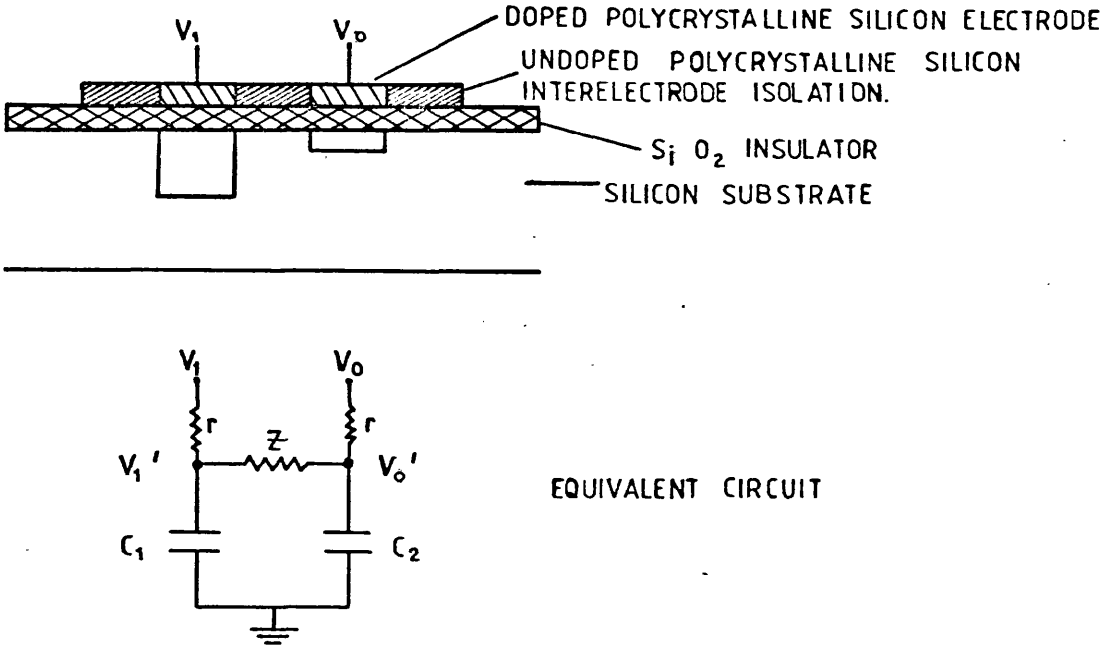


Figure 4.7: Diagram of CCD 202 and equivalent circuit showing how the inter-electrode isolation affects the surface voltages $V_1$ and $V_6$ on CCD cells.

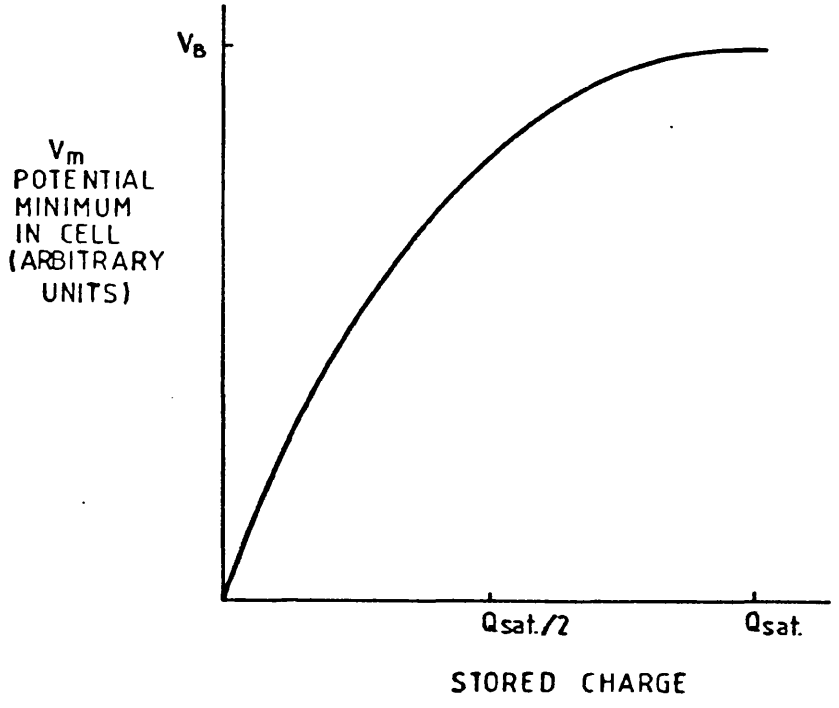


Figure 4.8: Variation of depth of potential minimum Vm with stored charge for a buried channel CCD (ref. Hobson)

If $Z$ is very large, as it is before irradiation, then

$$V_1' - V_o' = V_1 - V_o$$

and the bias voltages applied to the cells are those provided by the power supply. However if channelling occurs and $Z$ is low, then $V_1' - V_o'$ tends to zero as $Z$ tends to zero. As a result the bias voltages to the two cells become almost equal and the values of $V_m$, the potential minima in the cells also become equal. Charge will therefore spill from one cell to the next at low signal charges. The potential difference between the cells can be increased by increasing $V_1 - V_o$, so improving the potential profile. This explanation is again consistent with the observed results.

While the last explanation accounts for loss of signal due to spillage of signal charge to adjacent cells, it suggests that a sharp cut-off in output charge will occur below which the device is normal but above which no more charge can be transferred. However that this is not the case can be seen from the graphs of voltage output against number of incident electrons which show an increase, although a non-linear one, in output voltage against number of incident electrons above the maximum usable output voltage. This occurs in the following way. The variation of $V_m$, the minimum potential, with stored charge is not linear for a buried channel CCD but has the form shown in Figure 4.8. Saturation for the damaged CCD occurs when the stored charge increases $V_m$ to the point where it is equal to the $V_m$ of a neighbouring cell which does not have an applied bias voltage and therefore should not store charge. At this point, if an amount of charge is added to the original cell it will not all be stored there but will be shared between it and the neighbouring cell. This extra charge will increase the potential minimum $V_m$ of both cells, and the relative amounts of charge stored in the cells will be such as to maintain their equal values of $V_m$. Since the collecting cell contains more charge than the other, its increase in $V_m$ with stored charge will be smaller (see Figure 4.8) and it can therefore store more charge for an equal increase in $V_m$. Therefore more than half of the additional charge added after maximum usable output voltage is reached is retained in the original cell. This is consistent with the gain results obtained for irradiated areas (Section 4.3.9).

### 4.3.12 Summary

In summary, two main damage effects are seen in the Fairchild CCD202 as a result of electron irradiation in the electron microscope.

The first is an increase in dark current with total electron dose sufficient to half fill the potential wells of the CCD at a dose of typically $3 \times 10^6$ electrons/cell. This effect, while rendering the CCD unusable at room temperature, can be made negligible by cooling the device to $\approx 0^{\circ}C$ and so does not limit the useful lifetime of the device. These results apply to a CCD cycle time of 40 ms.

However the second manifestation of radiation damage, a decrease in the maximum usable output voltage as total electron dose increases, does restrict the CCD lifetime. The lifetime varies with electron energy but is typically $\sim 10^7$ electrons/photocell.

## SECTION 4.4 EXPERIMENTS TO REMOVE RADIATION DAMAGE IN CCD202 BY ANNEALING

### 4.4.1 Introduction

The reports of removal of radiation damage from MOS devices by heating to temperatures greater than 150°C (Section 4.2.9) led to an experiment to see if the same techniques could be applied to radiation damage in the Fairchild CCD202. The manufacturer's specifications quote a maximum storage temperature of 100°C, so the effect of elevated temperatures on the device packaging was uncertain before the experiment took place. A series of preliminary experiments were done in which the device was heated to temperatures within and slightly above the specification, culminating in a 4-hour anneal at 100°C. No improvement in transfer efficiency or dark current was seen after this anneal and it was necessary to exceed the manufacturer's specifications in subsequent experiments.

### 4.4.2 Experimental Arrangement

The CCD was heated under vacuum for one hour at temperatures of 150°C, 180°C, 208°C, 208°C again and 238°C, and in nitrogen for one hour at 238°C, 270°C, 300°C, 330°C and 370°C. The series of experiments under vacuum were performed in a Townson and Mercer vacuum oven with the temperature measured by a thermometer placed within the oven insulation. The second series in nitrogen was done in a furnace and the temperature measured with a thermocouple before the CCD was inserted. A slow nitrogen flow ( $\lesssim 0.3$ litres/minute) was passed over the device during annealing. The performance of the CCD was monitored after every anneal to detect whether any improvement had occurred. The CCD used in this experiment was that used in the radiation damage experiments described

in Section 4.3 and so contains seven damaged areas which have received various total doses at electron energies of 20, 60 and 100keV. This allows comparison of the dependence of the annealing temperature required to remove damage on the energy of the damaging radiation and the total dose.

The dark current at room temperature was measured for all the irradiated areas after each anneal at temperatures greater than 180°C (this was not done for the first two anneals at 150°C and 180°C). The maximum usable output voltage was measured for all seven areas for all but the first two anneals. In addition, oscilloscope photographs were taken of the scan across one line after each anneal at room temperature to show dark current, and cooled and illuminated to show transfer inefficiency. The CCD was not annealed to temperatures greater than 370°C because there were signs of new damage appearing after this anneal (See Section 4.4.5).

In the experiments described in this section the CCD driver system described in Section 2.1.3 which was used for previous experiments in this Chapter is replaced by the driver and accumulation system described in Section 2.2.6 . As a result the irradiation time and readout time are different from those of previous sections resulting in a different dark voltage for the same device dark current. In graphs where data obtained using both systems is presented the values of dark voltage obtained with the old system have been converted to those which would have been obtained with the new system. In addition, bypassing the amplifier on the Fairchild driver board SL61268 in the new system has resulted in the measured output voltage being smaller by a factor of two and as a result saturation occurs at a value of 1V.

### 4.4.3 Results of Annealing Experiments - Temperature required to remove Dark Voltage

From the results of the preliminary experiments anneals at temperatures less than 100°C produce no improvement in device performance. However the results of the experiments described in the previous section show that annealing to $\approx$ 330°C was sufficient to remove dark current from all the damaged areas of the CCD. Figure 4.9 shows oscilloscope photographs of the output of the same horizontal line of the CCD taken after successive anneals. The decrease in dark current after each anneal can be clearly seen. This line passes through two regions which had been irradiated, with cells 32 - 46 receiving a dose of $17.7 \times 10^6$ 60keV electrons, and cells 80 - 94 a dose of $7.2 \times 10^6$ 60keV electrons. In addition, dark current overflowing from

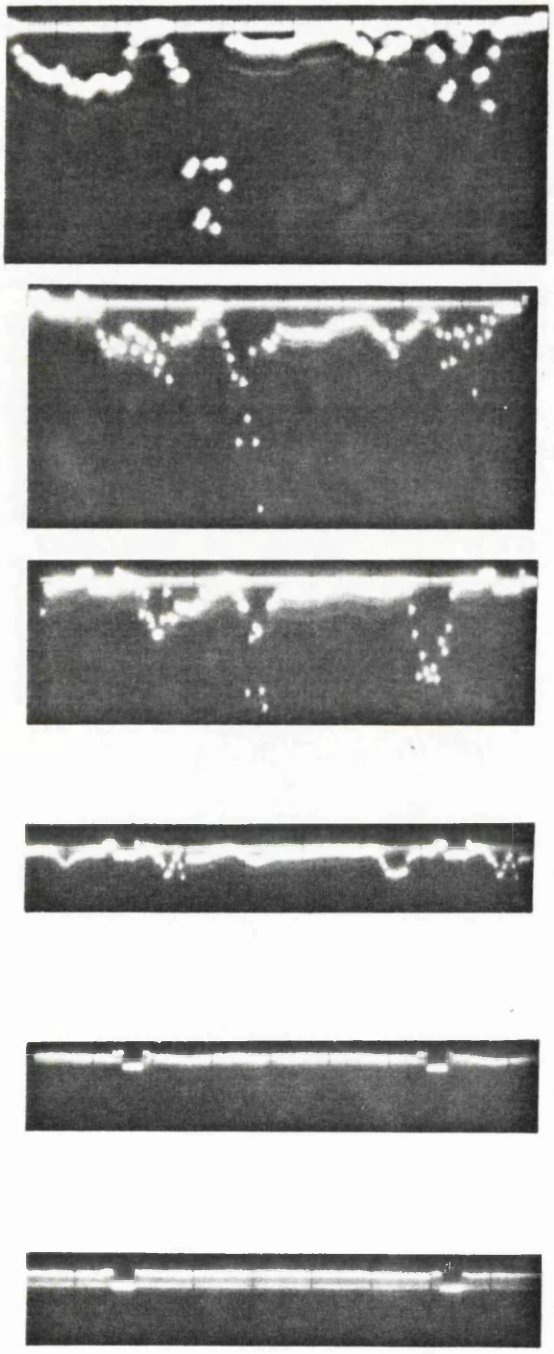


Figure 4.9: Output of horizontal row in damaged area taken after successive anneals, showing the decrease in dark current in the damaged area as annealing proceeds. The most heavily damaged region had received a dose of $17.7 \times 10^6$ electrons/photocell.

other damaged areas is seen in cells 6 - 30. After a one hour anneal at 150°C a small decrease in dark current could be discerned from the line photograph and a further small decrease was noted after the one hour 180°C anneal. A large decrease in dark current (by a factor of $\simeq$ 3) occurred after the 210°C anneal, and a further large decrease after the 240°C anneal. At this point almost all dark current had been removed, and a further anneal to 270°C reduced the dark current to an unmeasurable level ( $< \frac{1}{2}\%$ of saturation) in all but one area.

Comparison of three areas previously irradiated with 60keV electrons at various total doses shows the effect of previous dose on the rate of removal of dark current. The dark voltage after anneal is greatest for the area with highest previous electron dose, but all the damage in all three areas is removed by annealing to the same temperature. Therefore, regardless of previous dose, an anneal to 270°C is sufficient to remove dark voltage caused by bombardment with 60keV electrons. This is shown in figure 4.10(a).

It is difficult to determine the effect of electron energy on the rate at which dark current is removed by annealing because no areas have been irradiated to the same electron dose at different energies. Figure 4.11(a) shows three areas which have approximately equal dark voltages before annealing but have received different electron doses at different energies. The damage in all three areas is removed by 330°C. The area previously irradiated with 100keV electrons seems to require a higher temperature to remove the dark voltage, but it is not clear whether this is truly energy dependent or is simply a result of the very high electron dose received by this area.

### 4.4.4 Results of Annealing Experiments - Temperature required to improve Maximum Usable Output Voltage

No improvement in the maximum usable output voltage (as defined in Section 4.3.7) was achieved by the preliminary anneal to 100°C. In the experiments reported here, annealing to 370°C increased the maximum usable output voltage to the saturation voltage in almost all areas, so restoring the device performance.

Some improvement in maximum usable output voltage occurs after the first anneal to 150°C, and a further improvement occurs after 180°C, 210°C and 240°C. A further anneal to 270° results in a considerable improvement in efficiency, and the CCD output is restored almost to normal after the final anneal at 370°C. Figure 4.12 shows oscilloscope photographs of a line of output as the performance

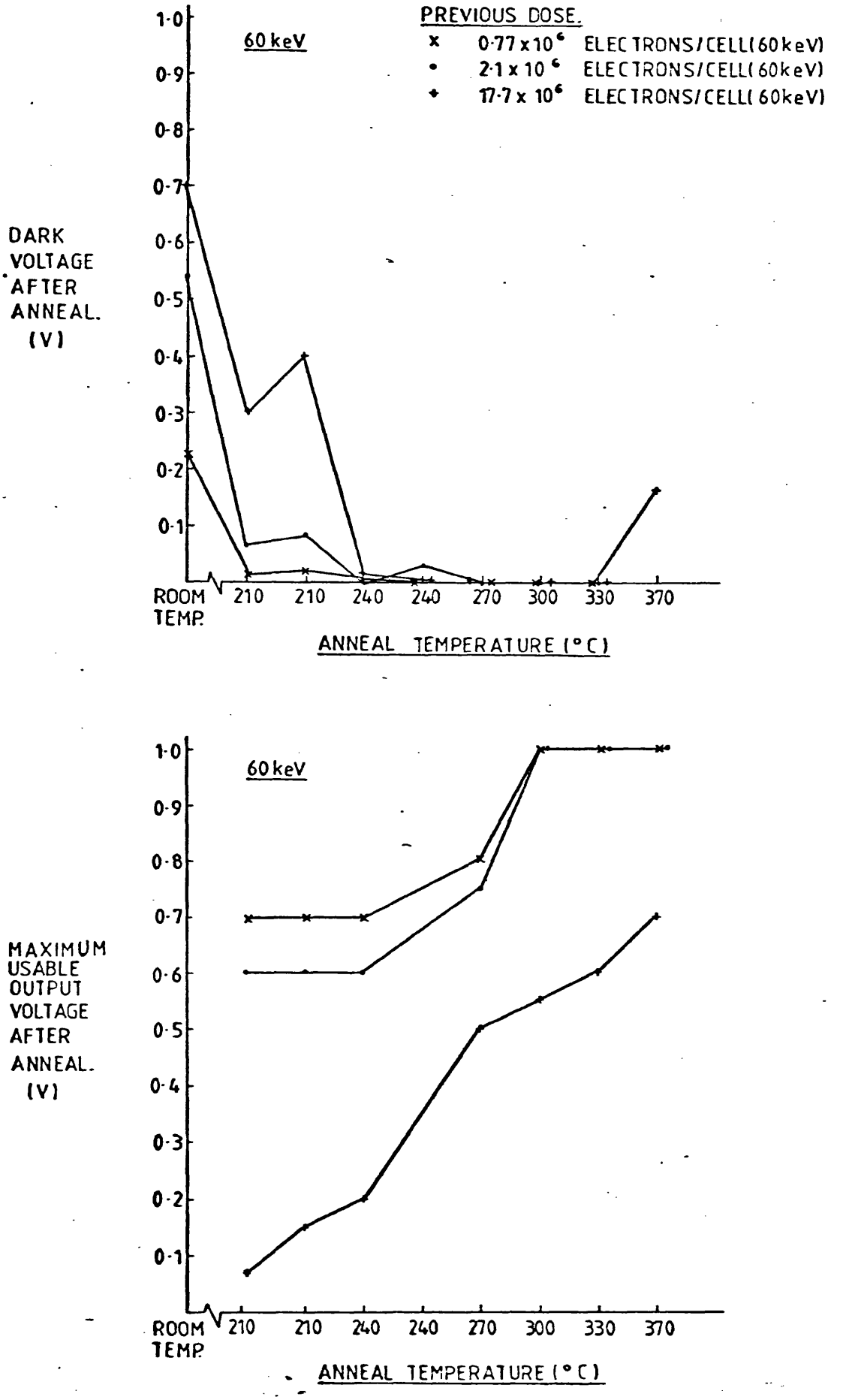


Figure 4.10: Improvement in CCD performance with annealing, showing dependence on previous electron dose.

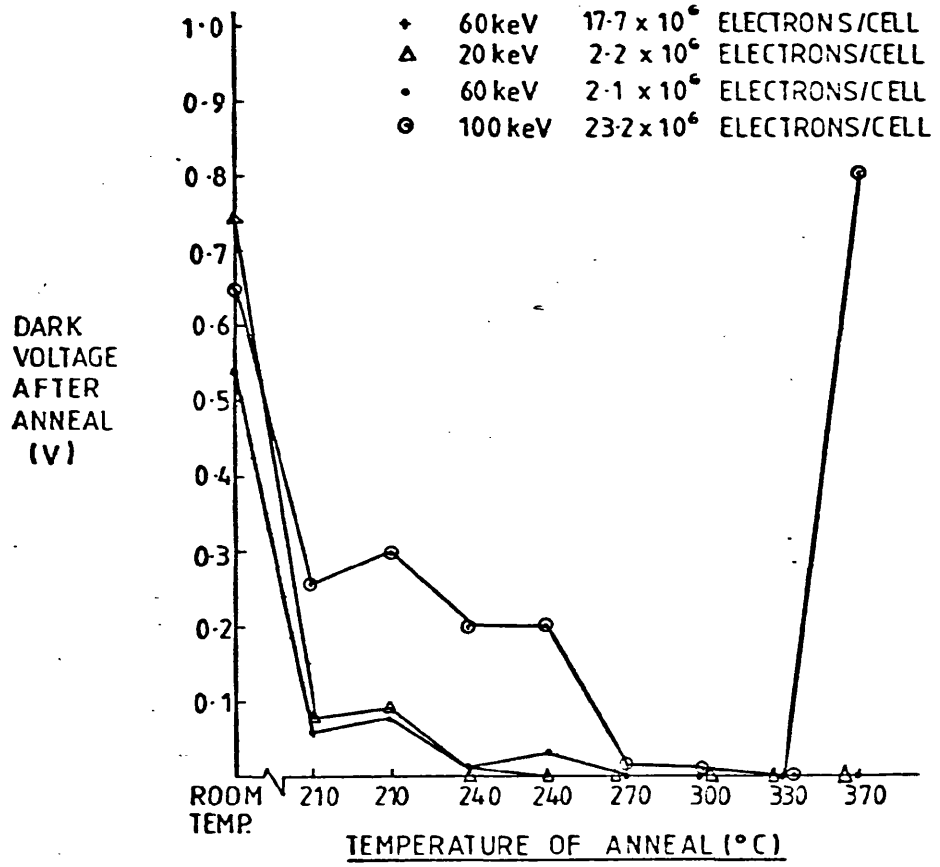


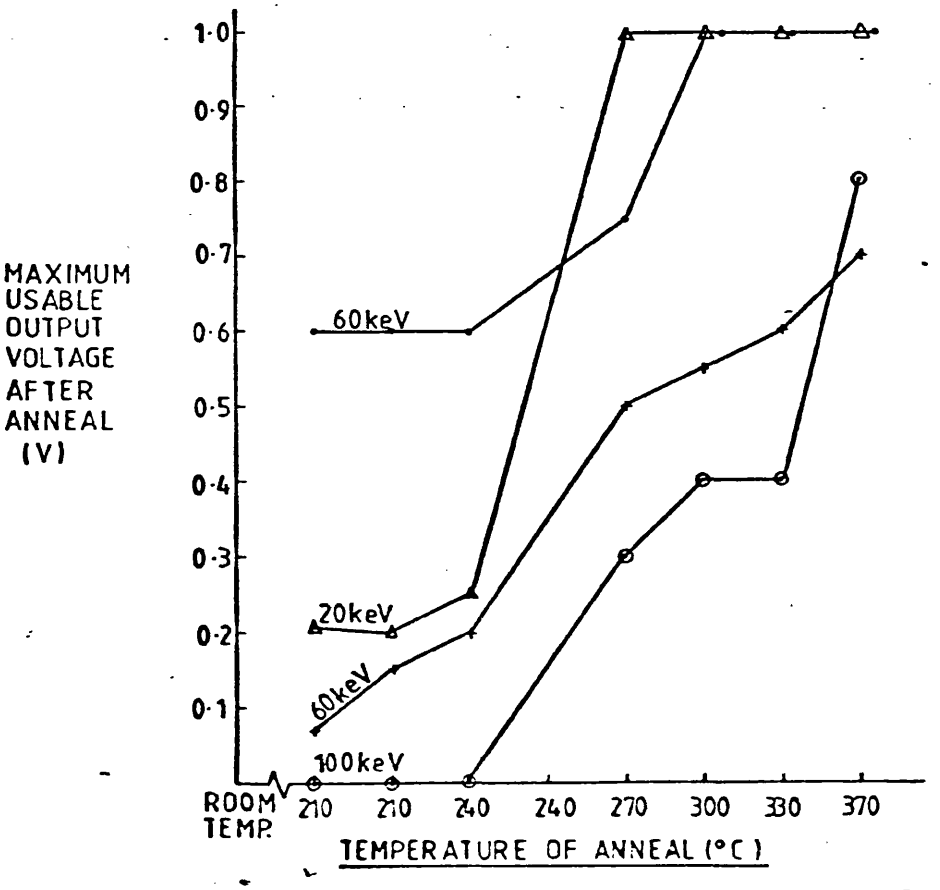


Figure 4.11: Improvement in CCD performance with annealing, showing effect of energy of incident electrons on rate of improvement.

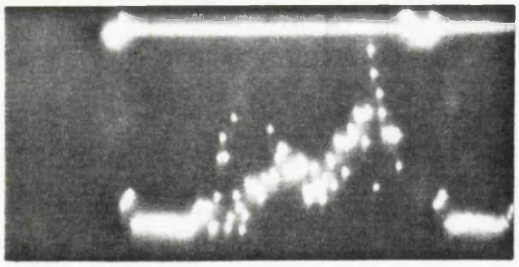

a) Before anneal

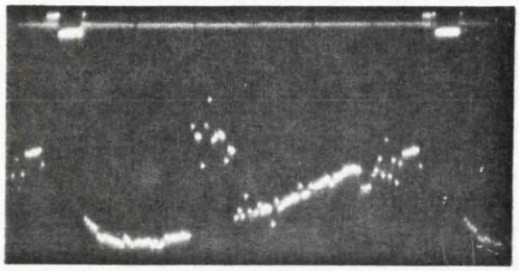

b) 180°C

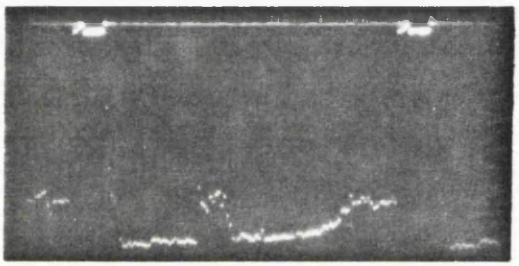

c) 240°C

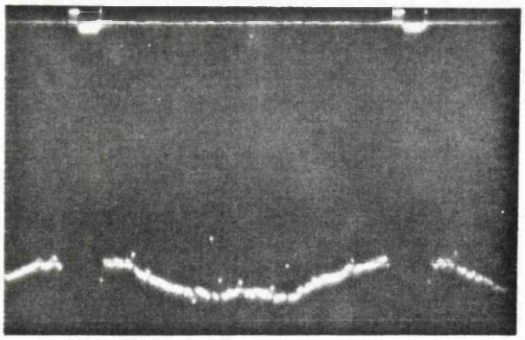

d) 370°C

Figure 4.12: Output of horizontal row in damaged area after successive anneals, showing the improvement in maximum output voltage in the damaged area as annealing proceeds. The most heavily damaged region had received a dose of 17.7 electrons/photocell.

improved. The intensity of light on the CCD is ≈ 75% of saturation in all four photographs. The previous doses in the damaged regions were $17.7 \times 10^6$ 60keV electrons in cells 32-44, $2.1 \times 10^6$ in cells 45 - 55 and $7.2 \times 10^6$ in cells 83 - 93.

Measurement of the maximum usable output voltage after each anneal showed that it had increased to the saturation voltage after 370°C in all but two of the seven areas studied. These two areas had been heavily irradiated, one with 60keV electrons and the other with 100keV electrons, and before annealing had a maximum usable output voltage of 0V. Their maximum usable output voltages after the 370°C anneal were respectively 70% and 80% of saturation.

Figure 4.10(b) shows the annealing curve for three areas damaged by 60 keV electrons. The two least damaged areas show a sudden improvement after annealing to 240 and 270°C while the most heavily damaged area shows a steady improvement in performance which is not complete by 370°C, the highest temperature to which the CCD was heated.

As in the case of dark current it is difficult to separate the effects of incident electron energy and total electron dose on the annealing temperature required to remove damage. Figure 4.11(b) shows the improvement in maximum usable output voltage with annealing for three different electron energies and four different doses. It is not clear whether the highest temperature required to remove the damage due to 100keV electrons is due to the electron energy or the high total dose received by the area.

Thus, for five of the seven areas studied the maximum usable output voltage was restored to the saturation voltage by annealing to 370°C. In the two areas which had previously received the highest total dose there was still evidence of damage after an anneal to 370°C.

4.4.5 Damage caused by Annealing

After the final anneal to 370°C the CCD became very sensitive to the clocking voltage levels. The following effects were noted:

1. The dark current in some areas of the device became very large, with saturation occurring in one region. All but one of the areas in which this occurred had been previously irradiated. The signal is known to be dark current because of its temperature dependence and can be removed completely by reducing the clocking voltage height to 4V for the vertical transfer pulse $\phi_v$ and to 2V for the photogate pulse $\phi_p$. These two facts suggest that the signal may

be due to incomplete depletion of the buried channel (described in Section 4.2.4), since it is probable that irradiated areas have a higher oxide charge, which can inhibit depletion, and that reducing the clocking voltages improves performance by opposing this effect. The voltage applied to the buried channel was previously sufficient to deplete the buried channel but the final anneal to 370°C could have caused an increase in the resistance of the gold wire-aluminium electrode contact, thus decreasing the voltage applied to the silicon. This effect, due to depletion of the aluminium from the area under the gold electrodes, is reported by Maissel & Glang[24] and can occur at temperatures of 300°C. If this is the correct explanation it will be possible to remove the dark current by increasing the reverse bias to the channel - substrate junction, but this has not been attempted. The CCD was not heated to temperatures above 370°C in case the dark current became worse. At this point it should be made clear that this dark current mechanism could not be responsible for the dark current increase observed when the device was irradiated since in that case there was no dependence of dark current on electrode voltage.

2. The saturation voltage of all cells of the CCD became dependent on the value of the clocking voltages and became lower as the clocking voltage increased. It could be restored to its former value of 1 V by reducing $\phi_v$ and $\phi_p$ to 5V and 4V respectively. This is consistent with the dependence of saturation voltage on electrode voltage described in Appendix 5, in which the saturation voltage is greatest for small electrode bias voltage. However it is not clear why this effect should only become important after annealing. Incomplete depletion of the buried channel may cause the effective number of donor atoms to decrease, thus decreasing the saturation charge, but this effect should be evident only in those regions which have been irradiated.

3. The CCD became very noisy with a noise signal of $\approx$ 30% superimposed on the signal. This could be removed for a short time by switching on and off nearby apparatus, suggesting a poor connection either within the CCD or in the external wiring. The external connections were checked and replaced, but the problem persisted, and was eventually solved by increasing the value of $\phi_v$ to 4V. This effect may once again be due to poor contact between the gold wires and aluminium interconnections.

4. A dependence of saturation voltage on device temperature was

observed, and since no such effect had been noticed before this is assumed to be a result of annealing. Figure 4.13 shows the decrease in saturation voltage with temperature. This effect is not due to a change in the gain of the CCD because a given output voltage does not decrease continuously as the device is cooled, but only shows a decrease after the temperature corresponding to maximum output voltage is reached. This may be due to an effect similar to that described in (2) in which an increase in the device clocking voltage caused the saturation voltage to decrease. The occupancy of states in the band gap depends on the position of the Fermi level and therefore on device temperature, with donor states becoming more negatively charged as temperature decreases, and acceptor states becoming more positively charged as temperature decreases[25]. Therefore, if there is an excess of acceptor states over donor states a decrease in temperature will result in an increase in the positive charge at the interface, increasing the effective bias voltage on the semiconductor and reducing the cell capacity as described in Appendix 5 . While the trivalent silicon states are donors, the non-bridging oxygen states are acceptors and may be responsible for this effect.

In summary, annealing to 370°C removes the effect of radiation damage in almost all irradiated areas but is insufficient to remove damage in areas which were heavily irradiated. However damage occurs as a result of annealing, and some of the damage effects may be due to the increased resistence of the gold wire-aluminium interconnection contacts.

### 4.4.6 Lifetime of Annealed Device under Electron Irradiation

If it can be shown that an annealed CCD damages under irradiation at the same rate as a new device, then it may be possible to extend the life of the CCD indefinitely by this process. To this end a series of experiments were performed in which the whole area of the annealed CCD was irradiated with 60keV electrons, and the deterioration in dark current and maximum usable output voltage measured. This allowed comparison of the rate at which damage occurred in irradiated areas with that of areas which had not previously been damaged. The following experimental conditions were in operation:

1. The border of the active area of the device was masked off by a copper aperture. As a result rows 6 - 94 and cells 8 - 99 were irradiated, with the remaining cells being shielded. Cells 1 - 7

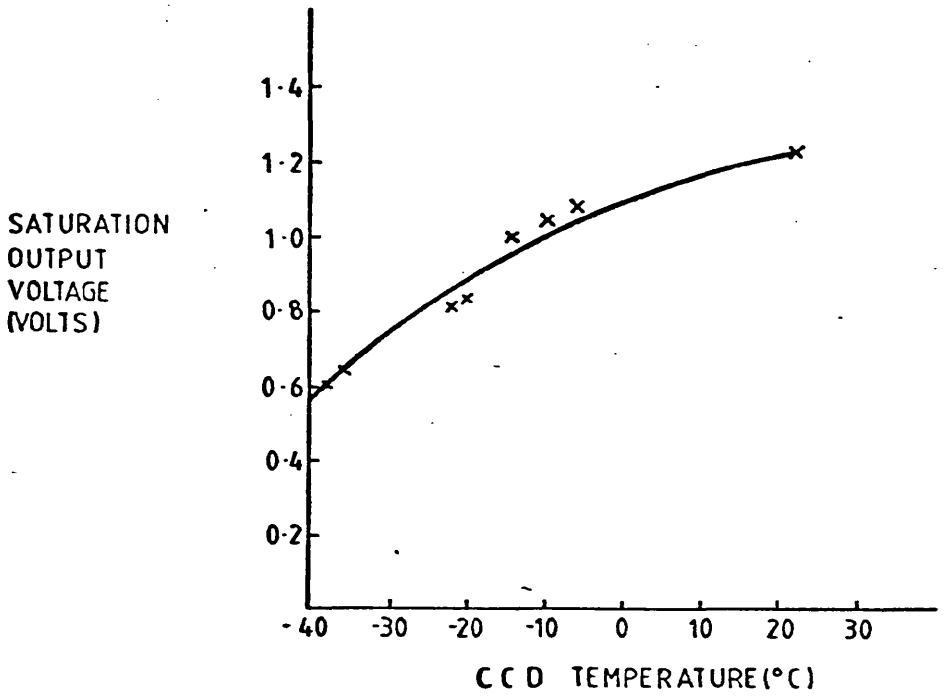


Figure 4.13: Effect of temperatures on CCD saturation voltage.

could therefore be used for comparison with the irradiated area to detect changes in the maximum usable output voltage.

2. The clocking voltages to the CCD were chosen to minimise the damage effects described in Section 4.4.4 above. The best performance was achieved with $\phi_v$ = 0-4V and $\phi_p$ = 0-5V, which, although in the correct range for minimising noise and maximising saturation voltage, allow a large dark current (95% of saturation at room temperature) in 3 areas. These areas cannot therefore be used to study the increase in dark current with irradiation but behave normally when cooled and so can be used for studying maximum usable output voltage.

3. The experiment was performed with the apparatus described in Section 2.2 . The beam current and irradiation time were chosen so that the electron signal half-filled the CCD wells, and the irradiation time was the shortest compatible with the speed of the counting system. Initially an irradiation time of 14.3 ms and a count rate of 26 electrons/photocell/irradiation was used, and latterly a rate of 50 electrons/photocell/irradiation with an irradiation time of 47 ms. The readout time in both cases was 56 ms.

4. Nine irradiations were performed with the CCD performance checked before the first and after each subsequent run. The total dose received by the device during this experiment was $14.2 \times 10^6$ electrons/photocell. The total irradiation time was approximately nine hours. Some additional irradiation of the CCD occurred while the gain of the device was measured after each run, and this is accounted for in calculating the total dose on the device.

5. Since the saturation voltage of the CCD varies with temperature (4.4.5), it is important that the device temperature is as high as possible so that early changes in maximum output voltage can be detected. If, for example, the maximum output voltage falls to 1V, this will be detectable at 22°C, with a saturation voltage of 1.2V, but not detectable at -40°C, where the saturation voltage is $\approx$ 0.6V. Thus the measurements were made at -6°C, which gives a saturation voltage of 1.08V and a reasonably low dark voltage of 20mV.

### 4.4.7 Results of Experiment on CCD Performance after Annealing - Increase in Dark Voltage with Irradiation

A comparison of the rates of dark current increase before and

after annealing is made in Figure 4.14(a). An area which was irradiated with 2.1 x $10^6$ electrons/photocell, annealed to 370°C and reirradiated damages more quickly than an area being irradiated for the first time. The cumulative dose required to half-fill the potential wells is 2.5 x $10^6$ electrons/cell for a CCD which has been neither irradiated nor annealed, is 1.4 x $10^6$ for an area which has not been irradiated but has been annealed, and is 0.7 x $10^6$ electrons/photocell for an area which had been previously irradiated and annealed. Figure 4.14(b) shows that an area damaged previously with 20keV electrons, annealed to 370°C and reirradiated with 60keV electrons, damages more slowly with 60keV electrons than it did in the earlier 20keV irradiation, demonstrating a considerable improvement in performance. Figure 4.15 shows the effect of previous total dose on the damage rate. For the two areas irradiated under positive gate bias and the previously unirradiated area the rate of damage increase as the total dose increases as can be seen from the following table:

| Previous Dose (electrons/photocell) | Dose required to increase Dark Current to half saturation voltage (electrons/photocell) |
|---|---|
| 0 | 1.3 x $10^6$ |
| 0.77 x $10^6$ | 1.1 x $10^6$ |
| 2.1 x $10^6$ | 0.75x $10^6$ |

TABLE 4.3
Effect of previous dose on dark current increase for 60keV electrons

The other area on this graph was previously irradiated under negative bias (Section 4.3.10). At that time there was no difference noted between the damage rates with positive and negative bias. However this area now seems to damage more slowly than would be expected from its previous total dose, with a damage rate less than that of another region with a considerably smaller total dose. It may be that the different location of the damaged areas in the $SiO_2$ under negative bias makes annealing more effective.

### 4.4.8 Results of Experiment on CCD Performance after Annealing - Change in Maximum Usable Output Voltage with Irradiation

The maximum usable output voltage decreases with total electron dose as described before (Section 4.3.8). As can be seen from Figures 4.16 and 4.17 the damage rate depends on the previous total electron dose, with the CCD lifetime being longest for those areas which were irradiated least. The following table gives device lifetimes after

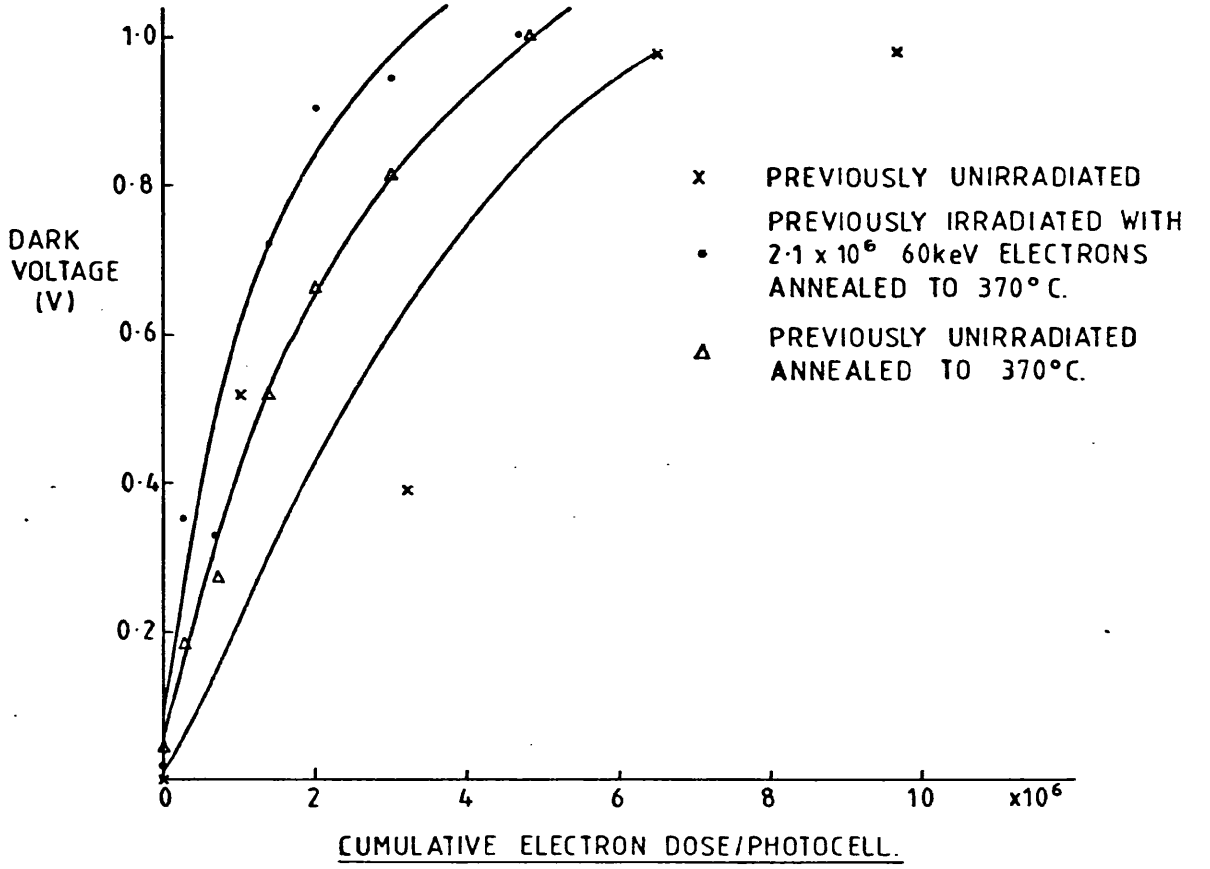


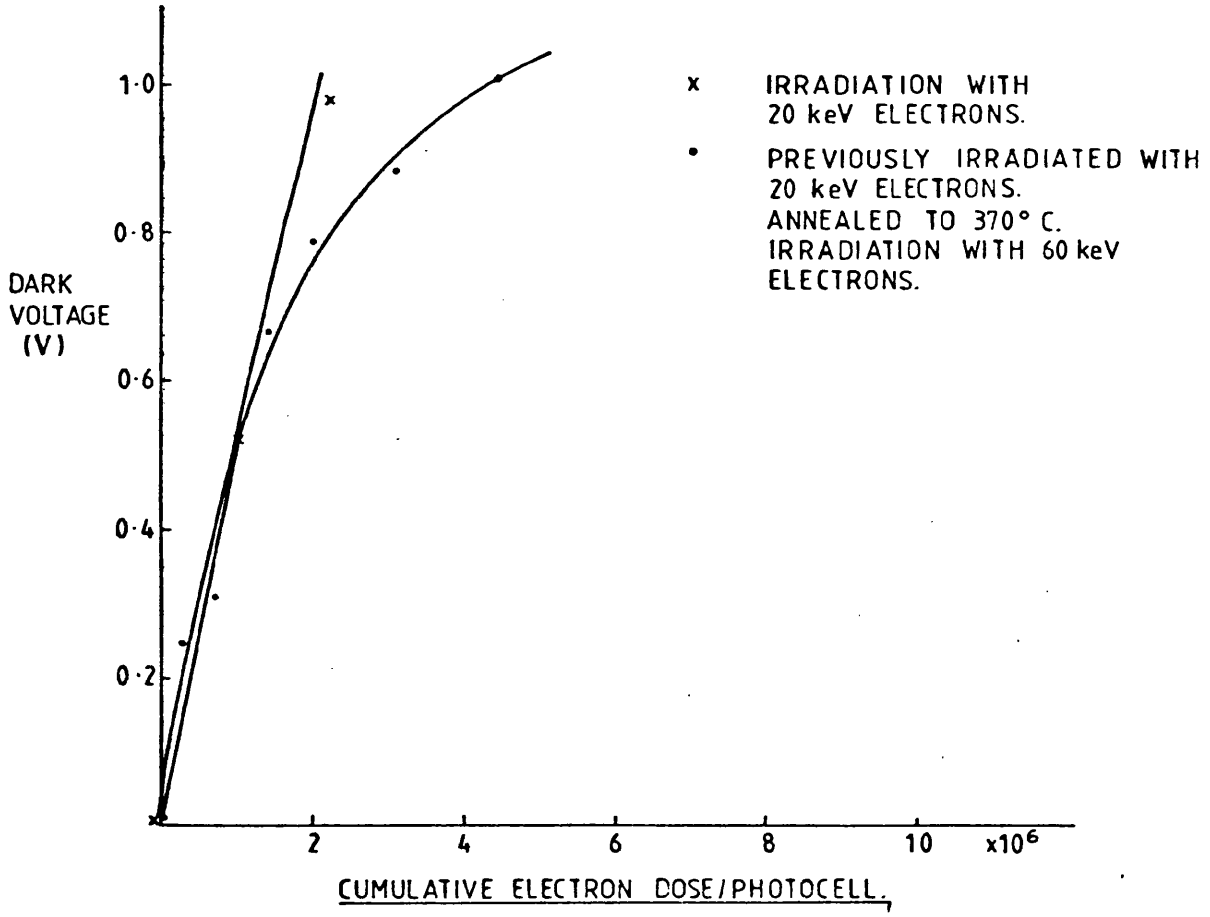


Figure 4.14 Damage rate of CCD 202 before and after annealing

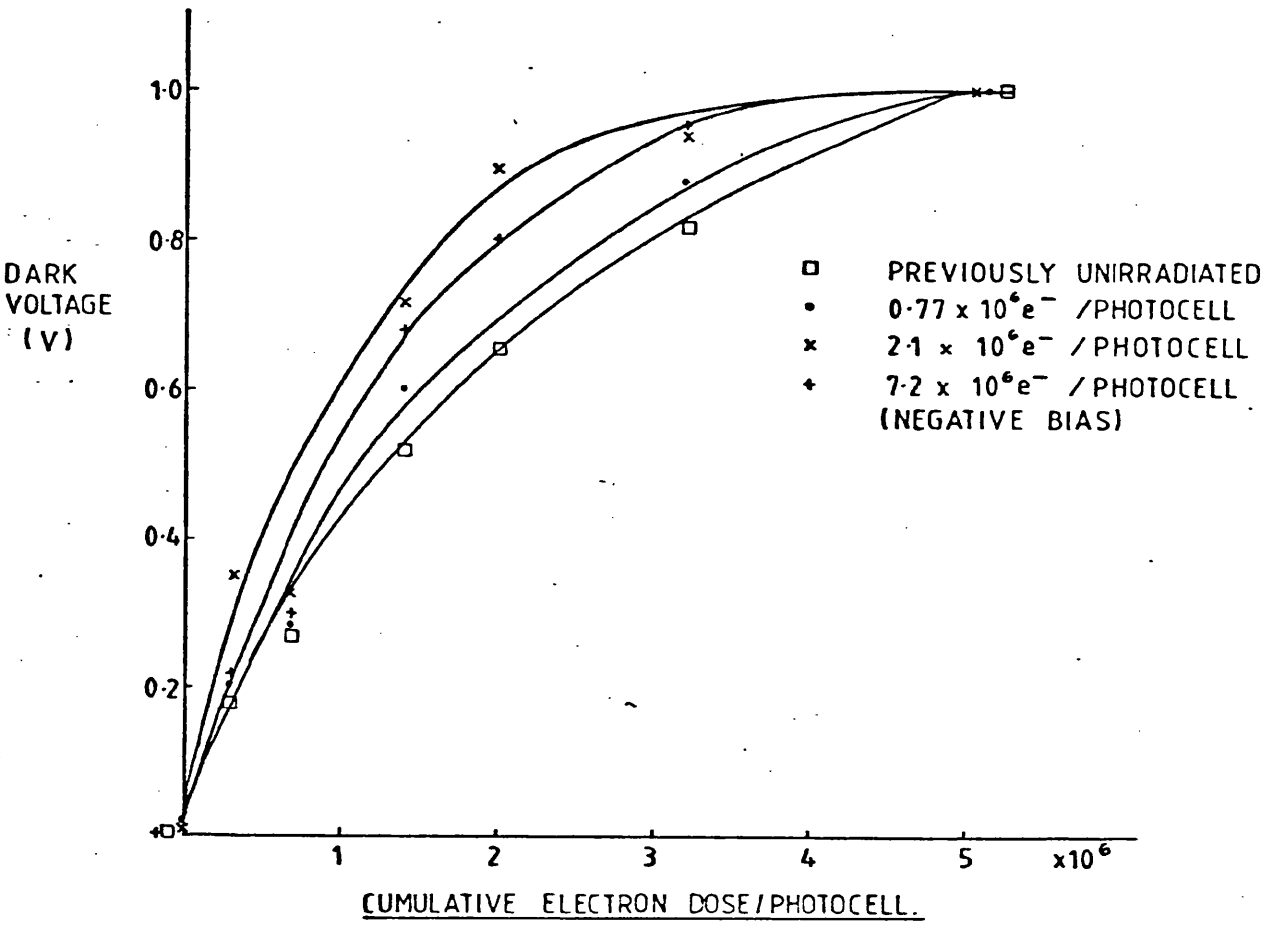


Figure 4.15: Effect of electron dose before annealing on rate at which annealed CCD damages - dark voltage.

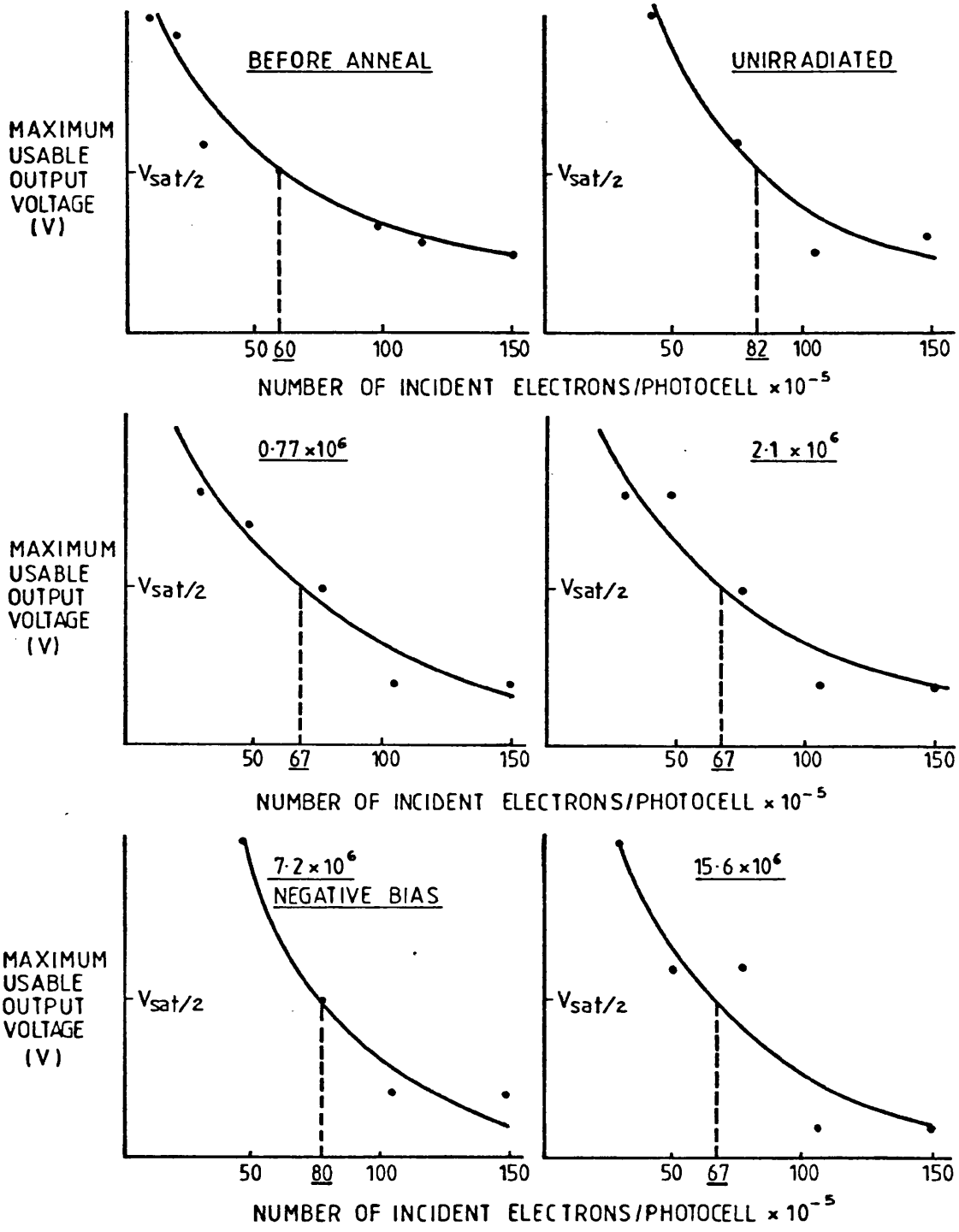


Figure 4.16:

Effect of electron dose before annealing on rate at which annealed CCD damages - maximum usable output voltage.

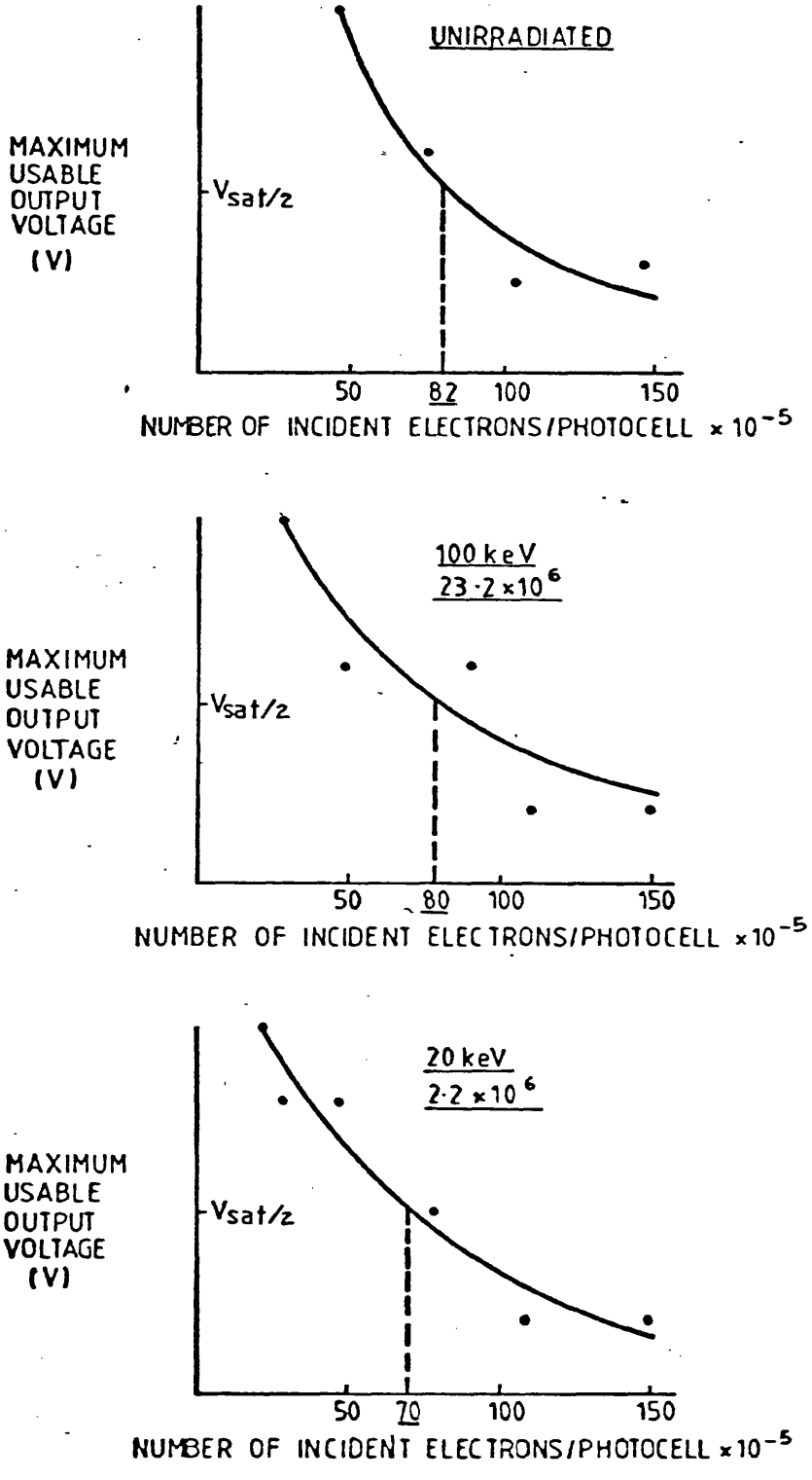


Figure 4.17: Effect of electron dose before annealing on rate at which annealed CCD damages - maximum usable output voltage

annealing to 370°C as a function of previous total electron dose of 60keV electrons:

| Previous Dose (electrons/photocell) | Lifetime (electrons/photocell) |
|---|---|
| 0 | $8.2 \times 10^6$ |
| $0.77 \times 10^6$ | $6.7 \times 10^6$ |
| $2.1 \times 10^6$ | $6.7 \times 10^6$ |
| $7.2 \times 10^6$ (negative bias) | $8.0 \times 10^6$ |
| $15.6 \times 10^6$ | $6.7 \times 10^6$ |
| $17.7 \times 10^6$ | $5.2 \times 10^6$ |

TABLE 4.4

Effect of previous dose on CCD lifetime for 60keV electrons

Once again the area previously irradiated with negative bias damages more slowly than the other areas. For all areas except the most heavily irradiated the CCD lifetime is greater than the value of $6.0 \times 10^6$ electrons/photocell measured in the original experiment when the device was first irradiated. This suggests that annealing the CCD to 370°C removes not only radiation induced oxide charge but also fixed oxide charge which was present in the device before irradiation. The lifetimes for areas previously irradiated with 20 and 100keV electrons are $7.0 \times 10^6$ and $8.0 \times 10^6$ respectively.

The main points arising from the experiments to measure the rate of damage after annealing are as follows:

1. The dark current increases more quickly with electron dose in a CCD which has been irradiated, annealed and reirradiated, than in a new device.

2. The maximum usable output voltage in most cases decreases more slowly in a damaged and annealed device than in a new one.

3. For areas previously irradiated with the same electron energy the rate at which damage occurs is greatest for those areas with highest previous total dose.

4. An area which had been previously irradiated under negative bias damaged more slowly than one which had been irradiated under positive bias.

It is not known whether these results which are observed after one cycle of irradiation and annealing will apply to a device which has

undergone many such cycles. Further investigation of this effect is required before a final figure can be put on CCD lifetime.

4.4.9 Reannealing CCD for Use in Imaging

To demonstrate that an annealed CCD can be used for imaging of specimens in the electron microscope, the device used in the experiments described in Sections 4.2 and 4.3 was annealed once again and used to record images of radiation sensitive materials. The work on imaging is described in Section 5.3. Annealing was done in a furnace as before in a $N_2$ atmosphere. The CCD was annealed three times, twice for one hour at 350°C, and once for one hour at 365°C. The maximum usable output voltage and the dark voltage were measured after each anneal, and, since a variation in output signal from different areas of the device was apparent, this was done for each of the irradiated areas discussed previously. The performance after each anneal was as follows:

1. After anneal to 350°C for one hour.

   The dark voltage in all areas was reduced to approximately 10% of saturation. The residual dark voltage was greatest in those areas which had received the greatest electron dose in the first set of irradiations. The maximum usable output voltage had increased to greater than 80% of saturation in four of the seven areas. Again the most heavily damaged areas in the first set of irradiations performed worst.

2. Anneal to 350°C for one hour

   This further anneal caused little improvement in performance.

3. Anneal to 365°C for one hour

   A dark voltage of 10% of saturation was present in all areas but those used in the first set of irradiations, in which the dark voltage was less. The most heavily damaged areas had the smallest dark voltage, it being as low as 5% of saturation in the area previously irradiated with $17.6 \times 10^6$ 60keV electrons. It is not clear why this dark voltage should be present or why it should depend in this way on electron dose since this seems to contradict the effects observed after the first set of anneals described in Section 4.4.5, and after the first of this set of anneals. No significant reduction in the dark voltage was observed when the clocking voltages were varied.

The maximum output voltage was restored to saturation voltage in

four out of the seven areas, was 90% of saturation in two areas, and 60% of saturation in the most heavily irradiated area. The CCD was used in this condition without a further anneal. No decrease in saturation voltage with temperature was seen after this anneal. When cooled to -24°C the dark current decreased to a negligible value and the CCD was capable of producing the images shown in Figure 5.

## SECTION 4.5 IMPLICATIONS OF DAMAGE RESULTS

The results outlined above are encouraging for the future of CCD as detectors in the electron microscope. The results on device lifetime show that $10^4$ images with a shot noise limit of 3% can be produced before the device becomes inoperable, using electrons of energy 60 and 100keV. The considerably greater damage rate of 20keV electrons reduces the lifetime to $10^3$ images. This suggests that the CCD is useful for recording separate images in the way that photographic plate is used but cannot be used continuously to view the specimen as can a phosphor screen. The lifetime of the CCD under continuous irradiation at a typical rate is approximately 5 hours.

The lifetime of the Fairchild CCD202 can be extended, after damage has rendered the device unusable, by annealing to 370°C. The minimum time required at this temperature to remove damage is not known, but is certainly less than one hour.

Due to the increase in dark voltage with irradiation a method of cooling the device to $\approx$ -20°C is necessary, and the increased sensitivity of the CCD saturation voltage to temperature after annealing requires that this be controllable to within a few degrees. A Peltier element bonded to the CCD base may allow more precise temperature control than the present system.

It is possible that commercial radiation hard devices may soon be manufactured with a lifetime which is a factor of 30-100 greater than the non-hardened devices presently available. If this is so, continuous electron irradiation of the CCDs will be possible, and the devices can be used both to continuously view and to record images.

# CHAPTER 5

# IMAGING WITH CCD 202

## SECTION 5.1 INTRODUCTION

This Chapter describes the use of the CCD 202 to record images of various specimens in the electron microscope and shows the images which were obtained. They range from perforated carbon film, a simple test specimen, to lattice fringes in chlorinated copper phthalocyanine, which is a radiation sensitive specimen. The experiments allow both visual assessment of the quality of images recorded by the CCD and experience of the practicalities of CCD operation as a routine viewing and recording device.

## SECTION 5.2 RECORDING PROCEDURE

The apparatus used in recording the images is described in Chapter 2. The recording procedure is as follows:

1. A suitable area of the specimen is selected and focused, using either the CCD alone or, more commonly, the phosphor screen for area selection and rough focusing and the CCD for fine focusing.

2. The electron beam intensity is suitably adjusted to match the CCD cell capacity and recording time.

3. An image is recorded by the Data Accumulation and Control Unit.

4. The image is displayed on the C.R.T. screen and photographed to produce a permanent record.

### Section 5.2.1 Area Selection and Focusing

This stage proved to be the most difficult and time-consuming. The Data Accumulation and Control Unit has the ability to store and continuously cycle image data so that a recorded image can be displayed without further irradiation of the specimen. This makes the CCD attractive for area selection and focusing of images of radiation sensitive specimens, where it is important to minimise the electron dose on the specimen. With a specimen of perforated carbon film an image recorded with a dose of $\approx$ 30 electrons/photocell was sufficient to assess whether an area was suitable for recording with better electron statistics. However, perforated carbon film is a particularly simple high contrast specimen, and most other specimens will require higher doses than this. The imaging system in its present state is

not suitable for selection of areas for recording. This is due to the limited number of picture elements in the device which means that only a small area of the specimen can be imaged at a given resolution. In addition, the CCD is mounted non-centrally in the electron microscope column, so that changes in magnification result in movement of the image on the CCD. Thus area selection has to be done at the magnification at which the image will be recorded. This proved to be difficult with the limited number of picture elements of the CCD even for perforated carbon film, which is a particularly simple specimen. Area selection could thus be made easier by mounting the CCD centrally in the microscope column. In addition, the trend in new CCDs is towards devices with greater numbers of picture elements, and devices are now available which can image considerably greater areas than the CCD 202.

Thus, although low dose area selection and focusing is highly desirable for radiation sensitive specimens, it is not practical to use the CCD for this purpose, with the present experimental system. For this reason, in recording images, the area was normally selected approximately using the phosphor screen, with the CCD being used only for fine focusing and for recording. The CCD position was marked by an indentation on the phosphor screen to facilitate positioning of the specimen.

Section 5.2.2 Beam Intensity

The electron counting system was used to adjust the electron dose rate before the image was recorded. This was normally done immediately before recording the image, but could take place before area selection and focusing to minimise the electron dose on the recorded area. The beam intensity was normally chosen to approximately half-fill the CCD photocells at each accumulation, with an irradiation time of normally 24 ms, chosen as giving reasonably short recording times, while being long compared with the beam deflection time. The exception to this was in the case of the images of chlorinated copper phthalocyanine where it proved necessary to continuously irradiate the specimen and CCD to avoid image blur (Section 5.3.4). In that case it was desirable to have the irradiation time long compared with the readout time of 56 ms, and so an irradiation time of 158 ms and a low beam intensity were used.

Section 5.2.3 Image Recording

An electron dose of $\approx 10^3$ electrons/photocell was normally used to record the images, giving an electron shot noise of $\approx 3\%$ in the recorded image. The number of accumulations/image was chosen accordingly, and was typically 31. This results in a typical recording time of $\approx$ 2.5 seconds for an image with 3% electron shot noise. After accumulation, an equal number of subtractions was performed with the CCD unirradiated to ensure that only signals due to incident electrons contribute to the data stored in the memory. The image was normally recorded in 3-frame mode, so that an 82 x 82 array of photocells and a 41 x 82 array of transport cells were recorded and could be displayed separately.

Section 5.2.4 Photography

The images were displayed on the Tektronix display monitor (Section 2.7) and were photographed with both a Shackman camera using Polaroid 107C film for an immediate record, and a Tektronix camera using 220 roll film (HP4 or HP5) to obtain negatives for printing. The photographs in this Chapter are reproduced from the images recorded on 220 roll film. There is a magnification of $\approx$ 20x between the image on the CCD and the image screen of the display oscilloscope. In addition, the magnification of the electron microscope is greater than the nominal value given by the instrumental displays, because of the different positions of the CCD and the photographic plate. The distance from the projector lens pole piece to the photographic plate is 35.4 cm, compared with a distance of 62.9 cm from the projector lens pole piece to the CCD, giving a magnification at the CCD greater by a factor of 1.78x than the nominal magnification. This has to be borne in mind in calculating the sizes of features on the recorded images.

SECTION 5.3 IMAGES

Section 5.3.1 Images of Perforated Carbon Film

This standard electron microscope test specimen was chosen for the first set of imaging experiments with the CCD 202. Figure 5.1 shows a through-focus series of images taken with an electron microscope magnification of 2000x ( $\equiv$ 3560x on the CCD) and an electron dose of typically 300 electrons/photocell. This gives an electron shot noise of $\approx$ 6%, and demonstrates the ability of the CCD to produce images at low electron doses. The irradiation time used for these images was 24

Figures 5.1 & 5.2

| | |
|---|---|
| Total accumulation time (seconds) | 5 |
| Irradiation time/accumulation (ms) | 24 |
| Readout time/accumulation (ms) | 56 |
| Number of accumulations | 64 |
| Average number of electrons/photocell | 300 |
| Electron intensity at CCD ($e^-$/photocell/second) | 195 |
| ($A/cm^2$) | $5.8 \times 10^{-6}$ |
| Electron intensity at specimen ($e^-/Å^2$) | 0.07 |
| ($A/cm^2$) | 74.14 |
| Electron energy (keV) | 60 |
| Full well capacity ($e^-$/photocell) | 65 |
| ($C/cm^2$) | $1.9 \times 10^{-10}$ |

(a) under focus (b) in focus (c) over focus

Figure 5.1: Electron image of perforated carbon film showing Fresnel fringes recorded with CCD.
Average number of electrons/photocell = 340
Electron microscope magnification = 2500
Electron energy = 60 keV

(a) (b) (c)

Figure 5.2: Electron image of perforated carbon film showing Fresnel fringe.
(a) Photocell image: average number of electrons/photocell = 300
(b) Transport cell image: average number of electrons/transport cell = 730
(c) Image recorded on Kodak Electron Image Film 4463
Electron microscope magnification = 2600
Electron energy = 60 keV

ms, the readout time was 56 ms, and the number of accumulations was 64 giving a total accumulation time of 5 seconds. Clearly this figure could have been much reduced by using a higher intensity electron beam, since for these images the electron dose/photocell/accumulation was, on average, only 5 electrons. Thus, the number of accumulations necessary to record the image could have been reduced by increasing the electron dose/photocell/accumulation. In changing from one focus position to the next, the image was examined before the final recording was made by accumulating for a small number of cycles. A typical figure of 30-50 electrons/photocell was sufficient to ascertain the suitability of the image for recording. This corresponds to a dose of 0.007- 0.010 electrons/$Å^2$ on the specimen.

These images were recorded in 3-frame mode, so that an image was also formed from the transport cell contents. Figure 5.2 shows one of the through-focus series of photocell images, together with the associated transport cell image, and the image of the same area taken on photographic plate at the same electron microscope magnification. The superior resolution of the photographic plate compared with the photocell image, and of the photocell compared with the transport cell image, can be seen from the sharpness of the Fresnel fringes around the holes in the carbon film. The "granularity" introduced into the image recorded on photographic film by statistical fluctuations in the electron beam intensity[1] can be seen in the variation in the thickness of the dark fringe round the small holes in the carbon film and in the apparent detail in the carbon film. This noise particle size corresponds to a distance of ≈ 30 μm on the photographic film, which is compatible with the expected figure for this type of photographic emulsion. Thus for 60 keV electrons, with images recorded at the same magnification, the resolution of photographic emulsion is better than that of the CCD. This is to be expected from the results of Section 3.4.2, since the charge spread caused by 60 keV electrons should be intermediate between that of 40 keV and 100 keV electrons, and so should be in the range 28 - 120 μm. The size of specimen detail which can be resolved in the image can clearly be reduced by increasing the electron microscope magnification, but this would bring a corresponding reduction in field of view.

Section 5.3.2 Images of Replica Diffraction Grating

A second specimen which was suitable for preliminary imaging tests was a carbon replica diffraction grating of spacing 0.46 μm, commonly

used in the electron microscope for calibration at low magnifications. Since the grating extends over the whole specimen no area selection was necessary in this case. Figure 5.3 shows a photocell and a transport cell image recorded at an electron energy of 60 keV, an electron dose of 629 electrons/photocell, and a magnification of 660x ($\equiv$ 1200x on CCD). The total time to accumulate the image was 4.1 seconds. The average number of electrons/photocell/accumulation was 20 which is $\approx \frac{1}{2}$ of cell saturation, so that a reduction in accumulation time could be achieved by increasing the electrons dose/photocell/accumulation and so decreasing the necessary number of accumulations. Comparison of the photocell and transport cell images shows the loss of resolution in the vertical direction for the transport cells due to the smaller number of picture elements (41 instead of 82).

Section 5.3.3 Images of Catalase Calibration Specimen

The next set of images shows a catalase calibration specimen with lattice fringes of spacing 8.75 nm. The electron energy in this case was 100 keV and the electron microscope magnification was 13,000x (23,400 on CCD). The electron dose on the CCD was typically 500 electrons/photocell, giving an electron shot noise of 4.4%. 32 accumulations were performed for each image, a total accumulation time of 2.6 seconds per image. Figure 5.4 shows a series of images of the catalase lattice fringes taken at different defocus values. The specimen was not irradiated between focus positions in this case, so that the full series of 7 images was recorded with a total dose on the CCD of 3,700 electrons/photocell (equivalent to an electron dose on the specimen of 37 electrons/$\text{Å}^2$).

Figure 5.5 shows the same specimen recorded under the same conditions as above with a lower electron dose of 280 electrons/photocell, giving a shot noise of $\approx$ 6%. The horizontal band seen across the image in this photograph is an artefact introduced by the CCD, which has not been satisfactorily explained. It appears intermittently when the CCD is cooled to $\approx -30^{\circ}$C and disappears when the device is heated. There are several possible reasons for this banding, all of which rely on the fact that the dark area lies approximately along the length of the copper braid under the CCD which cools the device. It may be expected, then, that this region will be colder than the rest of the device and so more susceptible to problems due to, eg, contamination or icing. However, since it is possible to cool the CCD to a temperature low enough to remove dark current, but above the temperature at which

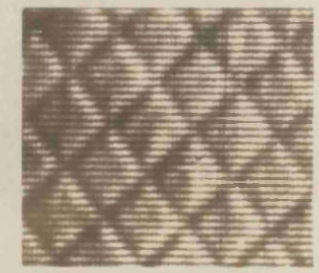

1 μm

(a) photocells (b) transport cells

Figure 3.4: Electron image of a replica diffraction grating recorded with CCD.
Average number of electrons/photocell = 630
Average number of electrons/transportcell = 1540
Electron energy = 60 keV
Electron microscope magnification = 660X

| | | |
|---|---|---|
| Total accumulation time (seconds) | | 4.1 |
| Irradiation time/accumulation (ms) | | 82 |
| Readout time/accumulation (ms) | | 56 |
| Number of accumulations | | 32 |
| Average number of electrons/photocell | | 630 |
| Electron intensity at CCD | (e-/photocell/second) | 240 |
| | ($A/cm^2$) | $7.2 \times 10^{-6}$ |
| Electron intensity at specimen | ($e^-/Å^2$) | 0.64 |
| | ($A/cm^2$) | 1036 |
| Electron energy (keV) | | 60 |
| Full well capacity | (e-/photocell) | 65 |
| | ($C/cm^2$) | $1.9 \times 10^{-10}$ |

Figure 5.4

| | |
|---|---|
| Total accumulation time (seconds) | 2.6 |
| Irradiation time/accumulation (ms) | 24 |
| Readout time/accumulation (ms) | 56 |
| Number of accumulations | 32 |
| Average number of electrons/photocell | 500 |
| Electron intensity at CCD ($e^-$/photocell/second) | 651 |
| ($A/cm^2$) | $2.0 \times 10^{-5}$ |
| Electron intensity at specimen ($e^-/Å^2$) | 6.6 |
| ($A/cm^2$) | 1067 |
| Electron energy (keV) | 100 |
| Full well capacity ($e^-$/photocell) | 45 |
| ($C/cm^2$) | $1.3 \times 10^{-10}$ |

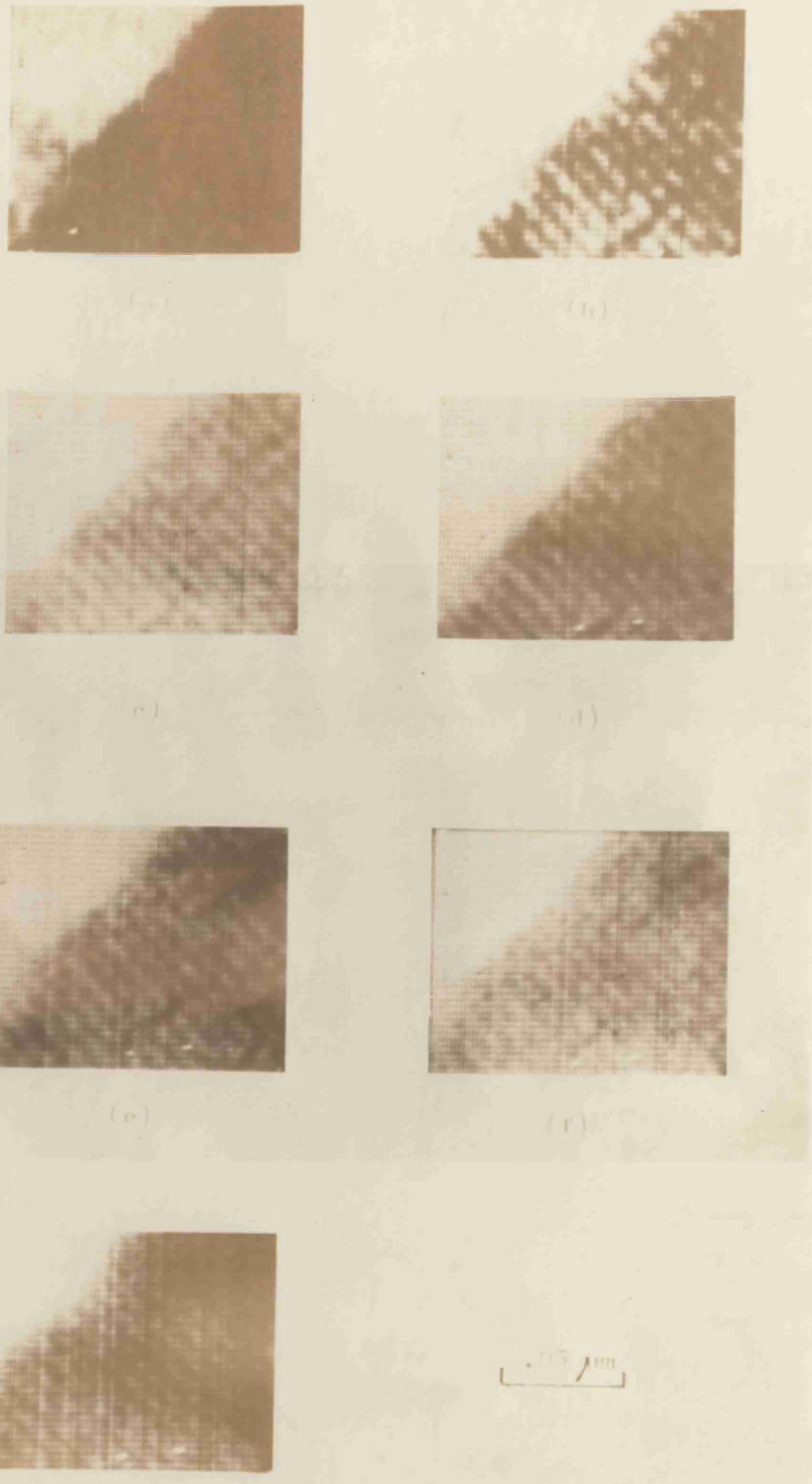


Figure 5.7: Series of electron images of gadolinium calibration specimen recorded with CCD.
Grid spacing = 8.73 nm
Average number of electrons/photocell = 500
Electron energy = 100 keV
Electron microscope magnification = 150,000

Figure 5.5

| | |
|---|---|
| Total accumulation time (seconds) | 2.6 |
| Irradiation time/accumulation (ms) | 24 |
| Readout time/accumulation (ms) | 56 |
| Number of accumulations | 32 |
| Average number of electrons/photocell | 280 |
| Electron intensity at CCD ($e^-$/photocell/second) | 364 |
| ($A/cm^2$) | $1.1 \times 10^{-5}$ |
| Electron intensity at specimen ($e^-/Å^2$) | 2.8 |
| ($A/cm^2$) | 5960 |
| Electron energy (keV) | 100 |
| Full well capacity ($e^-$/photocell) | 45 |
| ($C/cm^2$) | $1.3 \times 10^{-10}$ |

the horizontal band appears (ie to ≈ -10°C), this problem was subsequently avoided.

Section 5.3.4 Images of Chlorinated Copper Phthalocyanine

The final set of images produced with the CCD 202 were of a radiation sensitive specimen, chlorinated copper phthalocyanine. The specimens were provided by Dr W R K Clark of this department. The specimen is crystalline, with a monoclinic structure, and unit cell dimensions: $\underline{a}$ = 19.62Å, $\underline{b}$ = 26.04Å and $\underline{c}$ = 3.76 Å$^2$. The specimen preparation technique resulted in the growth of many small crystallites ( ≈ 1 μm diameter) with their c-axis at 26° to the film normal and the a- and b-axes in the horizontal plane of the substrate, lying along directions defined by the KCl substrate on which the crystallites were grown. Thus if the specimen is tilted through 26° in the electron microscope, a fraction of the molecules will lie with their c-axis vertical, resulting in stacked vertical columns of molecules from which phase contrast images of lattice fringes can be produced. For this form of chlorinated copper phthalocyanine the electron dose at which long range order disappears is ≈ 12,000 electrons/Å$^2$.

Initial attempts to record images of lattice fringes in chlorinated copper phthalocyanine with the CCD were unsuccessful, although the fringes could be recorded on photographic plate. This proved to be due to movement of the image on the CCD when the electron beam was deflected on and off the specimen, which blurred the image and washed out the lattice fringe detail. No such blurring was visible, under the same conditions, with specimens of perforated carbon film and with the replica diffraction grating. In addition, the image movement was greatest in the centre of a grid square, decreasing to zero near the grid bar. Figure 5.6 shows images of phthalocyanine crystals recorded on photographic plate. In Figure 5.6a the electron beam is steady on the specimen and no blurring is seen. In Figure 5.6b the electron beam is deflected on and off the specimen during recording and blurring occurs corresponding to a movement in the specimen plane of ≈ 200Å. Figure 5.6c shows an area of the specimen near a grid bar with beam deflection during recording, and that no image blurring occurs is demonstrated by the presence of lattice fringes.

From these observations the image movement seems to be due to charging effects in the poorly conducting crystals when the electron beam is deflected on and off the specimen. The crystals charge up while the beam is on the specimen, causing movement of the image and

area in which fringes are visible

blurring in the direction of movement. While the beam is removed from the specimen the charge on the crystals leaks away so that there is further charging and image blurring when the electron beam is restored. The fact that there is no blurring of the image near a grid bar is due to the conduction away of the charge along the grid bar. An attempt was made to record images of lattice fringes in crystallites near the grid bar, but this considerably increased the difficulty in finding suitable areas for recording in an already difficult specimen.

The phthalocyanine crystallites are supported on one side by a thin film of evaporated carbon, which should decrease the charging effect by conducting charge away from the crystallites. The other side of the specimen was originally uncoated and in an attempt to reduce the amount of specimen charging and thus the movement of the image, this side was also coated with a thin layer of evaporated carbon. However, no improvement in performance was seen and it seems that no beam deflection should be used in recording images of phthalocyanine and of other poorly conducting specimens. Thus, in order to record images of chlorinated copper phthalocyanine the electron beam was held steady on the specimen both during the integration time and the readout time.

In order to minimise image smearing due to penetration of the transport cells by incident electrons during readout, the integration time was made as long as possible compared with the readout time. The maximum integration time of the system is 158 ms, and the time taken for the signals from each field to be transferred through the transport cells is 14 ms. Due to the readout system of the CCD 202 (see Section 1.2.4) the first row of charge to be read out remains for a very short time ( $\approx$ 0.28 ms) in the transport register, whereas the last row is in the register for the full 14 ms. As a result the fraction of the output signal due to smeared charge varies from 0.16% to 8.1% with an average of 4.13%. This amount of smearing proved small enough to allow imaging of lattice fringes in the specimen.

Figure 5.7 shows the images recorded by the CCD of lattice fringes in chlorinated copper phthalocyanine. It is worth noting that the device used to record these images was one which had previously been rendered unusable by radiation damage, had been annealed to 370°C to remove the damage effects, and had been damaged and annealed a second time (see Section 4.4.9). The images were recorded with an electron energy of 80 keV, and an electron microscope magnification of 66,000x

Figure 5.7

| | |
|---|---|
| Total accumulation time (seconds) | 6.8 |
| Irradiation time/accumulation (ms) | 158 |
| Readout time/accumulation (ms) | 56 |
| Number of accumulations | 32 |
| Average number of electrons/photocell | 1000 |
| Electron intensity at CCD ($e^-$/photocell/second) | 198 |
| ($A/cm^2$) | $5.9 \times 10^{-6}$ |
| Electron intensity at specimen ($e^-/Å^2$) | 24.07 |
| ($A/cm^2$) | 77196 |
| Electron energy (keV) | 80 |
| Full well capacity ($e^-$/photocell) | 45 |
| ($C/cm^2$) | $1.3 \times 10^{-10}$ |

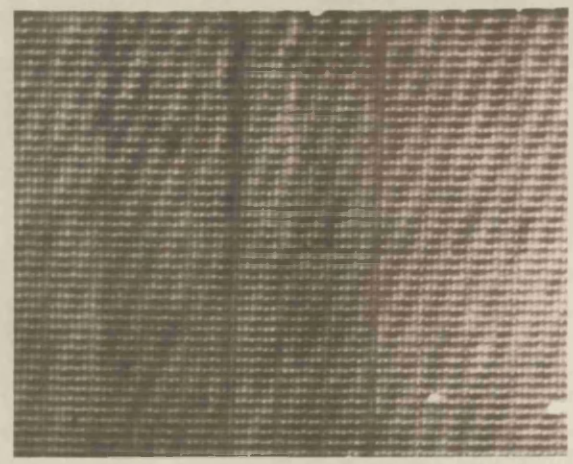

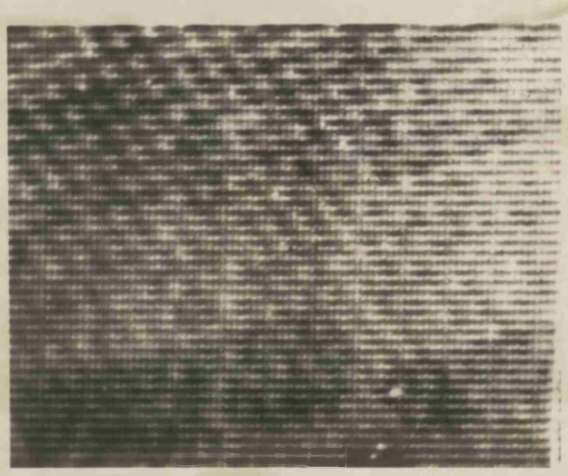

Figure 5.7: Electron images of lattice fringes in chlorinated copper phthalocyanine recorded with CCD.

a) Fringe spacing = 13.02Å (020 reflection)

b) Fringe spacings = 14.60Å (110 and $\bar{1}10$ reflections and 13.02Å (020 reflection)

Average number of electrons/photocell ≈ 10

Electron energy = 200keV

Electron microscope magnification = 600,000X

(equivalent to 114,000x on the CCD).

In order to identify areas for recording, the microscope was used in selected area diffraction mode to search for the known diffraction pattern from suitably aligned crystallites. When such a crystallite was identified, the phosphor screen was used for focusing to obtain lattice fringes. Since these are difficult to see at 66,000x magnification, a higher magnification (160,000x) was used for focusing. The focus controls were then altered in a previously determined manner to obtain the lattice fringes at 66,000x magnification. The fine focusing was done using the CCD.

To record the images, the d.c. voltage level which holds the electron beam off the specimen (Section 2.3) was switched off, so that the specimen and CCD were illuminated by the electron beam. Accumulation was then started and lasted for a preset number of cycles. Finally the d.c. voltage level was restored to remove the electron beam from the specimen and CCD. The delay in starting accumulation and in switching off the electron beam after accumulation means that the electron dose on the specimen and CCD is greater than that used in recording the image. Before recording, the electron beam intensity was set to $\approx$ 30 electrons/photocell/accumulation, and a total of 32 accumulations was performed for each image, giving an electron dose of $\approx$ 1000 electrons/photocell used to record the images of Figure 5.7. However the electron dose on the specimen and CCD for each image was 2000 and 1560 respectively for Figures 5.8a and b due to the recording method described above. The fringes in Figure 5.8a correspond to the 020 reflection and have a spacing of 13.02Å. Figure 5.8b is an underfocus image showing 3 sets of lattice fringes. The two sets on the top left-hand corner have spacings of 14.60Å, and an angle between them of 68°. These are the 110 and $\bar{1}10$ reflections. A third faint set of fringes can be seen in the bottom right-hand corner of the image, making an angle of 56° with the 110 fringes. These are the 020 reflection and have spacing 13.02Å.

The electron dose of $\approx$ 1000 electrons/photocell to record each image is equivalent to a dose on the specimen of $\approx$ 250 electrons/Å$^2$. The doses received by the specimen during recording of 2000 and 1560 electrons/photocell correspond respectively to doses of $\approx$ 500 electrons/Å$^2$ and $\approx$ 390 electrons/Å$^2$. However, the specimen received a considerably greater dose than this during focusing at 160 000x magnification, and greater use of the CCD during this phase is necessary in future to

reduce the total electron dose.

## SECTION 5.4 SUMMARY OF IMAGING RESULTS

These results show that the CCD can be used to record images of various types of specimen, and in particular can record useful images of radiation sensitive specimens.

The ability of the CCD to record images at low electron doses has been demonstrated, and it has been found to be useful for assessing the suitability of an image for recording at very low doses ($\approx$ 30 electrons/photocell in the case of perforated carbon film). However, if CCDs are to supersede phosphor screens as the only viewing system used in the field of radiation sensitive materials, a considerably larger field of view is clearly necessary. Fortunately, the trend in commercial CCDs is towards devices with larger numbers of image elements; for example, Texas Instruments have produced a CCD with 327 x 245 image elements with a cell size of 25 x 25 um.

From the results on signal spread to adjacent cells (Section 3.4) it may be expected that the size of detail that the CCD can resolve will be severely restricted. However, in the first image of lattice fringes in phthalocyanine, Figure 5.7a, the lattice fringe repeat in the horizontal direction is 4.6 photocells, and the fringes can be clearly seen on the photograph. This shows that although at this energy (80 keV), spreading of charge from the 'bright fringe' cells to the 'dark fringe' cells should result in all CCD photocells containing some charge, the fraction of charge spread is not enough to obscure the image detail. However, the contrast in this specimen is high, and it may be that for lower contrast specimens charge spreading will limit the CCD resolution. The loss of resolution compared with photographic plate can be seen in Figure 5.2.

The problems in using the beam deflection system with a poorly conducting specimen, chlorinated copper phthalocyanine, have highlighted the desirability of the frame transfer readout organisation, rather than the interline transfer method, for electron imaging (Section 1.2.4). The organisation of the frame transfer CCD would allow continuous irradiation with considerably less smearing and shorter readout time than that used in recording the images described above.

In summary, the CCD 202 has recorded qualitatively acceptable images of all the specimens studied, and has been used at low doses for focusing and image assessment. Its main drawback in practice is its

limited number of picture elements which causes difficulties in the selection of suitable areas for imaging.

# CHAPTER 6

## CONCLUSIONS AND SUGGESTIONS FOR FUTURE WORK

### Section 6.1 CCDs as Imaging Devices in CTEM

The initial aim of this research project was to evaluate the performance of CCDs as electron detectors in CTEM with a view to using them for the extraction of quantitative information from images. In this respect they have fulfilled their promise, meeting the main requirements for a detector for quantitative work. The important factors for this application are 1) electron gain, 2) linearity, 3) resolution and 4) uniformity of response. These will be discussed individually.

1. Electron Gain. The electron gain of the CCD is $\sim 10^3$ for 20 keV electrons and $\sim 10^4$ for 60 and 100 keV electrons. The efficiency of the CCD for 20 keV electrons is determined mainly by energy loss in the overlying layers, while the efficiency for 60 and 100 keV electrons is limited by diffusion and recombination of electrons in the silicon bulk. These gain figures, when compared with the CCD output noise of $\approx$ 300 electrons[1], suggest that single electron detection should be possible. However, an experiment to verify single electron detection ability showed that for very low signals, $\approx$ 0.2 incident electrons/photocell, the CCD performance is degraded, probably by bulk traps in the silicon substrate which trap signal charge and re-emit it into empty cells. This problem does not affect the CCD at high signal levels, since then charge emitted into a cell will be balanced by charge trapped from the signal charge packet. A possible solution to the problem which would allow the CCD to be used at low signal levels is to provide a small background charge ( $\approx$ 10% of the saturation charge) to ensure that the CCD potential wells are never empty and that charge emission is balanced by charge trapping[2].

2. Linearity. The output signal from the CCD 202 was linearly related to the number of electrons incident on the device for electrons of energy 20, 60 and 100 keV. This was studied for input signal levels up to 50 electrons/photocell. Thus the output signal can be digitised to provide quantitative data which is linearly related to the electron beam intensity, which is highly desirable for image processing.

3. Resolution. The resolution of the CCD was determined by measuring the spread of signal at an aperture edge. This gave diameters

of ≈ 28 μm and ∝ 100 μm respectively for the area over which significant charge is created by 40 and 100 keV electrons. Conventional photographic emulsion is typically of thickness 12 μm[3], so that the spread of signal in it is ∝ 24 μm[4,5] for 40 and 100 keV electrons, with only the first 12 μm of the electron-hole pair cloud for 100 keV electrons being collected. Thus the spread of signal for 40 keV electrons in the CCD is comparable with the figure for photographic plate, whereas for 100 keV electrons the resolution of the CCD is poorer than that of photographic plate due to the greater thickness of the detector material. The figures for both 40 and 100 keV electrons compare well with the resolution of TV camera tubes[6].

4. Uniformity of Response. The uniformity of response of the CCD was measured for signals which half-filled the photocells. At this signal level, the DQE of the CCD is determined mainly by non-uniformity in the response of individual cells, since the random noise in the output voltage is low. The DQE of the device was 0.6 for 40 keV electrons, comparable with that of camera tubes[6], and with that of some types of photographic emulsions[7]. For 100 keV electrons, the DQE is 0.46, which is still comparable with some types of photographic emulsion. The poorer DQE for 100 keV electrons is probably due to the fact that the signal collection for this energy is more dependent on the minority carrier lifetime, which can vary from cell to cell due to variations in cell composition[8]. This high DQE, which means that little noise is introduced into the image data by the CCD and recording system, shows that the CCD can be used for quantitative work, and in particular is useful in work with radiation-sensitive specimens. In this field it is desirable for the recording system to detect every electron incident on the detector, and so cause no noise in the image beyond the shot noise already present due to the small number of electrons collected.

Thus the imaging system based on the CCD 202 fulfils most of the requirements for a system for obtaining quantitative data for image processing. The possible uses to which the system may be put will be discussed in Section 6.6. However, there are several undesirable aspects of the CCD performance as an electron imager, and these will be discussed in the following Section.

## Section 6.2 Factors limiting the Range of Applications of the CCD 202 in Electron Microscopy

There are several factors which limit the range of application of the CCD 202-based imaging system in electron microscopy. These are 1) dynamic range, 2) number of picture elements, 3) readout speed and 4) lifetime under electron bombardment. The effects of each of these and the possibilities for their improvement will be discussed individually.

1. Dynamic Range. The dynamic range of the CCD for electrons is determined by the number of incident electrons which saturate a cell of the CCD. The figures for this are 45, 65 and 440 for 100, 60 and 20 keV electrons respectively. The Data Accumulation Unit allows data from successive cycles to be superimposed in the memory to form an image, and while this is acceptable for CTEM imaging, where dynamic range in the image is normally low, it is not satisfactory for data in which the dynamic range is high. This category includes, for example, EELS data, with a typical dynamic range of $\gtrsim 10^4$, and diffraction patterns, where there can be a factor of $\approx 10^4$ difference in intensity between zero and higher order spots.

2. Number of Picture Elements. This quantity determines the area of the specimen which can be recorded with a given resolution, and ideally, for ease of operation, should be as large as possible. In any recorder it is determined by the active area of the recorder and by the spatial resolution for electrons. In the case of the CCD 202, the active area is 3 mm x 4 mm, and the area over which an incident electron creates significant charge has diameter 28 um and 120 um respectively for 40 and 100 keV electrons. Thus the effective number of picture elements in the CCD is $\approx 10^4$ for 40 keV and $\approx 10^3$ for 100 keV electrons. This number of elements is adequate for recording images for computer processing, although a larger number would be desirable, but it makes area selection extremely difficult. It to some extent rules out the use of CCDs as replacements for the phosphor screen in the electron microscopy of radiation-sensitive materials.

3. Readout Speed. The readout speed of the present system of $\approx \frac{1}{2}$ MHz is not a drawback for image recording, since usable images can be accumulated in $\approx$ 2 - 5 seconds. However, it is certainly a limitation to the use of the CCD in STEM recording. One possibility for future uses of CCDs is that they can be used

to simulate different detector geometries in STEM imaging[9,10]. This is desirable because different information about the specimen can be extracted from different regions of the angular distribution of transmitted electrons. The detector geometries which are likely to be of most interest are 1) the split detector, which consists of 2 semicircles[11], 2) the quadrant detector, which consists of 4 quadrants of a circle[12], and 3) the Rose detector consisting of several concentric annular detectors[13]. Computer processing of the CCD output would allow it to simulate any of these geometries. However, this application requires at least one cycle of irradiation and readout of the CCD for each picture point in the STEM image. Thus for a 256 x 256 STEM image, the total recording time would be $\approx$ 1 hr. Clearly this is unacceptably long.

4. Lifetime under Electron Bombardment. As reported in Chapter 4, the lifetime of the CCD 202 is limited under electron bombardment to $2 \times 10^6$, $6 \times 10^6$, $1.5 \times 10^7$ electrons/photocell respectively for 20, 60 and 100 keV electrons. This figure is satisfactory for using the CCD purely as a recording device, but is unacceptably low when the CCD is to be irradiated over a long period or when a large dynamic range, and thus a large number of electrons, is required in the recorded data. The former case rules out, for example, the use of CCDs as routine area selection and focusing aids. This would have been of particular interest in the field of radiation sensitive materials. The second case includes EELS and diffraction pattern recording. Thus it is highly desirable that the radiation hardness of the CCD be increased. In Chapter 4 it was described how damaged CCDs can be restored to their former performance by annealing to $\approx$ 370°C. This has been done twice in the case of one CCD, which was subsequently used to record high resolution images of chlorinated copper phthalocyanine. However, an increased sensitivity to device temperature and clocking voltages was noted in the device which had been damaged and annealed twice, and it may be that some irreversible processes are occurring in the annealing process. Other methods by which device lifetime may be improved are discussed in Section 6.3.

## Section 6.3 Improvements to CCD for Electron Imaging

This Section deals with ways in which the design of CCDs could be optimised for electron imaging. Some of the features to be discussed are already available in some commercial devices, but unfortunately

there is no single device incorporating them all. The most important areas in which the CCD performance could be improved are 1) radiation damage, 2) cell capacity, 3) number of picture elements, 4) readout rate, 5) readout organisation. These will be discussed separately.

1. Radiation Damage. Possibly the most important area in which CCD performance could be improved is in the radiation hardness of the devices. The most desirable method of increasing device lifetime is to use a CCD which has been designed and fabricated using a radiation hard process. This has been extensively investigated by the Naval Research Laboratory[14,15,16] and by Hughes Aircraft Company[17], and the factors influencing radiation sensitivity have been determined. The radiation hard CCDs have structures which are relatively insensitive to positive charge trapped in the oxide layer, and, in addition, have a slow-grown oxide layer which has few ionizable traps and therefore is less likely to become positively charged. The lifetime of such a device has been shown to be $\approx$ 100X longer than that of conventional devices[18]. The research in the field is mainly concerned with military applications, and there is no commercial incentive at present to make radiation hard devices. However, Hughes Aircraft Company have marketed a new CCD, the HCC1 200A[19,20], which incorporates some of the features of their radiation hard military CCDs, and so might be expected to have a longer lifetime than other CCDs. The device is a 100 x 100 array, with a cell size of 25 x 25 $\mu$m, and with a line transfer readout organisation. This readout organisation is a drawback of the Hughes device, since it requires pulsed illumination to avoid signal smearing. In general for a CCD to be relatively radiation hard requires an n-buried channel structure and avoidance of the use of polycrystalline silicon electrodes[14]. It is also desirable that it should be able to withstand annealing to $\approx$ 370°C.

A second way in which CCDs can be improved for electron imaging is to use them in backface imaging mode, in which the radiation is incident on the substrate side of the device. In this case the incident electron beam does not pass through the electrode structure, and in particular deposits no energy in the $SiO_2$, so avoiding the creation of fixed positive charge. This mode of operation requires that the CCD substrate is thinned to $\approx$ 10-100 $\mu$m to minimise recombination of minority carriers. Experiments on backface imaging devices have shown that they have a considerably greater lifetime

than conventional devices under ionizing radiation. One manufacturer has produced a backface imaging device which is now commercially available. This is the RCA array with 500 x 350 picture elements[21]. However, this device is intended for photon imaging, and so the silicon substrate is thinned to ≈ 10 μm. Given the range of 60 and 100 keV electrons of ≈ 20 μm and ≈ 60 μm respectively it is clear that electrons in this energy range would penetrate the silicon substrate and would deposit some energy in the insulator and electrodes. Thus a backface imaging device for electron imaging would require a substrate thickness which was matched to the electron energy used.

One way in which the problem of radiation damage can be avoided altogether is to convert the electron image into an optical image by means of a fluorescent screen, so that the CCD is used in photon imaging mode. However, the inefficiency of the fluorescent screen results in a degradation of the DQE of the system, as described by Herrmann et al for the case of camera tubes. Thus, this imaging method is less attractive than direct bombardment mode, and a radiation hard CCD would be preferable.

2. Cell Capacity. As discussed in the previous section, the number of incident electrons which saturate a cell of the CCD determines the dynamic range of the device for electrons, and thus should be as large as possible to give the widest range of applications. The cell capacity of buried channel devices is smaller (by a factor of ≈ 10X) than that of surface channel devices. However, the other disadvantages of surface channel CCDs, such as increased radiation sensitivity and increased noise outweigh this advantage. Thus the cell capacity is limited to that available in buried-channel CCDs. The cell capacity of the CCD 201 of $4 \times 10^5$ electrons is reported by Hall to be considerably smaller than the maximum theoretical value[22]. He suggests that it may be improved by modifications to the device. The capacity of the Hughes HCC1 100A is also of this order[19]. Possible methods for increasing the dynamic range of CCDs for direct electron imaging include increasing photocell area, and decreasing the charge collection efficiency of the photocells. Unfortunately, neither of these options is commercially available. Since CCDs have been reported with active areas ≈ 26X greater than the CCD 202[23], it would clearly be possible to increase the cell size by this factor while retaining the same number of photocells, resulting, for example, in a cell capacity of ≈ $10^3$ 60 keV

electrons. The second proposal is highly tentative, and results from a suggestion by Kamins and Fong[24] for improving the spatial resolution of photosensing devices. They suggest the formation of a potential carrier at a distance of ≈ 10 μm from the substrate surface to exclude charge created far from the surface from the signal charge packet. Their intention was to use this method to reduce the number of charge carriers created far from the surface which could diffuse to other photocells, thus improving spatial resolution for, in particular, infra-red radiation. The potential barrier is formed by a highly doped layer of material of the same polarity as the substrate. Clearly, for electron detection, this would allow only charge from the top of the electron-hole pair cloud to contribute to the signal charge packet, so decreasing electron gain and improving dynamic range. However, no devices incorporating this principle have been manufactured commercially.

3. Number of Picture Elements. As discussed earlier, the area of the specimen which can be imaged at a given resolution depends on the effective number of picture elements in the CCD. An increase in the number of picture elements in the CCD is desirable for both area selection and for recording images for computer processing. The simplest way of increasing the number of picture elements is to use a device with a larger imaging area. There are now imaging CCDs available with considerably larger numbers of picture elements and larger active areas than the CCD 202. For example, Bell Laboratories have reported a 496 x 475 array, with a total active area of 320 $mm^2$, 26 times bigger than the CCD 202. Since this number of picture elements is necessary for US broadcast television it is likely that large devices will be made in greater numbers in future. The cell size in this particular array is 39 μm x 27 μm.

In some imaging CCDs, for example the Fairchild CCD 211, an increase in the number of picture elements is gained by a decrease in cell size, so that the area of silicon used is kept constant. For electron imaging, since the spread of charge in the silicon is large, there is therefore no advantage to be gained by using the Fairchild CCD 211 instead of the CCD 202. Thus both the number of picture elements and the cell size must be considered in any attempt to increase the effective number of picture elements of the CCD.

A second method of increasing the effective number of picture elements in the CCD is to improve the resolution of the device for

electrons, so that the number of elements is not limited by charge spread. The suggestion of Kamins and Fong for improving the resolution of silicon imaging devices has been discussed earlier. If this were applied to CCDs, it would considerably improve their resolution for higher energy electrons. However, since only a fraction of the created signal would be collected, the gain of the CCD would be reduced and this may have the effect of reducing the DQE of the device. Further investigation of this method to determine whether it is compatible with buried channel structures would be most interesting. However, there seems to be no commercial effort towards the manufacture of devices employing this "diffusion cut-off" principle.

4. Readout Rate. As discussed in the previous section, a considerably higher readout rate is required if the CCD is to be useful for STEM imaging. CCDs have been built which can operate at readout rates in excess of 100 MHz[25] although these devices are not commercially available. Unfortunately, the readout rate required for broadcast television is $\approx$ 25 - 35 frames/second, so there is little incentive to build imaging CCDs which operate at higher speed. Thus there may be no commercial development in this direction with imaging devices, although high speed is important for signal processing CCDs.

5. Readout Organisation. The most suitable readout organisation for electron imaging has been discussed in Chapter 1. This is the frame transfer organisation which allows continuous irradiation of the device with electrons. With the interline transfer organisation used in the Fairchild CCD 202, and the line transfer organisation used in the Hughes HCC1 100A it is necessary to stop clocking the CCD during the irradiation time, and is desirable that the electron beam should be removed from the device during readout to avoid image smearing. This last feature is unsatisfactory, since as discussed in Chapter 5, deflection of the electron beam on and off the specimen can result in charging and image movement in poorly-conducting specimens. Thus these readout organisations should be avoided if possible. All manufacturers other than Fairchild and Hughes are at present using the frame transfer readout organisation.

## Section 6.4 Other Solid State Devices for Electron Imaging

The other types of solid state imaging arrays are photodiode arrays

and CID (Charge Injection Devices) imagers. The former have been discussed in Chapter 3 and have been rejected on the grounds of the large readout noise associated with the high capacitance of the output bus[26]. This results in an output noise which increases as $\sqrt{N}$, where N is the number of picture elements in the device. While this factor is very important for recording images in CTEM, it is of lesser importance in EELS, since the number of image elements in linear arrays is normally smaller than in area arrays. Thus in direct electron bombardment mode in EELS, photodiodes would appear to be more suitable than CCDs because of their larger cell capacity and resistance to radiation damage. However, for electron-photon conversion mode, CCDs are preferable because of their lower noise. In STEM imaging mode, if a small number of image elements can be tolerated then it may be possible to use photodiode arrays instead of CCD arrays. However, if a large area array is required then CCDs are more suitable.

CID (Charge Injection Device) imagers collect and store charge in the same way as CCDs[27]. However, the readout of charge is not by charge transfer but by the removal of the potential well, so injecting the stored charge into the silicon substrate, and creating a signal in the external circuit. This readout method requires XY- addressing of cells, leading to fixed pattern noise and a high output capacitance. Thus there seems to be no advantage, for our application, in using CIDs rather than CCDs.

Section 6.5 Improvements to Apparatus

The Data Accumulation and Control Unit very satisfactorily allowed the CCD to be used for electron imaging. The main improvement which could be made to the Unit is the addition of memory cards to increase the memory capacity from 10k to 15k words to allow the storage of the full content of both photocells and transport cells. Having done this it would then be desirable to scale the output of the transport cells to match the photocell output, so that they can be used in reconstructing the image on the oscilloscope screen. Since there are only 50 rows of transport cells, as opposed to 100 rows of photocells, each transport cell content will have to appear in 2 consecutive rows.

For more general considerations, since it is unlikely that this research will continue with the CCD 202 alone, a more flexible Data Accumulation Unit would be desirable. The present unit incorporates the Fairchild Driver Board, and relies on it for clock and selection pulses. For a more flexible system, the Data Accumulation Unit should

use only the basic clock of the driver system, with the memory address being operated by a microprocessor unit with selectable controls. For the deflection pulse, too, if necessary, it would be desirable to avoid gating by pulses from the driver board, and to have instead a pulse derived from the basic clock controlled by a counter with selectable loading and resets.

On the output side of the system, an increase in the memory capacity of the output interface from 4k to 15k words is necessary to allow full images to be transferred to computer and to magnetic tape. In addition, the time taken to transfer data to the IBM 370/145 via the CRJE system is unacceptably long, and plans are underway to link the CCD output to a dedicated minicomputer. This should considerably increase the data rate, so reducing the transfer time. With this modification it will be possible to use the CCD for determining the focus of the microscope, by Fourier transformation of images of amorphous specimens, as well as for other types of image processing.

Two modifications to the CCD holder would be desirable. Firstly, since fine temperature control of the CCD becomes necessary as damage and annealing proceed , a Peltier element would be preferable to the present cooling system. Secondly, to facilitate area selection, it is desirable that the CCD is mounted centrally in the camera chamber, so that changes in magnification do not result in movement of the chosen area.

## Section 6.6 Future Work

There are several directions which future investigations can pursue. The first is the use of the present system, with the instrumental modifications suggested in the previous section, for image processing since the performance of the CCD 202 is adequate for this purpose. However, since this CCD is no longer available, it will be necessary to find a replacement device, and one which is more suitable for electron imaging. The choice in this case would seem to lie between the radiation hard Hughes device discussed earlier, and a larger frame transfer device. In the latter case it would be important to ensure that the device is relatively radiation hard. The use of a new device would require modification of the Data Accumulation and Control Unit, preferably with the final result being a more flexible system. A series of experiments along the lines reported in this thesis would be necessary to investigate the performance of the new device under electron bombardment. A third possibility in the selection of a replacement device for the

CCD 202 is to have a device made to our specifications for electron imaging. One CCD manufacturer, Thomson-CSF, has advertised that it intends producing custom-made devices in the future. However, this is a long-term prospect, and the cost of such devices is not known.

The third possible area of investigation with CCDs is in the optically coupled mode as detectors in EELS. This mode of operation avoids the problem of radiation damage, but it is likely that a decrease in the DQE of the system and perhaps in the spatial resolution, will result from inefficiency and charge spreading in the phosphor screen. In addition, a highly efficient optical system will be required to maximise the light collection efficiency. If such a system proves feasible, it will provide a parallel detection system for EELS, thereby considerably reducing the time and the specimen dose required to record a spectrum. An optically coupled CCD may also be of use in recording diffraction patterns, since it can give quantitative data about the intensities and positions of diffraction spots, which can be used for determining specimen structure.

APPENDICES

Appendix 1 Charge Storage in a Surface Channel CCD

Following Hobson, for a metal-oxide-semiconductor (MOS) capacitor the electric field in the semiconductor can be calculated from Poisson's equation:

$$\varepsilon_s \varepsilon_o \frac{\partial E}{\partial x} = e\,(p - N_A - n)$$

where p is the density of free holes

$N_A$ is the density of acceptor atoms in the semiconductor

n is the density of free electrons

If a positive potential is applied to the metal electrode, so depleting the semiconductor under the electrode, no free charge exists in that region and so

$$\varepsilon_s \varepsilon_o \frac{\partial E}{\partial x} = -eN_A$$

Integrating gives

$$\varepsilon_s \varepsilon_o E = -eN_A X$$

where X = 0 is chosen to be the edge of the depletion region.
The potential V in the depletion region is therefore:

$$V = Vo + \frac{N_A e}{\varepsilon_s \varepsilon_o} \frac{X^2}{2}$$

where Vo is the voltage in the undepleted region of semiconductor.
The surface voltage at the semiconductor-insulator interface, Vs, occurs at X = $\ell$, where $\ell$ is the depletion layer depth, and is

$$Vs = Vo + \frac{N_A e}{\varepsilon_s \varepsilon_o} \frac{\ell^2}{2}$$

The bias voltage, $V_B$ + Vo, applied to the electrode is related to Vs according to the following derivation.

From Maxwell's Equations, $D_I = D_S + \rho_A$

where $D_I$ is the electric displacement vector in the insulator

$D_S$ is the electric displacement vector in the semiconductor

$\rho_A$ is the charge stored at the interface (charge/area)

Therefore:

$$\varepsilon_o \varepsilon_I E_I = \varepsilon_s \varepsilon_o E_S + \rho_A$$

$$= -N_A e \ell + \rho_A$$

This gives $V_I$, the voltage in the insulator as

$$V_I = Vs + \frac{(N_A e \ell - \rho_A)}{(\varepsilon_o \varepsilon_I)} (x - \ell)$$

At the oxide-metal interface X = $\ell$ + d, where d is the oxide thickness and so

$$V_B + Vo = Vs + \frac{N_A e l - \rho_A}{\varepsilon_o \varepsilon_I} d$$

Therefore

$$V_B = (Vs - Vo) + \frac{\varepsilon_s}{\varepsilon_I} d \left[2 (Vs - Vo) \frac{N_A e}{\varepsilon_s \varepsilon_o}\right]^{\frac{1}{2}} - \frac{\rho_A d}{\varepsilon_I \varepsilon_o}$$

From this

$$Vs - Vo = V_B + \frac{\rho_A d}{\varepsilon_I \varepsilon_o} + V_A - \left\{2 V_A \left[V_B + \frac{\rho_A d}{\varepsilon_I \varepsilon_o}\right] + V_A^2\right\}^{\frac{1}{2}}$$

where $V_A = \frac{N_A e \varepsilon_s \varepsilon_o}{(\varepsilon_I \varepsilon_o/d)^2} \approx 0.3V$ in a typical device and the square root term is negligible for the voltages and doping in a normal CCD.

Finally, this simplifies to:

$$Vs - Vo \approx V_B + \frac{\rho_A d}{\varepsilon_I \varepsilon_o} + 0.3V$$

If a charge $\Delta \rho_A$ is added to the storage cell there will be a corresponding change $\Delta$ Vs in the surface voltage given by:

$\Delta$ Vs $\approx \Delta \rho_A \frac{d}{\varepsilon_i \varepsilon_o}$, since $V_B$ and Vo are fixed in normal use.

Thus, there is an approximately linear relationship between the stored charge $\rho_A$ and the surface potential Vs - Vo. The CCD potential well behaves as a capacitor with a capacitance due to the oxide of $\frac{\varepsilon_I \varepsilon_o}{d}$.

## Appendix 2 Relationship between Bias Voltage and Position of Potential Minimum for a Buried Channel Device

Referring to Figure A1, $V_B$, the bias voltage applied to the metal electrode, is given by:

$$V_B = -\int_{x=o}^{x=l_1} E_1\,dx - \int_{x=l_1}^{x=l_2} E_2\,dx - \int_{x=l_2}^{x=l_2+d} E_I\,dx$$

where $x = 0$ is the position of the edge of the depletion layer

$l_1$ = length of depleted region in the p-type substrate

$l_2$ = position of $Si - SiO_2$ interface

$d$ = thickness of $SiO_2$ insulator

$E_1$ = field in p-type substrate

$E_2$ = field in n-type channel

$E_I$ = field in $SiO_2$ insulator

Hence $V_B = -\frac{1}{2}Epl_1 - \frac{1}{2}Ept - \frac{1}{2}Ent - E_Id$

where Ep is field at interface of p and n-type regions

En is field at $Si - SiO_2$ interface

By Poisson's equation $\varepsilon_s\,\varepsilon_o \frac{\partial E}{\partial x} = \rho$

where $\varepsilon_s$ = relative permittivity of semiconductor

$\varepsilon_o$ = permittivity of free space

$\rho$ = positive charge density

In the n-channel, $\rho = N_De$

where $N_D$ = density of donor atoms

$e$ = electronic charge = $1.6 \times 10^{-19}$C

so

$$E_n = \frac{N_Del}{\varepsilon_s\,\varepsilon_o}$$

where $l$ is distance of point of zero field from interface

$$Ep = En - \frac{N_Det}{\varepsilon_s\,\varepsilon_o} = En\left(1 - \frac{t}{l}\right)$$

where $t = l_2 - l_1$ is thickness of n-channel

$$E_I = \frac{\varepsilon_s}{\varepsilon_I} En$$

where $\varepsilon_I$ = relative permittivity of insulator

Hence

$$V_B = -\tfrac{1}{2}\,En\,(l_1 + t)\left(1 - \frac{t}{l}\right) - \tfrac{1}{2}\,Ent - \frac{\varepsilon_s}{\varepsilon_I}\,En$$

Since by the position of the point of zero field

$$N_Ael_1 = N_D\,e\,(t - l)$$

where $N_A$ = density of donor atoms

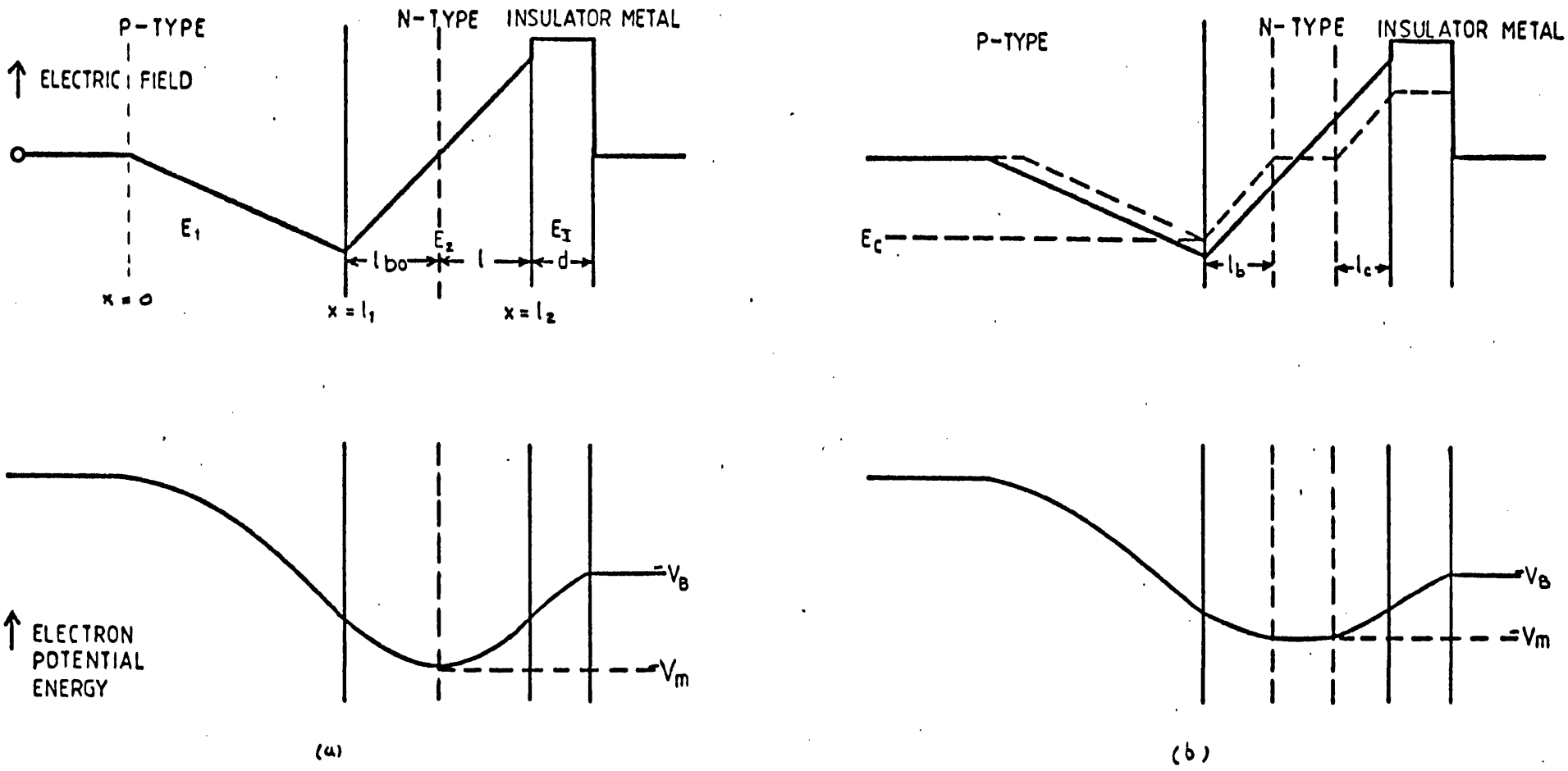


Figure A 1: Electric field and potential profiles in buried channel CCD
a) in absence of stored charge
b) with charge present

Then

$$l_1 = \frac{N_D}{N_A} (t - l)$$

So

$$V_B = En \left\{ -\tfrac{1}{2} \left(\frac{N_D}{N_A} (t - l) \left(1 - \frac{t}{l}\right) - \tfrac{1}{2} t - \frac{\varepsilon_s}{\varepsilon_I}\right\}\right.$$

$$= \tfrac{1}{2} \frac{N_D^2}{N_A} \frac{e}{\varepsilon_s \varepsilon_o} \left\{ l^2 - \frac{2N_A}{N_D} \left( \frac{N_D}{N_A} t + t + \frac{\varepsilon_s}{\varepsilon_I} d\right) l + t^2 + \frac{N_A}{N_D} t^2 \right\}$$

Hence

$$V_B = K (l^2 - cl + k)$$

where $K = \tfrac{1}{2} \frac{N_D^2}{N_A} \frac{e}{\varepsilon_s \varepsilon_o}$

$$c = \frac{2N_D}{N_A} \left(\frac{N_D}{N_A} t + t + \frac{\varepsilon_s}{\varepsilon_I} d\right)$$

$$k = t^2 \left(1 + \frac{N_A}{N_D}\right)$$

replacing by typical numerical values (Hobson) of

$N_D = 3 \times 10^{21}\ m^{-3}$

$N_A = 10^{20}\ m^{-3}$

$t = 2\ \mu m$

$d = 0.1 \mu m$

and with

$e = 1.6 \times 10^{-19}\ C$

$\varepsilon_s = 11.3$

$\varepsilon_I = 2.8$

$\varepsilon_o = 8.85 \times 10^{-12}\ Fm^{-1}$

gives $K = 7.2 \times 10^{13}\ Vm^{-2}$

$c = 4.12\ \mu m$

$k = 4\ \mu m^2$

Hence

$$V_B = 72 (l^2 - 4.12l + 4) \text{ Volts}$$

where $l$ is measured in $\mu m$

Thus as $l$ increases from zero $V_B$ is initially $\approx$ 288V at $l = 0$, decreases to a minimum of $\approx$ 0.24V at $l = 2.06\ \mu m$ and increases thereafter. Since in a practical CCD the value of $l$ can never exceed d, then only the region of the curve with $0 < l < 2\ \mu m$ is of interest. In this region, increasing $V_B$ causes $l$ to decrease ie causes the potential minimum to move nearer to the interface.

## Appendix 3 Relationship of Potential Minimum $V_{min}$ to Bias Voltage $V_B$ for a Buried Channel CCD

Referring to Figure A1

$$V_{min} = V_B + \int_{l_2}^{l_2 + d} E_I \, dx + \int_{l_2 - l}^{l_2} E_2 \, dx$$

Since $E_I = \frac{\varepsilon_s}{\varepsilon_I} En$

$$E_2 = \frac{N_D e}{\varepsilon_s \varepsilon_o} (x - (l_2 - l))$$

and $$En = \frac{N_D \, e l}{\varepsilon_s \, \varepsilon_o}$$

$$Vmin = V_B + \frac{N_D e l}{\varepsilon_s \varepsilon_o} \left( \frac{\varepsilon_s}{\varepsilon_I} d + \frac{l}{2} \right)$$

Therefore Vmin is always greater than $V_B$ by an amount which increases as $l$ increases. Since in the region in which a practical CCD operates an increase in $l$ causes a decrease in $V_B$, the first term in the expression decreases as $l$ increases, while the second term increases as $l$ increases. However, the first term dominates and so $V_{min}$ decreases as $l$ increases. To summarise, increasing $V_B$ moves the position of the minimum nearer to the interface, and also increases the depth of the potential minimum.

## Appendix 4 Rate of Change of $V_{min}$ with $V_B$

$$V_{min} = V_B + \frac{Noe\ell}{\varepsilon_s \varepsilon_o} \left(\frac{\varepsilon_s}{\varepsilon_I} d + \frac{\ell}{2}\right)$$

$$\frac{dV_{min}}{dV_B} = 1 + \frac{Noe}{\varepsilon_s \varepsilon_o} \left\{\frac{d\ell}{dV_B} \left(\frac{\varepsilon_s}{\varepsilon_I} d + \frac{\ell}{2}\right) + \frac{\ell}{2} \frac{d\ell}{dV_B}\right\}$$

$$= 1 + \frac{Noe}{\varepsilon_s \varepsilon_o} \left(\ell \frac{d\ell}{dV_B} + \frac{\varepsilon_s}{\varepsilon_I} d \frac{d\ell}{dV_B}\right)$$

$$= 1 + \frac{Noe}{\varepsilon_s \varepsilon_o} \frac{d\ell}{dV_B} \left(\ell + \frac{\varepsilon_s}{\varepsilon_I} d\right)$$

To determine how $\frac{dV_{min}}{dV_B}$ depends on $V_B$, it is necessary to examine the behaviour of $\frac{d\ell}{dV_B}$ and $\ell$ with $V_B$. Referring to Appendix 2, $\frac{d\ell}{dV_B}$ is negative in the region of interest and its absolute value decreases as $V_B$ increases. $\ell$ also decreases as $V_B$ increases. As a result $\frac{d\ V_{min}}{dV_B}$ increases as $V_B$ increases. Therefore if two adjacent electrodes, one with a high and the other with a low bias voltage both undergo the same d.c. offset in bias voltage, $V_{min}$ will increase more for the electrode with the higher initial bias voltage. The potential difference between the minima of the two electrodes will therefore increase.

## Appendix 5 Effect of Bias Voltage on Saturation Charge for a Buried Channel CCD

When signal charge is stored in the potential well of an n-buried channel CCD, it is stored in the region previously occupied by the majority charge carriers in the n-region. The maximum density of signal charge is therefore $N_D$, the density of donor atoms, and since the net charge is zero in the region of stored charge, the electric field is zero in that area. Figure A1 shows the change in the electric field profile with stored charge. As the amount of stored charge increases the region of zero field increases and the distances $l_c$ and $l_b$ decrease. Saturation occurs when $l_c$ becomes zero. At this point the amount of charge stored in the well is:

$N_D\ e\ (t - l_b)$ where t is the thickness of the n-channel

Therefore to maximise the saturation charge $l_b$ must be as small as possible. $l_b$ is related to $V_B$ in the following way

$$V_m = -Ep\ \left( \frac{l_i}{2} + \frac{l_b}{2} \right) = -Ep\ \frac{l_b}{2}\ \left( \frac{N_D}{N_A} + 1 \right)$$

$$= \frac{N_D e l_b}{\varepsilon_s \varepsilon_o}\ l_b\ \left(\frac{N_D}{N_A} + 1\right)$$

Since $V_B = V_m$ at saturation (since the field across the insulator is zero), then $l_b$ at saturation is:

$$l_{bsat} = \left\{ \frac{\varepsilon_s \varepsilon_o}{N_D e} \left(1 + \frac{1}{\frac{N_D}{N_A}}\right) V_B \right\}^{\frac{1}{2}}$$

Therefore to minimise $l_b$ and thus increase the saturation charge which can be collected the well $V_B$ must be reduced.

REFERENCES

INTRODUCTION


1. Farnell G.C, Flint R.B, "The Response of Photographic Materials to Electrons with Particular Reference to Electron Micrography", Journal of Microscopy, Vol 97, Pt 3, April 1973, p 271-291.

2. Burge R.E., Garrard D.F., Browne M.T., "The Response of Photographic Emulsions to Electrons in the Energy Range 7 - 60 keV" J. Scient. Instruments, 1, 707, 1968

3. Valentine R.C, "Characteristics of Emulsions for Electron Microscopy", Laboratory Investigation, Vol 14, No 6, Pt 2, p 596 - 602, 1965

4. Agar A.W, Alderson R.H, Chescoe D, "Principles and Practice of Electron Microscope Operation", publ North-Holland Publishing Company, Amsterdam, 1974.

5. Saxton W.O, "Digital Processing of Electron Images - a Survey of Motivations and Methods", Proceedings of Seventh European Congress on Electron Microscopy, The Hague, 1980, publ Foundation for Seventh European Congress on Electron Microscopy.

6. Williams R.C, Fisher H W, "Electron Microscopy of Tobacco Mosaic Virus under Conditions of Minimum Electron Beam Exposure", J Mol Biol 1970, 52, p 121-123.

7. Herrmann K.-H, Krahl D, Rust H.-P. "The DQE of an Electron Image Recording System", Proc 9th International Conference on Electron Microscopy, Toronto, 1978, Vol 1, p 100 - 101.

8. Rust H.-P, Krahl D, Herrmann K.-H "A Digital Storage and Processing System which permits Aposteriori Image Accumulation", Proc 9th International Conference on Electron Microscopy, Toronto 1978, Vol 1, p 90 - 91.

9. Herrman K.-H, Krahl D, Rust H.-P, "A T.V. System for Image Recording and Processing in Conventional Transmission Electron Microscopy", Ultramicroscopy, 3, (1978), p 227 - 235.

10 Herrmann K.-H, Krahl D, Kübler A, Muller K.-H, Rindfleisch V, "Image Recording with Semiconductor Detectors and Video Amplification Devices", Electron Microscopy in Material Science, ed U. Valdrè, publ Academic Press (London) 1971.

11. Herrmann K.-H, Krahl D, Rust H.-P, Ulrichs O, Optik, 44, No 4, 1976, p 393 - 412.

12. Kuo I.A.M, Glaeser R.M, "Development of Methodology for Low Exposure, High Resolution Electron Microscopy of Biological Specimens", Ultramicroscopy, 1 (1975) p 53 - 66

13 Kerzendorf W, Hoppe W, "High Resolution Image Recording with a Cooled Camera", Proc EUREM 80, Electron Microscopy 1980, Vol 1.

14. Kerzendorf W, PhD Thesis, 1979, Technischen Universität Munchen.

15. Hall J, "Comparison of Solid State Imagers and Electron Beam Scanning Imagers", Solid State Imaging, NATO Advanced Study Institute Series, Series E; Applied Science, No 16, ed Jespers P.G, Van de Wiele F, White M H, publ Noordhof.

16. Hobson G.S, "Charge Transfer Device", publ Arnold, London, 1978.

17. Fry P.W, "Silicon Photodiode Arrays", J. Phys E, Vol 8, 1975, p 337 - 343.

18. Weimer P.K, "Image Sensors for Solid State Cameras", Advances in Electronics and Electron Physics, Vol 37, 1975, ed L Marton.

19. Killiany, J.M, Baker W.D, Saks N.S, Barbe D.F, "Effects of Ionizing Radiation on Charge-Coupled Device Structures", IEEE Trans Nuc Sci, NS-21, Dec 74.

20. Killiany J.M, Saks N.S, Baker W.D, "Effects of Ionizing Radiation on a 256-Stage Linear CCD Imager", IEEE Trans Nuc Sci, NS-22, No 6, Dec 75.

21. Chang C.P, "Radiation Hardened p-surface Channel CCDs", IEEE Trans Nuc Sci, NS-23, Dec 76.

22. Egerton R.F, "Quantitative Energy Loss Spectroscopy", Scanning Electron Microscopy, 1978, Vol 1.

23. J. N Chapman, Private Communication

24. Dekkers N.H, De Lang H, Optik, 41, p 452, 1974

25. Morrison G.R, Chapman J.N, Craven A.J, "Applications of a STEM Equipped with a Quadrant Detector", Electron Microscopy and Analysis 1979, ed T Mulvey, Institute of Physics Conference Series No 52.

26. Rose H, Ultramicroscopy, 2, p 251, 1977

CHAPTER 1

1. Boyle W.S, Smith G.F, Bell Syst Tech. J., Vol 49, p587 - 593 (1970)
2. Hobson G.S, "Charge Transfer Devices", publ Edward Arnold, London, 1978
3. Fairchild CCD 201/202 Design Development Board Brochure, May 1976
4. Killiany J.M, Baker W.D, Saks N.S, Barbe D.F, "Effects of Ionizing Radiation on Charge-Coupled Device Structures", IEEE Trans Nuc Sci, NS - 21, Dec 1974
5. Currie D.G, "On a Photon Counting Array using the Fairchild CCD 201", Technical Report 75 - 082, May 1975, University of Maryland, Dept of Physics and Astronomy
6. Oatley C.W, "The Scanning Transmission Electron Microscope", Cambridge University Press, 1972
7. Katz L, Penfold A.S, "Range-Energy Relations for Electrons and the Determination of Beta-Ray End-Point Energies by Absorption", Rev. Modern Physics, 24, 1, Jan 1952, p 28-44.
8. Sequin C.H, Tompsett M.F, Charge Transfer Devices, Advances in Electronics and Electron Physics, Suppl 8, ed Marton L, publ Academic Press Inc 1975

CHAPTER 2

1. The Cambion Thermoelectric Handbook, Cambridge Thermionic Corpn, Massachusetts, 1971
2. Burstein P, Krieger A.S, Vanderhill M.J, Wattson R.B, "Soft X-Ray Imaging Experiments with Charge Coupled Devices (CCDs) and some Astronomical Applications", Society of Photo-optical Instrument Engineers, Vol 143, Applications of Electronic Imaging Systems, p 114 - 122, 1978.
3. Downing K.H, Ming-Hsiu Ho, Glaeser R.M, "A Charge Coupled Device Readout System for Electron Microscopy", Electron Microscopy, EMSA 1980
4. Nuclear Enterprises Ltd, Scintillator Catalogue, 1976
5. Birks J.B, "The Theory and Practice of Scintillation Counting", Pergamon Press, 1964
6. EMI Photomultiplier Tubes, Data Book

7. CCD 201/202 Design Development Board Brochure, May 1976, Fairchild Semiconductor

8. Saxton W.O, "Digital Processing of Electron Images - A Survey of Motivations & Methods", Electron Microscopy, 1980, Vol 1, p 486, publ Seventh European Congress on Electron Microscopy Foundation, Leiden, 1980

CHAPTER 3

1. Herrmann K.-H, Krahl D, Rust H.-P, "The DQE of an Electron Image Recording System", Proc 9th International Conference on Electron Microscopy, Toronto, 1978, Vol 1, p 100 - 101

2. Rust H.-P, Krahl D, Herrmann K.-H, "A Digital Storage and Processing System which permits Aposteriori Image Accumulation", Proc 9th International Conference on Electron Microscopy, Toronto, 1978, Vol 1, p 90 - 91.

3. Herrmann K.-H, Krahl D, Rust H.-P, "A T.V. System for Image Recording and Processing in Conventional Transmission Electron Microscopy", Ultramicroscopy 3 (1978), p 227 - 235.

4. Herrmann K.-H, Krahl D, Kübler A, Muller K.-H, Rindfleisch V, "Image Recording with Semiconductor Detectors and Video Amplification Devices", Electron Microscopy in Material Science, ed U. Valdrè, publ Academic Press (London),1971

5. Herrmann K.-H, Krahl D, Rust H.-P, Ulrichs C, Optik 44, No 4, 1976 p 393 - 412

6. Zeitler E, Hayes J.R, "Electronography", Laboratory Investigation, Vol 14, No 6, Pt 2, 1965, p 586 - 595

7. Russ J.C, "X-Ray Microanalysis at High Beam Voltages", Scanning Electron Microscopy, 1976, Pt 1, publ IIT Research Institute, Chicago

8. Weimer P.K, "Image Sensors for Solid State Cameras", Advances in Electronics and Electron Physics, Vol 37, 1975, ed L Marton

9. G C Farnell, Flint R.B, "The Response of Photographic Materials to Electrons with particular reference to Electron Micrography", Journal of Microscopy, Vol 97, Pt 3, April 1973, p 271 - 291

10. Egerton R.F, "Quantitative Energy-Loss Spectroscopy", Scanning Electron Microscopy, 1978, Vol 1

11. Hicks P.J, Daviel S, Wallbank B, Comer J, "An Electron Spectrometer using a New Multidetector System based on a Charge-Coupled Imaging Device", J. Phys E: Sci. Instrum. Vol 13, 1980

12. Esser L.J.M, "Peristaltic Charge-Coupled Devices: What is Special about the Peristaltic Mechanism", Solid State Imaging, NATO Advanced Study Institutes Series, Series E: Applied Science, No 16, ed Jespers P.G, Van de Wiele F, White M.H, publ Noordhoff.

13. Currie D.G, "On a Photon Counting Array using the CCD 201", Technical Report 75 - 082, May 1975, University of Maryland, Dept of Physics & Astronomy

14. Hobson G.S, "Charge Transfer Devices", publ Arnold, London, 1978

15. Katz I, Penfold A.S, "Range-Energy Relations for Electrons and the Determination of Beta-Ray End Point Energies by Absorption", Rev Mod Physics, Vol 24, No 1, January 1952, p 28 - 44

16. Fry P.W, "Silicon Photodiode Arrays", J Phys E, Vol 8 (1975), p 337 - 343

17. Agar A.W, Alderson R.H, Chescoe D, "Principles and Practice of Electron Microscope Operation ", North-Holland Publishing Company, Amsterdam, 1974

18. Mohsen A.M, Tompsett M.F, "The Effects of Bulk Traps on the Performance of Bulk Channel Charge-Coupled Devices", IEEE Trans on Electron Devices, ED-21 (11), 701 (Nov 74)

19. Sequin C.H, Tompsett M.F, Charge Transfer Devices, Adv Electronics & Electron Physics, Supplement 8, publ Academic Press, London, 1975

20. Kim C.-K, "The Physics of Charge-Coupled Devices", Charge-Coupled Devices and Systems, ed Howes M.J, Morgan D.V, publ John Wiley & Sons, Chichester

21. Burge R.E, Garrard D.F, "The Resolution of Photographic Emulsions for Electrons in the Energy Range 7 - 60 keV", J Scient Instrum (J Phys E) 1, 715 (1968)

22. Valentine R.C, "Characteristics of Emulsions for Electron Microscopy", Laboratory Investigation, Vol 14, No 6, Pt 2, p 596 - 602, 1965

23. Kuo I.A.M, Glaeser R.M, "Development of Methodology for Low Exposure, High Resolution Electron Microscopy of Biological Specimens", Ultramicroscopy, 1, (1975) p 53 - 66

24. Herrmann K.-H, "The Present State of Instrumentation in High Resolution Electron Microscopy", J Phys E (Sci Instrum) Vol 11, p 1076 - 1091, 1978

25. Kerzendorf W, Hoppe W, "High Resolution Image Recording with a Cooled Camera", Proc EUREM '80, Electron Microscopy, 1980, Vol 1.

26. Jones, B.L, Jenkins D.G, Booker G.R, Fry P,W, "Use of Silicon Linear Photodiode Arrays for Detection of High-Energy Electrons", Electron Microscopy and Analysis, 1977, Inst Phys Conf Series No 36

27. Jenkins D.G, Rossouw C.J, Jones B.L, Booker G.R, Fry P.W, "Use of Silicon Self-Scanned Linear Photodiode Arrays for the Direct Display of Transmission Electron Microscope Energy Loss Spectra", Electronics Letters, Vol 14, No 6, 1978, p 174 - 175

28. Jenkins, D.G, Rossouw C.J, Booker G.R, Fry P.W, "Direct Display of TEM Images and EEL Spectra using Self-Scanned Linear Silicon Photodiode Arrays", Developments in Electron Microscopy and Analysis 1979 (T Mulvey ed) publ Institute of Physics, Bristol (1979)

29. Reticon Data Sheet, RA 100 x 100 Photodiode Array

30. Integrated Photomatrix Ltd, IPL 2 DIA Information Sheet

CHAPTER 4

1. Zaininger K.H, Holmes-Siedle A.G, "A Survey of Radiation Effects in Metal-Insulator-Semiconductor Devices", RCA Review, June 1967

2. Snow E.H, Grove A.S, Fitzgerald, D.G, "Effects of Ionizing Radiation on Oxidized Silicon Surfaces and Planar Devices", Proc IEEE, Vol 55, No 7, July 1967

3. Mitchell J.P, Wilson D.K, "Surface Effects of Radiation on Semiconductor Devices", Bell System Technical Journal, Vol 46, Jan 1967

4. Zaininger K.H, "Irradiation of MIS Capacitors with High Energy Electrons", IEEE Trans on Nuclear Science, Vol NS-13, No 6, Dec 1966

5. Lamb D.R, "Some Electrical Properties of the Silicon-Silicon Dioxide System", Thin Solid Films, 5 (1970), p 247 - 276

6. Sah C.T, IEEE Trans Nuc Sci, NS-23, No 6, December 1976

7. Aubuchon K.G, "Radiation Hardening of P-MOS Devices by Optimisation of the Thermal $SiO_2$ Gate Insulator", IEEE Trans on Nuclear Science, NS-18, No 6, December 1971

8. Killiany J.M, Baker W.D, Saks N.S, Barbe D.F, "Effects of Ionizing Radiation on Charge-Coupled Device Structures", IEEE Trans on Nuclear Science, NS-21, December 1974

9. Killiany J.M, Saks N.S, Baker W.D, "Effects of Ionizing Radiation on a 256-Stage Linear CCD Imager", IEEE Trans on Nuclear Science, NS-22, No 6, December 1975

10. Killiany, J.M, "Low Temperature Radiation Damage Effects in a Room Temperature Radiation-Hard Surface Channel CCD", IEEE Trans Nuc Sci, NS-14, No 6, December 1977

11. Chang C.P, "Radiation Hardened P-Surface Channel CCDs", IEEE Trans on Nuclear Science, NS-23, December 1976

12. Powell R.J, Derbenwick G.F, "Vacuum Ultraviolet Radiation Effects in $SiO_2$", IEEE Trans Nuc Sci, NS-18, No 6, December 1971

13. Rewesz A.G, "Defect Structure and Irradiation Behaviour of Non-crystalline $SiO_2$", IEEE Trans Nuc Sci, NS-18, No 6, December 1971

14. Fathy D, Sparrow T.G, Valdrè U, "Application of EBIC to Displacement Energy Determination", Electron Microscopy and Analysis 1979, ed T Mulvey

15. Hartsell G.A, "Radiation Hardness of Surface and Buried Channel CCDs", Proceedings of 2nd International Conference on Charge-Coupled Devices, San Diego, 1975

16. Hobson G.S, "Charge Transfer Devices", p 74, publ Arnold, London, 1978

17. Nicollian E.H, "Electrical Properties of the Si-$SiO_2$ Interface", J Vac Sci Technol, Vol 14, No 5, Sept/Oct 1977

18. Killiany, J.M, "Ionizing & Neutron Radiation Effects in Charge-Coupled Devices", GOMAG 1978

19. Kim C.K, CCD Appl Conf, San Diego, Proc 7 (1975)

20. Borsuk G.M, Green J.A, De Witt R.N, Killiany J.M, "Electron Beam Irradiation of Thinned Backside Illuminated CCDs", Proc Conf on Charge-Coupled Device Technology and Applications, December 1976, Washington

21. Ma T.-P, Ma W.H.-L, "Effects of R F Annealing on the Excess Charge Centres in MIS Dielectrics", IEEE J Solid State Circuits, Vol SC-13, No 4, August 1978

22. Cosslett V.E, Thomas R.N, "Multiple Scattering of 5-30 keV Electrons in Evaporated Metal Films", British J Appl Phys, 1964, Vol 15, p 1283 - 1299

23. Kanaya K, Ono S, "Consistent Theory of Electron Scattering with Atoms in Electron Microscopes", J Phys D: Appl Phys, Vol 9, 1976

24. Maissel L.I and Glanz R (eds) "Handbook of Thin Film Technology", p 23 - 19, McGraw-Hill.

25. McKelvey J.P, Solid-State and Semiconductor Physics 1966, New York: Harper and Row

CHAPTER 5

1. Valentine R.C, "Characteristics of Emulsions for Electron Microscopy", Laboratory Investigation, Vol 14, No 6, Pt 2, p 596 - 602, 1965

2. Clark W.R.K, PhD Thesis, Glasgow University, 1979

CHAPTER 6

1. Currie D.G, "On a Photon Counting Array using the Fairchild CCD 201", Technical Report 25-082, May 1975, University of Maryland, Dept of Physics & Astronomy.

2. Mohsen A.M, Tompsett M.F, "The Effects of Bulk Traps on the Performance of Bulk Channel Charge-Coupled Devices", IEEE Trans Electron Devices, Vol ED-21, No 11, Nov 1974.

3. Agar A.W, Alderson R.H, Chescoe D, "Principles and Practice of Electron Microscope Operation", publ North Holland Publishing Company, Amsterdam, 1974.

4. Burge R.E, Garrard D.F, "The Resolution of Photographic Emulsions for Electrons in the Energy Range 7-60 keV", J Scient Instrum (J Phys E) 1, 715 (1968)

5. Zeitler E, Hayes J.R, "Electronography", Laboratory Investigation, Vol 14, No 6, Pt 2 (1965), p. 586-595.

6. Hermman R.-H, Krahl D, Rust H.-P, "A TV System for Image Recording and Processing in Conventional Transmission Electron Microscopy", Ultramicroscopy 3 (1978) p. 227-235.

7. Valentine R.C, "Characteristics of Emulsions for Electron Microscopy", Laboratory Investigation, Vol 14, No 6, Pt 2, p596-602, 1965

8. Fry P.W, "Silicon Photodiode Arrays", J Phys E, Vol 8 (1975), p 337-343.

9. Chapman J N, private communication.

10. Waddell E M, PhD Thesis, Glasgow University, 1978.

11. Dekkers N.H, De Lang H, Optik 41, p.452, 1974.

12. Waddell E.M, Chapman J.N, Optik, 54, p 83, 1979

13. Rose H, Ultramicroscopy, 2, p251, 1977.

14. Killiany J.M, Baker W.D, Saks, N.S, Barbe D.F, "Effects of Ionizing Radiation on Charge-Coupled Device Structures", IEEE Trans Nuclear Science, Vol NS-21, Dec 1974.

15. Killiany J.M, Saks N.S, Baker W.D, "Effects of Ionizing Radiation on a 256-stage Linear CCD Imager", IEEE Trans Nuclear Science, Vol NS-22, No 6, Dec 1975.

16. Killiany J.M, "Ionizing and Neutron Radiation Effects in Charge-Coupled Devices", GOMAG '78.

17. Chang C.P, "Radiation Hardened p-Surface Channel CCDs", IEEE Trans Nuclear Science, Vol NS-23, Dec 1976.

18. Chang C.P, "Radiation Effects in N-buried Channel CCDs Fabricated with a Hardened Process", IEEE Trans Nuclear Science, NS-24, Dec '77.

19. G Hershman, private communication.

20. HCC1 100A Data Sheet, Hughes Aircraft Company.

21. McMullan D, private communication.

22. Hall D.A, "Comparison of Solid-State Imagers and Electron Beam Scanning Imagers", Solid State Imaging, NATO Advanced Study Institutes Series, Series E: Applied Science-No 16, ed Jespers P.G, Van de Wiele F, White M.H, publ Noordhof.

23. Sequin C.H, Simany E.J, Tompsett M.F, Fuls E.N, "All Solid-State Camera for the 525-line TV Format", IEEE Journal Solid-State Circuits, SC-11,p115-121, 1976

24. Kamins T.I, Fong G.T, "Photosensing Arrays with Improved Spatial Resolution", IEEE Trans Electron Devices, Vol ED-25, No 2, Feb 1978.

25. Esser L.J.M, "Peristaltic Charge-Coupled Devices: What is Special about the Peristaltic Mechanism", Solid State Imaging, NATO

Advanced Study Institute Series, Series E: Applied Science, No 16, ed Jespers P.G, Van de Wiele F, White M.H, publ Noordhof.

26. Weimer P.K, "Image Sensors for Solid State Cameras", Advances in Electronics and Electron Physics, Vol 37, 1975, ed L Marton.

27. Hobson G.S, "Charge Transfer Devices", publ Arnold, London, 1978.

28. D M Walton, 'The Use of self-scanned Silicon Photodiode Arrays as Electron Detectors', Part II thesis, Department of Metallurgy & Science of Materials, University of Oxford, June 1980.

29. D M Walton, B L Jones, G R Booker & P W Fry, 'Director Display of Transmission Electron Microscope Images using self-scanned two-dimensional Silicon Photodiode Arrays', EMAG Meeting on Data Collection in Electron Microscopy & Analysis, City University, London, March 1980. (Abstract available).